



TESTING CERT # 2937.01

SAFETY INVESTIGATION AND GUIDANCE FOR RETROFITTING EXISTING APPROACH GUARDRAIL TRANSITIONS

Submitted by

Eric R. Jowza, M.S.C.E., E.I.T.
Graduate Research Assistant

Ronald K. Faller, Ph.D., P.E.
Research Assistant Professor

Scott K. Rosenbaugh, M.S.C.E., E.I.T.
Research Associate Engineer

Dean L. Sicking, Ph.D., P.E.
Professor and MwRSF Director

John D. Reid, Ph.D.
Professor

MIDWEST ROADSIDE SAFETY FACILITY

Nebraska Transportation Center
University of Nebraska-Lincoln
130 Whittier Research Center
2200 Vine Street
Lincoln, Nebraska 68583-0853
(402) 472-0965

Submitted to

WISCONSIN DEPARTMENT OF TRANSPORTATION

4802 Sheboygan Avenue
Madison, Wisconsin 53707

MwRSF Research Report No. TRP-03-266-12

August 21, 2012

TECHNICAL REPORT DOCUMENTATION PAGE

1. Report No. TRP-03-266-12	2.	3. Recipient's Accession No.	
4. Title and Subtitle SAFETY INVESTIGATION AND GUIDANCE FOR RETROFITTING EXISTING APPROACH GUARDRAIL TRANSITIONS		5. Report Date August 21, 2012	
		6.	
7. Author(s) Jowza, E.R., Faller, R.K., Rosenbaugh, S.K., Sicking, D.L., and Reid, J.D.		8. Performing Organization Report No. TRP-03-266-12	
9. Performing Organization Name and Address Midwest Roadside Safety Facility (MwRSF) Nebraska Transportation Center University of Nebraska-Lincoln 130 Whittier Research Center 2200 Vine Street Lincoln, Nebraska 68583-0853		10. Project/Task/Work Unit No.	
		11. Contract © or Grant (G) No. TPF-5(193) Supp. #26	
12. Sponsoring Organization Name and Address Wisconsin Department of Transportation 4802 Sheboygan Avenue Madison, Wisconsin 53707		13. Type of Report and Period Covered Final Report: 2010 – 2012	
		14. Sponsoring Agency Code TPF-5(193) Supp. #26	
15. Supplementary Notes Prepared in cooperation with U.S. Department of Transportation, Federal Highway Administration.			
16. Abstract (Limit: 200 words) A recent survey of approach guardrail transition systems in use along highways and roadways in the State of Wisconsin determined that a number of the transition systems were installed in a manner which deviated from the as-tested design details. These deviations included: missing transition posts; transition posts installed near or at slope break point of fill slope; insufficient soil backfill/grading behind transition posts; wood posts installed in asphalt surfacing; and the presence of drainage structures (i.e., flume) below the rail. These deviations in approach guardrail transition installations were examined using a combination of: prior research results; engineering experience; an extensive BARRIER VII computer simulation effort; and a total of eight dynamic component tests on wood and steel posts embedded in soil with varying terrain and/or foundation conditions. This investigation was performed to evaluate whether the noted design deviations degraded barrier performance for two commonly-used approach guardrail transition systems in the State of Wisconsin. When design deficiencies were determined based on computer simulations, dynamic component testing, and estimated critical limits, several design modifications were developed for use in retrofitting existing transition systems to resolve such deficiencies.			
17. Document Analysis/Descriptors Highway Safety, Roadside Appurtenances, Approach Guardrail Transitions, Retrofitting Existing Systems		18. Availability Statement No restrictions. Document available from: National Technical Information Services, Springfield, Virginia 22161	
19. Security Class (this report) Unclassified	20. Security Class (this page) Unclassified	21. No. of Pages 298	22. Price

DISCLAIMER STATEMENT

This report was funded in part through funding from the Federal Highway Administration, U.S. Department of Transportation. The contents of this report reflect the views and opinions of the authors who are responsible for the facts and the accuracy of the data presented herein. The contents do not necessarily reflect the official views or policies of the Wisconsin Department of Transportation nor the Federal Highway Administration, U.S. Department of Transportation. This report does not constitute a standard, specification, regulation, product endorsement, or an endorsement of manufacturers.

UNCERTAINTY OF MEASUREMENT STATEMENT

The Midwest Roadside Safety Facility (MwRSF) has determined the uncertainty of measurements for several parameters involved in standard full-scale crash testing and non-standard testing of roadside safety features. Information regarding the uncertainty of measurements for critical parameters is available upon request by the sponsor and the Federal Highway Administration. Test nos. WAGTMP-1, WAGTMP-4, WITB-1, WITB-2, and WIA-1 through WIA-4 were non-certified component tests conducted for research and development purposes only.

INDEPENDENT APPROVING AUTHORITY

The Independent Approving Authority (IAA) for the data contained herein was Ms. Karla Lechtenberg, Research Associate Engineer.

ACKNOWLEDGEMENTS

The authors wish to acknowledge several sources that made a contribution to this project:

(1) the Wisconsin Department of Transportation for sponsoring this project and (2) MwRSF personnel for constructing the barriers and conducting the crash tests.

Acknowledgement is also given to the following individuals who made a contribution to the completion of this research project.

Midwest Roadside Safety Facility

J.C. Holloway, M.S.C.E., E.I.T., Test Site Manager
K.A. Lechtenberg, M.S.M.E., E.I.T., Research Associate Engineer
R.W. Bielenberg, M.S.M.E., E.I.T., Research Associate Engineer
C.L. Meyer, B.S.M.E., E.I.T., Former Research Associate Engineer
M. Mongiardini, Ph.D., Post-Doctoral Research Assistant
A.T. Russell, B.S.B.A., Shop Manager
K.L. Krenk, B.S.M.A., Maintenance Mechanic
D.S. Charroin, Laboratory Mechanic
S.M. Tighe, Laboratory Mechanic
Undergraduate and Graduate Research Assistants

Wisconsin Department of Transportation

Jerry Zogg, P.E., Chief Roadway Standards Engineer
John Bridwell, P.E., Standards Development Engineer
Erik Emerson, P.E., Standards Development Engineer

TABLE OF CONTENTS

TECHNICAL REPORT DOCUMENTATION PAGE i

DISCLAIMER STATEMENT ii

UNCERTAINTY OF MEASUREMENT STATEMENT ii

INDEPENDENT APPROVING AUTHORITY ii

ACKNOWLEDGEMENTS iii

TABLE OF CONTENTS iv

LIST OF FIGURES viii

LIST OF TABLES xi

1 INTRODUCTION 1

 1.1 Background 1

 1.2 Problem Description 6

 1.2.1 Missing Transition Post(s) with Varied Locations 6

 1.2.2 Transition Posts Installed near or at Slope Break Point of Fill Slope 7

 1.2.3 Wood Transition Posts with Insufficient Soil Backfill/Grading 8

 1.2.4 Transition Posts Embedded in Asphalt 8

 1.2.5 Drainage Structures (Flume) Positioned Below Rail 10

 1.3 Research Objective 10

 1.4 Scope 10

2 LITERATURE REVIEW 12

 2.1 Safety Standards for Approach Guardrail Transitions 12

 2.2 Previous Research on Retrofitting Approach Guardrail Transitions 13

 2.2.1 Nebraska Missing Post Transition 13

 2.2.2 Tennessee Guardrail to Bridge Rail Transition 16

 2.2.3 Nebraska Prototype Thrie Beam Transition 19

 2.2.4 Modified Nebraska Thrie Beam Transition (Hidden Post) 20

 2.3 Iowa Thrie Beam Approach Guardrail Transition (18 ft – 9 in. Long) 20

 2.4 Kansas Thrie Beam Approach Guardrail Transition (31 ft – 3 in. Long) 26

 2.5 Other Relevant Approach Guardrail Transition Studies 28

 2.5.1 Missouri Thrie Beam Transition to Single-Slope CMB 28

 2.5.2 California Thrie Beam Approach Guardrail Transition 30

 2.5.3 Midwest Guardrail System Transition Element 33

 2.5.4 Midwest Guardrail System Approach Guardrail Transition 33

 2.6 Adhesive Anchor Research and Testing 34

 2.7 Post Testing Studies 36

 2.7.1 Posts Installed on Level Terrain 36

 2.7.1.1 Iowa Approach Guardrail Transition Posts 36

 2.7.1.2 Evaluation of Wood Post Quality on Guardrail Performance 39

2.7.1.3 MGS Wood-Post Approach Guardrail Transition	39
2.7.2 Posts Installed on Sloped Terrain	41
2.7.2.1 Metric-Height W-Beam Guardrail on Slopes	41
2.7.2.2 MGS Guardrail on Slopes – Phase I	42
2.7.2.3 MGS Guardrail on Slopes – Phase II	42
2.7.2.4 MGS Guardrail for Wire-Faced MSE Walls	43
2.7.3 Posts Installed in Asphalt/Concrete	46
2.7.4 Posts Installed in Rock Foundations	48
2.8 Curbs Installed Below Approach Guardrail Transitions	49
2.8.1 Texas Thrie Beam Approach Guardrail Transition	50
2.8.2 Guidelines for Curb-to-Barrier Installations	50
3 SURVEY DATA	52
3.1 Overview	52
3.2 Site Analysis	53
3.2.1 Missing Transition Post(s) with Varied Locations	53
3.2.2 Transition Posts Installed near or at Slope Break Point of Fill Slope	55
3.2.3 Transition Posts with Insufficient Soil Backfill/Grading	55
3.2.4 Transition Posts Embedded in Asphalt	56
3.2.5 Drainage Structures (Flume) Positioned Below Rail	56
3.3 Priority Ranking	56
4 BARRIER VII COMPUTER SIMULATION	59
4.1 Overview	59
4.2 Model Components	59
4.2.1 6-in. x 8-in. x 6-ft Long Wood Posts	60
4.2.2 6-in. x 8-in. x 7-ft Long Wood Posts	62
4.2.3 Rail Elements	65
4.2.4 Concrete Bridge Rail	66
4.3 Model Assembly and Validation	66
4.3.1 18-ft 9-in. Long Transition System	66
4.3.2 31-ft 3-in. Long Transition System	67
4.4 Baseline Runs	70
4.5 Evaluation Criteria for BARRIER VII Models	71
4.5.1 Vehicle Pocketing	71
4.5.2 Vehicle Snag	72
4.5.3 Dynamic Deflections	73
5 RESEARCH APPROACH – MISSING TRANSITION POSTS	74
5.1 Overview	74
5.2 Analysis	74
5.3 Retrofit Development	76
5.3.1 Retrofit 1 – Positions Adjacent to Blunt-End Parapets	77
5.3.1.1 Anchor Design	77
5.3.1.2 Base Plate Design	80
5.3.1.3 Horizontal Beam Design	82
5.3.1.4 Weld Design	84

5.3.1.5 Additional Design Considerations	85
5.3.2 Retrofit 2 – Positions Adjacent to Sloped-End Parapets	86
5.3.2.1 Anchor Design	86
5.3.2.2 Base Plate Design	87
5.3.2.3 Horizontal Beam Design.....	88
5.3.2.4 Weld Design.....	88
5.3.2.5 Additional Design Considerations	89
5.3.3 Retrofit 3 – Positions Not Adjacent to Concrete Bridge Parapets	89
5.3.3.1 Surrogate Member Selection.....	90
5.3.3.2 Surrogate Member Connection.....	96
5.4 Summary.....	96
6 COMPONENT TEST CONDITIONS.....	99
6.1 Test Facility	99
6.2 Equipment and Instrumentation.....	99
6.2.1 Bogie.....	99
6.2.2 Accelerometers	100
6.2.3 Pressure Tape Switches.....	101
6.2.4 Digital Cameras	101
6.3 End of Test Determination.....	102
6.4 Data Processing.....	102
6.5 Results.....	103
7 DYNAMIC COMPONENT TESTING – MISSING TRANSITION POSTS	104
7.1 Purpose.....	104
7.2 Scope.....	104
7.3 Bogie Testing and Results	114
7.3.1 Test No. WAGTMP-1.....	114
7.3.1.1 Discussion.....	118
7.3.2 Test No. WAGTMP-4.....	121
7.3.2.1 Discussion.....	125
7.4 Analysis.....	125
8 SUMMARY, CONCLUSIONS, AND RECOMMENDATIONS – MISSING TRANSITION POSTS.....	132
8.1 Summary and Conclusions	132
8.1.1 Retrofit 1 – Missing Transition Post Adjacent to Sloped-End Parapets	134
8.1.2 Retrofit 2 – Missing Transition Posts Adjacent to Blunt-End Parapets.....	135
8.1.3 Retrofit 3 – Missing Transition Posts Not Adjacent to Bridge Rail	135
8.1.3.1 Retrofit 3A – Applications on Level Terrain.....	136
8.1.3.2 Retrofit 3B – Applications Near a 2H:1V Fill Slope.....	136
8.2 Recommendations.....	136
9 TRANSITION POSTS INSTALLED NEAR OR AT SLOPE BREAK POINT OF FILL SLOPES	157
9.1 Overview.....	157
9.2 Dynamic Component Testing	158
9.2.1 Scope.....	158

9.2.2 Bogie Testing and Results	162
9.2.2.1 Test No. WITB-1	162
9.2.2.2 Test No. WITB-2	164
9.2.3 Discussion	166
9.3 BARRIER VII Analysis.....	169
9.4 Retrofit Development.....	171
9.4.1 Extra Driven Steel Post Concept.....	172
9.4.2 Backside Beam Concept	175
9.5 Summary and Conclusions	177
9.6 Recommendations.....	179
10 TRANSITION POSTS WITH INSUFFICIENT SOIL BACKFILL/GRADING	180
10.1 Overview.....	180
10.2 Analysis.....	180
10.3 Summary, Conclusions, and Recommendations.....	188
11 WOOD TRANSITION POSTS EMBEDDED IN ASPHALT.....	189
11.1 Overview.....	189
11.2 Discussion on Direct Confinement of a Guardrail Post.....	190
11.3 Dynamic Component Testing	192
11.3.1 Scope – Round 1	192
11.3.2 Bogie Testing and Results – Round 1	196
11.3.2.1 Test No. WIA-1	196
11.3.2.2 Test No. WIA-2	199
11.3.3 Scope – Round 2	202
11.3.4 Bogie Testing and Results – Round 2.....	202
11.3.4.1 Test No. WIA-3	202
11.3.4.2 Test No. WIA-4	205
11.3.5 Discussion.....	208
11.4 Summary, Conclusions, and Recommendations.....	209
12 DRAINAGE STRUCTURES POSITIONED BELOW TRANSITION	216
12.1 Overview.....	216
12.2 Longitudinal Curbs	216
12.3 Lateral Drainage Flumes.....	218
13 SUMMARY, CONCLUSIONS, AND RECOMMENDATIONS.....	220
14 REFERENCES	223
15 APPENDICES	228
Appendix A. Wisconsin Detailed Drawings	229
Appendix B. BARRIER VII Input Data.....	235
Appendix C. BARRIER VII Execution Procedures.....	244
Appendix D. BARRIER VII Simulation Results.....	247
Appendix E. Test Results.....	269
Appendix F. Material Specifications and Documentation	286

LIST OF FIGURES

Figure 1. Example of Vehicle Pocketing in Rail, Test No. MWT-2 [1].....	2
Figure 2. 18-ft 9-in. (5.7-m) Long, Wisconsin Approach Guardrail Transition [2]	4
Figure 3. 31-ft 3-in. (9.5-m) Long, Wisconsin Approach Guardrail Transition [3]	5
Figure 4. Common Deviations in Approach Guardrail Transition Installation	9
Figure 5. 1987 NDOR Missing Post Transition Design Alternatives [15].....	14
Figure 6. 1987 NDOR Missing Post Transition Configuration [16]	15
Figure 7. 1994 Tennessee DOT Steel-Post Transition (Original Configuration) [17]	17
Figure 8. 2000 Nebraska Thrie Beam Transition – Hidden Post Detail [19]	21
Figure 9. 1998 Iowa Transition Wood-Post with Curb [20].....	22
Figure 10. 1998 Iowa Steel-Post Transition Detail [20].....	23
Figure 11. 1998 Iowa Wood-Post Transition Detail [20].....	24
Figure 12. 1988 Kansas Thrie Beam Transition – Fifth Design Option [21]	27
Figure 13. 1995 Missouri Thrie Beam Transition to Single-Slope CMB [22]	29
Figure 14. 2000 CALTRANS Approach Guardrail Transition, Design No. 3 [23].....	32
Figure 15. Schematic of Vehicle Pocketing.....	33
Figure 16. Iowa Transition Post Testing in Soil – Force vs. Deflection [32].....	37
Figure 17. IBT Testing Series, W6x9 Posts with 43 in. E.D. – Force vs. Deflection [20,32].....	40
Figure 18. IBT Testing Series, W6x9 Posts with 43 in. E.D. – Energy vs. Deflection [20,32] ...	40
Figure 19. Texas Approach Guardrail Transition Detail [43].....	51
Figure 20. Schematic of Transition Post Numbering System.....	52
Figure 23. Blunt-End Parapet Retrofit Concept.....	78
Figure 24. Blunt-End Parapet Retrofit - Proposed Anchor Layout	79
Figure 25. Blunt-End Parapet Retrofit – Base Plate Model.....	81
Figure 26. Blunt-End Parapet Retrofit – Base Plate Weld Design	84
Figure 27. Blunt-End Parapet Retrofit – Steel Spacer Tubes	85
Figure 28. Sloped-End Parapet Retrofit – Proposed Anchor Layout.....	87
Figure 29. Sloped-End Parapet Retrofit Concerns.....	89
Figure 30. Level Terrain Dual W6x9 Retrofit - Force vs. Deflection	91
Figure 31. Proposed Dual Post Retrofit for Missing Posts	92
Figure 32. Sloped Terrain Dual W6x9 Retrofit – Force vs. Deflection.....	95
Figure 33. Rigid Frame Bogie on Guidance Track.....	100
Figure 34. WAGTMP Bogie Testing Matrix and Setup – Elevation View	106
Figure 35. WAGTMP Bogie Testing Setup – Plan View.....	107
Figure 36. WAGTMP Bogie Testing Concrete Wall Assembly – Back View.....	108
Figure 37. WAGTMP Bogie Testing Concrete Wall Assembly – Side View.....	109
Figure 38. WAGTMP Bogie Testing Concrete Wall Reinforcement Layout	110
Figure 39. WAGTMP Bogie Testing Weld Details.....	111
Figure 40. WAGTMP Bogie Testing Anchor Plate Assembly.....	112
Figure 41. WAGTMP Bogie Testing Bill of Materials	113
Figure 42. Force vs. Deflection and Energy vs. Deflection, Test No. WAGTMP-1	115
Figure 43. Time Sequential Photographs, Test No. WAGTMP-1	116
Figure 44. Post Assembly Damage, Test No. WAGTMP-1	117
Figure 45. Anchor and Parapet Damage, Test No. WAGTMP-1	118
Figure 46. Horizontal Post Loading.....	119
Figure 47. Distribution of Forces in the Base Plate.....	119

Figure 48. Anchor Force vs. Time Comparison	120
Figure 49. Force vs. Deflection and Energy vs. Deflection, Test No. WAGTMP-4.....	122
Figure 50. Time Sequential Photographs, Test No. WAGTMP-4.....	123
Figure 51. Post Assembly Damage, Test No. WAGTMP-4.....	124
Figure 52. Anchor and Parapet Damage, Test No. WAGTMP-4.....	125
Figure 53. Force vs. Deflection Results, WAGTMP Bogie Testing	127
Figure 54. Energy vs. Deflection Results, WAGTMP Bogie Testing.....	128
Figure 55. Retrofit 1 – Sloped-End Concrete Wall Assembly – Back View.....	139
Figure 56. Retrofit 1 – Sloped-End Concrete Wall Assembly – Side View.....	140
Figure 57. Retrofit 1 – Sloped-End Weld Detail	141
Figure 58. Retrofit 1 – Sloped-End Anchor Plate Assembly.....	142
Figure 59. Retrofit 1 – Sloped-End Bill of Materials	143
Figure 60. Retrofit 2 – Blunt-End Concrete Wall Assembly – Back View	144
Figure 61. Retrofit 2 – Blunt-End Concrete Wall Assembly – Side View.....	145
Figure 62. Retrofit 2 – Blunt-End Weld Detail.....	146
Figure 63. Retrofit 2 – Blunt-End Anchor Plate Assembly.....	147
Figure 64. Retrofit 2 – Blunt-End Bill of Materials.....	148
Figure 65. Retrofit 3A – General Missing Post Installation Detail.....	149
Figure 66. Retrofit 3A – General Missing Post Cross-Beam Detail.....	150
Figure 67. Retrofit 3A – General Missing Post Cross-Beam Assembly.....	151
Figure 68. Retrofit 3A – General Missing Post Bill of Materials.....	152
Figure 69. Retrofit 3B – General Missing Post Installation Detail.....	153
Figure 70. Retrofit 3B – General Missing Post Cross-Beam Detail.....	154
Figure 71. Retrofit 3B – General Missing Post Cross-Beam Assembly.....	155
Figure 72. Retrofit 3B – General Missing Post Bill of Materials.....	156
Figure 73. WITB Bogie Testing Matrix and Setup.....	160
Figure 74. WITB Bogie Testing Post Details.....	161
Figure 75. Force vs. Deflection and Energy vs. Deflection, Test No. WITB-1	162
Figure 76. Time-Sequential and Post-Impact Photographs, Test No. WITB-1	163
Figure 77. Force vs. Deflection and Energy vs. Deflection, Test No. WITB-2	164
Figure 78. Time-Sequential and Post-Impact Photographs, Test No. WITB-2	165
Figure 79. Force vs. Deflection Comparison Plot, WITB Bogie Testing.....	167
Figure 80. Energy vs. Deflection Comparison Plot, WITB Bogie Testing	168
Figure 81. Backside Beam Concept.....	171
Figure 82. Extra Driven Steel Post Concept.....	175
Figure 83. Base Moment Calculation – Wood Post Configuration	181
Figure 84. Resistances and Base Moments for Various Improper Exposure Lengths.....	184
Figure 85. Asphalt Placement on Sloped Terrain.....	191
Figure 86. WIA Bogie Testing Matrix and Setup – Round 1	194
Figure 87. WIA Bogie Testing Post Detail – Round 1	195
Figure 88. Force vs. Deflection and Energy vs. Deflection, Test No. WIA-1.....	197
Figure 89. Time-Sequential and Post-Impact Photographs, Test No. WIA-1	198
Figure 90. Force vs. Deflection and Energy vs. Deflection, Test No. WIA-2.....	200
Figure 91. Time-Sequential and Post-Impact Photographs, Test No. WIA-2	201
Figure 92. Force vs. Deflection and Energy vs. Deflection, Test No. WIA-3.....	203
Figure 93. Time-Sequential and Post-Impact Photographs, Test No. WIA-3	204
Figure 94. Force vs. Deflection and Energy vs. Deflection, Test No. WIA-4.....	206

Figure 95. Time-Sequential and Post-Impact Photographs, Test No. WIA-4	207
Figure 96. Force vs. Deflection Results, WIA Bogie Testing	212
Figure 97. Force vs. Deflection Results, 2H:1V Fill Slope Bogie Testing.....	213
Figure 98. Energy vs. Deflection Results, 2H:1V Fill Slope Bogie Testing	214
Figure 99. Energy vs. Deflection Results, WIA Bogie Testing.....	215
Figure A-1. Wisconsin Sloped Face Parapet “LF” [45]	230
Figure A-2. Wisconsin Sloped Face Parapet “B” (Voided) [46].....	231
Figure A-3. Wisconsin Concrete Surface Drains Flume Type at Structures [47]	232
Figure A-4. Wisconsin Concrete Surface Drains Drop Inlet Type at Structures [48]	233
Figure A-5. Wisconsin Double and Triple Blocked-Out Guardrails [53]	234
Figure B-1. BARRIER VII Model Deck for the 18-ft 9-in. Long System	236
Figure B-2. BARRIER VII Model Deck for the 18-ft 9-in. Long System – Cont.....	237
Figure B-3. BARRIER VII Model Deck for the 18-ft 9-in. Long System – Cont.....	238
Figure B-4. BARRIER VII CAD Drawing of the 18-ft 9-in. Long System	239
Figure B-5. BARRIER VII Model Deck for the 31-ft 3-in. Long System	240
Figure B-6. BARRIER VII Model Deck for the 31-ft 3-in. Long System – Cont.....	241
Figure B-7. BARRIER VII Model Deck for the 31-ft 3-in. Long System – Cont.....	242
Figure B-8. BARRIER VII CAD Drawing of the 31-ft 3-in. Long System	243
Figure E-1. Results of Test No. WAGTMP-1 (EDR-3)	270
Figure E-2. Results of Test No. WAGTMP-1 (DTS).....	271
Figure E-3. Results of Test No. WAGTMP-4 (EDR-3)	272
Figure E-4. Results of Test No. WAGTMP-4 (DTS)	273
Figure E-5. Results of Test No. WITB-1 (EDR-3).....	274
Figure E-6. Results of Test No. WITB-1 (DTS).....	275
Figure E-7. Results of Test No. WITB-2 (EDR-3).....	276
Figure E-8. Results of Test No. WITB-2 (DTS).....	277
Figure E-9. Results of Test No. WIA-1 (EDR-3).....	278
Figure E-10. Results of Test No. WIA-1 (DTS).....	279
Figure E-11. Results of Test No. WIA-2 (EDR-3)	280
Figure E-12. Results of Test No. WIA-2 (DTS).....	281
Figure E-13. Results of Test No. WIA-3 (EDR-3).....	282
Figure E-14. Results of Test No. WIA-3 (DTS).....	283
Figure E-15. Results of Test No. WIA-4 (EDR-3).....	284
Figure E-16. Results of Test No. WIA-4 (DTS).....	285
Figure F-1. W6x12 Beam Material Specifications, Test No. WAGTMP-1	287
Figure F-2. Base Plate Material Specifications, Test No. WAGTMP-1	288
Figure F-3. Back-up Plate Material Specifications, Test No. WAGTMP-1	289
Figure F-4. W6x12 Beam Material Specifications, Test No. WAGTMP-4	290
Figure F-5. Base Plate Material Specifications, Test No. WAGTMP-4.....	291
Figure F-6. Back-Up Plate Material Specifications, Test No. WAGTMP-4	292
Figure F-7. Gusset Plate Material Specifications, Test No. WAGTMP-4.....	293
Figure F-8. 6-in. x 8-in. Wood Post Material Specifications.....	294
Figure F-9. Soil Characteristic Data, Test Nos. WITB-1 and WITB-2	295
Figure F-10. Soil Characteristic Data, Test Nos. WIA-1 and WIA-2.....	296
Figure F-11. Soil Characteristic Data, Test Nos. WIA-3 and WIA-4.....	297

LIST OF TABLES

Table 1. MwRSF Adhesive Anchor Dynamic Test Results [30-31] 35
Table 2. Dynamic Test Results, IBT Bogie Testing Series in Soil [32] 38
Table 4. Dynamic Component Results for MGS Posts on 2H:1V Terrain [7] 44
Table 5. Dynamic Testing of Wood and Steel Posts for MGS on a MSE Wall [8]..... 45
Table 6. Dynamic Testing of Wood Posts on 3H:1V Terrain [9]..... 46
Table 7. Survey Summary of 18-ft 9-in. Long Wisconsin Transition System 54
Table 8. Survey Summary of 31-ft 3-in. Long Wisconsin Transition System 54
Table 9. System Deficiency Rankings 58
Table 10. 6-in. x 8-in. Wood Post Test Results [32]..... 60
Table 11. Input Properties for BARRIER VII Wood Posts 61
Table 12. Input Properties for BARRIER VII Rail Elements..... 65
Table 13. 18-ft 9-in. Long System Validation with Crash Test No. ITNJ-4 Results..... 69
Table 14. Previous Approach Transition Simulation and Testing Results with Critical Limits... 72
Table 15. Simulation Summary of 18-ft 9-in. Long System Missing Transition Posts..... 75
Table 16. Simulation Summary of 31-ft 3-in. Long System Missing Transition Posts..... 75
Table 17. Blunt-End Parapet Retrofit – Base Plate Analysis Results..... 81
Table 18. Flexural Capacities of Common W-Shapes..... 84
Table 19. Sloped-End Parapet – Base Plate Analysis Results 87
Table 20. Flexural Capacities of Common W-Shapes with 4-in. Flange Widths..... 88
Table 21. Relative Dynamic Deflections between Consecutive Wood Transition Posts [20]..... 93
Table 22. Bogie Testing Results – W6x12 Horizontal Retrofit Design 126
Table 23. Input Properties for BARRIER VII W6x12 Retrofit..... 130
Table 24. Summary of Simulation Results for W6x12 Retrofit Design 131
Table 25. Wood Post Properties – WITB Testing Series..... 159
Table 26. Testing Results – 6-in. x 8-in. Wood Posts Embedded 52 in. on 2H:1V Fill Slope... 166
Table 27. Input Properties – 6 in. x 8 in. Wood Posts Embedded 52 in. on 2H:1V Fill Slope... 169
Table 28. Summary of Simulation Results for 2H:1V Fill Slopes 170
Table 29. Input Properties for BARRIER VII – Backside Beam 176
Table 30. Calculations for Various Exposure Lengths 183
Table 31. Input Properties for BARRIER VII Improperly Exposed Posts 185
Table 32. Maximum Wheel Rim Snag for Improperly Exposed Posts..... 186
Table 33. Summary of Simulation Results for Improperly Exposed Posts 187
Table 34. Wood Post Properties – WIA Testing Series..... 193
Table 35. Bogie Testing Results – Wood Posts Confined by 2-in. Thick Asphalt Layer 209
Table D-1. 18-ft 9-in. Long System – Baseline 248
Table D-2. 18-ft 9-in. Long System – Missing Post Position 1 249
Table D-3. 18-ft 9-in. Long System – Retrofitted Post Position 1 (W6x12) 250
Table D-4. 18-ft 9-in. Long System – Missing Post Position 2 251
Table D-5. 18-ft 9-in. Long System – Missing Post Position 3 252
Table D-6. 18-ft 9-in. Long System – Missing Post Position 4 253
Table D-7. 18-ft 9-in. Long System – Missing Post Position 5 254
Table D-8. 18-ft 9-in. Long System – Missing Post Position 6 255
Table D-9. 18-ft 9-in. Long System – 3-in. Improper Post Exposure 256
Table D-10. 18-ft 9-in. Long System – 4-in. Improper Post Exposure 257
Table D-11. 18-ft 9-in. Long System – Break Point of a 2H:1V Fill Slope 258

Table D-12. 31-ft 3-in. Long System – Baseline	259
Table D-13. 31-ft 3-in. Long System – Missing Post Position 1	260
Table D-14. 31-ft 3-in. Long System – Retrofitted Post Position 1 (W6x12)	261
Table D-15. 31-ft 3-in. Long System – Missing Post Position 2	262
Table D-16. 31-ft 3-in. Long System – Missing Post Position 3	263
Table D-17. 31-ft 3-in. Long System – Missing Post Position 4	264
Table D-18. 31-ft 3-in. Long System – Missing Post Position 6	265
Table D-19. 31-ft 3-in. Long System – 3 in. Improper Post Exposure	266
Table D-20. 33-ft 3-in. Long System – 4-in. Improper Post Exposure	267
Table D-21. 31-ft 3-in. Long System – Break Point of a 2H:1V Fill Slope	268

1 INTRODUCTION

1.1 Background

Throughout the United States, various approach guardrail transition systems are routinely employed by State Highway Departments to connect standard strong-post, W-beam guardrail systems to the blunt end of bridge rails. These transition systems, as compared to more flexible W-beam guardrails, utilize increased post sizes, reduced post spacing, longer post embedment depths, and additional rail elements to gradually increase the lateral stiffness of the system and achieve a smooth transition from flexible or semi-rigid guardrail to a more rigid bridge rail. Without these stiffness transitions, errant vehicles which are captured and redirected by the upstream guardrail system could pocket and/or snag on the blunt end of the rigid bridge rail, thus resulting in dangerous levels of rapid deceleration and/or vehicle instabilities. For this reason, approach guardrail transitions are essential roadside features that improve motorist safety near bridge ends.

Still, it is important that the additional stiffness and strength of a transition system be applied gradually over its length. A short and overly stiff transition system may prevent contact with the upstream end of the bridge rail, but it may also induce vehicle pocketing during impacts farther upstream of the transition system. The phenomenon of vehicle pocketing occurs when a vehicle approaches a stiffened, semi-rigid approach guardrail transition region from a relatively flexible guardrail region. Small lateral deflections in the transition region as compared to large lateral deflections in the preceding guardrail region can cause a sharp bend to develop in the barrier system directly before the transition region, as shown in Figure 1. This rail bend or pocket, if steep enough, has the potential to produce high longitudinal forces on the vehicle which could lead to excessive decelerations, rail rupture, or even rollover.



Figure 1. Example of Vehicle Pocketing in Rail, Test No. MWT-2 [1]

Two W-beam to three beam approach guardrail transition systems constitute the majority of transition systems currently found along highways and roadways in the State of Wisconsin. The first system measures approximately 18 ft – 9 in. (5.7 m) long, as currently specified in the Wisconsin Department of Transportation's (DOT's) standard plans (Wisconsin DOT Standard Detail Drawing 14B20-9a [2]). The second system was installed for many years and measured approximately 31 ft – 3 in. (9.5 m) long [3]. These two three beam transition systems are shown in Figures 2 and 3, respectively. For clarification, the 31 ft – 3 in. (9.5 m) long system represented Wisconsin's standard transition for treating rigid concrete parapets from 1990 through 2004, while the 18 ft – 9 in. (5.7 m) long system represented Wisconsin's primary approach guardrail transition from 2004 through 2011. In this report, each system will be referred to by its length. In 2011, the State of Wisconsin adopted another three beam transition that was based on the Midwest Guardrail System (MGS), although older three beam transitions remain in service.

Historically, approach guardrail transition systems have been designed, tested, and evaluated according to various impact safety standards. Subsequently, many of these crashworthy approach guardrail transitions have also been approved for use along U.S. highways and roadways by the Federal Highway Administration (FHWA). When installed correctly, these systems significantly reduce the propensity for wheel snag and vehicle pocketing throughout the transition region. Unfortunately, approach guardrail transitions that are installed in the field may not always resemble that of the as-tested configuration. These deviations can reduce the desired lateral stiffness and strength of the transition system, thus potentially resulting in rail rupture, vehicle instabilities, vehicle pocketing, vehicle snagging, and other hazardous consequences. Consequently, deviations from the as-tested approach guardrail transition can render the system as a liability rather than as a safety device.

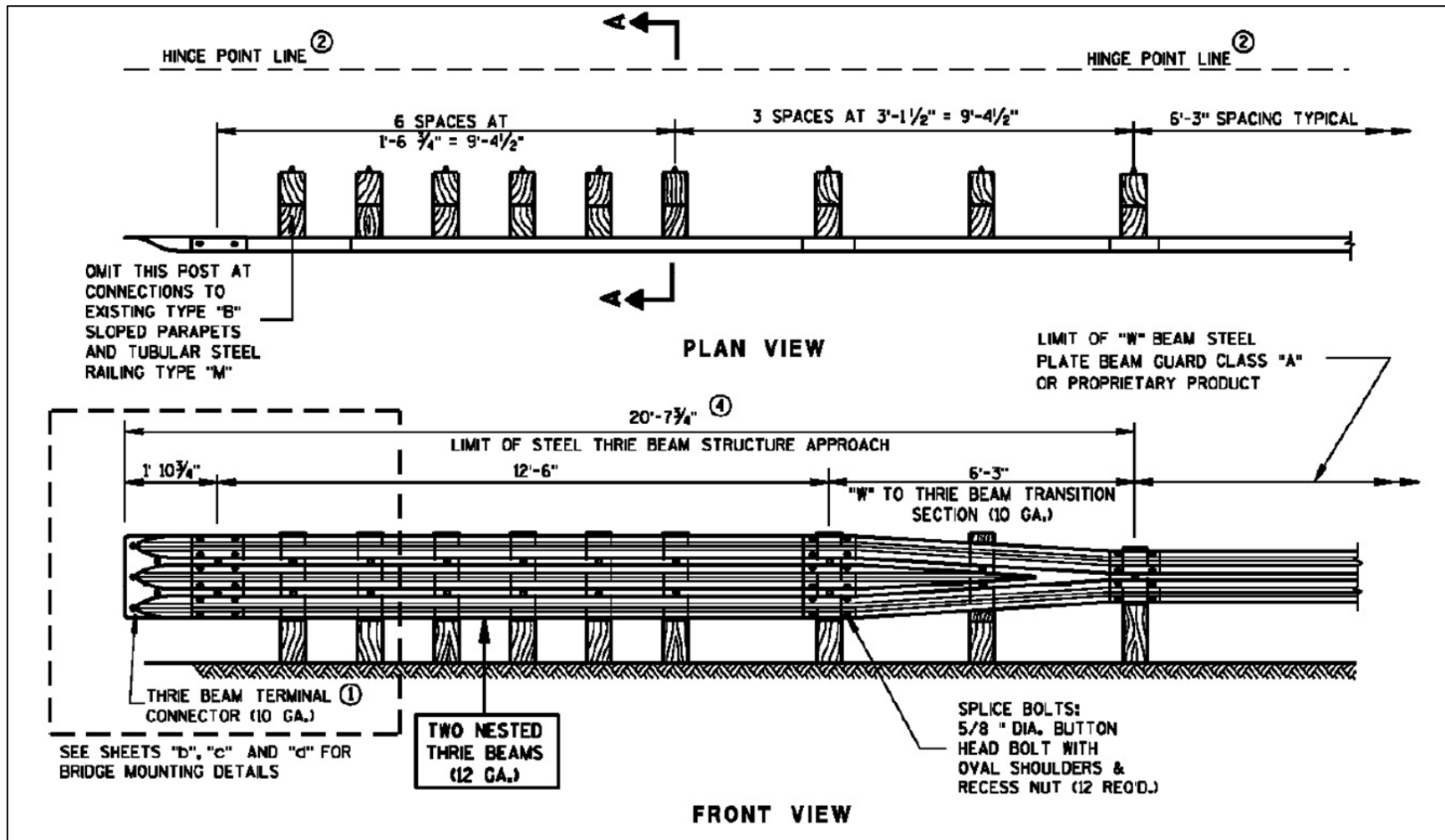


Figure 2. 18-ft 9-in. (5.7-m) Long, Wisconsin Approach Guardrail Transition [2]

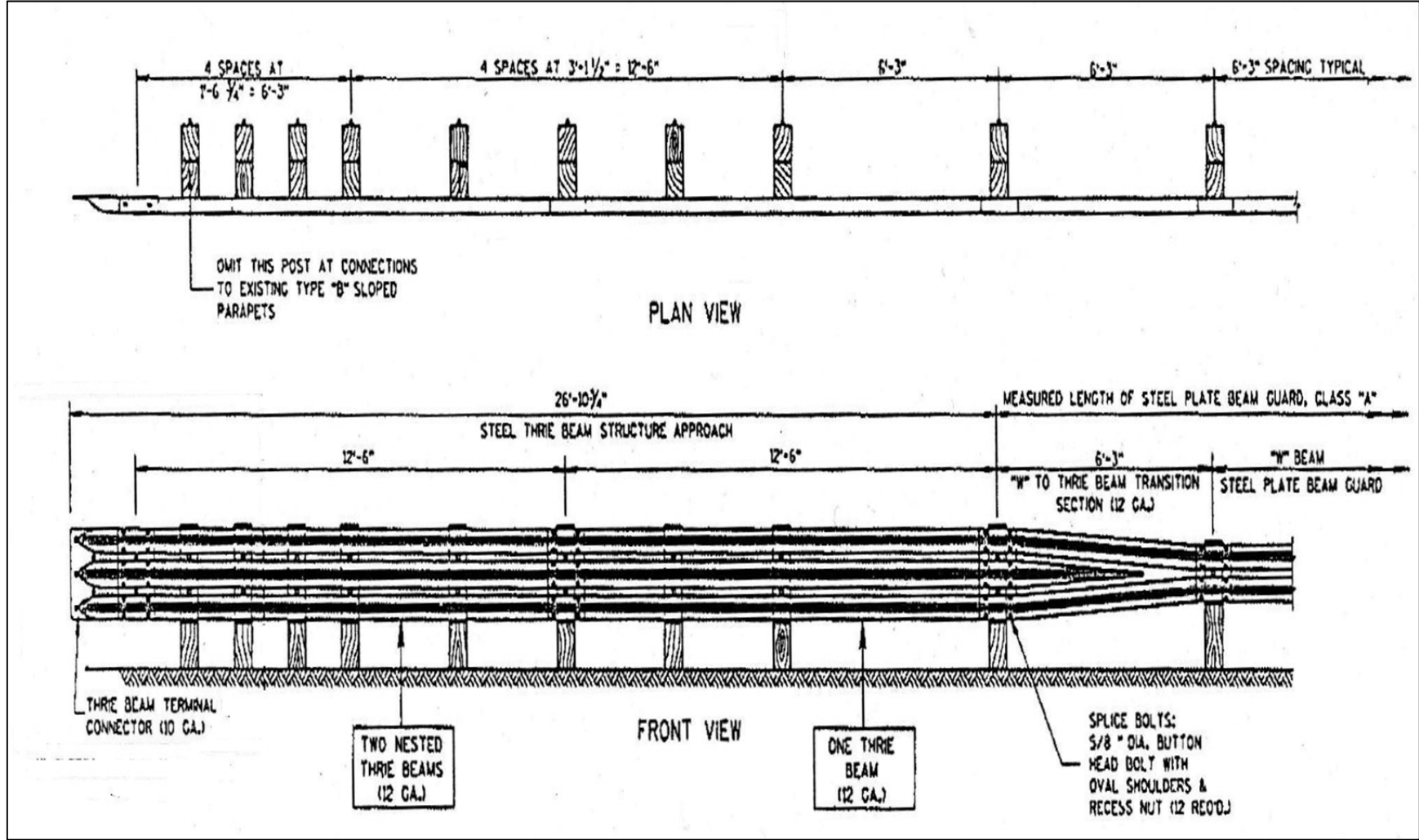


Figure 3. 31-ft 3-in. (9.5-m) Long, Wisconsin Approach Guardrail Transition [3]

5

1.2 Problem Description

In recent years, Wisconsin DOT personnel reviewed numerous approach guardrail transition installations across the State including configurations measuring 18 ft – 9 in. (5.7 m) and 31 ft – 3 in. (9.5 m) long. As part of this review, it was determined that a number of the transition systems were installed in the manner which deviated from the standard plans and as-tested design details. The most common deviations included: missing transition posts; transition posts installed near or at slope break point of fill slope; insufficient soil backfill/grading behind transition posts; wood posts installed in asphalt surfacing; exposed posts due to erosion; and the presence of drainage structures (i.e., flumes) below the rail. Any one of these system deviations can negatively affect a transition system's safety performance, as explained in the following sections of the report.

1.2.1 Missing Transition Post(s) with Varied Locations

The omission of even a single post in any type of guardrail installation creates a discontinuity or 'weak spot' in the barrier system. A 'weak spot' can allow for larger than desired deflections when struck by a vehicle. These excessive deflections can ultimately lead to: a vehicle striking fixed objects outside of the system's working width; vehicle pocketing within the system; severe vehicle instabilities (e.g., rollovers); wheel snag on the end of a rigid concrete bridge rail, road barrier, or parapet (i.e., buttress); or even rail rupture. In fact, a recent simulation study conducted by researchers at the Virginia Polytechnic Institute in 2009 demonstrated that a single missing post resulted in greater barrier deflections, increased the propensity for a vehicle to strike a fixed object otherwise protected by the guardrail, and provided greater propensity for rail rupture [4-5].

The vehicle pocketing issue only becomes magnified for missing posts within a transition system. Transitions are already sensitive to pocketing due to the gradual increase in lateral

stiffness and strength between the W-beam guardrail and the rigid bridge rail. Omitting a post within a transition system can disrupt the gradual increase in stiffness and instead create a rapid increase in stiffness immediately downstream of the missing post. Thus, vehicle pocketing and snag become more likely.

The location of the missing post is also critical. As one moves along an approach guardrail transition toward the rigid bridge rail, the lateral barrier resistance increases and the lateral rail deflections decrease. Thus, different posts in a transition system are expected to provide different structural capacities, dissipate varying levels of energy, and produce different lateral barrier deflections. Therefore, different consequences may be associated with different missing post positions within a transition system. In particular, missing posts adjacent to a bridge rail will likely result in vehicle pocketing and/or wheel snag on the bridge rail end, while missing posts further upstream will likely produce vehicle pocketing, vehicular instabilities, and wheel snag on posts. In the data review of actual field installations, missing posts were noted in a wide variety of positions along transition systems, ranging from locations adjacent concrete bridge rails to locations near the narrow end of the W-beam to thrie beam transition element. An example of an approach guardrail transition system with multiple missing posts is depicted in Figure 4 (a).

1.2.2 Transition Posts Installed near or at Slope Break Point of Fill Slope

Numerous studies have indicated that a guardrail post installed on a slope will rotate under lower force levels as compared to a guardrail post installed on level terrain [6-9]. This outcome is due to a reduction in soil backfill for confining the backside of the post. As such, the lateral stiffness, strength, and energy absorbing potential of a transition system located on a fill slope will be reduced from that observed in crash-tested transitions on level terrain. In particular, a reduction in these parameters can result in excessive system deflections. As noted previously,

excessive system deflections can especially become a problem near the rigid bridge rail end where there is an inherent propensity for vehicle snag on the upstream end of a concrete buttress. An example of an approach guardrail transition system with wood posts installed on a steep slope is provided in Figure 4 (b).

1.2.3 Wood Transition Posts with Insufficient Soil Backfill/Grading

The consequences associated with transition posts placed with insufficient compacted soil are similar to those for transition posts installed on fill slopes, In addition to reduced post-soil resistance, transition posts with inadequate soil backfill correspond with increased post exposure above ground line. As a result, the impact load imparted to an exposed post is applied at a greater height about grade, this amplifying the bending moment applied to the affected post. Larger bending moments translate to premature yielding of steel posts and premature fracture of wood posts. Further, increased exposure lengths correlate with shallow embedment depths. Posts with excessively shallow embedment depths can be pulled out of the ground without providing sufficient lateral resistance. An example of transition posts with insufficient soil backfill material is shown in Figure 4 (c).

1.2.4 Transition Posts Embedded in Asphalt

Asphalt that has been compacted and hardened is much stiffer than a typical roadside soil. Thus, layers of relatively rigid asphalt which surround and confine guardrail posts can prevent post rotation and potentially lead to the premature yielding of steel posts or the premature fracture of wood posts. As a result, the amount of energy absorbed by each post confined by asphalt will be significantly reduced below its expected value, and the possibility of total system failure can occur. An example of a transition post installed in asphalt is provided in Figure 4 (d).



(a)



(b)



(c)



(d)



(e)

Figure 4. Common Deviations in Approach Guardrail Transition Installation

1.2.5 Drainage Structures (Flume) Positioned Below Rail

A lateral drainage structure (i.e., flume) placed under a guardrail system and perpendicular to the roadway can create a hazardous condition for a vehicle being contained and redirected by the barrier system. In particular, this obstacle can provide a more abrupt change in terrain as compared to a sloped longitudinal curb. A rapid change in terrain could easily result in vehicle instabilities and lead to rollovers. An example of a blunt lateral drainage structure or flume positioned beneath an approach guardrail transition system is shown in Figure 4 (e).

1.3 Research Objective

The objective of this study was to investigate the potential hazards associated with each of the five previously described configurations found in combination with existing approach guardrail transition systems in terms of vehicle snag, vehicle pocketing, and vehicle instabilities. If feasible, a design modification or retrofit was evaluated in order to alleviate each particular deficiency. It should be noted that the design modifications provided herein were only developed to provide an immediate solution for upgrading the deficient condition. As such, it may not be appropriate to implement all of these design modifications within the initial installation of an approach guardrail transition system unless deemed necessary, as in the case of flumes below the rail. Further, those transition systems deemed deficient should be upgraded in a timely manner with the appropriate safety modifications which would likely improve barrier performance and resemble that provided by the original FHWA-accepted configurations.

1.4 Scope

The research objective was achieved through the completion of several tasks. A literature review was conducted to identify key design considerations and features for approach guardrail transition systems. Brainstorming sessions were held to develop concepts for treating each of the five noted system deficiencies. BARRIER VII computer simulations were performed to evaluate

the effect that selected deficiencies had on system performance [10]. Dynamic component tests were conducted to quantify the negative effects of particular deficiencies and to evaluate potential design solutions. BARRIER VII computer simulation was again employed to examine the safety performance of proposed solutions during vehicular impact events.

It should be noted that the approach guardrail transition systems under investigation herein adhere to the standards set forth by the National Cooperative Highway Research Program (NCHRP) Report No. 350 [11]. As such, the simulation, analysis, and design efforts employed herein to address these deficiencies utilized this criteria as well.

2 LITERATURE REVIEW

2.1 Safety Standards for Approach Guardrail Transitions

In 1981, the National Cooperative Highway Research Program (NCHRP) released Report No. 230 *Recommended Procedure for the Safety Performance Evaluation of Highway Appurtenances* [12]. These criteria were effective for over a decade and required that all high-speed approach guardrail transitions satisfy the requirements of one Multiple Service Level 2 (MSL-2) full-scale vehicle crash test (test designation 30). This test consisted of a 4,500-lb (2,401-kg) sedan impacting the barrier system at 60 mph (97 km/h) and at an angle of 25 degrees. The impact location for this test was specified to be 15 ft (4.6 m) upstream of the bridge rail end. Three general evaluation criteria were considered to determine whether a system was adequate or not: (i) structural adequacy of the system; (ii) occupant risk in terms of impact velocity (OIV) and ride down acceleration (ORA); and (iii) post-impact vehicle trajectory.

In 1989, the American Association of State Highway and Transportation Officials (AASHTO) released *Guide Specifications for Bridge Railings* [13]. This document had similar evaluation criteria as that found in NCHRP Report No. 230, but concentrated on bridge railings and the approach guardrail transitions which preceded them. It required that all high-speed approach guardrail transitions satisfy the requirements of two Performance Level (PL) full-scale vehicle crash tests. A new vehicle, the pickup truck, was introduced for the PL crash tests. The first test, PL-1, consisted of a 5,400-lb (2,449-kg) pickup truck impacting the barrier system at 45 mph (72 km/h) and at an angle of 20 degrees. The second test, PL-2, consisted of a 5,400-lb (2,449-kg) pickup truck impacting the barrier system at 60 mph (97 km/h) and at an angle of 20 degrees. In addition, these criteria specified varied test conditions for a smaller 1,800-lb (816-kg) vehicle.

In 1993, NCHRP released Report No. 350 *Recommended Procedures for the Safety Performance Evaluation of Highway Features* [11]. As such, the MSL-2, PL-1, and PL-2 full-scale vehicle crash tests were replaced with Test Levels 1 (TL-1) through 4 (TL-4). In particular, it specified that all high-speed approach guardrail transitions satisfy TL-3 safety requirements (test designation 21). The TL-3 test consisted of a 4,409-lb (2,000-kg) pickup truck impacting the barrier system at 62.1 mph (100 km/h) and at an angle of 25 degrees. The impact point of the test was no longer set at 15 ft (4.6 m) upstream of the bridge rail. Instead, the impact point was to be determined based on the predicted worst case scenario for the system, known as the critical impact point (CIP). In addition, a second test with varied conditions was also specified using a smaller 1,808-lb (820-kg) vehicle to evaluate occupant risk and post-impact trajectory criteria.

In 2010, the American Association of State Highway and Transportation Officials (AASHTO) released the *Manual for Assessing Safety Hardware (MASH)* [14] performance criteria. Again, several parameters were altered from previous full-scale vehicle crash testing criteria, including changes in vehicle types, weights, impact conditions, as well as a specification for the center of gravity for the pickup truck.

2.2 Previous Research on Retrofitting Approach Guardrail Transitions

2.2.1 Nebraska Missing Post Transition

In 1987, researchers at the University of Nebraska-Lincoln (UNL) evaluated four guardrail-to-bridge rail transition designs for the State of Nebraska [15]. The goal of the study was to determine the most cost-effective design that satisfied full-scale crash test criteria. The base design in the study consisted of six 6-ft (1.8-m) long wood posts of varying sizes spaced at 37¹/₂ in. (953 mm). For this configuration, the first wood post upstream from the bridge rail was omitted in each of the designs as the result of a common field problem in which a concrete abutment and/or wingwall system prevented installation of this post. As such, several design

alternatives were considered to compensate for the missing rigidity from the omitted post, including the use of additional beam members.

A total of six full-scale vehicle crash tests were used to evaluate the four different rail designs, as shown in Figure 5. The researchers found that the performance of only two of the four designs were deemed satisfactory according to the safety criteria set forth in NCHRP Report No. 230 for MSL-2 sedan tests. Both satisfactory designs incorporated two 12-gauge (2.7-mm) thrie beam rails as compared to a single thrie beam rail or two nested W-beam rails. Therefore, it was concluded that transition configurations which omitted the first post upstream from the bridge rail could be permitted if nested thrie beam rails were specified. The final transition design, as shown in Figure 6, was accepted under *Technical Advisory T5040.26* [16].

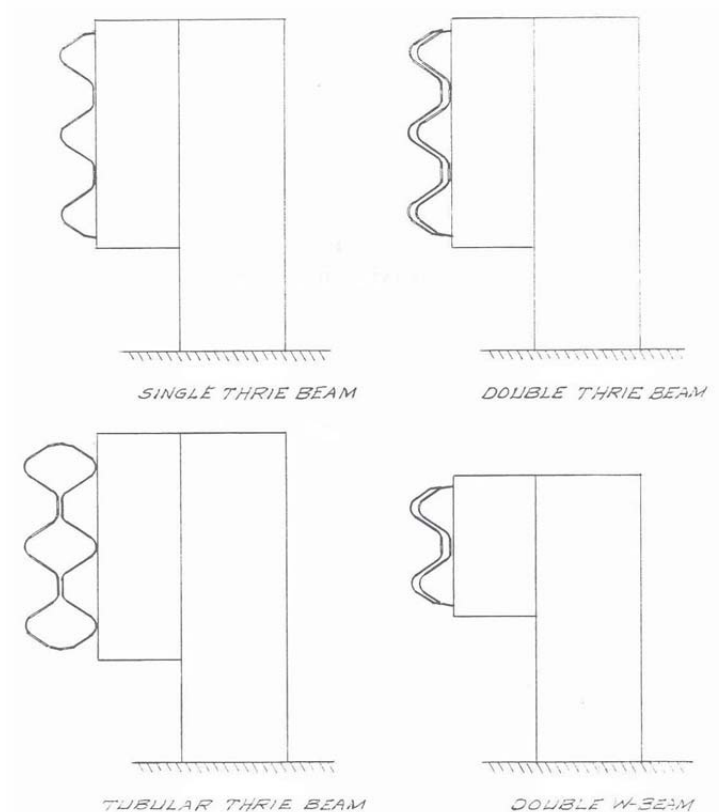


Figure 5. 1987 NDOR Missing Post Transition Design Alternatives [15]

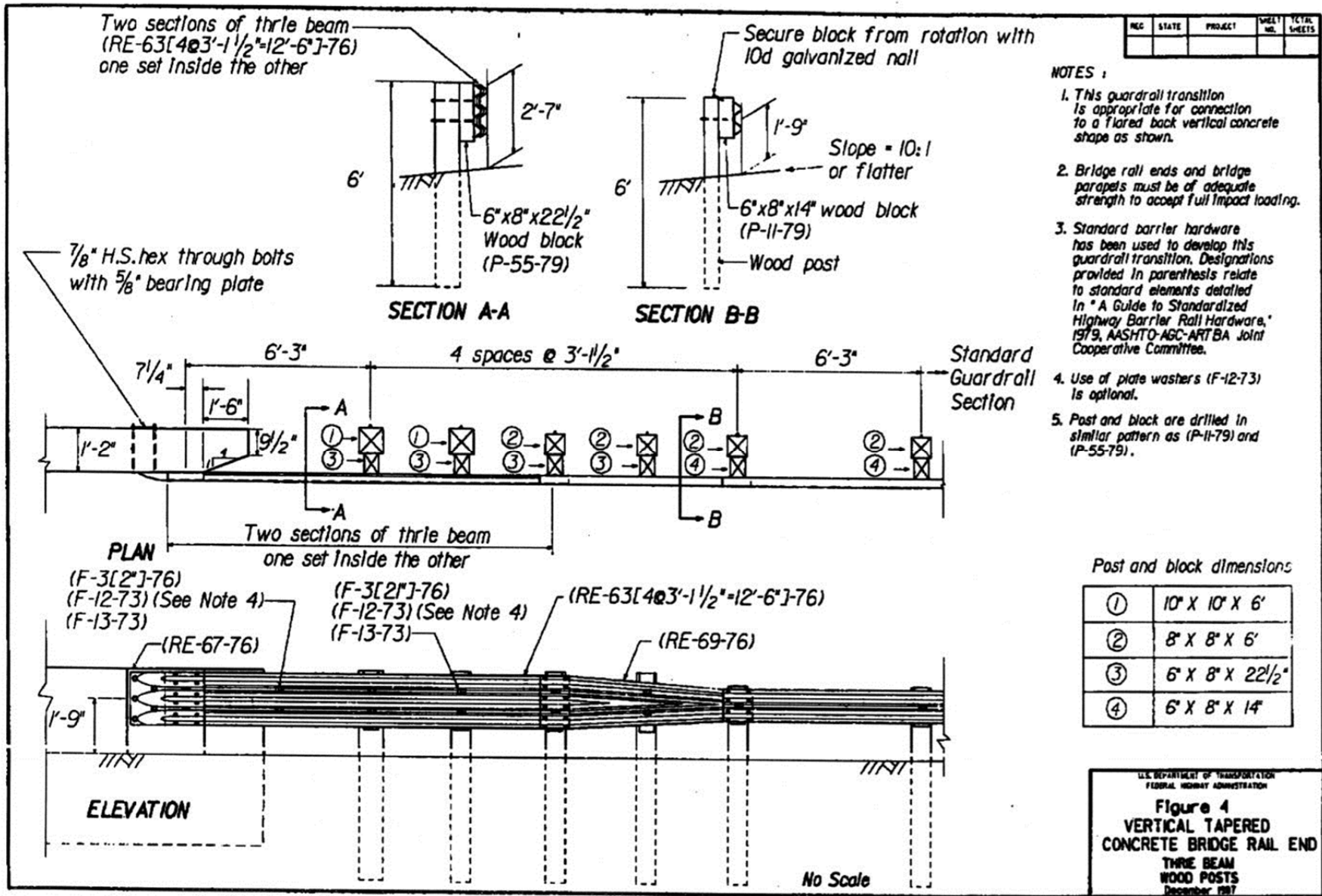


Figure 6. 1987 NDOR Missing Post Transition Configuration [16]

2.2.2 Tennessee Guardrail to Bridge Rail Transition

Another study involving the investigation of approach guardrail transitions was published in 1994 by researchers at the Texas Transportation Institute (TTI) [17]. The goal of the study was to investigate the impact performance of a bridge rail transition that was used by the Tennessee Department of Transportation (DOT) using the MSL-2 criteria found in NCHRP Report No. 230. The steel-post transition system, as shown in Figure 7, consisted of one 10-gauge (3.4-mm) W-beam rail supported by six W6x15 (W152x22.3) steel posts spaced at 37¹/₂ in. (953 mm) and embedded 44 in. (1,118 mm) into the soil. This transition configuration was examined when attached to two different concrete bridge rails: (i) a vertical, tapered parapet and (ii) a safety shape parapet.

The performance of each transition-bridge rail attachment was analyzed with the BARRIER VII computer program. For this study, the researchers utilized an upper limit of 2 in. (51 mm) for lateral wheel contact with the lower bridge rail end. It was determined that maintaining a wheel overlap distance of 2 in. (51 mm) or less would reduce the propensity for severe vehicle decelerations because such contact would primarily involve the vehicle's tire, exclusive of the actual steel wheel assembly. This finding was based on average dimensions of typical passenger car tires and wheels.

Computer simulations of the baseline Tennessee DOT steel-post transition attached to either bridge rail type predicted wheel snag which violated this established limit. Consequently, design modifications which attempted to minimize the amount of wheel snag on the upstream end of the bridge rail were developed through BARRIER VII computer simulation. Certain characteristics of the transition were varied by the researchers including beam strength, post size, post strength (i.e., embedment depth), and post spacing.

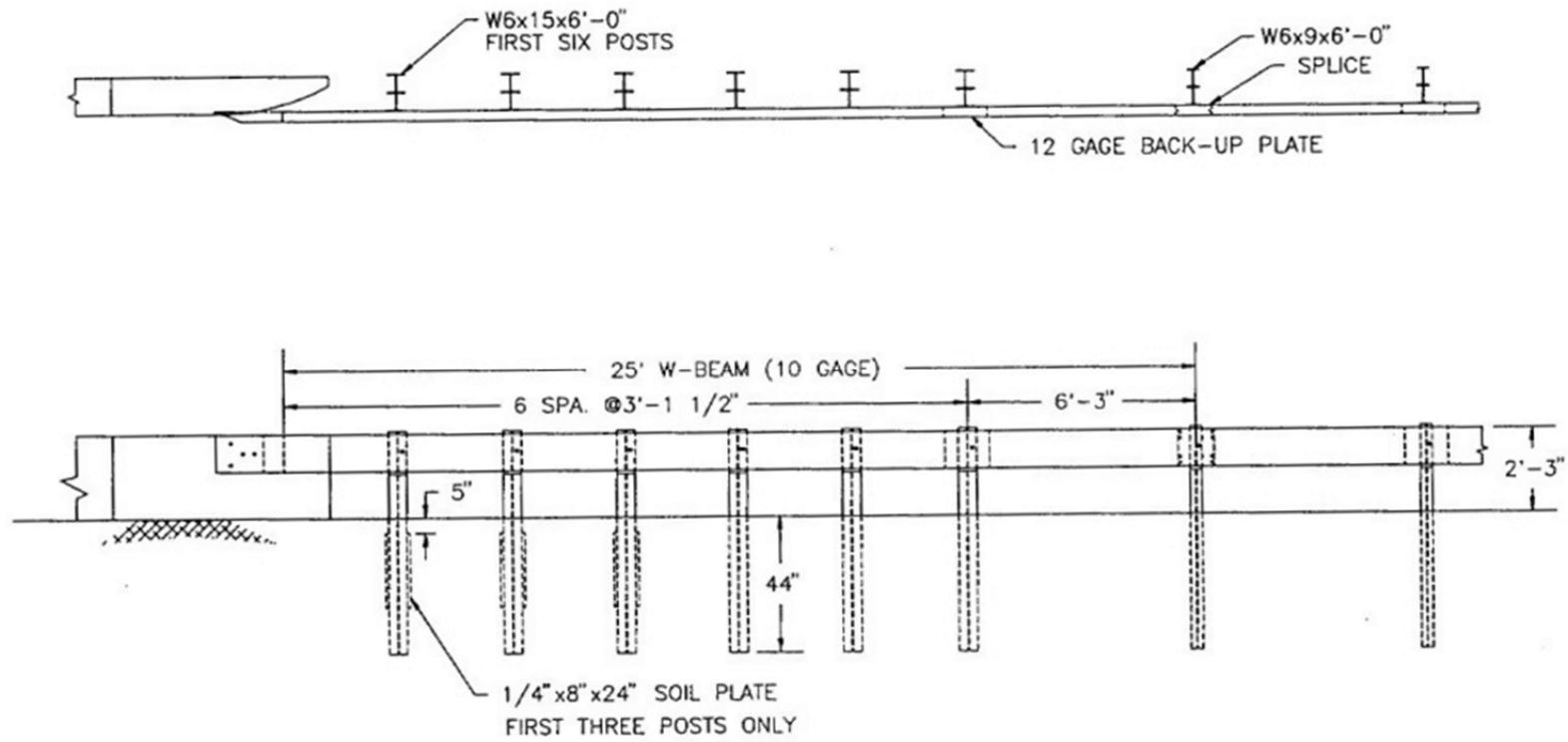


Figure 7. 1994 Tennessee DOT Steel-Post Transition (Original Configuration) [17]

Following the computer simulation effort for transition attachment to vertical parapets, three approach guardrail transition retrofits were selected for full-scale crash testing:

1. replace first three 6-ft (1.8-m) long, W6x15 (W152x22.3) steel posts adjacent to bridge rail with 8-ft (2.4-m) long, W8x21 (W203x31.3) steel posts;
2. install two additional W6x15 (W152x22.3) steel posts between first three existing posts; and
3. install C6x8.2 steel channel rubrail below the W-beam rail and utilize additional nested W-beam in transition region.

In addition, a 6-in. (152-mm) I.D. by 12-in. (305-mm) long schedule 40 steel pipe was vertically positioned between the rail and the flared portion of the concrete barrier for each retrofit.

Following the computer simulation effort for transition attachment to safety shape parapets, one approach guardrail transition retrofit was selected for full-scale testing. This design utilized special steel spacers to block the W-beam rail away from the face of the parapet. In addition, a nested W-beam rail, a C6x8.2 rubrail, and an 8-in. (203-mm) I.D. by 12-in. (305-mm) long schedule 40 vertical steel pipe were utilized for the modified design. These features are depicted in schematics that are provided in the original TTI research report [17].

Each of the three potential retrofit designs for vertical parapets and the one potential retrofit design for safety shape parapets successfully contained and redirected a test vehicle during MSL-2 impact events according to the safety criteria presented in NCHRP Report No. 230. The researchers concluded that each successfully crash tested system performed similarly during high-speed impacts with sedans. Thus, the choice of which alternative design to use in the field became a consideration of economics and site specific requirements. Further, each design was also applicable for new construction.

2.2.3 Nebraska Prototype Thrie Beam Transition

In 1998, researchers at the Midwest Roadside Safety Facility (MwRSF) re-evaluated the Nebraska thrie beam approach guardrail transition that was previously crash tested at UNL in 1987 but instead using the NCHRP Report No. 350 criteria [15,18]. Several new variables associated with a pickup truck, such as a higher center of gravity and increased weight, as compared to the previous sedan, created concerns as to whether the system would perform satisfactorily under TL-3 impacts.

Following a BARRIER VII computer simulation analysis, the dimensions and flare rate of the upstream end of the bridge rail were slightly modified to minimize the propensity for wheel snag and better ensure that adequate safety was provided. Further, a 4-in. (102-mm) thick concrete mow-strip with 13-in. x 15³/₄-in. (330-mm x 400-m) leave outs filled with a 2-in. (51-mm) thick layer of 'weak' fill material was utilized for vegetation control purposes. In addition, comparably-sized steel posts were specified for a modified design. This design modification was considered based on the Nebraska Department of Road's desire to utilize steel posts instead of wood posts in guardrail installations. As a result, an alternate steel-post transition system was developed to replace the wood-post configuration with a missing post.

During test no. NEBT-1, a 4,418-lb (2,004-kg) pickup truck traveling at 64.1 mph (103.2 km/h) and 24.9 degrees impacted the transition between post nos. 1 and 2. The system was able to adequately contain and redirect the vehicle. However, the vehicle experienced excessive wheel snag in excess of 3 in. (76 mm) during the impact event, subsequently causing severe occupant compartment deformations. Therefore, the full-scale crash test was deemed unsuccessful according to NCHRP Report No. 350. Still, the researchers concluded that the addition of a rubrail would likely prevent wheel snag and reduce subsequent occupant compartment deformations to an acceptable level.

2.2.4 Modified Nebraska Thrie Beam Transition (Hidden Post)

In 2000, researchers at TTI again examined the Nebraska thrie beam transition according to NCHRP Report No. 350 TL-3 safety performance criteria [19]. However, an additional ‘hidden post’ was incorporated into the design. The ‘hidden post’ consisted of a TS 4-in. x 4-in. x $\frac{5}{16}$ -in. (102-mm x 102-mm x 7.9-mm) steel tube rail that attached to the upstream end of the concrete parapet and to the side of post 1, as shown in Figure 8. The steel tube supported a 6-in. x 8-in. x $15\frac{3}{4}$ -in. (150-mm x 200-mm x 400-mm) wood block which connected to the nested thrie beam at the location of the missing post. This configuration eliminated the use of an embedded post at this location. The steel tube attached to the parapet with a $\frac{1}{2}$ -in (13-mm) thick ASTM A36 steel plate. Two $\frac{5}{8}$ -in (16-mm) diameter A325 mechanical anchors and two $\frac{3}{4}$ -in. (19-mm) diameter ASTM 193 Grade B7 chemically-bonded threaded rods were utilized to mount the steel plate to the parapet.

During test no. 404211-7, a 4,409-lb (2,000-kg) pickup truck traveling at 61.9 mph (99.6 km/h) and 24.6 degrees impacted the transition 6 ft – 4 in. (1.93 m) upstream from the end of the parapet. Following the test, the transition system was found to adequately contain and redirect the vehicle, thus meeting the required TL-3 criteria for NCHRP Report No. 350.

2.3 Iowa Thrie Beam Approach Guardrail Transition (18 ft – 9 in. Long)

In 1998, researchers at MwRSF developed two approach thrie beam guardrail transitions for the Midwest States Pooled Fund Program and the Iowa DOT for use with concrete safety shape barriers [20]. Both transition designs were constructed with two nested 12-gauge (2.7-mm) thrie beam rails and a 12-gauge (2.7-mm) W-beam to thrie beam transition element. A 4-in. (102-mm) tall, triangular-shaped, concrete curb was constructed below the nested thrie beam rails on each system, as shown in Figure 9. The first transition design was supported by nine W6x9 (W152x13.4) steel posts, while the second transition design was supported by nine 6-in. x 8-in.

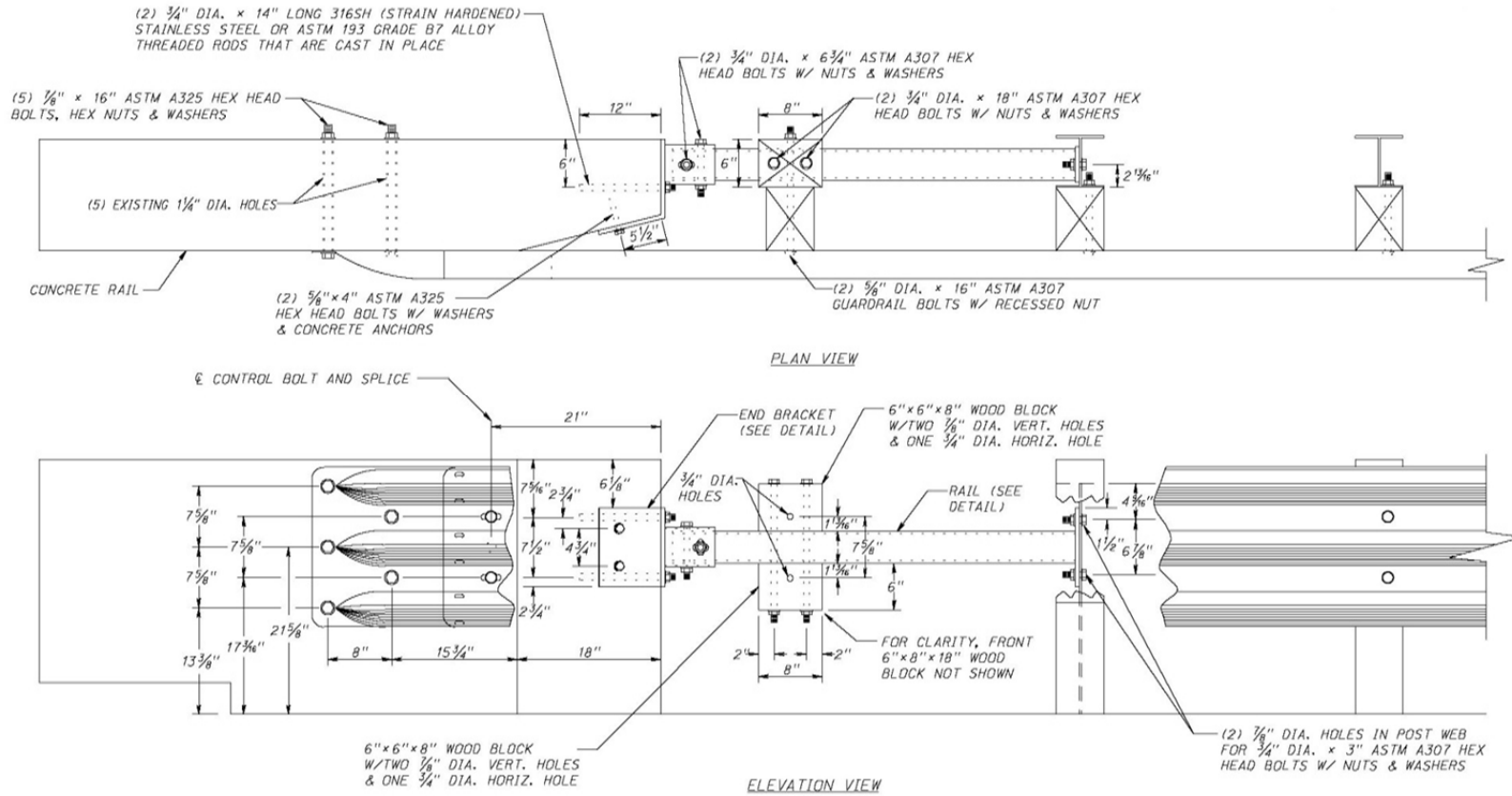


Figure 8. 2000 Nebraska Thrie Beam Transition – Hidden Post Detail [19]

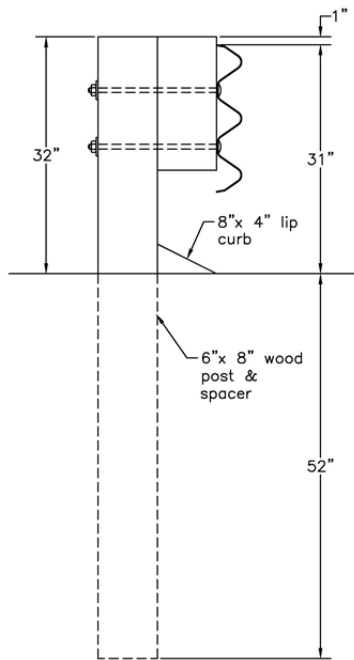


Figure 9. 1998 Iowa Transition Wood-Post with Curb [20]

(152-mm x 203-mm) wood posts. For both systems, a varied post spacing consisted of one at 11¹/₂ in. (292 mm), five at 18³/₄ in. (476 mm), and three at 37¹/₂ in. (953 mm). The steel- and wood-post versions of the transition are shown in Figures 10 and 11, respectively. Two full-scale crash tests were conducted on each design (4 total) according to TL-3 requirements specified in NCHRP Report No. 350.

The first test was conducted on the steel-post design which utilized a post embedment depth of 43 in. (1,092 mm) along the thrie beam. Test no. ITNJ-1 consisted of a 4,396-lb (1,994-kg) pickup truck impacting the system at 62.1 mph (100 km/h) and 25.0 degrees. During the test, the barrier deflected farther than predicted, and a sharp pocketing angle formed just upstream from the bridge rail end. Upon redirection, the vehicle was subjected to a high exit angle along with significant roll, pitch, and yaw angular motions, which eventually resulted in vehicle rollover. Subsequently, the performance of test no. ITNJ-1 was deemed unacceptable.

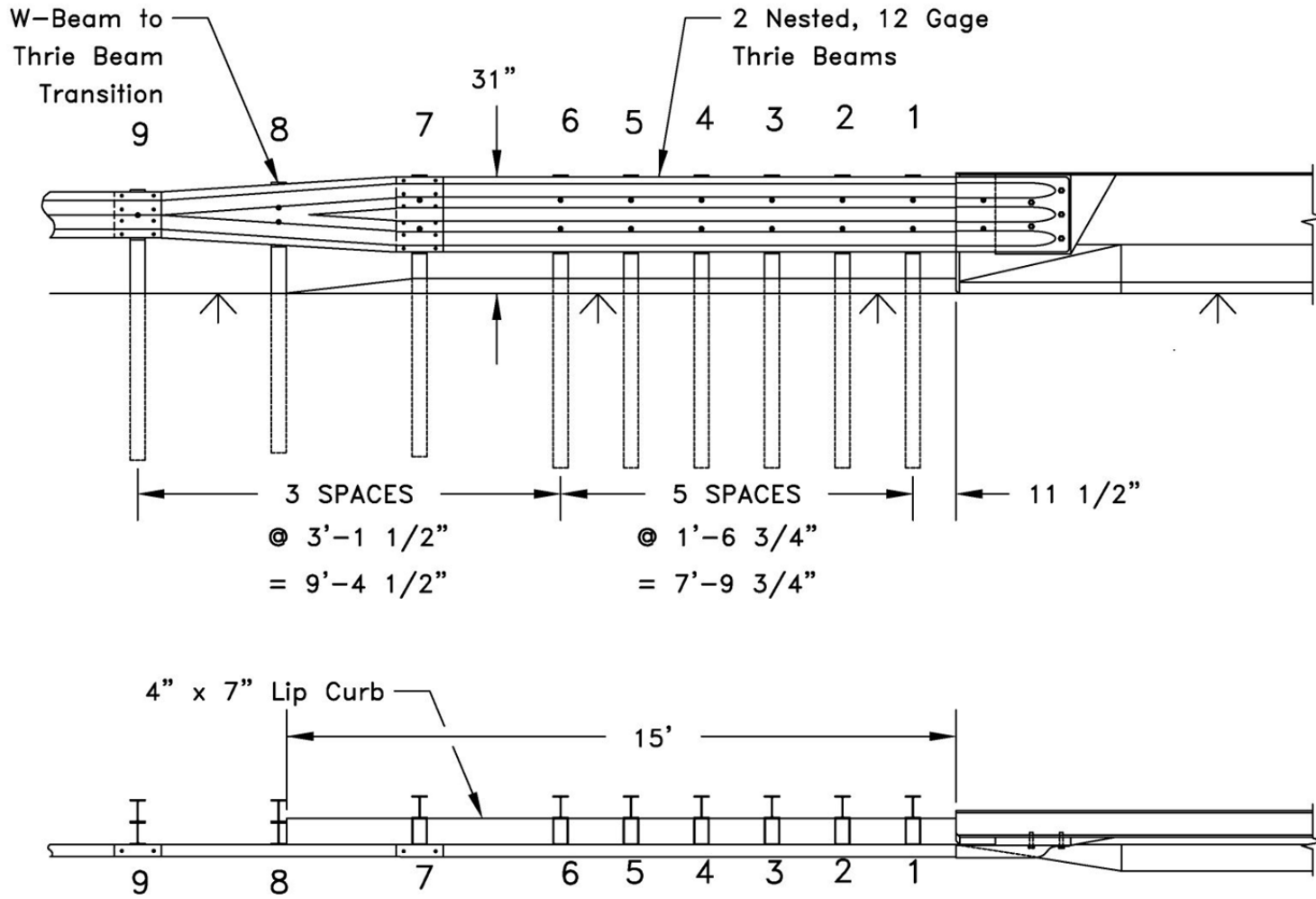


Figure 10. 1998 Iowa Steel-Post Transition Detail [20]

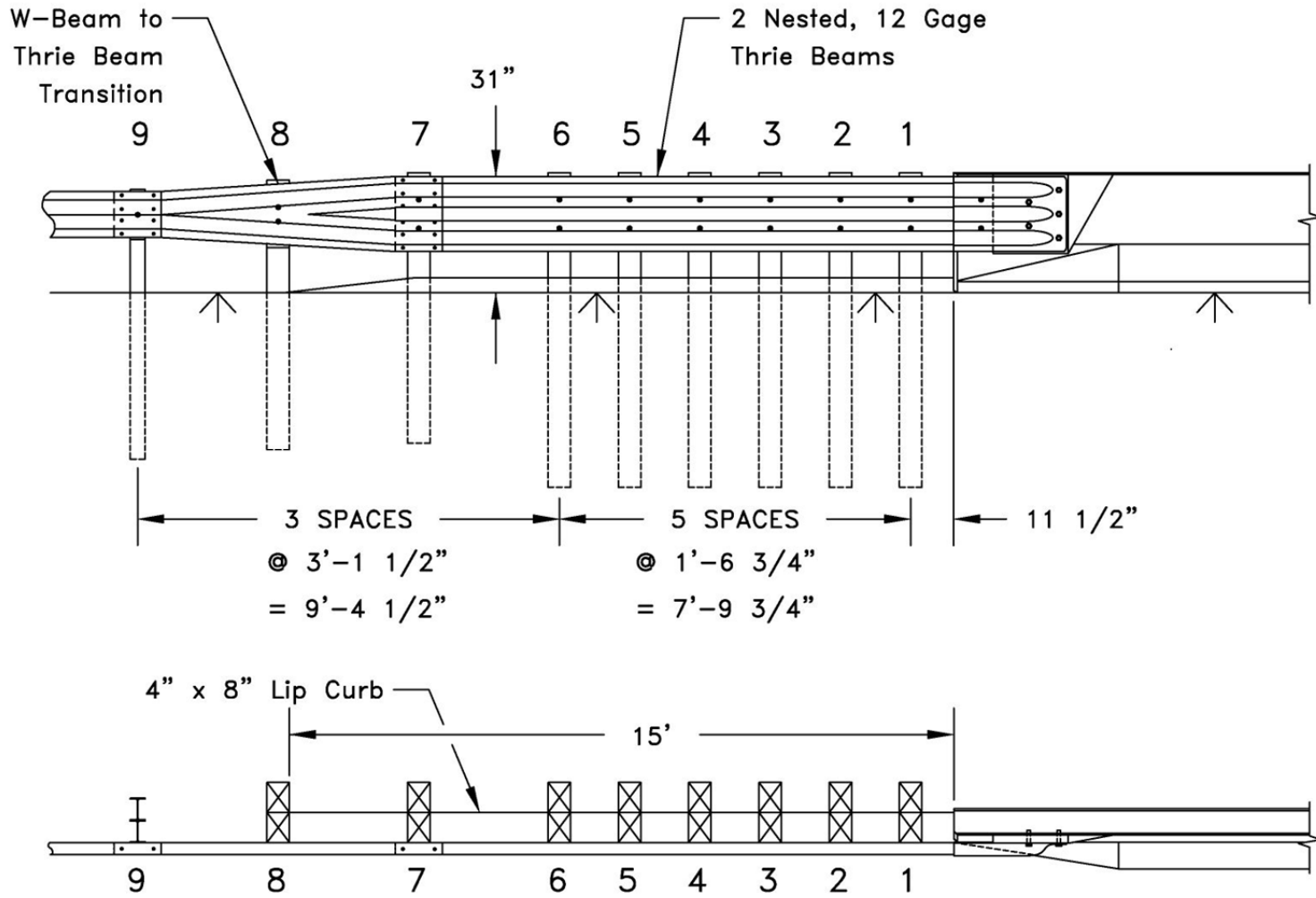


Figure 11. 1998 Iowa Wood-Post Transition Detail [20]

Several modifications were made in an attempt to stiffen the system before further testing was conducted. Most notably, the post embedment depth was increased to 49 in. (1,245 mm) for the first seven posts. The upstream corner on the traffic-side face of the concrete parapet was also chamfered to mitigate vehicle snag on the sharp, leading edge of the parapet. A retest, test no. ITNJ-2, was conducted on the steel-post design using a 4,359-lb (1,977-kg) pickup truck impacting the system at 63.1 mph (102 km/h) and 25.7 degrees. The vehicle was contained and smoothly redirected, and the system performance of test no. ITNJ-2 was deemed acceptable.

The third full-scale crash test in the transition study, test no. ITNJ-3, was conducted on a wood-post design which utilized 6-in. x 8-in. (152-mm x 203-mm) posts with an embedment depth of 43 in. (1,092 mm) throughout the thrie beam region. In test no. ITNJ-3, a 4,381-lb (1,987-kg) pickup truck impacted the system at 63.4 mph (102 km/h) and 26.9 degrees. Similar to test no. ITNJ-1, the system deflected farther than expected which created vehicle instabilities during redirection, eventually resulting in vehicle rollover. Subsequently, the system performance of test no. ITNJ-3 was deemed unacceptable according to NCHRP Report No. 350 safety criteria.

To provide additional stiffness and limit barrier deflections of the wood-post design, the post embedment depth was increased to 52 in. (1,321 mm) for the first seven posts. A retest on the revised wood-post system, test no. ITNJ-4, consisted of a 4,407-lb (1,999-kg) pickup truck impacting the system at 63.6 mph (102 km/h) and 24.6 degrees. The vehicle was contained and smoothly redirected. Subsequently, the redesigned wood-post transition system was deemed acceptable according to NCHRP Report No. 350 safety performance criteria.

As a result of the successful research noted above, the Wisconsin DOT generally adopted the 18-ft 9-in. (5.7-m) long Iowa transition system. The final Wisconsin system was composed of two nested 12-gauge (2.7-mm) thrie beam rails and a 10-gauge (3.4-mm) W-to-thrie transition

element. The rails were supported by nine 7-ft (2.1-m) long, 6-in. x 8-in. (152-mm x 203-mm) wood posts, each embedded in soil to a depth of 52 in. (1,321 mm). The varied post spacing consisted of six at $18\frac{3}{4}$ in. (476 mm) and three at $37\frac{1}{2}$ in. (953 mm). Details of the 18-ft 9-in. (5.7-m) long Wisconsin transition system were shown previously in Figure 2.

2.4 Kansas Thrie Beam Approach Guardrail Transition (31 ft – 3 in. Long)

In 1988, researchers at MwRSF conducted a BARRIER VII computer simulation study to evaluate suitable bridge rail transition designs for the State of Kansas [21]. The goal of the study was to determine feasible alternatives to those crashworthy FHWA designs previously accepted under *Technical Advisory T5040.26* [16]. Five different transition design options were examined according to the requirements specified for MSL-2 impacts in NCHRP Report No. 230. For this effort, full-scale crash test results and findings from previous studies were used to develop and validate the computer models. Each transition design was evaluated on its ability to prevent wheel snag on the end of the bridge rail and also on its implied risk to occupants of errant vehicles. Wheel snag was categorized as minor, 0 to 1 in. (0 to 25 mm), moderate, 1 to 3 in. (25 to 76 mm), or severe, 3 to 6 in. (76 to 152 mm).

The fifth transition design option consisted of a tapered concrete bridge rail end, two nested 12-gauge (2.7-mm) thrie beam rails, a single 12-gauge (2.7-mm) thrie beam rail, and a 12-gauge (2.7-mm) W-to-thrie transition element, as shown in Figure 12. The thrie beam region was supported by nine 6-ft (1.8-m) long, steel posts embedded 41 in. (1,041 mm) into the soil. A varied post spacing consisted of four at $18\frac{3}{4}$ in. (476 mm), four at $37\frac{1}{2}$ in. (953 mm), and two at 75 in. (1,905 mm).

During the simulation study, the fifth transition design was determined to be the only configuration that did not result in wheel snag on the bridge rail end during impact events. Further, simulation of the fifth transition configuration predicted lower occupant risk values than

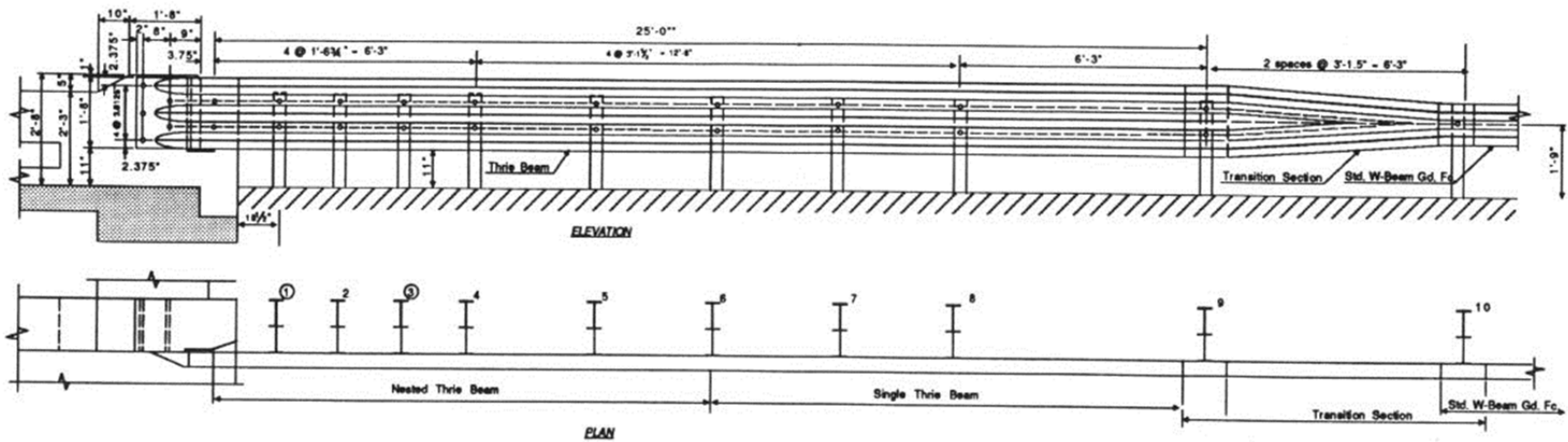


Figure 12. 1988 Kansas Thrie Beam Transition – Fifth Design Option [21]

observed for the accepted FHWA transition designs. The researchers determined that the fifth transition design would provide equal or better safety performance than predicted for the FHWA-approved transition designs. Thus, the MwRSF researchers recommended that the FHWA adopt the fifth transition design.

Therefore, the 31-ft 9-in. (9.5-m) long Wisconsin thrie beam transition system was configured using the recommendations from the MwRSF research study on Kansas DOT transition designs. The final Wisconsin system was composed of two nested 12-gauge (2.7-mm) thrie beam rails, a single 12-gauge (2.7-mm) thrie beam rail, and a 12-gauge (2.7-mm) W-to-thrie transition element. The rails were supported by nine 7-ft (2.1-m) long, 6-in. x 8-in. (152-mm x 203-mm) wood posts, each embedded in soil to a depth of 52 in. (1,321 mm). The varied post spacing consisted of four at $18\frac{3}{4}$ in. (476 mm), four at $37\frac{1}{2}$ in. (953 mm), and two at 75 in. (1,905 mm). Details of the 31-ft 3-in. (9.5-m) long Wisconsin transition system were shown previously in Figure 3.

2.5 Other Relevant Approach Guardrail Transition Studies

2.5.1 Missouri Thrie Beam Transition to Single-Slope CMB

In 1995, MwRSF researchers developed an approach guardrail transition for the Midwest States Pooled Fund Program and the State of Missouri for use with a single-slope concrete median barrier (CMB) [22]. The transition design was constructed with a 10-gauge (3.4-mm) thrie beam rail and a 12-gauge (2.7-mm) W-to-thrie transition element on both faces of the median barrier, as shown in Figure 13. The system was supported by nine 6-ft (1.8-m) long, W6x9 (W152x13.4) steel posts embedded 41 in. (1,041 mm) into the soil. A varied post spacing consisted of one at $11\frac{1}{2}$ in. (292 mm), five at $18\frac{3}{4}$ in. (476 mm), and three at $37\frac{1}{2}$ in. (953 mm). Two full-scale crash tests were conducted on the system according to TL-3 requirements specified in NCHRP Report No. 350.

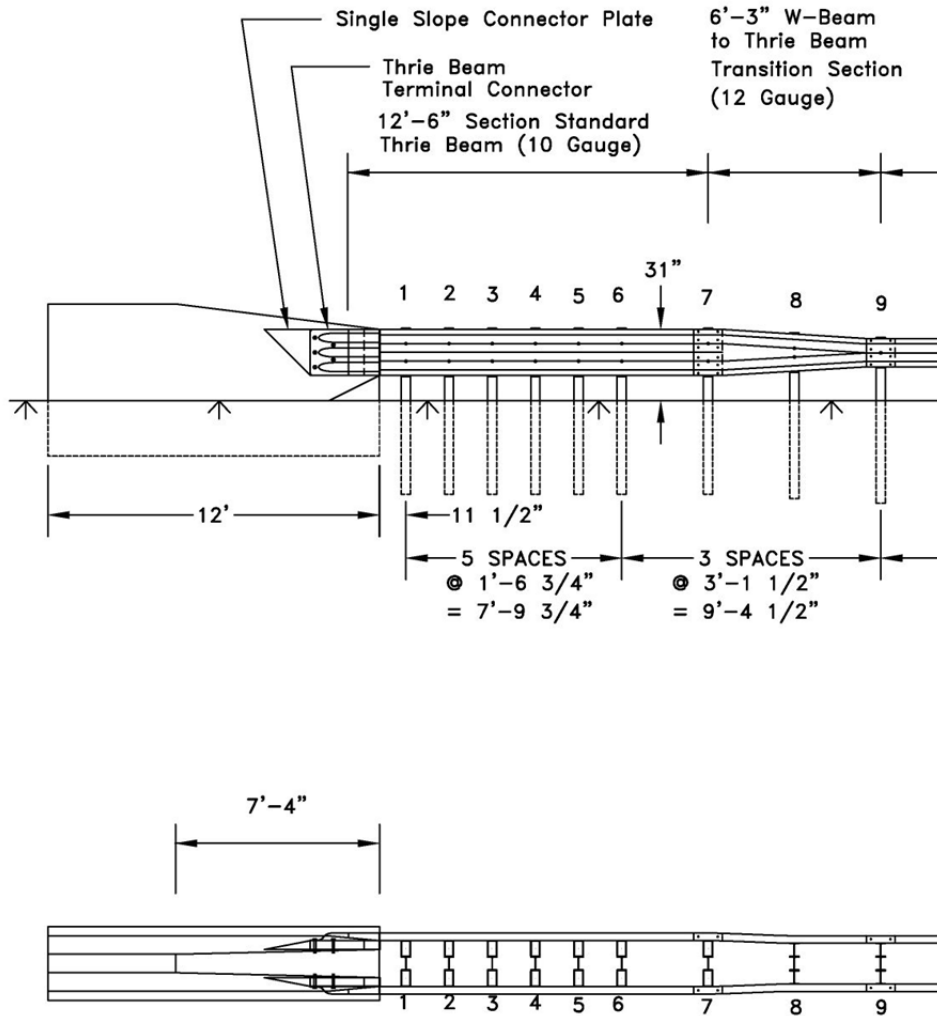


Figure 13. 1995 Missouri Thrie Beam Transition to Single-Slope CMB [22]

Several small modifications were made to the system in an attempt to improve the safety performance of the barrier before further testing was conducted. These modifications included shortening the thrie beam spacer blocks to $17\frac{7}{16}$ in. (443 mm), reducing the height of the thrie beam posts above ground by increasing the embedment depth to $43\frac{7}{16}$ in. (1,103 mm), and reducing the propensity for vehicle snag on the top of posts as well as on the upper end of the parapet.

During test no. MTSS-2, a 4,484-lb (2,034-kg) pickup truck impacted the transition approximately 10 ft (3 m) upstream from the end of the CMB at a speed of 57.5 mph (92.5 km/h)

and at an angle of 28.7 degrees. The vehicle was contained and safely redirected, and the tests results satisfied all safety performance criteria.

2.5.2 California Thrie Beam Approach Guardrail Transition

In 2000, researchers at the California Department of Transportation (CALTRANS) developed and tested three approach guardrail transition system designs [23]. The goal of the study was to develop a transition system capable of satisfying TL-3 requirements specified in NCHRP Report No. 350. A total of five full-scale crash tests were conducted during the study, four of which are presented below. The fifth test utilized the TL-4 criteria and therefore was not deemed relevant.

The initial transition design consisted of a 12-gauge (2.7-mm) thrie beam rail and a 12-gauge (2.7-mm) W-to-thrie transition element. The thrie beam rail was connected to a single-slope parapet and supported by three 6-ft (1.83-m) long, 10-in. x 10-in. (254-mm x 254-mm) wood posts each spaced 37¹/₂ in. (953 mm) apart. During test no. 516, a 4,328-lb (1,963-kg) pickup truck traveling at 62.4 mph (100.5 km/h) impacted the transition system between the second and third post upstream from the end of the bridge rail and at an angle of 25 degrees. Upon impact, severe pocketing in the rail and major snagging on the bridge rail were observed. Consequently, the vehicle experienced extreme deformation, and the test was deemed unsuccessful.

To alleviate the pocketing and snagging issues observed in the first test, four major changes were made to the system. First, the 12-gauge (2.7-mm) W-to-thrie transition element was replaced with a similar 10-gauge (3.4-mm) element. Second, the single thrie beam rail was replaced with nested 12-gauge (2.7-mm) thrie beam rails, and an additional 12-gauge (2.7-mm) thrie beam rail was attached to the back side of the parapet and to the first three posts. Third, the

first three posts were lengthened to 7 ft (2.13 m). Finally, the single-slope parapet was replaced with a vertical-faced parapet.

During test no. 517, a 4,409-lb (2,000-kg) pickup truck impacted the revised (second) design at the third post upstream from the end of the bridge rail at a speed of 62.4 mph (100.5 km/h) and at an angle of 26 degrees. The system contained and redirected the vehicle without severe pocketing or snag. However, upon exiting the system, the vehicle rolled over, thus causing the test to fail.

Although vehicle pocketing and snag were not an issue during the second test, the researchers still felt that the amount of deflection observed in the system was excessive. To reduce these deflections, three more changes were made. First, one of the nested 12-gauge (2.7-mm) thrie beam rails was replaced with a 10-gauge (3.4-mm) thrie beam rail. Next, the fourth, fifth, and sixth system posts were replaced with 10-in. x 10-in. (254-mm x 254-mm) wood posts (originally 6-in. x 8-in. (152-mm x 203-mm)). Finally, the first five posts were lengthened to 8 ft (2.44 m).

During test no. 519, a 4,352-lb (1,974-kg) pickup truck impacted the third design, as shown in Figure 14, at the third post upstream from the end of the bridge rail at a speed of 62.1 mph (100.0 km/h) and at an angle of 25.5 degrees. The system adequately contained and redirected the vehicle without excessive deformations or instabilities.

In addition, another test was conducted to evaluate the third design farther upstream from the end of the bridge rail. During test no. 518, a 4,400-lb (1,996-kg) pickup truck impacted the transition system at the sixth post upstream from the end of the bridge rail at a speed of 62.1 mph (99.9 km/h) and at an angle of 25 degrees. The vehicle was contained and smoothly redirected without any indication of pocketing within the rail. Test nos. 518 and 519 were deemed

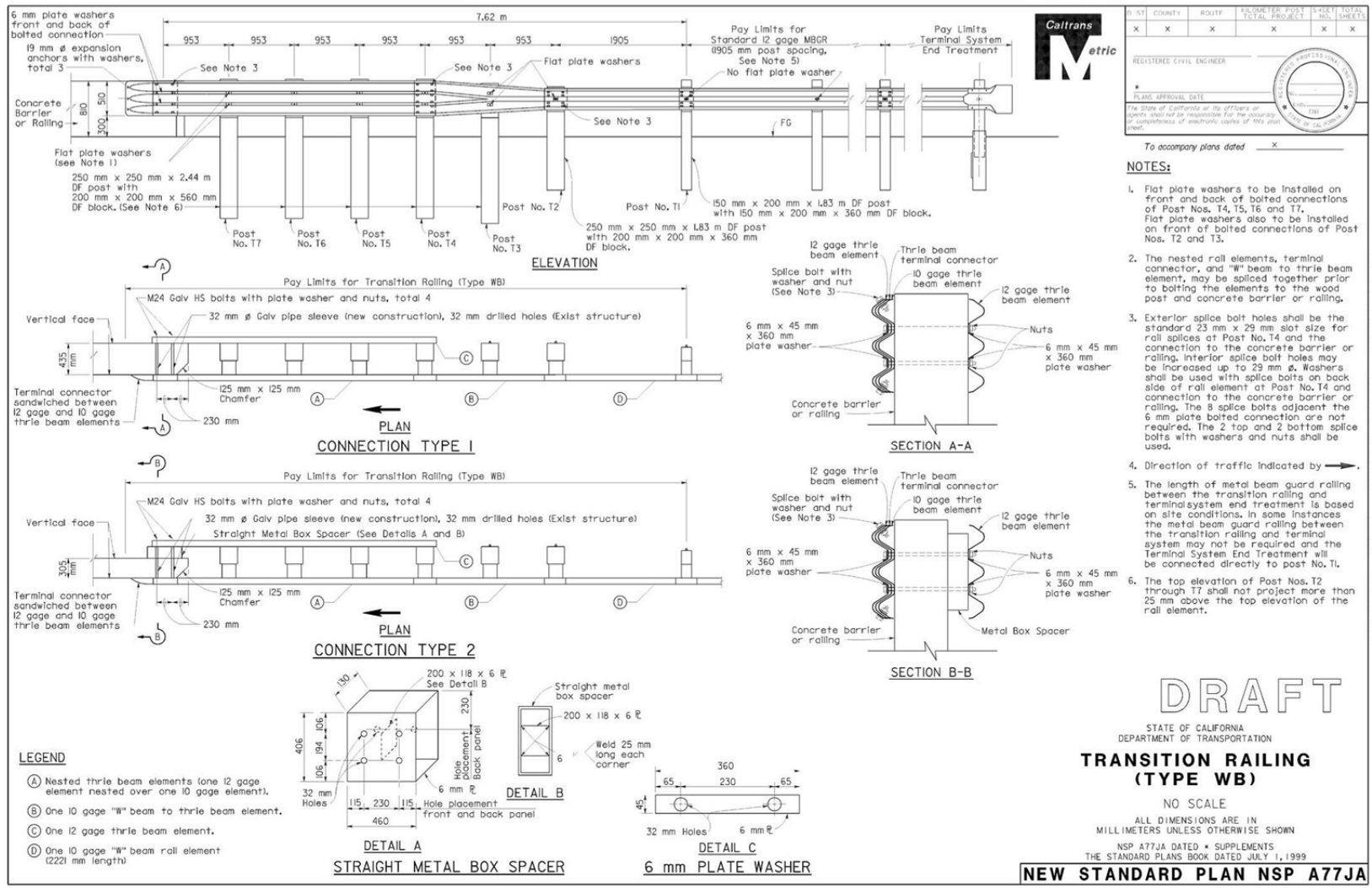


Figure 14. 2000 CALTRANS Approach Guardrail Transition, Design No. 3 [23]

successful according to NCHRP Report No. 350 safety criteria, and the third design, as shown in Figure 14, was recommended for use along high-speed roadways.

2.5.3 Midwest Guardrail System Transition Element

In 2007, researchers at MwRSF conducted a study to develop an improved stiffness transition to existing three beam approach guardrail transitions [24]. As part of this effort, various asymmetric W-beam to three beam transition sections were investigated in order to adapt the Midwest Guardrail System (MGS) for attachment to three beam transitions. A portion of the study was devoted to identifying a critical pocket angle, θ , as shown in Figure 15, which would result in undesirable vehicle responses (e.g., rollover). In order to identify θ , various successful and unsuccessful 2000P crash tests into both guardrail systems and approach guardrail transition systems were analyzed. The analyses determined a critical pocketing angle of 23 degrees. Every test that exhibited a pocketing angle greater than 23 degrees resulted in excessive deformations or vehicle rollover.

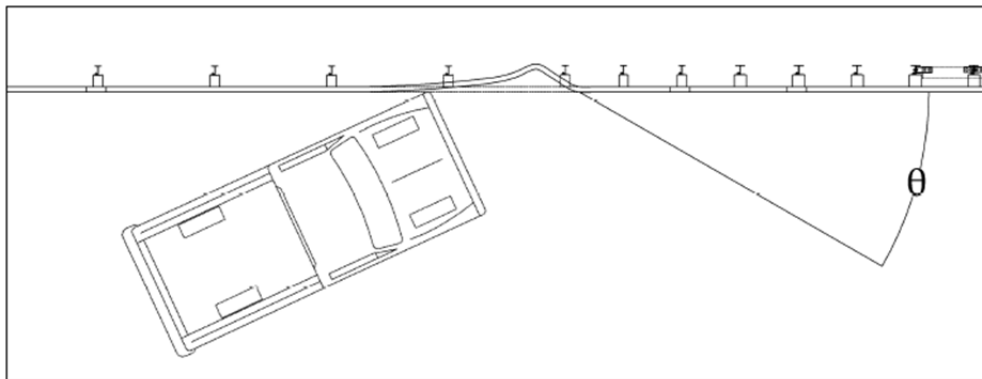


Figure 15. Schematic of Vehicle Pocketing

2.5.4 Midwest Guardrail System Approach Guardrail Transition

Later and in 2010, researchers at MwRSF increased the critical pocketing angle from 23 degrees for the NCHRP Report No. 350 pickup truck (2000P) to 30 degrees for the MASH pickup truck (2270P) [25]. During test no. MWTSP-2, a 5,158-lb (2,340-kg) pickup truck

impacted a three beam transition system at a speed of 61.2 mph (98.5 km/h) and at an angle of 26.3 degrees. The transition system adequately contained and redirected the vehicle in a stable manner, satisfying the safety criteria of MASH. Video analysis of the impact event illustrated a maximum pocketing angle of approximately 30.8 degrees within the system. Thus, a transition system was successful in containing and redirecting a 2270P vehicle when vehicle pocketing angles reached 30 degrees.

2.6 Adhesive Anchor Research and Testing

Prior research pertaining to adhesive anchors has primarily been focused on sustained loading [26-27]. Further, the uncertainty associated with bond-concrete performance led to the development of rather conservative design procedures [28-29]. Unfortunately, there have been limited tests conducted on adhesive anchors subjected to impact conditions.

As part of a Wisconsin DOT study conducted in 2011 at MwRSF, Dickey *et al.* examined the dynamic capacities of single and paired anchors embedded in concrete [30-31]. The goal of the research project was to develop design guidelines regarding the use of adhesive tie down anchors for temporary and permanent concrete barrier applications. The majority of the study consisted of dynamic testing on Grade 60 #5 (15.9 mm) and #6 (19.1 mm) deformed reinforcing bars. All bars were embedded 5¹/₄ in. (133 mm) in concrete. An adhesive with 2,145 psi (14.8 MPa) design strength was used to create a bond between the concrete and steel. A summary of the tensile test results from that study can be found in Table 1.

The lowest tensile load for an individual #5 (15.9 mm) rebar was 35.1 kips (156 kN), whereas the lowest tensile load for an individual #6 (19.1 mm) rebar was 41.0 kips (182.34 kN). Further, the lowest combined tensile load for an anchor pair composed of two #5 (15.9 mm) rebar spaced at 8 in. (203 mm) on center was 72.6 kips (323 kN), whereas the lowest combined tensile load for an anchor pair composed of two #6 (19.1 mm) rebar spaced at 8 in. (203 mm) on

center was 60.9 kips (271 kN). It should be noted that these values corresponded to the average loads observed at failure (e.g., steel fracture or concrete break out) of the specimen. In particular, these results demonstrated that the utilization of 8 in. (203 mm) spacing between anchors in a pair produced a capacity relatively similar to that of two individual steel anchors, especially for #5 (15.9 mm) rebar.

Table 1. MwRSF Adhesive Anchor Dynamic Test Results [30-31]

Test No.	Test Type	Bar Coating	Bar Size, US (Metric)	Anchor Configuration and Spacing	Bogie Speed, mph (km/h)	Maximum Anchor Load, kips (kN)	Result
WEAB-1	Tensile	None	#5 (#16)	Single	9.78 (15.74)	38.80 (172.60)	Anchor fracture
WEAB-2	Tensile	None	#5 (#16)	Single	10.40 (16.74)	39.83 (177.19)	Anchor fracture
WEAB-3	Tensile	Epoxy	#5 (#16)	Single	9.47 (15.24)	35.12 (156.23)	Anchor fracture
WEAB-4	Tensile	Epoxy	#5 (#16)	Single	8.86 (14.26)	36.83 (163.83)	Anchor fracture
WEAB-7	Tensile	Epoxy	#5 (#16)	2 @ 8 in. (2 @ 203 mm)	16.64 (26.78)	73.80 (328.30)	Anchor fracture/ core pullout
WEAB-8	Tensile	Epoxy	#5 (#16)	2 @ 8 in. (2 @ 203 mm)	14.05 (22.61)	72.64 (323.14)	Core pullout
WEAB-9	Tensile	Epoxy	#6 (#19)	Single	14.23 (22.91)	40.99 (182.34)	Core pullout
WEAB-10	Tensile	Epoxy	#6 (#19)	Single	15.73 (25.31)	42.69 (189.90)	Core pullout
WEAB-11	Tensile	Epoxy	#6 (#19)	2 @ 8 in. (2 @ 203 mm)	15.11 (24.32)	60.88 (270.80)	Core pullout
WEAB-12	Tensile	Epoxy	#6 (#19)	2 @ 8 in. (2 @ 203 mm)	15.08 (24.26)	75.66 (336.55)	Core pullout
WEAB -14	Tensile	None	1 1/8 in. (29 mm)	Single	15.19 (24.45)	43.73 (194.51)	Anchor fracture
WEAB-16	Tensile	None	#6 (#19)	Single	15.90 (25.58)	49.56 (220.43)	Core pullout

2.7 Post Testing Studies

2.7.1 Posts Installed on Level Terrain

2.7.1.1 Iowa Approach Guardrail Transition Posts

In 1998, MwRSF conducted a component study to examine the dynamic properties of various posts when installed on level terrain [32]. A total of 14 component tests were conducted on steel posts, while 15 tests were conducted on SYP wood posts. Each post was impacted 21.65 in. (550 mm) above ground line and perpendicular to the front face of the posts by a 2,086-lb (946-kg) bogie vehicle traveling at approximately 20 mph (32 km/h).

The first component test, IBT-1, was conducted on a W6x9 (W152x13.4) A36 steel post embedded in soil to a depth of 49 in. (1,245 mm). In that test, the steel post reached a peak force within the first few inches of deflection. Subsequently, the post yielded, and average force levels dropped off for the remainder of the test as the post experienced significant deflections. As a result, the embedment depth for subsequent steel and wood component tests was reduced to 43 in. (1,092 mm). Force-deflection curves for the posts embedded 43 in. (1,092 mm) in soil are shown in Figure 16. Selected results for W6x9 (W152x13.4) steel posts and 6-in. x 8-in. (152-mm x 203-mm) wood posts are shown in Table 2.

In addition, two component tests were conducted with stronger W6x16 (W152x23.8) steel posts for the following reasons: (i) the larger capacity of these members would prevent yielding during impact and (ii) post-soil interaction would remain relatively the same since the two shapes shared the same flange width. The embedment depth remained at 43 in. (1,092 mm) for both tests, the results of which are also shown in Table 2. During tests IBT-11 and IBT-12, the W6x16 (W152x23.8) steel posts successfully rotated through the soil without yielding. Thus, the results provided the expected dynamic strength capacity of the soil for an embedment depth of 43 in. (1,092 mm).

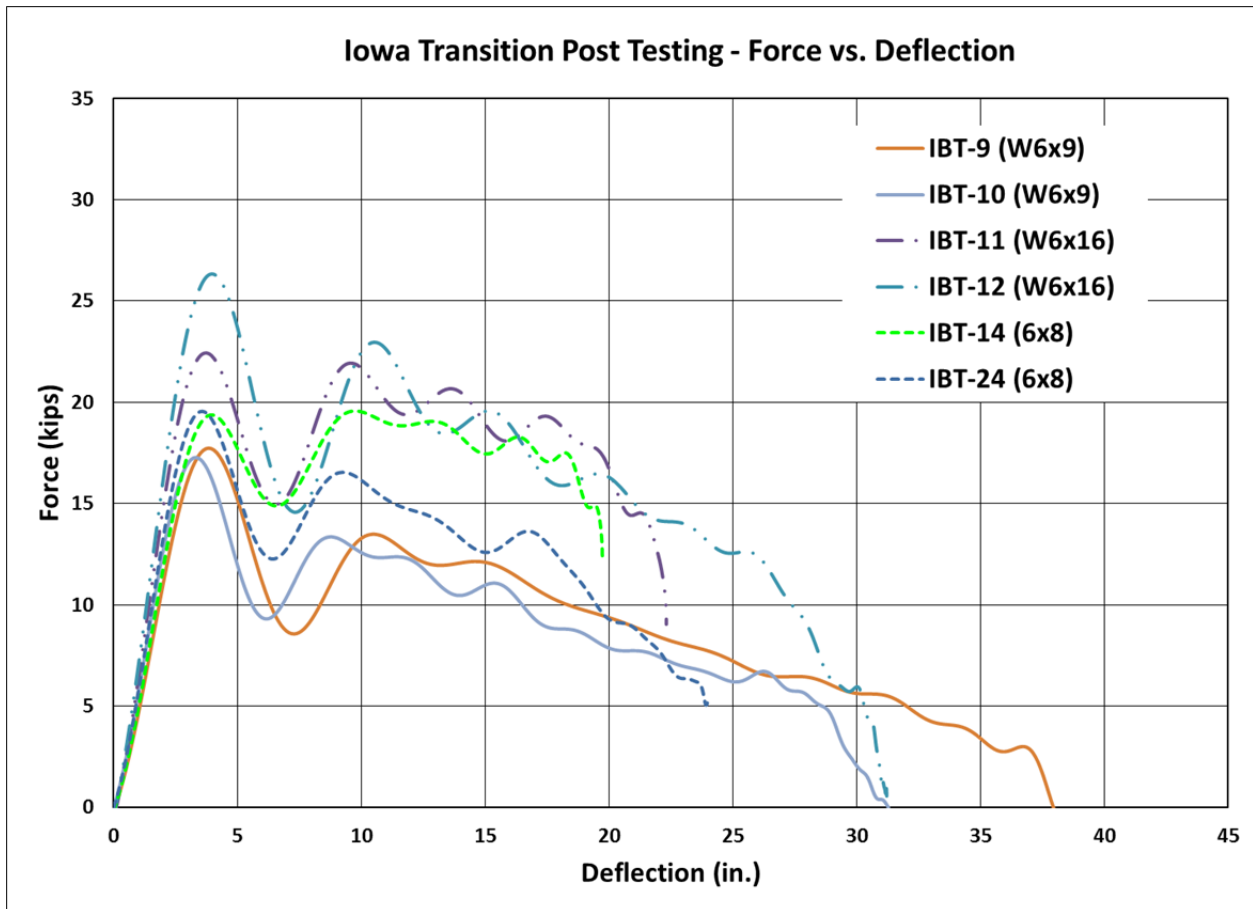


Figure 16. Iowa Transition Post Testing in Soil – Force vs. Deflection [32]

In addition to these bogie tests and the subsequent full-scale tests conducted in the 1998 MwRSF Iowa transition study [20], three unpublished dynamic component tests were also conducted to investigate the effects of tight post spacing in regards to post-soil interaction and strength. Each test was conducted with two W6x9 (W152x13.4) A36 steel posts placed side-by-side and spaced at $18\frac{3}{4}$ in. (476 mm) on center. This distance represented the closest spacing between consecutive posts along the transition. The dual post configuration utilized an embedment depth of 43 in. (1,092 mm) with the posts oriented such that each individual post was simultaneously impacted perpendicular to its strong axis of bending by a bogie vehicle traveling at 20 mph (32 km/h). The first two tests involved the use of soil plates, and therefore were invalid for this discussion. However, the third test, post test no. ITNJ-3, did not involve the use

Table 2. Dynamic Test Results, IBT Bogie Testing Series in Soil [32]

Test No.	Impact Velocity (mph)	Peak Force		Average Force			Absorbed Energy			Failure Type
		Deflection (in.)	Force (kips)	@ 5 in. (kips)	@ 10 in. (kips)	@ 15 in. (kips)	@ 5 in. (kip-in.)	@ 10 in. (kip-in.)	@ 15 in. (kip-in.)	
W6x9 Steel Post at 49 in. Embedment										
IBT-1	22.3	4.0	20.4	13.4	13.0	12.3	69.0	131.4	184.8	Post Yielding
W6x9 Steel Posts at 43 in. Embedment										
IBT-9	21.6	3.8	17.7	11.6	11.2	11.7	59.3	113.6	176.4	Post Yielding
IBT-10	18.5	3.3	17.3	11.6	11.6	11.6	59.7	116.9	174.5	Small Deflection/ Post Yielding
Series Average				11.6	11.4	11.6	59.5	115.3	175.5	
Dual W6x9 Steel Posts at 43 in. Embedment										
ITNJ-3	20.0	3.3	35.8	24.1	22.4	21.9	122.7	226.3	330.1	Post Rotation
W6x16 Steel Posts at 43 in. Embedment										
IBT-11	21.9	3.7	22.4	14.9	16.6	17.8	76.5	166.9	268.1	Post Rotation
IBT-12	24.3	3.9	26.3	17.2	17.6	18.5	87.5	180.1	280.8	Post Rotation
Series Average				16.0	17.1	18.1	82.0	173.5	274.5	
6 in. x 8 in. Wood Posts at 43 in. Embedment										
IBT-14	20.0	3.9	19.4	12.6	14.8	16.1	65.5	150.0	243.3	Post Rotation
IBT-24	19.0	3.6	19.6	13.1	13.8	14.0	67.5	138.9	210.6	Post Rotation
Series Average				12.8	14.3	15.0	66.5	144.5	227.0	

of soil plates. In that test, the two closely-spaced steel posts demonstrated the ability to collectively endure a peak force of 35.8 kips (159.2 kN) and an average force of 24.1 kips (107.2 kN), 22.4 kips (99.6 kN), and 21.9 kips (97.4 kN) over the first 5 in. (127 mm), 10 in. (254 mm), and 15 in. (381 mm) of deflection. Further, the two closely-spaced steel posts absorbed 226.3 kip-in. (25.6 kJ) of energy over the first 10 in. (254 mm) of deflection. These values were

approximately twice that of a single W6x9 (W152x13.4) A36 steel post embedded 43 in. (1,092 mm) in soil, as shown in Figures 17 and 18.

The key observation gathered from this additional component test was that neither of the closely-spaced posts yielded under those force levels, whereas the individual W6x9 posts had yielded. As such, this test illustrated that a relatively small spacing between posts had a positive effect in allowing the posts and surrounding soil to move together and absorb energy while withstanding an impact load that would not result in yielding of the dual steel posts.

2.7.1.2 Evaluation of Wood Post Quality on Guardrail Performance

In 2004, researchers at MwRSF conducted a study to determine the dynamic properties of various wood species when used as guardrail posts and under impact loading conditions [33]. The goal of the study was to determine an acceptable alternative to the then currently acceptable Southern Yellow Pine (SYP) guardrail post. A total of 60 dynamic component tests were conducted on 6-in. x 8-in. (152-mm x 203-mm) Red and White Pine wood posts which were confined in a rigid steel sleeve and embedded in concrete. Each post was impacted 21.65 in. (550 mm) above ground line and perpendicular to the front face of the posts by a bogie vehicle traveling at approximately 20 mph (32 km/h). Results from that testing series were compared against a previous MwRSF testing series involving 57 dynamic tests conducted on 6-in. x 8-in. (152-mm x 203-mm) wood posts [34]. It was determined that the SYP wood species had the highest average Modulus of Rupture, followed by the Red Pine species, and then the White Pine species, or 4.07 ksi (28.1 MPa), 3.30 ksi (22.7 MPa), and 2.34 ksi (16.1 MPa), respectively.

2.7.1.3 MGS Wood-Post Approach Guardrail Transition

In 2011, researchers at MwRSF conducted a study to determine a wood-post MGS approach guardrail transition system that was equivalent to the steel-post MGS stiffness transition transition [35]. A total of 20 dynamic component tests were conducted on W6x15 (152x22.3)



Figure 17. IBT Testing Series, W6x9 Posts with 43 in. E.D. – Force vs. Deflection [20,32]

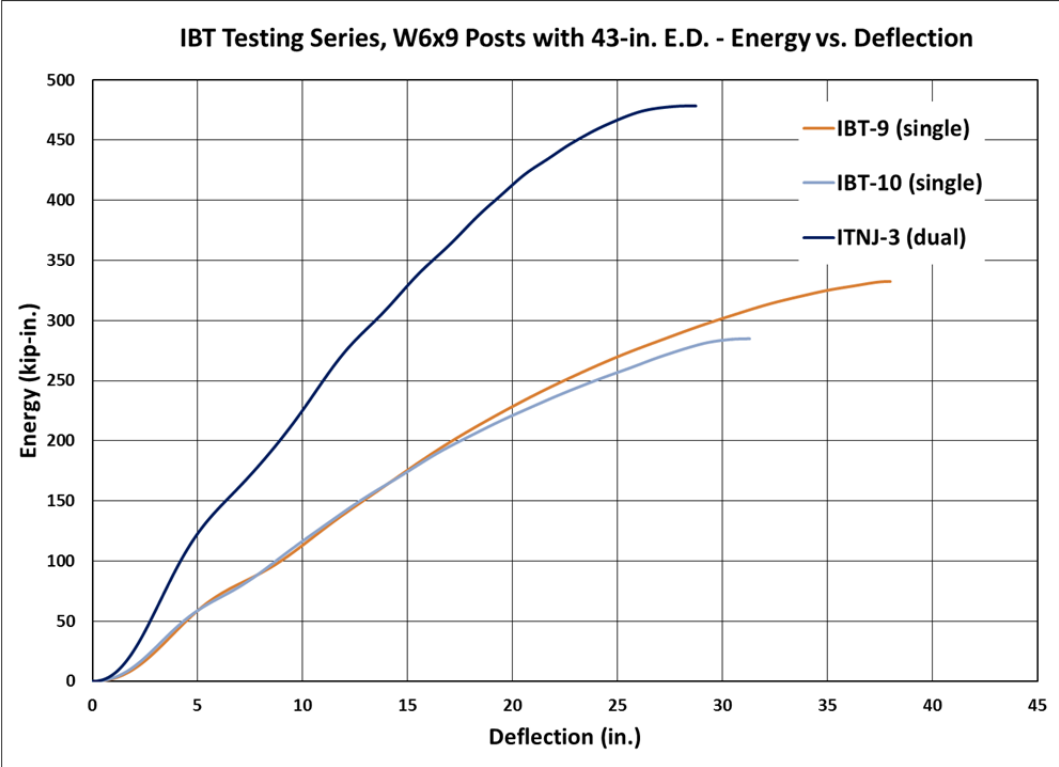


Figure 18. IBT Testing Series, W6x9 Posts with 43 in. E.D. – Energy vs. Deflection [20,32]

steel posts and various wood post sizes in soil. Each post was impacted 24⁷/₈ in. (632 mm) above ground line and perpendicular to the front face of the posts by a bogie vehicle traveling at approximately 20 mph (32 km/h). In particular, test nos. MGSATB-18 through MGSATB-20 of that series were conducted on 6-in. x 10-in. x 7-ft (152-mm x 254-mm x 2.1-m) long SYP wood posts embedded 52 in. (1,321 mm) into soil. Two out of those three wood posts fractured 12 in. (305 mm) below ground line during impact loading (test nos. MGSATB-19 and MGSATB-20), however, the wood post that did not fracture (test no. MGSATB-18) demonstrated a peak force of 21.8 kips (96.8 kN) and an average resistive force of 18.4 kips (81.9 kN) over the first 15 in. (381 mm) of deflection. The results from those three component tests are provided in Table 3.

2.7.2 Posts Installed on Sloped Terrain

2.7.2.1 Metric-Height W-Beam Guardrail on Slopes

In 2000, researchers at MwRSF conducted a study to develop a W-beam guardrail system for use on a 2H:1V fill slope [6]. The key variables investigated during the study were post size, embedment depth, and spacing. As such, a portion of the study consisted of dynamic component tests on various steel members. In particular, three tests were conducted on 7-ft (2.1 m) long, W6x9 (W152x13.4) steel posts embedded 55.2 in. (1,403 mm) at the slope break point of a 2H:1V fill slope. Each post was impacted 21.65 in. (550 mm) above ground line and perpendicular to the front face of the posts by a 2,143-lb (972-kg) bogie vehicle traveling at approximately 15 mph (24 km/h). The results from these three tests demonstrated an average force of approximately 5.0 kips (22.2 kN) over 15 in. (381 mm) of deflection.

Table 3. Select Dynamic Test Results, MGS Wood-Post Testing Series [35]

Test No.	Post Type	Embedment Depth (in.)	Impact Velocity (mph)	Peak Force (kips)	Average Force			Total Energy (kip-in.)	Maximum Deflection (in.)	Failure Type
					@ 5 in. (kips)	@ 10 in. (kips)	@ 15 in. (kips)			
MGSATB-18	SYP 6x10	52	21.0	21.8	14.7	17.7	18.4	352.2	18.0	Rotation in Soil
MGSATB-19	SYP 6x10	52	19.7	17.0	11.8	11.5*	NA	124.3	13.1**	Post Fracture
MGSATB-20	SYP 6x10	52	24.5	13.9	5.5*	NA	NA	28.5	4.2**	Post Fracture

* Fracture had already been initiated.

** Displacement associated with the end of fracture.

2.7.2.2 MGS Guardrail on Slopes – Phase I

In 2007, researchers at MwRSF conducted another dynamic component study to further evaluate the behavior of W6x9 (W152x13.4) steel posts when placed at the slope break point of a 2H:1V fill slope [36-37]. The goal of the study was to determine the necessary length of post required to provide an average resistance representative of the resistance provided by a standard steel post used in the Midwest Guardrail System (MGS) when installed on level terrain. A total of 17 dynamic component tests were conducted with varying post lengths and embedment depths. Each post was placed at the break point of a 2H:1V fill slope and impacted 24⁷/₈ in. (632 mm) above ground line by a 1,605-lb (728-kg) bogie vehicle traveling at speeds ranging from 15 to 20 mph (24 to 32 km/h). It was observed from that test series that a 9-ft (2,743-mm) long, W6x9 (W152x13.4) steel post embedded 76 in. (1,930 mm) at the slope break point of a 2H:1V fill slope provided the comparable force vs. deflection characteristics to a standard 6-ft (1.8-m) long steel post installed on level terrain.

2.7.2.3 MGS Guardrail on Slopes – Phase II

In 2010, researchers at MwRSF conducted yet another study on guardrail posts placed at the slope break point of a 2H:1V fill slope [7]. However, the goal of this study was to determine a suitable wood post alternative to the 9-ft (2,743-mm) long, W6x9 (W152x13.4) steel posts

originally recommended for MGS installations on 2H:1V sloped terrain. A total of five dynamic component tests were conducted on 6-in. x 8-in. (152-mm x 203-mm) wood posts with varying lengths and embedment depths. Two additional component tests were conducted on 9-ft (2,743-mm) long, W6x9 (W152x13.4) steel posts embedded 76 in. (1,930 mm) for comparative purposes. Each post was placed at the slope break point of a 2H:1V fill slope and impacted 24⁷/₈ in. (632 mm) above ground line by a 1,860-lb (844-kg) bogie vehicle traveling 15 mph (24 km/h). The results from all 7 component tests are shown in Table 4. In particular, the results from the two steel post component tests, test nos. MGS221PT-27 and MGS221PT-28, demonstrated that an average force of 8.65 kips (38.5 kN) could be expected over the first 15 in. (381 mm) of deflection.

2.7.2.4 MGS Guardrail for Wire-Faced MSE Walls

In 2012, researchers at MwRSF published results for a series of dynamic component tests on standard wood and steel posts placed in various soils and on different terrains [8]. The goal of the study was to develop an economical, longitudinal barrier system for placement on a wire-faced, Mechanically-Stabilized Earth (MSE) wall. A total of 26 tests were conducted through four different testing rounds during the study.

In the first round of testing, 11 tests were conducted on 6-in. x 8-in. (152-mm x 203-mm) wood posts embedded 40 in. (1,016 mm) on level terrain. A rigid frame bogie traveling at various speeds impacted the posts 24⁷/₈ in. (632 mm) above ground line. The researchers concluded from those tests that an increase in impact speed resulted in an increase in force and energy absorbed by the post (e.g., inertial effects).

The second round of testing consisted of two tests on 6-in. x 8-in. (152-mm x 203-mm) wood posts and two tests on W6x16 (W152x23.8) steel posts, all embedded 40 in. (1,016 mm) on level terrain and impacted 24⁷/₈ in. (632 mm) above ground line. Results from these tests are

Table 4. Dynamic Component Results for MGS Posts on 2H:1V Terrain [7]

Test No.	Post Type	Post Length (ft)	Embedment Depth (in.)	Impact Velocity (mph)	Peak Force		Average Force		Total Energy (kip-in.)	Maximum Deflection (in.)	Failure Type
					Force (kips)	Deflection (in.)	@ 15 in. (kips)	@ 20 in. (kips)			
MGS221PT-22	6x8 wood	8.0	64	15.1	12.7	4.7	NA	NA	48.8	6.2	Post Fracture
MGS221PT-23	6x8 wood	8.0	64	16.0	11.2	8.3	NA	NA	75.0	9.8	Post Fracture
MGS221PT-24	6x8 wood	8.0	64	18.5	17.4	7.3	NA	NA	103.4	9.0	Post Fracture
MGS221PT-25	6x8 wood	7.5	58	15.1	12.1	4.9	9.9	NA	161.7	18.4	Rotation in Soil
MGS221PT-26	6x8 wood	7.5	58	16.0	15.6	4.7	11.3	NA	180.9	15.1	Rotation in Soil
MGS221PT-27	W6x9 steel	9.0	76	13.7	13.2	2.4	8.4	NA	131.8	16.2	Rotation in Soil & Post Yielding
MGS221PT-28	W6x9 steel	9.0	76	16.4	13.0	2.3	8.9	8.0	189.8	30.4	Rotation in Soil & Post Yielding

shown in Table 5 as test nos. GWB-12 through GWB-15. The researchers concluded from those tests that the post-soil resistances for standard wood and steel posts were nearly identical.

The third round of testing consisted of five tests on wood and steel posts placed at the slope break point of a 3H:1V fill slope with various embedment depths. A rigid frame bogie vehicle traveling at 20 mph (32 km/h) impacted the posts 24⁷/₈ in. (632 mm) above ground line. Results from these tests are shown in Table 5 as test nos. GWR4-1 through GWR5-4. The steel posts from those tests provided similar resistances regardless of the embedment depth due to plastic bending occurring in the posts. On the contrary, the single test on a 6-in. x 8-in. (152-mm x 203-mm) wood post embedded 52 in. (1,321 mm) resulted in post fracture.

Table 5. Dynamic Testing of Wood and Steel Posts for MGS on a MSE Wall [8]

Test No.	Post Type	Terrain	Embedment Depth (in.)	Impact Velocity (mph)	Peak Force		Average Force		Total Energy (kip-in.)	Maximum Deflection (in.)	Failure Type
					Force (kips)	Deflection (in.)	@ 15 in. (kips)	@ 20 in. (kips)			
GWB-12	W6x16 steel	Level	40	19.0	12.8	9.9	11.0	10.3	236.1	33.8	Rotation in Soil
GWB-13	W6x16 steel	Level	40	19.2	12.8	6.6	11.0	10.4	247.7	31.3	Rotation in Soil
GWB-14	6x8 wood	Level	40	19.3	14.6	2.9	11.6	10.5	232.0	31.7	Rotation in Soil
GWB-15	6x8 wood	Level	40	19.6	13.5	4.0	11.3	10.3	225.6	30.0	Rotation in Soil
GWR4-1	6x8 wood	3H:1V	52	20.5	11.1	1.6	NA	NA	21.0	4.1	Post Fracture
GWR5-1	W6x9 steel	3H:1V	52	20.0	15.1	3.7	10.9	9.8	237.4	35.4	Rotation in Soil & Post Yielding
GWR5-2	W6x9 steel	3H:1V	52	20.8	15.6	2.8	11.1	10.2	251.2	33.2	Rotation in Soil & Post Yielding
GWR5-3	W6x8.5 steel	3H:1V	46	19.9	14.7	2.7	9.9	9.0	221.5	34.8	Rotation in Soil & Post Yielding
GWR5-4	W6x8.5 steel	3H:1V	40	20.6	14.0	2.9	9.9	9.3	237.1	34.5	Rotation in Soil & Post Yielding

Later in 2011, MwRSF continued the investigation of dynamic post-soil behavior for standard wood posts located on 3H:1V sloped terrain [9]. Four dynamic component tests were conducted on 6-in. x 8-in. (152-mm x 203-mm) wood posts placed at the slope break point of a 3H:1V fill slope. Each post was impacted 24⁷/₈ in. (632 mm) above ground line by a rigid frame bogie vehicle traveling 20 mph (32 km/h). The results from those tests are shown in Table 6. The researchers concluded that 6-ft (1.8-m) and 6.5-ft (2.0-m) long, 6-in. x 8-in. (152-mm x 203-mm) wood posts embedded 40 in. (1,016 mm) on 3H:1V sloped terrain provide lower average resistance force and energy dissipation as compared to 6-ft (1.8-m) long W6x8.5 (W152x12.6) steel posts under similar conditions.

Table 6. Dynamic Testing of Wood Posts on 3H:1V Terrain [9]

Test No.	Post Type	Post Length (ft)	Embedment Depth (in.)	Impact Velocity (mph)	Peak Force		Average Force		Total Energy (kip-in.)	Maximum Deflection (in.)	Failure Type
					Force (kips)	Deflection (in.)	@ 15 in. (kips)	@ 20 in. (kips)			
GWPB-1	6x8 wood	6.0	40	22.7	12.6	1.9	6.4	6.0	158.7	40.4	Rotation in Soil
GWPB-2	6x8 wood	6.0	40	20.5	12.3	2.0	7.1	6.4	174.6	45.3	Rotation in Soil
GWPB-3	6x8 wood	6.5	46	21.5	10.8	3.3	NA	NA	53.6	7.2	Post Fracture
GWPB-4	6x8 wood	6.5	46	20.1	10.1	5.4	8.4	8.3	254.6	42.2	Rotation in Soil

2.7.3 Posts Installed in Asphalt/Concrete

Research on guardrail posts confined in asphalt and concrete mow strips was conducted in 2004 by researchers at TTI [38]. In that study, 7-in. (178-mm) diameter wood posts and W6x9 (W152x13.4) steel posts installed in confined foundations were examined through a total of 17 dynamic component tests, multiple computer simulations, and two full-scale crash tests. Each post was placed in a 44-in. (1,118-mm) deep hole composed of both soil and a confining layer of pavement. The layer of pavement was composed of either 5-in. (127-mm) thick low-strength concrete (2,031 psi) or 8-in. (203-mm) thick PG64-22 asphalt. These pavement surfaces were evaluated with posts placed within the mow strip material and either with or without leave outs. Varied fill materials were examined for use within the leave outs. The dimension of the leave outs for the concrete pavement were either 18 in. x 18 in. (457 mm x 457 mm) or 18 in. x 24 in. (457 mm x 607 mm) rectangles, while leave-out dimensions in the asphalt pavement were either 12-in. (305-mm) or 18-in. (457-mm) diameter circles. Four different leave out setups were analyzed: (i) 8-in. (203-mm) deep hand-tamped asphalt; (ii) 4-in. (102-mm) deep hand-tamped asphalt; (iii) 4-in. (102-mm) deep low strength (120 psi) two-sack grout; and (iv) a rubber mat.

Dynamic component testing was performed with an 1,850-lb (839-kg) bogie vehicle impacting at a target speed of 22 mph (35 km/h). Posts were impacted at a height of 21.65 in.

(550 mm) above ground line. Results from these tests demonstrated that both the 8-in. (203-mm) and 4-in. (102-mm) deep leave-outs filled with hand-tamped, asphalt provided excessive resistance for both the steel and wood posts and did not allow for the desired post rotation. Conversely, posts tested in the 4-in. (102-mm) deep leave-outs filled with low-strength, grout allowed substantial deflection through the back of the leave outs before fracture or yield. The single test conducted with a rubber-mat leave out also allowed substantial deflection, but the amount of damage incurred by the mat was undesirable. Therefore, low-strength grout was deemed the most capable leave out material for allowing post displacement and adequate energy dissipation. Although results for low-strength grout were positive, the post response did not fully match that obtained for posts exclusively embedded in soil.

Subsequently, two full-scale crash tests were conducted employing guardrail posts encased in the 5-in. (127-mm) thick concrete mow strip with 18-in. x 18-in. x 4-in. (457-mm x 457-mm x 102-mm) low-strength grout leave outs. The first test, test no. 441622-1, consisted of a W-beam guardrail mounted at a height of 27 in. (686 mm) on W6x9 (W152x13.4) steel posts spaced at 6 ft – 3 in. (1.91 m). A 4,504-lb (2,045-kg) pickup truck impacted the system at 62.0 mph (99.7 km/h) and at an angle of 25 degrees. The vehicle was successfully contained and redirected in a stable manner, thus meeting the criteria set forth by NCHRP Report 350. The second test, test no. 441622-2, consisted of a W-beam guardrail mounted at a height of 27 in. (686 mm) on 7-in. (178-mm) diameter wood posts spaced at 6 ft – 3 in. (1.91 m). A 4,498-lb (2,042-kg) pickup truck impacted the system at 63.2 mph (101.7 km/h) and at an angle of 25 degrees. Again, the vehicle was successfully contained and redirected in a stable manner, thus meeting the criteria of NCHRP Report 350.

The researchers concluded that the successfully tested mow strip and leave out system was representative of the most severe confinement conditions allowable. Thus, any increase in

post confinement beyond the 4-in. (102-mm) deep low-strength grout backfill material used in the leave out sections should undergo additional analysis when used in combination with either an 8-in. (203-mm) thick asphalt or a 5-in. (127-mm) thick concrete mow strip. This finding included barrier systems featuring guardrail posts directly encased in concrete or asphalt. The research findings from this study were later incorporated into an FHWA memorandum which detailed the accepted method for the application of a mow strip in guardrail installations [39].

Later in 2009, a follow up study was conducted at TTI to explore alternate backfill materials for guardrail systems encased in pavement mow strips [40]. Products examined in the study included two-part urethane foam, a molded rubber mat, a flat rubber mat, and a concrete pop-out wedge. Results from dynamic component testing demonstrated that the two-part urethane foam, the molded rubber mat, and the concrete pop-out wedge each provided comparable resistances and energy dissipation to that observed for the low-strength grout backfill. Thus, the researchers concluded each of the three materials were a suitable alternative for mow strip and leave-out applications.

2.7.4 Posts Installed in Rock Foundations

In 1998, MwRSF researchers initiated a research study to develop a strong-post, W-beam guardrail system for use along roadsides which contain a combination of sub-surface rock and soil [41]. BARRIER VII computer simulations were performed to determine a minimum absorbed-energy requirement for a post rotating in a selected backfill material that could be placed and compacted into drilled holes within a rock foundation. Later, dynamic bogie testing was conducted on guardrail posts to determine the appropriate backfill material and proper embedment depth that would fulfill the minimum absorbed-energy requirement. One full-scale vehicle crash test with a 2000P pickup truck was successfully performed according to the TL-3 criteria specified in NCHRP Report No. 350. This crash test was conducted to verify that the

critical post placement design would work within a W-beam guardrail system. From these efforts, design guidelines were developed for the placement of guardrail posts in rock with varied thickness and depth below the ground line. In addition, recommendations were also extrapolated for placing guardrail posts in mow strips using a specific coarse aggregate backfill material.

2.8 Curbs Installed Below Approach Guardrail Transitions

According to the *Roadside Design Guide* [42], curbs can be used along roadways to provide effective drainage control. Although curbs provide limited redirective capacity, they are generally deemed undesirable along high-speed roadways due to a propensity to contribute to vehicular instabilities (i.e., vaulting, overturn, etc.) during impact events. When utilized, curb structures should be designed to be traversable and/or present minimal obstruction to errant motorists. However, curbs have been used in combination with barrier systems when appropriately stiffened to reduce lateral deflections and/or when its use did not excessively degrade system performance, such as with strong-post W-beam guardrails and some approach guardrail transition systems. In fact, approach guardrail transition systems have incorporated a curb to reduce the probability of wheel snagging on the end of a concrete bridge rail, while others were developed with curbs used for drainage control only. However, when utilized in a transition region, curb and curb inlets may induce vehicular instabilities which can adversely affect the crashworthiness of a transition system. Although several TL-2 and TL-3 combination curb-to-guardrail systems have been successfully crash tested and evaluated over the years, these designs are not applicable to thrie beam approach guardrail transitions to rigid barrier ends. Therefore, curb-to-barrier combinations should be crash tested if extensive use exists or is planned.

2.8.1 Texas Thrie Beam Approach Guardrail Transition

In 2003, researchers at TTI conducted a study to evaluate the performance of a variation to the Texas approach guardrail to concrete bridge rail transition system [43]. In particular, the purpose of the study was to determine if the 5.75-in. (146-mm) tall curb specified in the original design of the transition system, as shown in Figure 19, was necessary to satisfy the safety criteria set forth in NCHRP Report No. 350 for TL-3 impacts. Eliminating this portion of the design would significantly reduce construction costs. In test no. 445643-1, a 4,504-lb (2,045-kg) pickup truck impacted the transition at a speed of 61.3 mph (98.7 km/h) and an angle of 24.7 degrees. As the vehicle was redirected, it rolled on its side and therefore did not meet the requirements of NCHRP Report No. 350. Thus, the researchers concluded that the transition system without the 5.75-in. (146-mm) tall curb from the original design was unable to safely redirect a vehicle.

2.8.2 Guidelines for Curb-to-Barrier Installations

In 2005, recommendations for the design and placement of curb-to-barrier combinations were reported in NCHRP Report No. 537 [44]. Those recommendations focused on strong-post W-beam guardrails and were developed using knowledge obtained in prior curb-to-barrier design and testing studies, numerous computer simulations, and several full-scale crash vehicle crash tests. In particular, on roadways with operating speeds above 55.9 mph (90 km/h), it was recommended that curb-to-barrier combinations should only be used if the curb is 4 in. (100 mm) or shorter and has a 3H:1V or flatter sloping face. Further, the curb toe should be placed flush with the face of the guardrail.

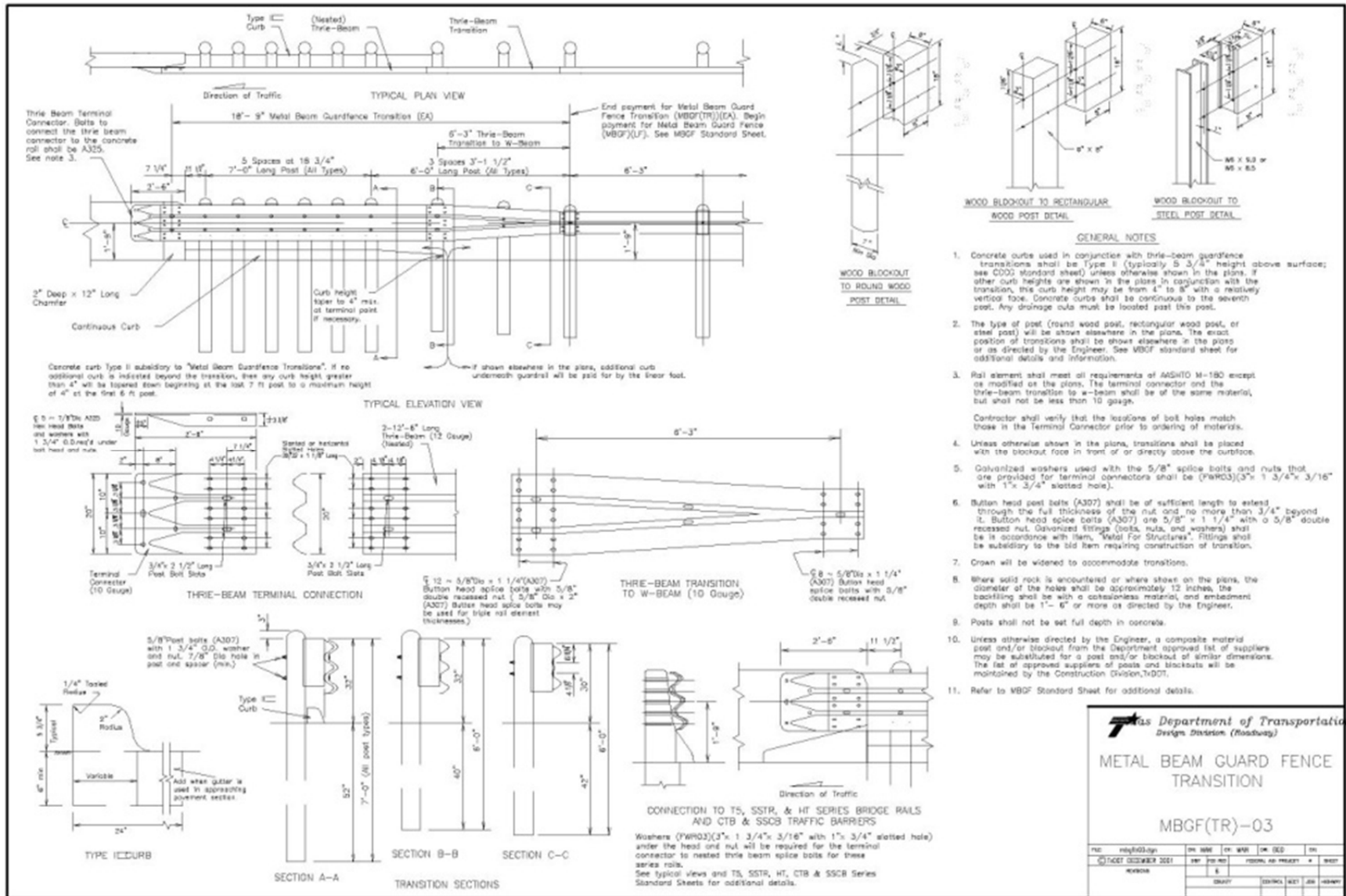


Figure 19. Texas Approach Guardrail Transition Detail [43]

3 SURVEY DATA

3.1 Overview

For this study, a sample set of field data was obtained from the Wisconsin DOT. In particular, participating personnel documented the following parameters:

1. Location of system
2. Type and length of system
3. Type of connecting bridge rail
4. Type of drainage structure utilized
5. Presence of improper grading behind post
6. Presence of improper post exposure
7. Presence of erosion on the surrounding terrain
8. Curb height and shape
9. Location of any damaged or missing posts

In addition, photographs were included to illustrate any of the above parameters. The compiled data represented a sampling of 223 approach guardrail transition systems located along high-speed highways. The information obtained from the sample set of field data was assumed to be representative of the State of Wisconsin. A schematic detailing the numbering system that was used by participating personnel to identify post position is shown in Figure 20.



Figure 20. Schematic of Transition Post Numbering System

3.2 Site Analysis

Two primary three beam transition systems within the data set are: (i) the 18-ft 9-in. (5.7-m) long transition system and (ii) the 31-ft 3-in. (9.5-m) long transition system. Data pertaining to each system design was analyzed separately, as shown in Tables 7 and 8, respectively. The sample size for the 18-ft 9-in. (5.7-m) long system (51 systems) was three times less than that utilized for the 31-ft 3-in. (9.5-m) long system (172 systems), which can be attributed to the relatively short time the shorter system has been used by the State. Nonetheless, both data sets illustrated the same concern – a significant number of these existing approach guardrail transition systems contained one or more of the listed deficiencies.

3.2.1 Missing Transition Post(s) with Varied Locations

Although missing posts appeared to be more common in the 18-ft 9-in. (5.7-m) long transition system as compared to the 31-ft 3-in. (9.5-m) long transition system, both systems indicated a higher propensity for missing a post near the bridge rail end and the region around post five. Examination of survey photographs illustrated that obstructions at ground line were often responsible for inability to install a post at a particular location. Poorly-placed drainage outlets were responsible for the majority of missing posts in the upstream region, while the bridge rail and its abutment/wingwall foundation system was often responsible for missing posts near the bridge rail end. Further, two different concrete bridge rail shapes were documented in the survey: (i) blunt-end parapets and (ii) sloped-end parapets. For clarification, the actual design of the blunt-end and sloped-end parapets can be found in Appendix A [45-46]. More recent installations utilizing the 18-ft 9-in. (5.7-m) long transition system did not demonstrate an issue with the first post for connections to blunt-end parapets. However, installation of the first post was a consistent problem across data sets for connections to sloped-end parapets.

Table 7. Survey Summary of 18-ft 9-in. Long Wisconsin Transition System

	Problem Description													
	Transition Missing at Least One Post	Missing Post Position							Posts Installed on Slopes Without 2-ft Grading	Transitions Posts with Insufficient Soil Backfill/Grading	Transitions Posts Embedded in Asphalt ^b	Drainage Structure (Lateral Curb) Below Rail	Transitions with 1 Deviation	Transitions with Multiple Deviations
		1			2	3	4	5						
	Blunt End Parapet	Sloped End Parapet	Other											
Number of Total Surveyed ^a	20	0	13	1	2	2	5	7	19	44	NA	16	22	29
Percent of Total Surveyed ^a	39%	0%	25%	2%	4%	4%	10%	14%	37%	86%	NA	31%	43%	57%

^a 51 systems.

^b Not documented in survey.

Table 8. Survey Summary of 31-ft 3-in. Long Wisconsin Transition System

	Problem Description														
	Transition Missing at Least One Post	Missing Post Position							Posts Installed on Slopes Without 2-ft Grading	Transitions Posts with Insufficient Soil Backfill/Grading	Transitions Posts Embedded in Asphalt ^b	Drainage Structure (Lateral Curb) Below Rail	Transitions with 1 Deviation	Transitions with Multiple Deviations	
		1			2	3	4	5 ^b							6
	Blunt End Parapet	Sloped End Parapet	Other												
Number of Total Surveyed ^a	24	4	6	2	2	1	7	NA	6	48	93	NA	62	95	77
Percent of Total Surveyed ^a	14%	2%	3%	1%	1%	1%	4%	NA	3%	28%	54%	NA	36%	55%	45%

^a 172 systems.

^b Transition does not have post at this position; any system documented with this missing post was excluded from consideration.

^c Not documented in survey.

3.2.2 Transition Posts Installed near or at Slope Break Point of Fill Slope

Approximately one third of the documented transition systems were supported by posts located on slopes or with insufficient grading behind them. This deficiency may ultimately describe a situation where the soil grading does not extend past the shoulder of the roadway. Possible causes for this lack of grading include economic motives directed to save costs, time, and soil fill material. In addition, approach guardrail transitions to bridge railing systems are typically located directly above a region where surface water runoff is diverted away from the roadway. Further, this region is often associated with a pivot location where roadside slopes begin as perpendicular to the roadway but curve through an arc, thus ending under the bridge and below the abutment in an orientation that is parallel to the roadway.

Thus, transition systems are prone to erosion, and the formation of undesirable slopes is a common occurrence. In fact, a significant amount of systems were documented to exhibit eroded terrain around the posts. However, the majority of those systems were reported to only contain minor erosion. Although measurement for the actual slope or eroded terrain was not required in the survey, several photographs illustrated posts located at the slope break point of very steep terrain.

3.2.3 Transition Posts with Insufficient Soil Backfill/Grading

The most common deficiency documented in the survey for either system was a transition supported by posts which were improperly exposed above ground line. Soil erosion, as mentioned in the previous section, is a probable cause for this deficiency. For an individual transition system, as many as nine posts were reported to be excessively exposed. However, the majority of these exposure lengths were reported as minor, in the range of 1 to 4 in. (25 to 102 mm). Still, some individual exposure lengths exceeded 10 in. (254 mm).

3.2.4 Transition Posts Embedded in Asphalt

No specific documentation was provided regarding transition posts embedded in soil with asphalt surfacing surrounding the posts. As such, there was no specific data available to quantify the extent of the problem. However, this deficiency was directly noted by State officials and was also observed in several site photographs. The research team was informed that Wisconsin contractors were having difficulty creating and applying the FHWA-recommended low-strength grout backfill material into leave outs formed in asphalt mow strips. Instead, contractors were either applying a stronger material (e.g., asphalt) in the leave outs, or even placing asphalt surfacing around the posts and sufficiently behind. In 2009, the WisDOT updated its policy regarding the installation of guardrail posts within asphalt or concrete mow strips by requiring the use of a low-strength, concrete grout material within the specified leave-out regions.

3.2.5 Drainage Structures (Flume) Positioned Below Rail

Approximately one third of all documented transition systems incorporated a drainage flume-curb structure below the three beam rail. For clarification, the actual design of the drainage flume-curb structure in question is shown in Figure A-3 of Appendix A [47]. These lateral drainage flumes were the main reason for missing posts in the region near post five upstream from the bridge rail end. On the other hand, another Wisconsin DOT drainage feature, a drop inlet, was available but utilized less frequently. For clarification, the actual design of the drop inlet structure can be found in Figure A-4 of Appendix A [48]. Both drainage structures were utilized in combination with a 6-in. (152-mm) tall vertical curb.

3.3 Priority Ranking

As described previously, a significant number of the existing approach guardrail transition systems contained deviations, as described in Tables 7 and 8. However, numerous systems contained more than one of these reported deviations. The combination of several

deficiencies likely complicated the research team's ability to accurately predict the degree of degraded barrier performance when impacted. Therefore, each deficiency type was evaluated independently regarding its frequency of occurrence and its implied safety risk based on engineering judgment in order to simplify the analysis and retrofitting process. These evaluations would then be combined to create a priority ranking for further analysis. The deficiency with the highest priority was examined first, followed by the next most critical defect, and continued until all five system deficiencies had been investigated.

Each of the five system deficiencies was assigned a rank from 1 to 5 to evaluate frequency of occurrence. The order of frequency ranking was based on the cumulative percentage of occurrences provided from Tables 7 and 8. A rank of 5 corresponded to the most common occurrence in both transitions, while a rank of 1 corresponded to the least common occurrence. The deficiency of transition posts embedded in asphalt was not documented in the survey, thus it was automatically assigned the lowest ranking. The most common deficiency documented in the survey was transition posts with insufficient soil backfill/grading, whereas the least common was missing transition posts. These deficiencies represented a cumulative percentage in both transition systems of 61 and 20 percent, respectively. The frequency of occurrence for each deficiency is shown in the first column of Table 9.

To determine which deficiency presented the largest hazard to errant motorists, each of the five system deficiencies was assigned a safety risk value based strictly on engineering judgment. Implied safety risks to errant motorists included the propensity for a deficiency to cause vehicle instabilities, vehicle snag, rail rapture, and/or vehicle penetration/override. Risk values were considered more critical than frequency of occurrence because low risk deficiencies found in high frequency would still safely redirect the majority of errant vehicles. As such, safety risk values were assigned to each deficiency on a scale from 1 to 10. This allowed the safety risk

values to potentially have twice the weight of the frequency of occurrence ranking. A rank of 10 represented the highest predicted safety risk to motorists, while a rank of 1 represented a minimal safety risk. The highest safety risk associated with a deficiency was applied to missing transition posts, whereas the lowest risk was applied to transitions posts with insufficient soil backfill/grading and drainage structures (i.e., lateral curbs) below the transition rail. The estimated safety risk for each deficiency is shown in the second column of Table 9.

The values in the first and second columns of Table 9 were summed to create a weighted total for each of the five deficiencies, as shown in the third column of Table 9. The highest weighted total represented the most critical deficiency. Then, a final priority ranking was assigned to each of the deficiencies. The deficiency with the highest weighted total was assigned a value of 1, while the deficiency with the lowest weighted total was assigned a value of 5. The final priority rankings for each deficiency, as shown in the fourth column of Table 9, were confirmed with the Wisconsin DOT.

Table 9. System Deficiency Rankings

System Deficiency	Frequency of Occurrence	Estimated Safety Risk	Weighted Total	Priority Ranking
Missing Transition Posts	2	10	12	1
Transition Posts Installed on Fill Slopes	4	7	11	2
Transition Posts with Insufficient Soil Backfill/Grading	5	5	10	3
Transition Posts Embedded in Asphalt	1	7	8	4
Drainage Structure (Lateral Curb) Below Rail	3	4	7	5

4 BARRIER VII COMPUTER SIMULATION

4.1 Overview

The two-dimensional, non-linear, finite element computer program, BARRIER VII [10], was utilized to investigate the impact performance of both Wisconsin DOT approach guardrail transitions with various deficiencies and several design modifications. The BARRIER VII computer program was developed to simulate vehicle impacts with safety barriers consisting of post and beam elements. In particular, beam (i.e., rail) elements were allowed to yield at all nodal points, and posts were treated as elastic, perfectly-plastic components with failure criteria guided by either defined shear or deflection limits. Due to its simplistic coding, BARRIER VII has aided roadside engineers for over four decades in analyzing and designing barrier systems as well as accurately predicting the dynamic crash performance of various roadside barriers under various impact conditions and vehicle types.

Results from previous component and full-scale vehicle crash tests were considered to develop accurate baseline models for both the 18-ft 9-in. (5.7-m) long and 31-ft 3-in. (9.5-m) long transitions systems, as shown previously in Figures 2 and 3, respectively. Next, the effects of missing posts, posts located on fill slopes, and posts with insufficient soil backfill/grading were investigated and compared to the simulation results obtained for the baseline configurations. In addition, the BARRIER VII computer simulations were used to evaluate the effectiveness of various retrofit alternatives in mitigating the degrading effects of such deficiencies.

4.2 Model Components

The Wisconsin DOT approach guardrail transitions were composed of five primary components: (i) 6-in. x 8-in. x 6-ft (152-mm x 203-mm x 1.8-m) long wood posts embedded 43 in. (1,092 mm) into soil; (ii) 6-in. x 8-in. x 7-ft (152-mm x 203-mm x 2.1-m) long wood posts

embedded 52 in. (1,321 mm) into soil; (iii) W-beam rails, (iv) thrie beam rails; and (v) a concrete bridge rail end section. The development of each of these components is described in the following sections.

4.2.1 6-in. x 8-in. x 6-ft Long Wood Posts

Dynamic test results from a 1998 MwRSF post study were utilized to develop the BARRIER VII component models for 6-in. x 8-in. x 6-ft (152-mm x 203-mm x 1.8-m) long wood posts installed on level terrain [32]. In particular, test nos. IBT-14 and IBT-24 from that testing series involved 6-in. x 8-in. (152-mm x 203-mm) wood posts embedded 43 in. (1,092 mm) in strong soil, as shown in Table 10.

Table 10. 6-in. x 8-in. Wood Post Test Results [32]

Test No.	Post Type	Embedment Depth (in.)	Impact Height (in.)	Impact Velocity (mph)	Average Force		Failure Type
					@ 10 in. (kips)	@ 15 in. (kips)	
IBT-14	6x8 wood	43	21.65	20.0	14.8	16.1	Post Rotation
IBT-24	6x8 wood	43	21.65	19.0	13.8	14.0	Post Rotation
Average					14.3	15.0	

Rotation through the soil was the primary mode of failure for both tests. As such, the peak force and average force over 15 in. (381 mm) of deflection, were 19.5 kips (86.7 kN) and 15.0 kips (66.7 kN), respectively. The average force provided the basis for strong-axis resistance for the BARRIER VII model. Utilizing an impact height of 21.65 in. (550 mm) to the center of the guardrail element, the strong-axis bending moment, M_A , was calculated to be 325 k-in. (36.7 kN-m). A post stiffness, K_B , of 6 kips/in. (1.1 kN/mm) was approximated from force vs. deflection curves obtained from the two component tests. Finally, the post was given a maximum deflection of 15 in. (381 mm) prior to failure, δ_{FB} . This displacement was selected for two reasons. First, after 15 in. (381 mm) of deflection, the resistive forces began to decrease

significantly. Second, full-scale vehicle crash testing has shown that a W-beam guardrail will release away from a post after large deflections, i.e., 15 in. (381 mm) to 20 in. (508 mm), thus causing a post to lose its effectiveness.

To obtain the weak-axis bending moments, M_B , the strong-axis values were artificially increased by approximately 12 percent according to data observed in a study on BARRIER VII applications for flexible barrier design [49]. This selection follows the assumption that the resistance to post rotation for the weak-axis of bending is initially higher; since, the side of the post is larger as compared to the front of the post, 8 in. (203 mm) compared to 6 in. (152 mm), respectively. This adjustment without test data was deemed acceptable, because the longitudinal post deflections in a transition are minimal and not as significant as the lateral deflections. Further, the failure deflection for the post rotating longitudinally or parallel with the barrier system, δ_{FA} , was set at 6 in. (152 mm) to minimize any energy absorption in the longitudinal direction, as this form of energy absorption is typically not anticipated for a transition system.

Additional input properties for the strong and weak axis of 6-in. x 8-in. x 6-ft (152-mm x 203-mm x 1.8-m) long wood posts embedded 43 in. (1,092 mm) on level terrain can be found in Table 11.

Table 11. Input Properties for BARRIER VII Wood Posts

BARRIER VII Input Parameters		6-in. x 8-in. x 7-ft Wood Post	6-in. x 8-in. x 6-ft Wood Post
Load Height	in.	21.65	21.65
K_B - Strong-Axis Post Stiffness Along B	kips/in.	8	6
M_A - Strong-Axis Bending Moment About A	kips-in.	476	325
δ_{FB} - Strong-Axis Displacement Failure Along B	in.	15	15
V_{FB} - Strong-Axis Shear Failure Along B	kips	25	25
K_A - Weak-Axis Post Stiffness Along A	kips/in.	14	11
M_B - Weak-Axis Bending Moment About B	kips-in.	400	368
δ_{FA} - Weak-Axis Displacement Failure Along A	in.	4.5	6
V_{FA} - Weak-Axis Shear Failure Along A	kips	25	25

4.2.2 6-in. x 8-in. x 7-ft Long Wood Posts

Component testing of 7-ft (2.1-m) long wood posts with an impact height of 21.65 in. (550 mm) and a soil embedment depth of 52 in. (1,321 mm) could not be found. Thus, the post-soil strength for a 6-in. x 8-in. x 6-ft (152-mm x 203-mm x 1.8-m) long wood post embedded 43 in. (1,092 mm) into soil on level terrain was extrapolated utilizing Equation 1 to account for an embedment depth of 52 in. (1,321 mm). This post configuration and larger embedment depth was successfully crash tested in the 1998 Iowa wood-post transition study. Equation 1 was obtained from NCHRP Report No. 350 and states that post-soil interaction can be approximated as a function of the square of the embedment depth ratio.

$$F'_s = F_s \left[\frac{D'_e}{D_e} \right]^2 \quad (1)$$

Where:

- F'_s = soil dynamic yield force at alternate embedment depth
- F_s = soil dynamic yield force at known embedment depth
- D'_e = alternate embedment depth
- D_e = known embedment depth

The modified post-soil resistance corresponding to this increased embedment depth was 21.9 kips (97.4 kN).

As previously noted, a recent MwRSF research study was conducted which included the testing of three 6-in. x 10-in. (152-mm x 254-mm) by 7-ft (2.1-m) long Southern Yellow Pine (SYP) wood posts embedded 52 in. (1,321 mm) into the soil and using a 24⁷/₈-in. (632-mm) load height [35]. During this testing program, two posts fractured and one post rotated in the soil. For the post (test no. MGSATB-18) that rotated through the soil and modified for a 21.65-in. (550-mm) load height, an average soil resistance of 21.1 kips (93.9 kN) through 15 in. (381 mm) of displacement was obtained. Further, the two posts (test nos. MGSATB-19 and MGSATB-20) which fractured demonstrated a point of maximum bending 12 in. (305 mm) below ground level.

As a result, the wood post in test no. MGSATB-18 had the strong-axis bending potential of 778 kip-in. (87.9 kN-m). As such, a post-soil resistance and strong-axis bending moment of approximately 22 kips (98 kN) and 476 kip-in. (53.8 kN) seemed reasonable for a 6-in. (152-mm) wide by 7-ft (2.1-m) long rectangular post. Unfortunately, the fracture of two out of three 6-in. x 10-in. (152-mm x 254-mm) by 7-ft (2.1-m) long SYP wood posts embedded 52 in. (1,321 mm) created concern for the 6-in. x 8-in. (152-mm x 203-mm) by 7-ft (2.1-m) long wood posts.

From a prior research study, 6-in. x 8-in. (152-mm x 203-mm) wood posts subjected to strong-axis bending using a cantilevered load height of 21.65 in. (550 mm) carried a peak lateral load of approximately 12.1 kips (53.8 kN), which corresponded to an average Modulus of Rupture (MOR) of 4,100 psi (28.27 kPa) [33-34]. This capacity was observed in dynamic testing of SYP wood posts placed in a rigid sleeve versus in a soil foundation.

From the 1998 Iowa transition post testing program, two tests (test nos. IBT-14 and IBT-24) on 6-in. x 8-in. x 6-ft (152-mm x 203-mm x 1.8-m) long wood posts provided a peak force and an average resistive force over 15 in. (381 mm) of deflection of 19.5 kips (86.7 kN) and 15.0 kips (66.7 kN), respectively, when embedded 43 in. (1,092 mm) into the soil [32]. As such, these dynamic post-soil tests revealed a MOR in excess of 6,596 psi (45,480 kPa) without post fracture as well as the ability to resist a lateral load much greater than 12.1 kips (53.8 kN).

From the 2012 FHWA post testing program pertaining to guardrail for wire-faced MSE walls, two tests (test nos. GWB-14 and GWB-15) on 6-in. x 8-in. x 6-ft (152-mm x 203-mm x 1.8-m) long wood posts provided a peak force and an average resistive force over 15 in. (381 mm) of deflection of 16.2 kips (72.1 kN) and 13.2 kips (58.7 kN), respectively, when embedded 43 in. (1,092 mm) into the level terrain soil and modified for a 21.65-in. (550-mm) load height [8-9]. As such, these dynamic post-soil tests revealed a MOR in excess of 5,412 psi (37,310 kPa)

without post fracture as well as the ability to resist a lateral load much greater than 12.1 kips (53.8 kN).

Based on the Iowa and FHWA post testing programs, it was realized that the peak lateral capacity of a wood post placed in soil at a 21.65-in. (550-mm) load height could easily exceed 12.1 kips (53.8 kN), and may even reach peak capacities greater than 19.5 kips (86.7 kN).

As part of the Iowa transition study, several unpublished component tests were performed to evaluate closely-spaced posts with and without soil plates [20,32]. For unpublished post test no. ITNJ-3, as depicted in Figures 17 and 18, two closely-spaced W6x9 (W152x13.4) steel posts embedded 43 in. (1,092 mm) into soil revealed interesting results. The peak force and average resistive force at various deflections for the dual post system were approximately twice that provided by a single steel post with identical embedment. However, neither of the dual posts showed signs of yielding, while the single post had clearly yielded. As a result, it was somewhat apparent that slightly different soil behavior occurred for closely-spaced posts such that yielding in the dual posts was mitigated. From this unpublished component testing and comparison of results, there is increased confidence that 6-in. x 8-in. (152-mm x 203-mm) by 7-ft (2.1-m) long SYP wood posts embedded in soil and closely spaced may be capable of carrying loads higher than that which was observed in the rigid sleeve testing of single wood posts. For lateral deflections ranging between 4 to 8 in. (102 to 203 mm) and those expected in the thrie beam transition region, this confidence increases even more so. Further and as found in the 1998 Iowa transition study, no 6-in. x 8-in. (152-mm x 203-mm) by 7-ft (2.1-m) long wood posts with 52 in. (1,321 mm) embedment depths were reported to fracture during crash test no. ITNJ-4 [20].

Similar to 6-in. x 8-in. x 6-ft (152-mm x 203-mm x 1.8-m) wood posts and based on the information noted above, the strong-axis bending moment, M_A , was calculated to be 476 k-in. (53.8 kN-m). A post stiffness, K_B , equal to 8 kips/in. (1.4 kN/mm) was determined. Finally, the

post was given a maximum deflection of 15 in. (381 mm) prior to failure, δ_{FB} . The weak-axis bending moment, M_B , was calculated to be 400 k-in. (45.2 kN-m). A post stiffness, K_A , equal to 14 kips/in. (2.5 kN/mm) was determined. However, the weak-axis failure deflection was reduced to 4.5 in. (114 mm), as forces of this magnitude would surely result in post fracture. Input properties utilized for 6-in. x 8-in. x 7-ft (152-mm x 203-mm x 2.1-m) wood posts embedded 52 in. (1,321 mm) on level terrain can be found in Table 11.

4.2.3 Rail Elements

Input values for the various rail sections were determined from the cross sectional properties of each member, as shown in Table 12. A yield stress of 50 ksi (345 MPa) was used to calculate the elastic tensile and moment capacities. For nested rail sections, all strength and cross sectional input values were doubled. Properties for the symmetric, 10-gauge (3.4-mm) W-to-thrie beam transition piece were calculated at the center of each $9^{3/8}$ in. (238 mm) rail segment using a linear interpolation between the W-beam and the thrie beam ends, as shown in the sample model decks of Appendix B.

Table 12. Input Properties for BARRIER VII Rail Elements

BARRIER VII Parameters		Beam Type				
		12-Gauge W-Beam	10-Gauge W-Beam	12-Gauge Thrie Beam	Nested 12-Gauge Thrie Beam	10-Gauge Thrie Beam
I - Second Moment of Area	in. ⁴	2.29	3.00	3.76	7.52	4.82
A - Area of Cross Section	in. ²	1.99	2.56	3.10	6.20	4.00
W - Weight	lb/ft	6.92	8.90	10.81	21.62	13.95
F _y - Yield Force	kip	99.5	128	155	310	200
S - Section Modulus	in. ³	1.37	1.76	2.19	4.38	2.80
M _y - Yield Moment	kip-in.	68.5	88	109.5	219.0	140

4.2.4 Concrete Bridge Rail

To represent the concrete bridge rail, two special members were created. First, a post member was generated utilizing very high values for each adjustable stiffness and strength parameters. Second, a rail element was also generated utilizing extremely high values for each adjustable stiffness and strength parameters. Combining these two members produced a nearly-rigid structure when compared to the semi-rigid barrier which preceded it. Thus, these two members were used to represent a concrete bridge parapet which would not deflect during impact.

4.3 Model Assembly and Validation

4.3.1 18-ft 9-in. Long Transition System

The component data described in the previous section was organized into a comprehensive barrier model to replicate the 18-ft 9-in. (5.7-m) long thrie beam and symmetric W-to-thrie beam transition sections. W-beam rail elements supported by 6-in. x 8-in. x 6-ft (152-mm x 203-mm x 1.8-m) long wood posts spaced at 6 ft – 3 in. (1.9 m) intervals preceded the transition system for 81 ft – 3 in. (24.8 m). A breakaway cable end terminal (BCT) supported by two breakaway wood posts was utilized to anchor the upstream end of the W-beam rail. ‘Concrete’ rail elements supported by ‘concrete’ post members spaced at 6 ft – 3 in. (1.9 m) intervals extended 28 ft – 1.5 in. (8.6 m) beyond the thrie beam transition system to replicate the rigid concrete bridge parapet. The total length of the barrier model was 127 ft – 6¹/₄ in. (38.9 m). The computer data deck of the baseline barrier model and a schematic of the barrier can be found in Appendix B.

Results from crash test no. ITNJ-4 of the 1998 MwRSF Iowa transition study [20] were used to validate the barrier model. For the validation simulation, a 2000P vehicle model was prescribed with the exact impact conditions of crash test no. ITNJ-4. The pickup truck weighed

4,407 lb (1,999 kg) and impacted the transition at a speed of 63.6 mph (102 km/h) and at an angle of 24.6 degrees using an impact point of 96 in. (2,438 mm) upstream from the end of the bridge rail. After multiple trials, the coefficient of friction for vehicle-barrier interaction was optimized at 0.25 to provide the most accurate results. Plots and results comparing simulated and actual full-scale test results are shown in Figure 21 and Table 13, respectively.

It is clear from the sequential time plots shown in Figure 21 and the results shown in Table 13 that the barrier model of the 18-ft 9-in. (5.7-m) long transition system accurately replicated the results obtained from the full-scale crash test and could be used to evaluate system performance under various impact conditions and design variations. Note that some measurements from crash test no. ITNJ-4 could not be documented because the hood of the vehicle obstructed the camera view.

4.3.2 31-ft 3-in. Long Transition System

The main difference between the 18-ft 9-in. (5.7-m) long transition system and the 31-ft 3-in. (9.5-m) long transition system was an additional 12¹/₂-ft (3.8-m) long section of thrie beam between the nested thrie section and the W-to-thrie transition element. Both systems utilized the same type of components within their respective configurations. Therefore, the components used within the validated model from the previous section for the 18-ft 9-in. (5.7-m) long system were reorganized into a comprehensive model to replicate the 31-ft 3-in. (9.5-m) long system. The computer data deck of the baseline barrier model and a schematic of the barrier can be found in Appendix B. The 1988 MwRSF Kansas transition study did not have any full-scale test results for which to directly validate the 31-ft 3-in. (9.5-m) long model. Nonetheless, the research team believed that the validation of the 18-ft 9-in. (5.7-m) long system and its components was suitable for predicting the baseline safety performance of the 31-ft 3-in. (9.5-m) long system due to the limited differences between them.

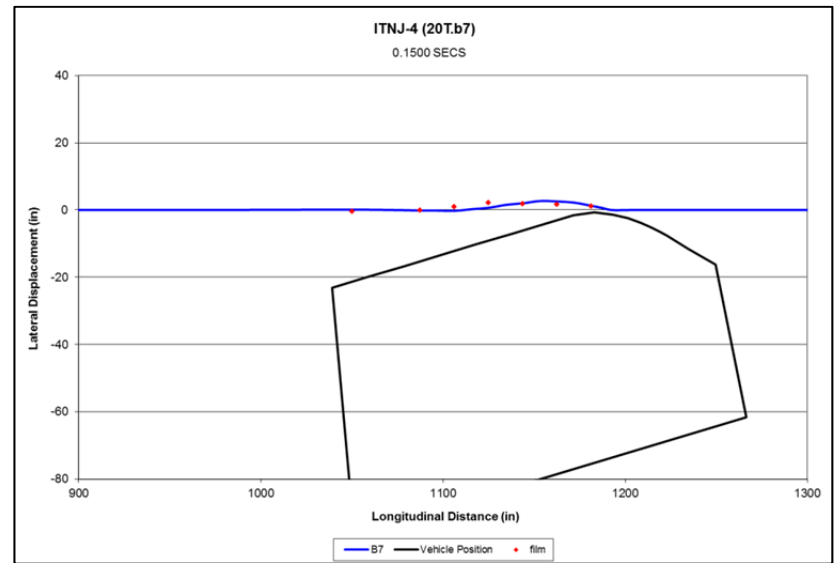
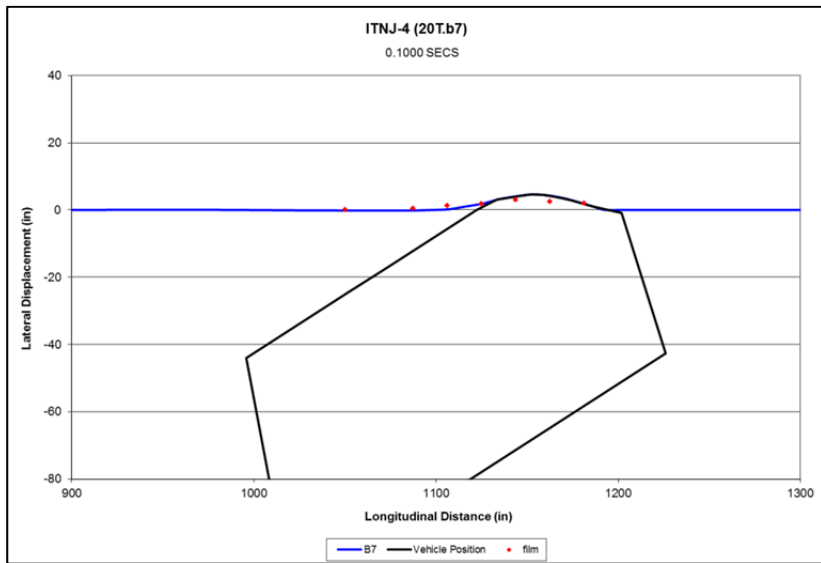
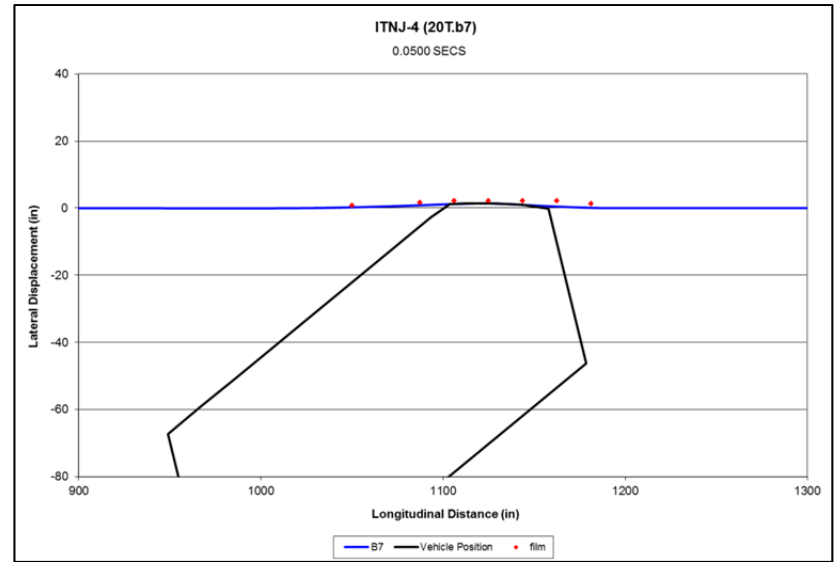
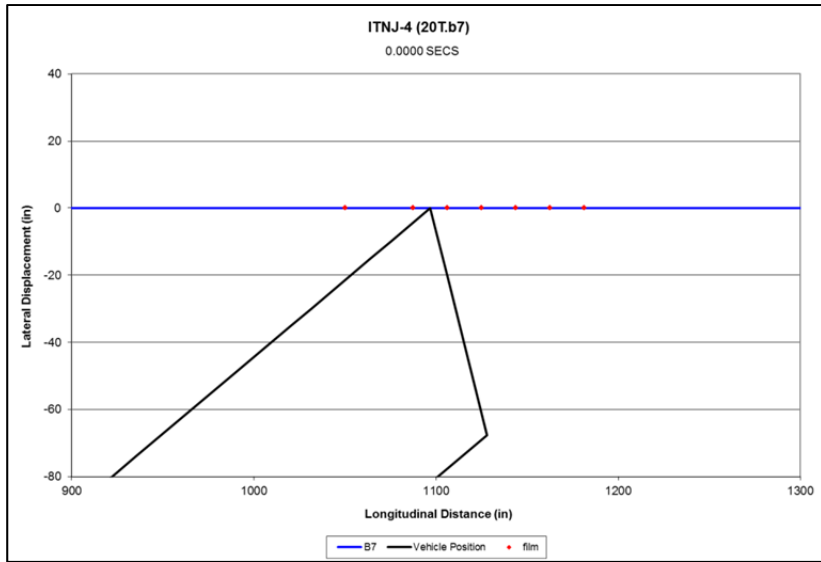


Figure 21. 18-ft 9-in. Long Transition System Validation with Crash Test No. ITNJ-4 Results

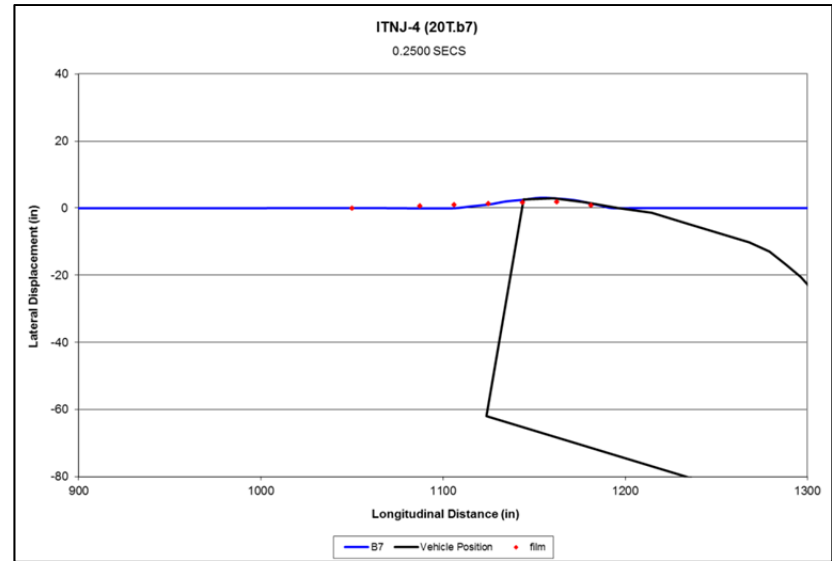
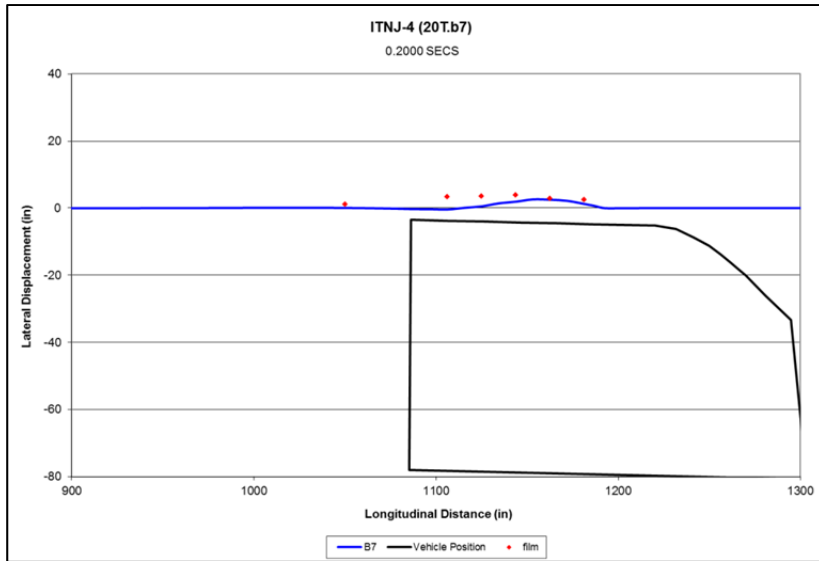


Figure 22. 18-ft 9-in. Long Transition System Validation with Crash Test No. ITNJ-4 Results – Cont.

69

Table 13. 18-ft 9-in. Long System Validation with Crash Test No. ITNJ-4 Results

Parameter		Test No. ITNJ-4 Results	BARRIER VII Simulation Results
Maximum Dynamic Rail Deflection	Value (in.)	3.9 ^a	4.8
	Location U.S. from Bridge Rail End (in.)	49 ^a	40
Maximum Pocketing Angle	Value (deg)	NA ^{a,b}	8.3
	Location U.S. from Bridge Rail End (in.)	NA ^{a,b}	30
Vehicle Parallel Time (sec)		0.190	0.197
Vehicle Exit Angle (deg)		7.2	11.4
Vehicle Exit Speed (mph)		44.9	47.6

^a Some measurements were obstructed from overhead camera view.

^b No excessive pocketing documented in field book.

4.4 Baseline Runs

The validated models of both transition systems were utilized to gain an understanding of how each system (without deficiencies) would perform when subjected to TL-3 impacts at various locations throughout the two systems. The results from these series of simulations would later be used to determine how a specific deficiency altered the safety performance of a transition system. All baseline simulations were modeled with a 4,409-lb (2,000-kg) pickup truck impacting at a speed of 62.1 mph (100 km/h) and at an angle of 25 degrees, conditions consistent with NCHRP Report No. 350 TL-3 impacts. Each model was iteratively impacted at $9^{3/8}$ -in. (238-mm) intervals along the transition systems. A total of 24 runs were conducted at impact points within the 18-ft 9-in. (5.7-m) long system, and a total of 40 runs were conducted at impact points within the 31-ft 3-in. (9.5-m) long system. Comprehensive results from these baseline simulations can be found in Appendix D.

Data was collected for each baseline system pertaining to the three following parameters: (i) maximum wheel rim snag on the upstream edge of the bridge rail; (ii) maximum dynamic deflection within the nested thrie section of the barrier; and (iii) maximum vehicle pocketing angle within and upstream from the system. To calculate wheel rim snag, the node corresponding to the left-front tire of the simulated vehicle was examined, as described in Appendix C. This node was fixed with respect to the vehicle center of gravity, was not prescribed to contact the barrier, and did not deform with the bumper/quarter panel. Any lateral displacement of this node beyond the face of the barrier at the upstream edge of the bridge rail would signify wheel rim snag. For the purpose of calculating vehicle pocketing angles within the rail, a linear regression was used to fit lines to five consecutive nodes of the rail. Angles over a five-node spread represent a rail length of $37^{1/2}$ in. (953 mm). The same spacing was utilized previously to determine the critical pocketing angle for 2000P impacts [24].

4.5 Evaluation Criteria for BARRIER VII Models

As discussed in previous sections, the two major concerns associated with the design of a transition from a flexible guardrail system to a rigid bridge rail are vehicle snag on the upstream end of the bridge rail and vehicle pocketing within the system. In addition, excessive dynamic deflection is not desired in approach guardrail transition systems as it can lead to vehicle pocketing, high exit angles, and vehicle instabilities. It was important to denote critical limits for each concern.

4.5.1 Vehicle Pocketing

Although BARRIER VII has the capability to predict values of vehicle pocketing angles, its 2-D formulation limits the ability to measure the risk or consequences associated with pocketing. Nonetheless, the 23-degree limit established by MwRSF in 2007 [24] for a 2000P vehicle seemed logical as the upper limit for vehicle pocketing angles; since, the research herein was focused on satisfying NCHRP Report No. 350 safety criterion. BARRIER VII baseline results for both Wisconsin transition systems were well within this limit for impacts within the nested thrie section of the transition system. However, results from the 18-ft 9-in. (5.7-m) long system exceeded this value for upstream impacts originating in the W-beam sections, while results from the 31-ft 3-in. (9.5-m) long system approached this limit for similar impacts. Unfortunately, impacts upstream of the thrie beam regions were not considered during the original design and evaluation of either transition system, so these results could not be verified against previous testing. As a result, the performance of these systems upstream of the transition region was deemed outside of the scope of this study.

Results from the baseline simulations in which the vehicle impacted inside the thrie beam transition region showed maximum pocketing angles of less than half the previous 23-degree limit. Thus, the research team determined that any potential retrofit should maintain pocketing

angles within 2 to 3 degrees of that observed in the corresponding baseline runs. This choice ensured that, at a minimum, any designed retrofit would perform as well as the original system.

4.5.2 Vehicle Snag

Although vehicle wheel snag is undesirable, minor snag may have minimal effects on the safety performance of the system as well as the trajectory of the vehicle. As such, small amounts of wheel overlap (or snag) are typically allowed during the design process. The BARRIER VII maximum allowable design values for wheel rim snag in both the 1998 MwRSF Iowa transition study [20] and the 1989 MwRSF Kansas transition study [21], as well as a few other similar transition studies [17,22], as shown in Table 14, ranged between 2.0 and 3.0 in. (51 and 76 mm). Therefore, the upper limit of allowable wheel rim snag on the rigid bridge rail for both Wisconsin transition systems was selected as 2 in. (51 mm) to ensure consistency with historical testing and BARRIER VII simulation. This value accounted for both the geometry of a vehicle’s tire and the offset created by the thickness of the rail itself. Results for both baseline system runs were well within this limit at 1.58 in. (40 mm) and 1.61 in. (41 mm) for the 18-ft 9-in. (5.7-m) and 31-ft 3-in. (9.5-m) long systems, respectively.

Table 14. Previous Approach Transition Simulation and Testing Results with Critical Limits

Study	System Description	Maximum Wheel Rim Snag		Maximum Dynamic Deflection		
		BARRIER VII Simulation Results (in.)	Critical Design Limit (in.)	BARRIER VII Simulation Results (in.)	Full-Scale Crash Test Results	
					Fail (in.)	Pass (in.)
Iowa [20]	12-gauge Nested Thrie Beam with Steel Posts	1.9	2.0	7.5	13.74 [ITNJ-1]	5.24 [ITNJ-2]
	12-gauge Nested Thrie Beam with Wood Posts				10.39 [ITNJ-3]	3.90 [ITNJ-4]
Kansas (Fifth Design) [21]	12-gauge Nested Thrie Beam and 12-gauge Single Thrie Beam with Steel Posts	0.0	3.0	10.7	N/A	N/A
Tennessee [17]	Various W-beam configurations with Steel Posts	1.2 - 1.8	2.0	8.0 - 9.0	N/A	N/A
Missouri [22]	10-gauge Single Thrie Beam (both sides) with Steel Posts	2.1	2.1	6.9	9.88 [MTSS-1]	7.60 [MTSS-2]

4.5.3 Dynamic Deflections

Full-scale vehicle crash test results, as shown in Table 14, demonstrated that transition systems were deemed unsuccessful when barrier dynamic deflections within the thrie beam region approached or exceeded 10 in. (254 mm). On the other hand, transition systems were deemed successful when dynamic deflections within the system were less than or equal to 7.6 in. (193 mm). Further, the original BARRIER VII design value utilized for dynamic deflections within the 1998 MwRSF Iowa transition system was 7.5 in. (191 mm), right below the successful threshold value for transition systems. Thus, 7.5 in. (191 mm) was selected as the dynamic deflection limit within the thrie beam region for the 18-ft 9-in. (5.7-m) long transition system. Results from the baseline simulation of the 18-ft 9-in. (5.7-m) long system were well within this limit, at a maximum value of 6.2 in. (157 mm).

In contrast, the 31-ft 3-in. (9.5-m) long transition system has been shown to provide slightly larger deflections than the previous 7.5 in. (191 mm) limit. However, it was deemed inappropriate to hold the barrier to a higher standard than originally designed. Thus, dynamic deflections within the nested thrie beam region of the 31-ft 3-in. (9.5-m) long transition system were required to fall within the maximum observed value in the baseline simulations, or less than or equal to 8.2 in. (208 mm).

5 RESEARCH APPROACH – MISSING TRANSITION POSTS

5.1 Overview

Data from Section 3.2 indicated that missing posts within both the 18-ft 9-in. (5.7-m) long transition system and the 31-ft 3-in. (9.5-m) long transition system were a common occurrence in Wisconsin. This specific deficiency was believed to have the potential to cause system failure and allow a vehicle to snag on the upstream end of the bridge rail. BARRIER VII models representing each excluded post position within each transition system were created to analyze the consequences associated with such a deficiency. Although survey data indicated the possibility of multiple missing posts along a single transition, only a single missing post position was considered for each simulation to simplify the analysis effort. Results were compared against the evaluation criteria, as established in Chapter 4. Three retrofits with comparable stiffness and strength were developed to rectify location dependent deficiencies created by a missing post.

5.2 Analysis

The validated BARRIER VII models developed in Chapter 4 were altered to represent a system with a single missing post in the nested three beam region of the transition. Six post locations were examined for the 18-ft 9-in. (5.7-m) long system, while five post locations were examined for the 31-ft 3-in. (9.5-m) long system. Simulations were modeled with a 4,409-lb (2,000-kg) pickup truck impacting at a speed of 62.1 mph (100 km/h) and at an angle of 25 degrees, conditions consistent with NCHRP Report No. 350 TL-3 impacts. Each model was iteratively impacted at $9^{3/8}$ -in. (238-mm) intervals along the system, spanning between the W-to-three transition element and the bridge rail end. Results concerning wheel rim snag on the upstream edge of the bridge rail and dynamic deflection and pocketing angles within the nested three section of the barrier were analyzed to determine how each system with a variable missing

post would perform during TL-3 impact events. Thus, 24 simulations were conducted on each of the six missing post models for the 18-ft 9-in. (5.7-m) long transition system (144 total), and 40 simulations were conducted on each of the five missing post models for the 31-ft 3-in. (9.5-m) long transition system (200 total). Comprehensive results from this series of BARRIER VII simulations can be found in Appendix D. As shown in Tables 15 and 16, the maximum values corresponding to each of the three critical evaluation parameters are provided for each transition model. Any evaluation parameter found to violate these critical limits was highlighted for clarification. Further, the 31-ft 3-in. (9.5-m) long transition system does not incorporate a post in the fifth position, as shown previously in Figure 3. To maintain consistency with the numbering associated with the 18-ft 9-in. (5.7-m) long transition system, the fifth position in the 31-ft 3-in. (9.5-m) long transition system was skipped over. Thus, the sixth post position represents the same location for both systems.

Table 15. Simulation Summary of 18-ft 9-in. Long System Missing Transition Posts

Parameter	Missing Post Location					
	1	2	3	4	5	6
Maximum Wheel Rim Snag (in.)	2.32	2.22	1.98	1.68	1.62	1.60
Maximum Dynamic Deflection (in.)	6.22	6.24	6.43	7.52	8.15	8.17
Maximum Pocket Angle (deg)	8.9	10.3	9.2	9.3	8.9	8.3
Maximum Pocket Angle - Baseline ¹ (deg)	8.0	8.3	8.3	8.3	8.3	8.3

¹ Corresponding to same impact location.

Table 16. Simulation Summary of 31-ft 3-in. Long System Missing Transition Posts

Parameter	Missing Post Location					
	1	2	3	4	6	
Maximum Wheel Rim Snag (in.)	2.36	2.27	2.06	1.76	1.64	
Maximum Dynamic Deflection (in.)	8.14	8.26	8.83	9.43	9.64	
Maximum Pocket Angle (deg)	9.7	11.5	10.5	10.7	10.1	
Maximum Pocket Angle - Baseline ¹ (deg)	8.9	8.9	8.9	8.9	8.8	

¹ Corresponding to same impact location.

Although the 31-ft 3-in. (9.5-m) long system had higher values for the evaluation parameters as compared to those obtained for the 18-ft 9-in. (5.7-m) long system, the overall trend associated with both systems was similar. Missing posts from positions 1 to 3 violated the criterion for wheel rim snag on the upstream end of the bridge rail, while missing posts in positions 2 to 6 violated the criterion for dynamic deflection. Further, the maximum pocketing angle in the nested three beam region of the 18-ft 9-in. (5.7-m) long transition system only exceeded its corresponding maximum baseline value by as much as 2 degrees, while the 31-ft 3-in. (9.5-m) long transition system only exceeded its corresponding maximum baseline value by as much as 2.6 degrees. Nonetheless, the results indicated that a single missing post, regardless of its relative location within the transition, sufficiently reduced the stiffness and strength of either system to potentially cause failure. Therefore, retrofits were necessary to provide the appropriate stiffness and strength for each deficient system.

5.3 Retrofit Development

When possible, the best option in repairing a guardrail system with a missing or severely damaged post is to re-install an appropriate post in the prescribed location. This resolution brings the system up to the standard in which it was originally designed, tested, and/or evaluated. However, this alternative is not always possible due to various below or above grade obstructions at the location where the post should be installed. Thus, new design retrofits were needed.

Development of an exclusive retrofit design for each post position within a given transition system was not feasible or necessary. Retrofits developed for a particular post location can typically be applied to adjacent positions within the system. As described in Section 3.2, the two most prominent causes for missing posts were poorly-placed drainage outlets or the bridge

rail itself. Also, two different concrete bridge rail ends were identified throughout the survey, each posing a new challenge for a retrofit. Therefore, it was concluded that the minimum of three interchangeable retrofit designs were required to completely satisfy the deficiency created by missing posts and are as follows: (i) one retrofit for the post location directly adjacent to blunt-end bridge rail parapets; (ii) one retrofit for the post location directly adjacent to sloped-end bridge rail parapets; and (iii) one retrofit for all post locations not directly adjacent to the bridge rail end.

5.3.1 Retrofit 1 – Positions Adjacent to Blunt-End Parapets

Modifications to the bridge rail shape itself were considered outside of the scope of this project. Therefore, a structure element of sufficient stiffness and strength would attach to the transition rail and serve as a surrogate to the missing post at this location. The concept developed for this post location utilized a horizontal cantilever beam mounted on the back side of the bridge rail, a concept somewhat similar to that used in the Nebraska thrie beam transition that was tested in 2000 at TTI [19]. It was believed that properly-designed adhesive anchors would provide the required strength and not affect parapet integrity. The horizontal beam would be vertically centered with the thrie beam at a height of 21.65 in. (550 mm) and directly connected to the back side of the thrie beam rail with breakout and attachment hardware. This configuration, as shown in Figure 23, would maintain basic system function and allow the bridge rail, horizontal beam, and anchors rather than the soil to provide the necessary lateral resistive forces.

5.3.1.1 Anchor Design

Chemical-adhesive anchors presented the most efficient and least invasive method available for connecting the horizontal beam to the concrete bridge rail end. Further, these anchor devices utilized relatively short embedment depths and would not protrude from the front

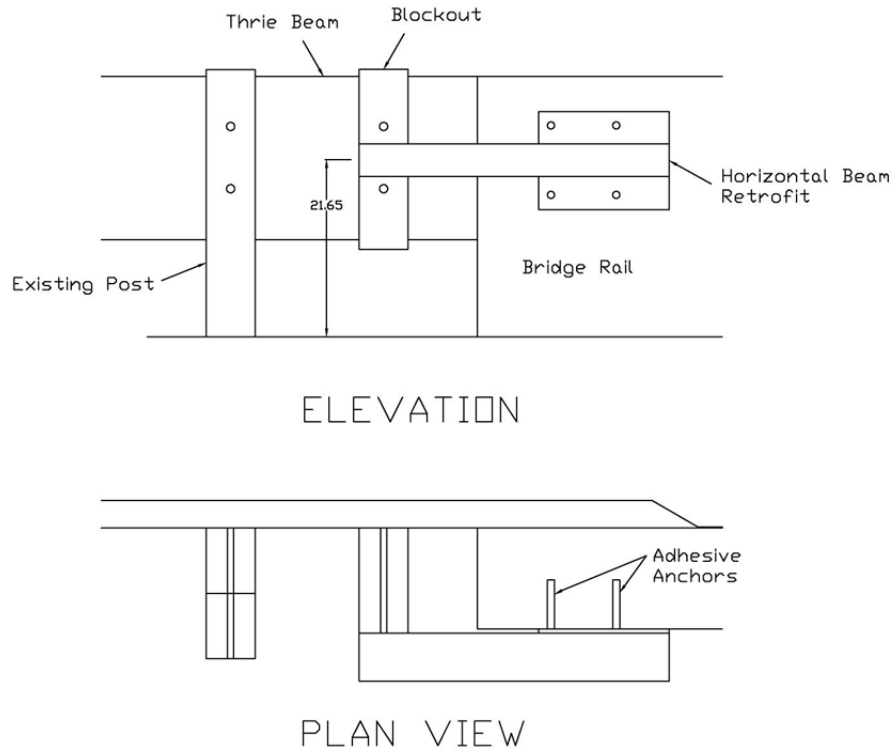


Figure 23. Blunt-End Parapet Retrofit Concept

face of the bridge rail as would a through-bolt configuration. Supplementary design variables (e.g., required size of the base plate, length of the beam, etc.) were dependent upon the anchor configuration itself. Factors considered regarding the layout of anchors included: (i) number of anchors required to resist impact loading; (ii) minimum spacing between anchors; (iii) anchor clear distance from concrete edge; (iv) anchor embedment depth; and (v) specific geometric characteristics of the bridge rail.

The horizontal beam represented a cantilever member which was restrained along the upstream plane of anchors. From simple solid mechanics, the moment reaction at the fixed end of a cantilever beam is linearly dependent upon the moment arm of the applied load. To minimize the loading induced into the anchors, it was essential to place the anchors as close to the vertical face of the parapet as feasibly possible. Due to the uncertainty associated with concrete edge effects, a lateral distance of no smaller than 8 in. (203 mm) was considered.

Wisconsin DOT standards for blunt-end parapets illustrated vertical reinforcing steel approximately 8 in. (203 mm) away from the edge of the parapet. As such, 9 in. (229 mm) was chosen for the lateral distance between the center of the upstream anchors and the edge of the parapet. For the purpose of redundancy, two pairs (4 anchors) were chosen. The proposed anchor placement, as shown in Figure 24, created a 20¹/₂-in. (521-mm) long moment arm from the adjacent post position to the center of the upstream anchor. In addition, no retrofit anchor obstructed the placement of any existing thrie beam attachment through-bolts. In fact, each retrofit anchor was spaced at least 3 in. (76 mm) away from the nearest thrie beam attachment through-bolt.

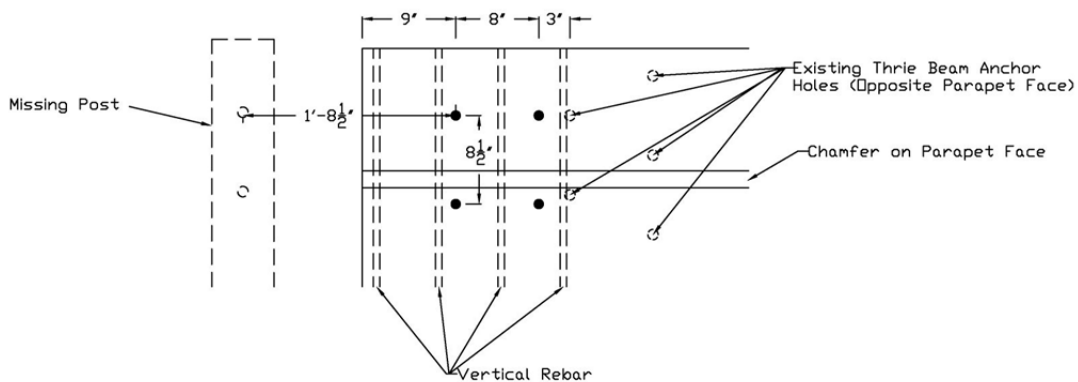


Figure 24. Blunt-End Parapet Retrofit - Proposed Anchor Layout

Dynamic component data utilized in Section 4.2.2 for the BARRIER VII simulation of 6-in. x 8-in. x 7-ft (152-mm x 203-mm x 2.1-m) long wood guardrail posts embedded 52 in. (1,321 mm) on level terrain was used to establish the necessary loading conditions for the retrofit. As such, an average resistive force of 22 kips (98 kN) was to be carried by the horizontal beam to supplement the deficiency created from a missing transition post at location 1. Subsequently, a concentrated load of this magnitude created a moment reaction of 451 kip-in. (51.0 kN-m) for the proposed retrofit beam.

Based on 2011 MwRSF research conducted on adhesive anchors [30], $\frac{5}{8}$ -in. (16-mm) diameter anchors, each with a minimum embedment depth of $5\frac{1}{4}$ in. (133 mm), were chosen for the design. Anchors were positioned in pairs of two and spaced 8 in. (203 mm) apart in an attempt to duplicate the 72.6 kip (323.1 kN) observed resistance, shown previously in Table 1. However, the embedment depth of each anchor was increased to 6 in. (152 mm) to reduce the propensity for anchor pullout. This embedment depth conservatively left $4\frac{3}{4}$ in. (121 mm) of concrete between the end of the anchor and the front face of the parapet.

5.3.1.2 Base Plate Design

Due to the relatively wide spacing required between anchors, direct anchor-flange attachment to the bridge rail was not feasible. Thus, a base plate was required to transfer the loading from the anchors to the horizontal beam. Design parameters examined for the base plate included: (i) width of base plate to satisfy spacing; (ii) length of base plate to develop reasonable forces; and (iii) thickness of base plate to limit yielding.

Anchors were symmetrically oriented away from the x-axis (longitudinal) of loading, as shown in Figure 25. Therefore, loads imparted to anchors equidistant apart and in the same vertical plane would be equivalent. An arbitrary height of 12 in. (305 mm) was chosen for plate design. This height allowed for an anchor spacing of $8\frac{1}{2}$ in. (216 mm), which provided adequate workable space for welds, bolt holes, and placement of a beam flange.

In contrast, anchors were not symmetrically placed about the y-axis (vertical) of loading, as shown in Figure 25. The y-axis of loading was set in line with the upstream pair of anchors, while the second pair of anchors was spaced 8 in. (203 mm) downstream. This loading condition replicated a cantilever beam fully restrained along the upstream plane of anchors. As such, selection of the y-axis dimension (e.g., length) of the base plate was dependent upon minimizing the applied load imparted to the anchors. As such, the y-axis plate dimension was determined

based on an analysis performed with Hilti Anchor Profis software [50]. Various plate lengths were examined in an attempt to produce reasonable tension and compression zones in the plate and minimize individual anchor loads, as shown in Table 17.

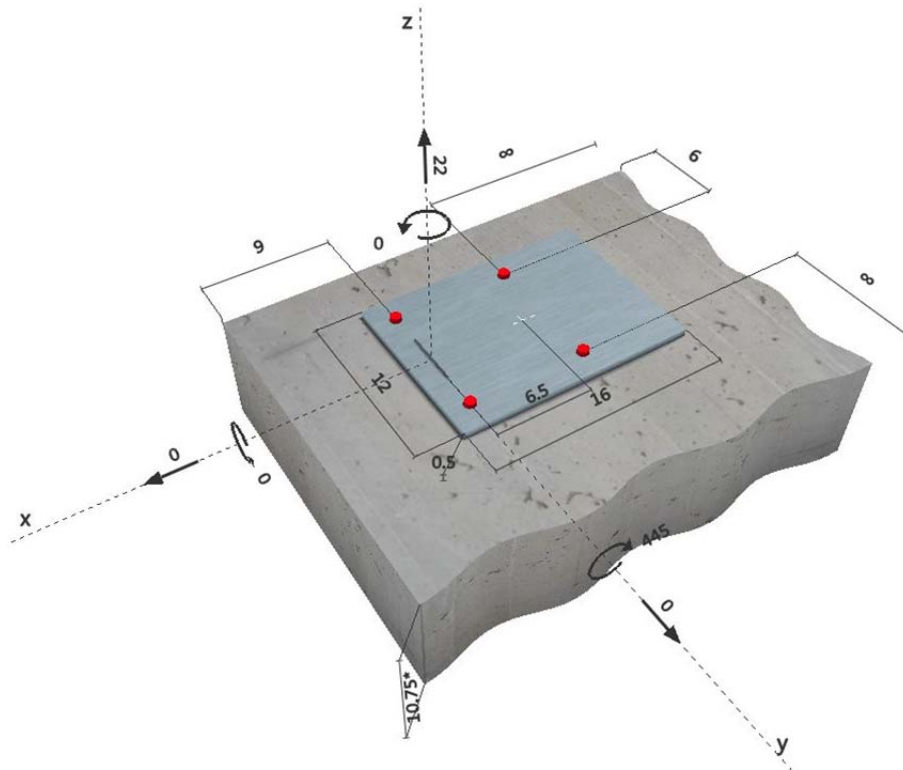


Figure 25. Blunt-End Parapet Retrofit – Base Plate Model

Table 17. Blunt-End Parapet Retrofit – Base Plate Analysis Results

Total Plate Length (in.)	Tension Per Anchor (kips)	
	Upstream Pair	Downstream Pair
11	36.4	0.0
12	33.8	0.6
14	28.6	5.1
16	24.5	7.3
18	21.5	8.4

A $\frac{5}{8}$ -in. (16-mm) diameter, ASTM A193 Grade B7 threaded rod has an ultimate tensile capacity of 28.2 kips (126 kN). Results from the base plate analysis demonstrated that a 16-in.

(406-mm) long plate was necessary to reduce the tensile force in the bolts below their ultimate threshold. At this plate length, each of the anchors in the upstream pair would carry a tensile force of 24.5 kips (109 kN), while each of the anchors in the downstream pair would carry a tensile force of 7.3 kips (32.5 kN). This projected load is approximately 30 percent less than the tested capacity of similar anchors, as shown previously in Table 1. Thus, it was determined that the anchors would not fracture or breakout from the concrete during impact events.

Although these values were less than the ultimate tensile strength for $5/8$ -in. (16-mm) diameter bolts, these calculations did not include any factors of safety. To ensure that the anchors do not fail, the diameter of each anchor was increased to $3/4$ in. (19 mm). The research team believed that increasing the diameter of the anchors was more economically feasible than increasing the length of the base plate and beam. A $3/4$ -in. (19-mm) diameter, ASTM A193 Grade B7 threaded rod has an ultimate tensile capacity of 41.8 kips (186 kN), thus providing a safety factor of 1.7 without considering reduction factors and based solely on ultimate strengths.

Base plates are typically designed as rigid members that prohibit prying action and subsequent deflections of the members which they support. As such, the methods utilized in the *Steel Construction Manual* [51] to calculate the minimum thickness of steel required to avoid flexural yielding of the base plate produced a plate thickness in excess of 2 in. (51 mm). However, for the purpose of this device, yielding in the base plate was desired to disperse some of the impact energy through plate deformation. Therefore, a value of $1/2$ in. (13 mm) was specified as the thickness of the base plate.

5.3.1.3 Horizontal Beam Design

Two performance criteria were considered during the design of the horizontal beam member: (i) its ability to adequately resist impact loading and (ii) its ability to efficiently transfer impact loading to the anchors. To optimize flexural resistance and minimize weight, only

sufficiently-sized, wide-flanged beam sections that are typically utilized in roadside design were considered. Additionally, the horizontal member was purposely designed to plastically deform in flexure. The onset of plastic behavior would allow a portion of the impact forces to be absorbed through beam deformation and limit the forces transferred to the anchors. Subsequently, this selection would reduce the propensity for anchor pull-out and damage to the concrete parapet.

The standard equation for the static, plastic flexural capacity of a beam is shown below in Equation 2. However, steel sections subjected to dynamic loads typically have the ability to withstand higher forces than during static loading. A notable study involving the testing of structural steel members attributed this phenomena to an inverse relationship between the yield strength of the material and the rate at which the material strains (e.g., strain rate) [52]. To account for this increase in strength and avoid over-designing the member, a dynamic factor was incorporated into the bending equation, as shown in Equation 3. Based on the research team's prior experience with dynamically-loaded, anchored steel posts, a magnification factor of 1.5 was selected. As such, a yield strength of 50 ksi (345 MPa) in combination with a design moment of 451 kip-in (51.0 kN-m) and a magnification factor produced a required plastic section modulus of 6.01 in.³ (98.5 cm³). Two standard wide-flange sections, W6x8.5 (W152x12.6) and W6X9 (W152x13.4), closely matched this value, as shown in Table 18. Although either section was suitable, the research team selected a W6x9 (W152x13.4) member for beam design.

$$\text{Static} \qquad \qquad \qquad M_{p,S} = \sigma_y Z_x \qquad \qquad \qquad (2)$$

$$\text{Dynamic} \qquad \qquad \qquad M_{p,D} = 1.5\sigma_y Z_x \qquad \qquad \qquad (3)$$

Where:

- M_p = moment capacity
- σ_y = yield strength
- Z_x = plastic section modulus
- 1.5 = dynamic increase factor

Table 18. Flexural Capacities of Common W-Shapes

Common W-Beam Sections	Z_x (in. ³)	$M_{p,D}$ ^a (kip-in.)
W6x25	18.90	1418
W6x20	14.90	1118
W6x16	11.70	878
W6x15	10.80	810
W6x12	8.30	623
W6x9	6.23	467
W6x8.5	5.73	430

^a With 1.5 dynamic increase factor.

5.3.1.4 Weld Design

To achieve proper stiffness and strength, the beam needed to be rigidly attached to the base plate. Therefore, the connection between the base plate and the flange of the horizontal beam consisted of three fillet welds, as shown in Figure 26: (i) a 1/4-in. (6-mm) thick vertical fillet weld along the entire upstream edge of the beam-plate overlap; (ii) a 3/16-in. (5-mm) thick longitudinal fillet weld along the upper beam flange edge; and (iii) a 3/16-in. (5-mm) thick longitudinal fillet weld along the lower beam flange edge. All sizing parameters developed for the connection design were consistent with criteria presented in the *Steel Construction Manual* [51] and were also confirmed by the fabricator.

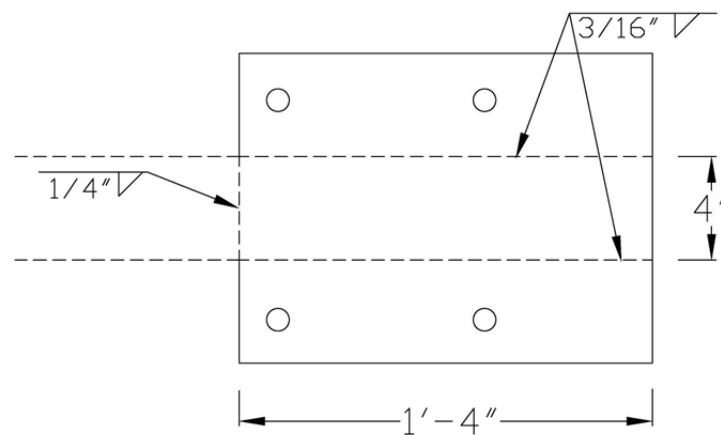


Figure 26. Blunt-End Parapet Retrofit – Base Plate Weld Design

5.3.1.5 Additional Design Considerations

Initially, there was concern regarding the mounting of this retrofit onto a blunt-end concrete parapet. In particular, a 1⁵/₈-in. (41-mm) deep chamfer exists on the backside face of the parapet, which created an overhang along the entire bottom edge of the base plate. As such, the contact area between the parapet and the base plate in the compression region was reduced, which had the potential to cause local plate buckling. To alleviate these concerns, a material (or object) of high compressive strength was needed to fill this gap between the bottom of the base plate and the back face of the concrete parapet. One such remedy would be to weld three 1⁵/₈-in. (41-mm) long 2-in. x 2-in. x 1/4-in. (51-mm x 51-mm x 6-mm) tubes to the plate, as shown in Figure 27. One tube would surround each of the two exposed anchors and one tube at the downstream edge of the base plate would compensate for the missing contact pressure. The three tubes need only be tack-welded into place as they will only be subjected to compressive loading. Many other objects of adequate strength and durability, including washers, wood blocks, and other steel shapes, could also be used to fill the gap.

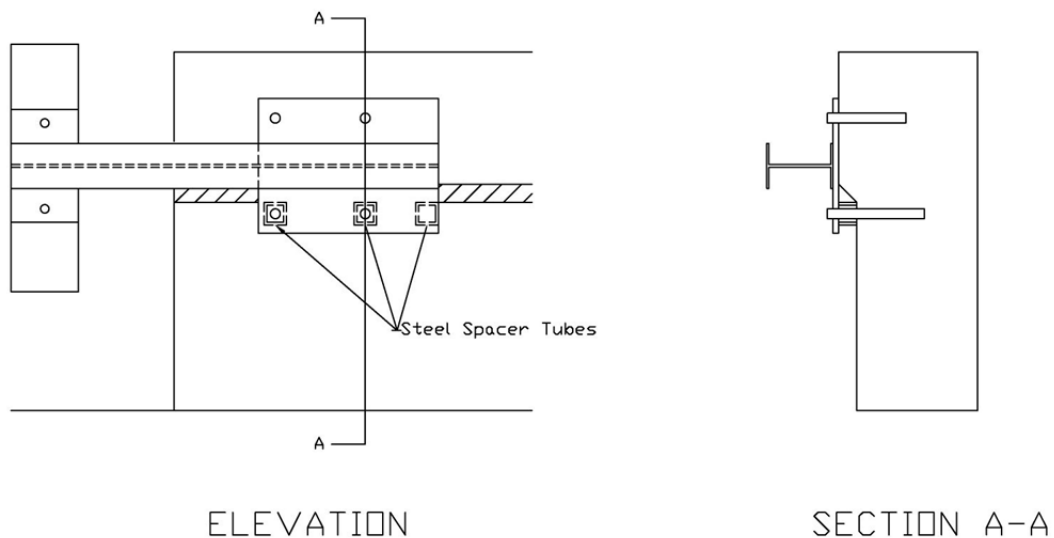


Figure 27. Blunt-End Parapet Retrofit – Steel Spacer Tubes

5.3.2 Retrofit 2 – Positions Adjacent to Sloped-End Parapets

Similar to the previous retrofit adjacent to blunt-end concrete parapets, modifications to the sloped-end bridge rail itself were again outside the scope of this project. As such, a horizontally-mounted retrofit design similar to the one developed for the blunt-end parapet was considered. Anchor, base plate, and beam details were altered accordingly to satisfy the new loading conditions. Effort was taken to ensure that both designs were as comparable as possible.

5.3.2.1 Anchor Design

It was desired to utilize the same anchorage design for both the blunt-end and sloped-end concrete barriers. Thus, four $\frac{3}{4}$ -in. (16-mm) diameter anchors (2 pairs) embedded 6 in. (152 mm) into the concrete parapet were chosen for retrofit design. To minimize the loading induced into the anchors, it was essential to place the anchors as close to the adjacent post position as feasibly possible. Due to the uncertainty associated with concrete edge effects, no location upstream of the upper slope break point of the parapet was considered for anchor placement. Further, Wisconsin DOT standards for sloped-end parapets illustrated reinforcing steel 4 in. (102 mm) downstream from the slope break point of the parapet. Therefore, the first line of anchors was positioned 2 in. (51 mm) downstream of the slope break point. The proposed anchor placement, as shown in Figure 28, created a $33\frac{1}{2}$ -in. (851-mm) long moment arm from the center of the first post position to the center of the nearest anchor. In addition, no retrofit anchor obstructed the placement of any existing thrie beam attachment through-bolts. In fact, each retrofit anchor was spaced at least 3 in. (76 mm) from the nearest thrie beam attachment through-bolt. Utilizing the same design load of 22 kips (98 kN) to replace the stiffness and strength of the missing post, the design moment for the retrofit beam was calculated to be 737 kip-in. (83.3 kN-m).

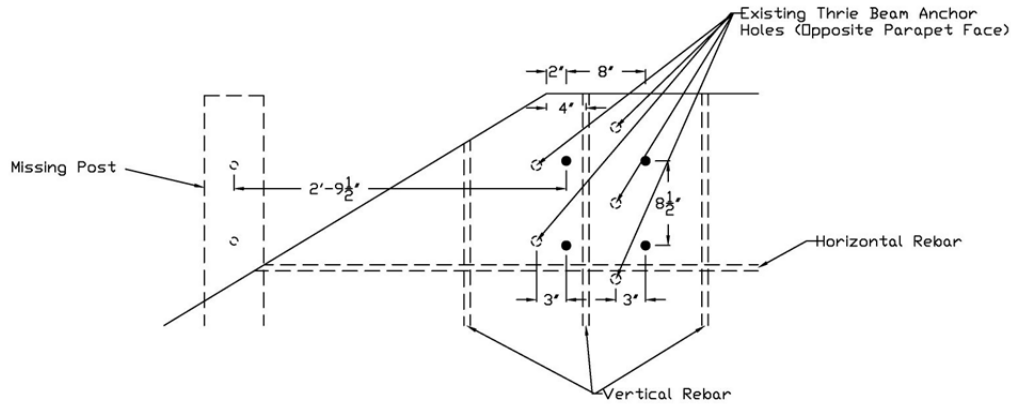


Figure 28. Sloped-End Parapet Retrofit – Proposed Anchor Layout

5.3.2.2 Base Plate Design

The base plate utilized the same 12 in. (305 mm) length as the previous design. Likewise, the anchor pairs were spaced 8 in. (203 mm) longitudinally and 8¹/₂ in. (216 mm) vertically. The y-axis dimension (e.g., length) of the base plate was again determined based on analysis performed with Hilti Anchor Profis software [50]. Various plate lengths were examined in an attempt to minimize individual anchor loading, as shown in Table 19. The analysis demonstrated that a 20-in. (406-mm) long plate produced similar anchor loadings to those predicted for the blunt-end design. At this plate length, each of the anchors in the upstream vertical pair would carry a tensile force of 25.7 kips (114 kN), while each of the anchors in the downstream vertical pair would carry a tensile force of 11.7 kips (52 kN). The plate thickness of ½ in. (13 mm) was also retained to allow for the absorption of some impact energy through plate yielding.

Table 19. Sloped-End Parapet – Base Plate Analysis Results

Total Plate Length (in.)	Tension Per Anchor (kips)	
	Upstream Pair	Downstream Pair
16	34.0	9.8
18	29.3	11.2
20	25.7	11.7
22	23.0	11.8

5.3.2.3 Horizontal Beam Design

To resist impact loading, only sufficiently-sized wide-flanged beam sections that are typically utilized in roadside design were considered. However, to keep the vertical spacing of the anchors the same, only members with 4 in. (102 mm) flange widths were considered. Equation 3 along with a design moment of 737 kip-in. (83.3 kN-m), a yield strength of 50 ksi (345 MPa), and a dynamic magnification factor, produced a plastic section modulus of 9.83 in.³ (161 cm³). Recall, the beam was to deform plastically during impact to ensure that the anchors would not be overloaded. Thus, a plastic section modulus of 9.83 in.³ (161 cm³) was deemed the maximum. The closest standard beam section for this plastic section modulus, without exceeding it, was a W6x12 (W152x17.9), as shown in Table 20.

Table 20. Flexural Capacities of Common W-Shapes with 4-in. Flange Widths

Common W-Beam Sections	Z _x (in. ³)	M _{p,D} ^a (kip-in.)
W6X16	11.70	878
W6X12	8.30	623
W6X9	6.23	467
W6X8.5	5.73	430

^a With 1.5 dynamic increase factor.

5.3.2.4 Weld Design

Similar weld details to those used in the previous design were utilized to rigidly attach the beam and base plate together as part of the sloped-end missing post retrofit design. Therefore, the connection between the base plate and the flange of the horizontal beam consisted of three fillet welds: (i) a 1/4-in. (6-mm) thick vertical fillet weld along the entire upstream edge of the beam-plate overlap; (ii) a 3/16-in. (5-mm) thick longitudinal fillet weld along the upper beam flange edge; and (iii) a 3/16-in. (5-mm) thick longitudinal fillet weld along the lower beam flange edge. All sizing parameters developed for the connection design were consistent with

criteria presented in the *Steel Construction Manual* [51] and were also confirmed by the fabricator.

5.3.2.5 Additional Design Considerations

There were concerns regarding the mounting of this retrofit onto a sloped-end concrete parapet. First, the position of the base plate configuration prevented the installation of the thrie beam anchor through-bolts, as shown in Figure 29. Thrie beam anchor bolts are essential in resisting shear loading and prying action at the attachment location of the thrie beam end shoe to the parapet. As such, it is recommended that those affected through-bolts be re-installed using a shorter, chemical-adhesive anchor sleeve with bolt or threaded rod with limited excess threads using the same or modified hole. This solution should provide adequate shear resistance for the end shoe anchor while not intruding upon the retrofit hardware on the opposite face. Second, the sloping end of the parapet interfered with the installation of a standard blockout, as shown in Figure 29. As such, the bottom third of the blockout was specified to be removed to fit within the available space.

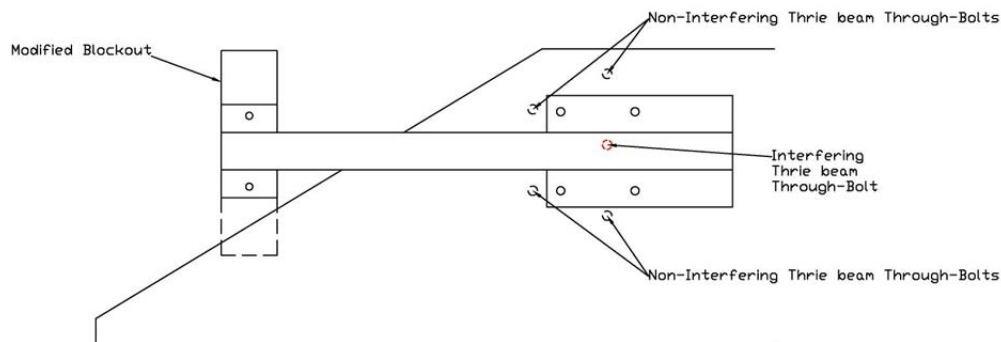


Figure 29. Sloped-End Parapet Retrofit Concerns

5.3.3 Retrofit 3 – Positions Not Adjacent to Concrete Bridge Parapets

The most straightforward concept involved the attachment of additional blockouts to an affected post to laterally shift the post beyond an above or below grade obstruction. In fact,

existing Wisconsin DOT standards permitted the use of double and triple blocked-out posts on level terrain to mitigate posts beyond underground obstructions, as shown in Figure A-5 of Appendix A [53]. However, transition posts not adjacent to the bridge rail were commonly affected by the placement of drainage outlets directly in the position specified for post installation. This drainage structure extended 6 ft (1.8 m) laterally beyond the roadway. As such, the addition of two or three blockouts to an affected post would not project the post sufficiently beyond the path of the drainage structure.

As a result, relocation of the drainage structure upstream of the W-to-thrie element was considered. This solution was ideal from a safety standpoint as it allowed for proper post installation throughout the transition region. However, this extreme alternative had significant construction costs associated with it and was deemed economically infeasible.

Subsequently, a concept was developed which utilized two surrogate posts in an attempt to ‘straddle’ over the lateral drainage structure rather than beyond it. The two surrogate posts would be linked by a horizontally-mounted beam and attached at mid-span to the thrie beam transition (i.e., location of missing post) with the use of several blockouts.

5.3.3.1 Surrogate Member Selection

Although the 18-ft 9-in. (5.7-m) long transition system and the 31-ft 3-in. (9.5-m) long transition system utilized wood posts as the supporting members, W6x9 (W152x13.4) steel posts were chosen as the surrogate post members. This choice was made due to the fact that steel posts can easily be driven into the ground with minimal site work, a quality conducive to retrofitting a permanent structure. In addition, steel posts can easily be modified for accepting cross-beam members. The spacing between each of the surrogate posts was dependent upon the clear distance required to span over a lateral drainage structure. As such, a center-to-center spacing of 3 ft (0.9 m) between surrogate posts was chosen. This distance allowed the retrofit to span over

2-ft (0.6-m) wide drainage structures. In particular, Wisconsin DOT standards illustrated that surface drainage flumes adjacent to bridge rails were configured with a 2 ft (0.6 m) width.

As shown previously in Figure 17, two W6x9 (W152x13.4) steel posts embedded 43 in. (1,092 mm) on level terrain, spaced $18\frac{3}{4}$ in. (476 mm) apart, and acting in parallel can provide an average post-soil resistance of 21.9 kips (97.4 kN). This resistance was also the maximum design resistance determined for a single 6-in. x 8-in. x 7-ft (152-mm x 203-mm x 2.1-m) long wood post embedded 52 in. (1,321 mm) into the soil on level terrain, as shown in Figure 30.

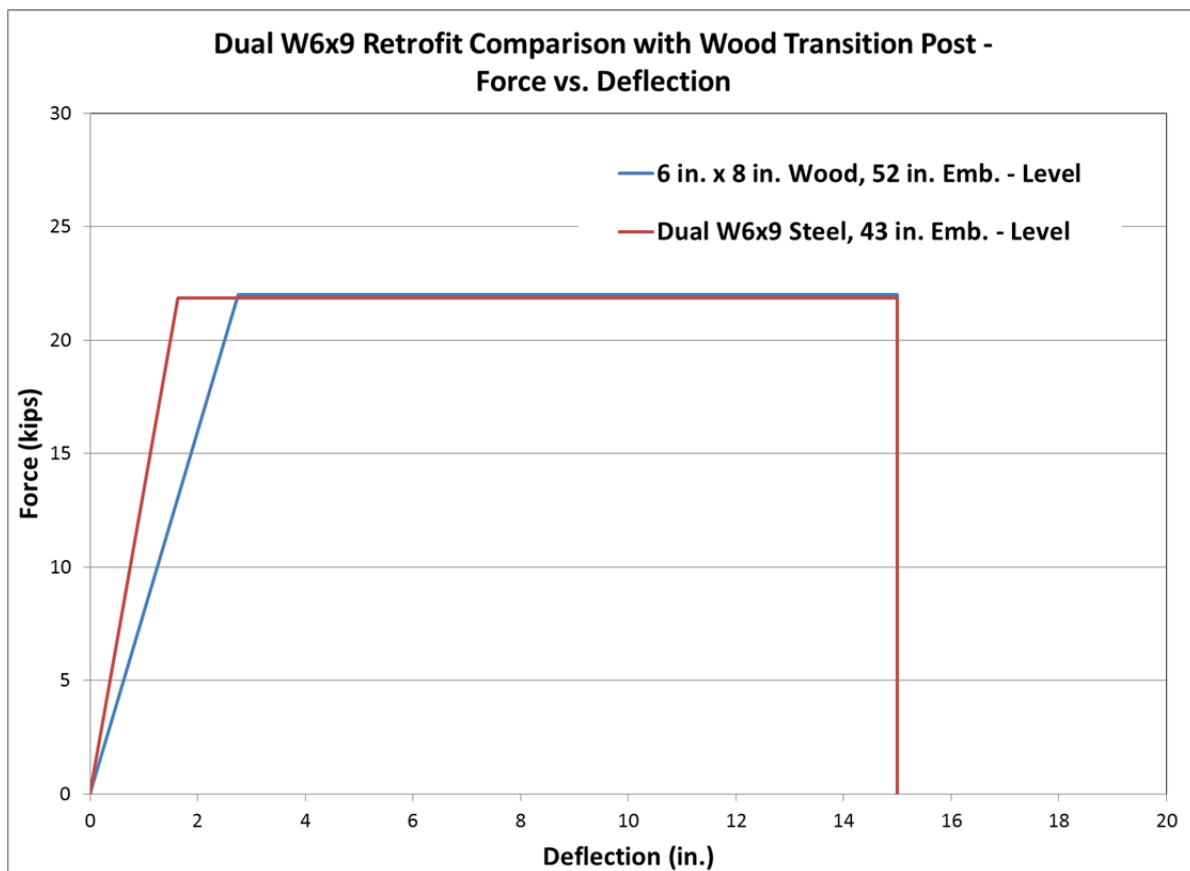
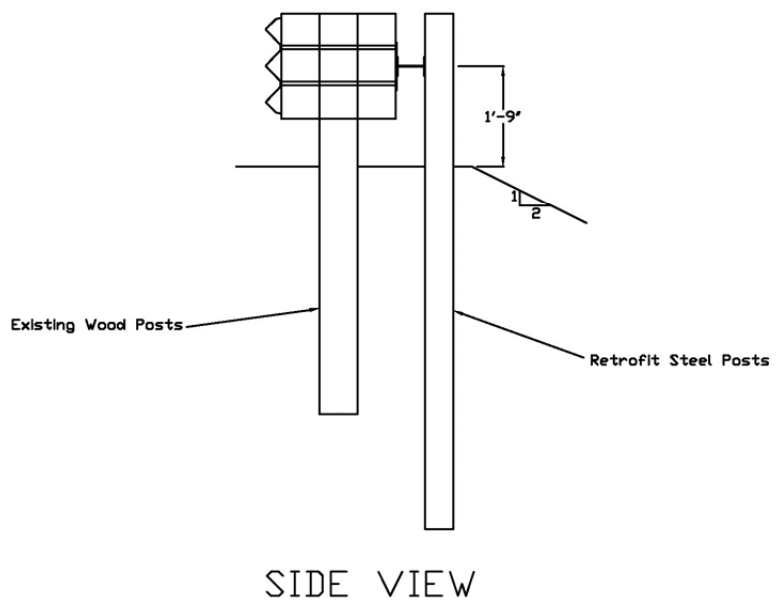
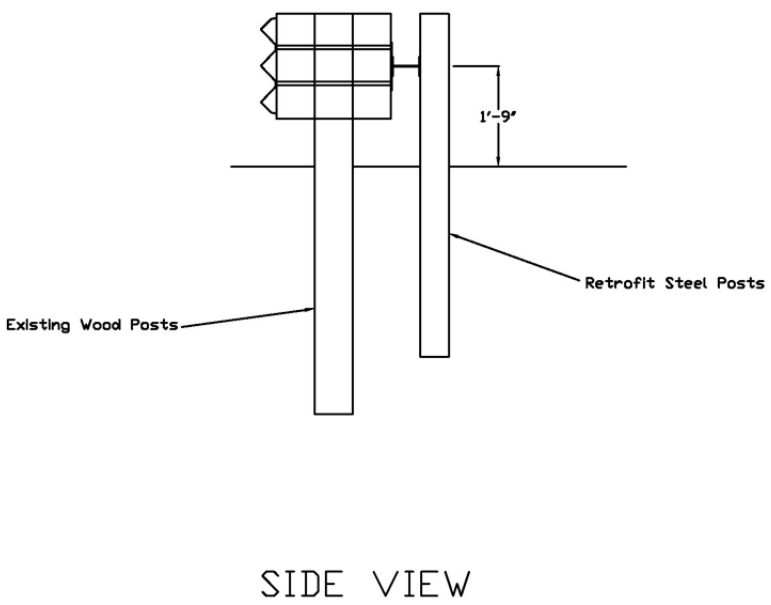
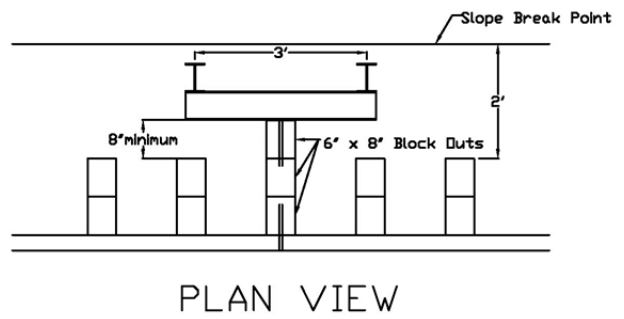
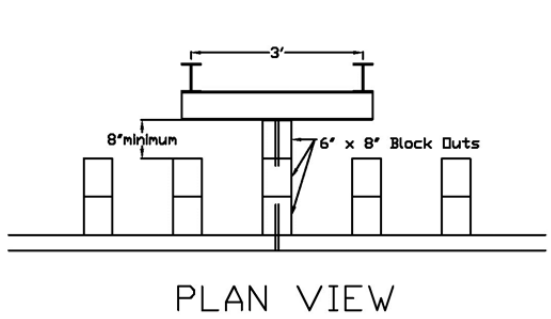


Figure 30. Level Terrain Dual W6x9 Retrofit - Force vs. Deflection

Three 6-in. x 8-in. (152-mm x 203-mm) wood blockouts would laterally offset the retrofit hardware away from the thrie beam rail, as shown in Figure 31.



(a) Level Terrain

(b) 2H:1V Sloped Terrain

Figure 31. Proposed Dual Post Retrofit for Missing Posts

This lateral offset was ideal because it created an 8-in. (203-mm) clear spacing between the front face of the horizontal beam and the backside of any existing transition post directly nearby. A review of film data from the original 1998 MwRSF Iowa transition study [20] revealed that no wood transition post dynamically deflected more than 2.3 in. (58 mm) relative to an adjacent transition post, as shown in Table 21. Therefore, the 8-in. (203-mm) lateral offset ultimately minimized the propensity for a vehicle to snag on the retrofit itself and did not cause increased barrier stiffness and additional propensity for vehicle pocketing.

Table 21. Relative Dynamic Deflections between Consecutive Wood Transition Posts [20]

Crash Test No. ITNJ-4	Maximum Relative Dynamic Deflection Between Posts					
	1 & 2 (in.)	2 & 3 (in.)	3 & 4 (in.)	4 & 5 (in.)	5 & 6 (in.)	6 & 7 (in.)
	1.12	1.12	1.07	1.20	2.30	0.99

In addition, roadsides containing drainage structures are often associated with sloped terrain. When slopes lay parallel to the roadside, 2 ft (0.6 m) of generally level grading (i.e., 10H:1V terrain) is required behind the back face of a transition post. The previously mentioned lateral offset created by three 6-in. x 8-in. (152-mm x 203-mm) wood blockouts would position the surrogate steel posts within the 2 ft (0.6 m) region of level terrain. This choice allowed the surrogate posts to essentially remain at an impact height of 21.65 in. (550 mm).

Although each surrogate post would be located within the 2 ft (0.6 m) of level grading, the lateral offset positioned the posts near the slope break point of the roadside. Subsequently, sloped terrain has a major effect on guardrail post performance. The post-soil resistance is dependent upon the slope of terrain as well as a post’s proximity to the slope break point. Posts placed near or at steeper slopes will produce lower average resistive forces. Thus, different fill slopes require different post embedment depths and corresponding lengths to develop adequate

resistive forces sufficient to redirect errant vehicles. As such, consideration of a 2H:1V fill slope behind the transitions would produce a design alternative with longer surrogate post members; since, it corresponded with the minimum post-soil resistance condition.

Results from recent dynamic component tests conducted on 9-ft (2,743-mm) long, W6x9 (W152x13.4) steel posts embedded 76 in. (1,930 mm) at the slope break point of a 2H:1V fill slope, test nos. MGS221PT-27 and MGS221PT-28, were used for the second design alternative of the surrogate posts [7]. For the two tests, the results revealed an average force of 8.65 kips (38.5 kN) over 15 in. (381 mm) of deflection. However, this average force corresponded to an impact height of $24\frac{7}{8}$ in. (632 mm), whereas the surrogate posts would utilize an impact height of 21.65 in. (550 mm). Therefore, it was necessary to relate the two impact heights and modify the post-soil forces.

Post yielding was the primary mode of failure during the recent testing series. Each post was assumed to represent a linear-elastic, cantilever beam restrained at ground line. As such, the yield moment of each post was dependent upon the impact height utilized in the tests. For linear-elastic behavior, identical post members composed of the same material should behave similarly. Therefore, the yield moment for a steel post corresponding to an impact height of $24\frac{7}{8}$ in. (632 mm), $M_{y,MGS}$, should be the same as the yield moment for an identical steel post corresponding to an impact height of 21.65 in. (550 mm), $M_{y,metric}$. Solving for the average load in Equation 4 resulted in an average force of 9.94 kips (44.2 kN) for a 9-ft (2.7-m) long W6x9 (W152x13.4) steel post placed at the break point of a 2H:1V slope and impacted at a height of 21.65 in. (550 mm).

$$24.875 \times 8.65 = 21.65 \times P_{ave} \quad (4)$$

In addition, it was also assumed that the post-soil resistance corresponding to a single post could be scaled accordingly to represent multiple identical posts acting in unison. As such,

the combined average post-soil force over 15 in. (381 mm) of deflection for two 9-ft (2,743-mm) long W6x9 (W152x13.4) steel posts placed in parallel and near the slope break point of a 2H:1V fill slope was 19.9 kips (88.4 kN). This idealized post-soil response is shown in Figure 32 along with the idealized BARRIER VII response for a 6-in. x 8-in. x 7-ft (152-mm x 203-mm x 2.1-m) long wood post embedded 52 in. (1,321 mm) into soil on level terrain. The difference in absorbed energy between a wood transition post and two steel surrogate posts was only 3, 5, and 6 percent over 8 in. (203 mm), 10 in. (254 mm), and 15 in. (381 mm) of deflection, respectively. As such, the anticipated differences in barrier performance during vehicular impact events would generally be negligible.

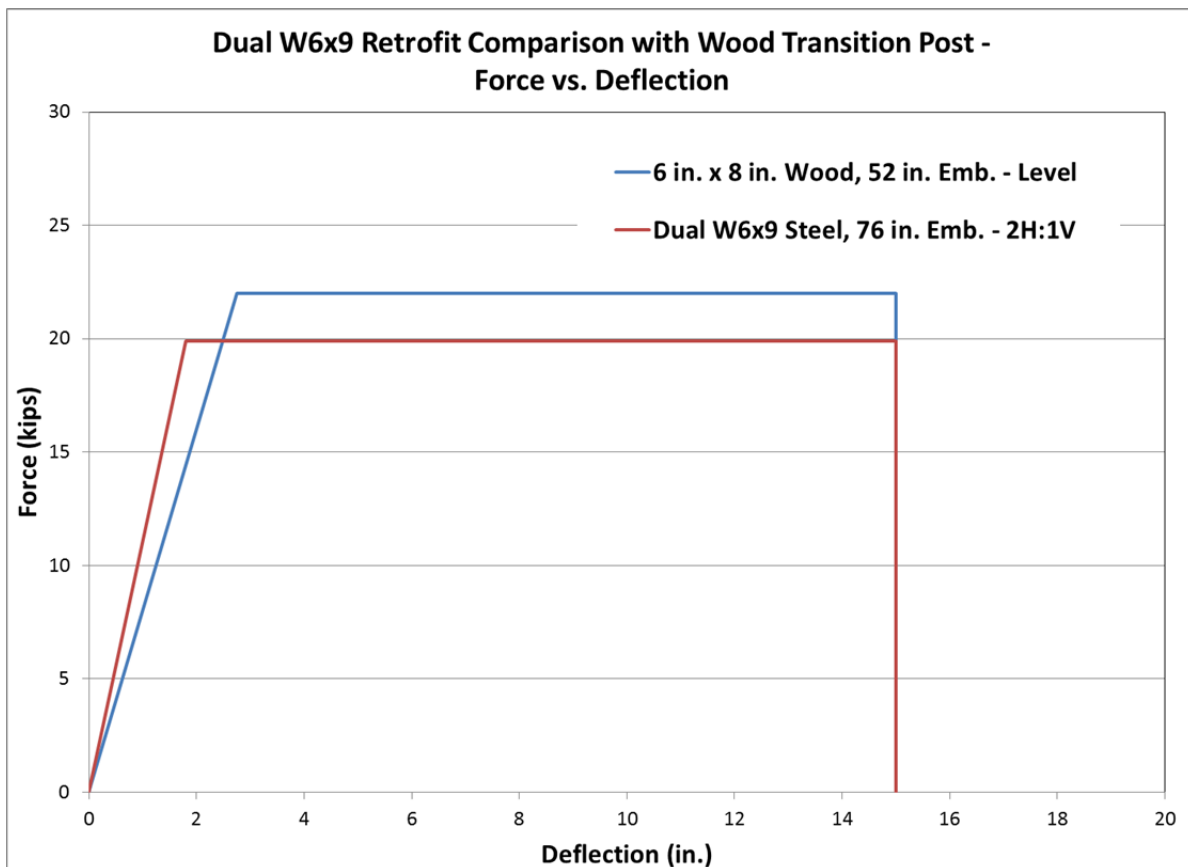


Figure 32. Sloped Terrain Dual W6x9 Retrofit – Force vs. Deflection

5.3.3.2 Surrogate Member Connection

It was necessary to provide an adequate connection between the two surrogate posts to ensure both posts would indeed act in unison. This behavior was accomplished by selecting a connecting member that could be treated as virtually rigid under the specified loading conditions (i.e., no yielding during impact). In particular, the loading conditions of the horizontal connecting member consisted of a 3-ft (0.9-m) long pinned-pinned beam with a concentrated load of 19.9 kip (88.4 kN) at mid-span. The maximum moment imparted to a simply supported beam with a concentrated load at mid-span is shown in Equation 5.

$$M_{u,mid} = \frac{PL}{4} \quad (5)$$

Where:

$M_{u,mid}$ = ultimate moment at midspan

P = applied load

L = beam length

The aforementioned values for applied load and beam length were input into Equation 5 to produce an ultimate moment of 179 kip-in. (20.2 kN-m). A common roadside hardware element, the W6x9 (W152x13.4) ASTM Grade 50 steel post, has a plastic bending capacity of 312 kip-in. (35.2 kN-m). As such, a W6x9 (W152x13.4) Grade 50 steel member was chosen for the horizontal connection member.

5.4 Summary

Initial BARRIER VII simulations of the 18-ft 9-in. (5.7-m) long and 31-ft 3-in. (9.5-m) long transition systems with missing posts indicated that retrofit designs were necessary to provide the appropriate stiffness and strength for each deficient system. Therefore, three interchangeable retrofit designs were developed to satisfy various missing post locations within the transition region of both barrier systems. The first design consisted of a W6x9 (W152x13.4) steel post horizontally mounted to a blunt-end concrete parapet by four $\frac{3}{4}$ -in. (19-mm) diameter

ASTM A193 Grade B7 threaded rods placed in the concrete parapet with a chemical-adhesive anchor system. The upstream end of the post directly attached to the thrie beam at the post location adjacent to the bridge rail with a wood blockout. Similarly, the second design consisted of a W6x12 (W152x17.9) steel post horizontally mounted to a sloped-end concrete parapet by four $\frac{3}{4}$ -in. (19-mm) diameter ASTM A193 Grade B7 threaded rods placed in the concrete parapet with a chemical-adhesive anchor system. Again, the upstream end of the post directly attached to the thrie beam at the post location adjacent to the bridge rail with a wood blockout. Both designs required validation through dynamic component testing. However, due to the similarity between designs, it was only deemed necessary to test of one of the two retrofit designs. The sloped-end design was selected for further examination; because, it represented the more critical loading condition for the chemical-adhesive anchors.

The third design consisted of two W6x9 (W152x13.4) steel posts placed in parallel: (i) 6-ft (1.8-m) long and embedded 43 in. (1,092 mm) into the soil with sufficient level terrain or (ii) 9-ft (2.7-m) long and embedded 76 in. (1,930 mm) into the soil at the slope break point of a 2H:1V fill slope. The steel posts would be inter-connected using a W6x9 (W152x13.4) horizontal steel beam which directly attaches to the thrie beam at the appropriate post location upstream from the bridge rail with three wood blockouts. Data from previous dynamic component tests was utilized to develop the retrofit design. Thus, further testing of the surrogate posts was deemed unnecessary, and it was concluded that the retrofit design would be applicable for an individual missing post in either the 18-ft 9-in. (5.7-m) long transition system or the 31-ft 3-in. (9.5-m) long transition system.

In some cases, alternative dual-post retrofit designs may be desired beyond those provided for level terrain and 2H:1V fill slope applications. For example, specific alternatives may be desired for steel posts placed at or near 3H:1V or 4H:1V fill slopes. Based on the best

available information, limited bogie testing data, and engineering judgment, it would seem reasonable to utilize lengths of 6.5 ft (1,981 mm) and 7 ft (2,100 mm) in combination with embedment depths of 46 in. (1,168 mm) and 52 in. (1,321 mm) for steel posts located at or near the slope break point of 4H:1V and 3H:1V fill slopes, respectively.

6 COMPONENT TEST CONDITIONS

6.1 Test Facility

Physical testing was conducted at the MwRSF outdoor testing facility, which is located at the Lincoln Air Park on the northwest side of the Lincoln Municipal Airport. The facility is approximately 5 miles (8 km) northwest from the University of Nebraska-Lincoln's city campus.

6.2 Equipment and Instrumentation

Equipment and instrumentation utilized to collect and record data during the dynamic impact tests included a bogie vehicle, accelerometers, pressure tape switches, high-speed and standard-speed digital video, and digital still cameras.

6.2.1 Bogie

A rigid-frame bogie was used to impact the various posts. A variable-height, detachable impact head was used in the testing program. The bogie head was constructed of 8-in. (203-mm) diameter, ½-in. (13-mm) thick standard steel pipe, with ¾-in. (19-mm) neoprene belting wrapped around the pipe to prevent local damage to the post from the impact. The impact head was bolted to the bogie vehicle, creating a rigid frame with an impact height of 27³/₈ in. (695 mm). The bogie with the impact head is shown in Figure 33. The weight of the bogie with the addition of the mountable impact head and accelerometers was approximately 1,720 lbs (780 kg), but it varied between tests. The actual measured bogie weight for each test can be found in the test data sheets provided in Appendix E.

The tests were conducted using a steel corrugated beam guardrail to guide the tire of the bogie vehicle. A pickup truck was used to push the bogie vehicle to the targeted impact velocity. After reaching the target velocity, the push vehicle braked, thus allowing the bogie to be free rolling as it came off the track. A remote-control braking system was installed on the bogie, thus allowing it to be brought safely to rest after the test. Due to space limitations, test no.

WAGTMP-4 utilized a special pickup truck with a reverse cable tow system to propel the bogie to the target impact speed. When the bogie approached the end of the corrugated beam, it was released from the tow cable, thus allowing it to be free rolling when it impacted the post.



Figure 33. Rigid Frame Bogie on Guidance Track

6.2.2 Accelerometers

Two accelerometer systems were mounted on the bogie vehicle near its center of gravity to measure the acceleration in the longitudinal, lateral, and vertical directions. The first accelerometer, Model EDR-3, was a triaxial piezoresistive accelerometer system manufactured by IST of Okemos, Michigan. The EDR-3 was configured with 256 kB of RAM, a range of ± 200 g's, a sample rate of 3,200 Hz, and a 1,120 Hz low-pass filter. The "DynaMax 1 (DM-1)" computer software program and a customized Microsoft Excel worksheet were used to analyze and plot the accelerometer data.

The second accelerometer system was a two-arm piezoresistive accelerometer system manufactured by Endevco of San Juan Capistrano, California. Three accelerometers were used to measure the longitudinal, lateral, and vertical accelerations independently at a sample rate of 10,000 Hz. The accelerometers were configured and controlled using a system developed and manufactured by Diversified Technical Systems, Inc. (DTS) of Seal Beach, California. More specifically, data was collected using a DTS Sensor Input Module (SIM), Model TDAS3-SIM-16M. The SIM was configured with 16 MB SRAM and 8 sensor input channels with 250 kB SRAM/channel. The SIM was mounted on a TDAS3-R4 module rack. The module rack was configured with isolated power/event/communications, 10BaseT Ethernet and RS232 communication, and an internal backup battery. Both the SIM and module rack were crashworthy. The “DTS TDAS Control” computer software program and a customized Microsoft Excel worksheet were used to analyze and plot the accelerometer data.

6.2.3 Pressure Tape Switches

Three pressure tape switches, spaced at approximately 39-in. (1-m) intervals and placed near the end of the bogie track, were used to determine the speed of the bogie before the impact. As the front tire of the bogie passed over each tape switch, a strobe light was fired sending an electronic timing signal to the data acquisition system. The system recorded the signals and the time each occurred. The speed was then calculated using the spacing between the sensors and the time between the signals. Strobe lights and high-speed video analysis are used only as a backup in the event that vehicle speeds cannot be determined from the electronic data.

6.2.4 Digital Cameras

At least one AOS VITcam high-speed digital video camera and one JVC digital video camera were used to document each test. The AOS high-speed cameras had a frame rate of 500 frames per second and the JVC digital video camera had a frame rate of 29.97 frames per second.

Generally, both cameras were placed laterally from the post, with a view perpendicular to the bogie's direction of travel. The WAGTMP testing series incorporated additional AOS and JVC cameras positioned at an angle to observe localized component behavior during impact. A Nikon D50 digital still camera was also used to document pre- and post-test conditions for all tests.

6.3 End of Test Determination

When the impact head initially contacts the test article, the force exerted by the surrogate test vehicle is directly perpendicular and completely transferred to the anchors. However, as the post begins to yield and deform plastically, the surrogate test vehicle's orientation and path moves farther from perpendicular. This behavior introduces two sources of error: (1) the contact force between the impact head and the post has a vertical component and (2) the impact head slides upward/downward along the test article. Therefore, only the initial portion of the accelerometer trace may be used since variations in the data become significant as the system deforms and the surrogate test vehicle overrides/underrides the system. For this reason, the end of the test needed to be defined.

Guidelines were established to define the end of test time using the high-speed video of the crash test. The first occurrence of any one of the following three events was used to determine the end of the test: (1) the test article fractures; (2) the anchors detach from the concrete parapet; or (3) the surrogate vehicle loses contact with the test article.

6.4 Data Processing

The electronic accelerometer data obtained in dynamic testing was filtered using the SAE Class 60 Butterworth filter conforming to the SAE J211/1 specifications [54]. The pertinent acceleration signal was extracted from the bulk of the data signals. The processed acceleration data was then multiplied by the mass of the bogie to get the impact force using Newton's Second Law. Next, the acceleration trace was integrated to find the change in velocity versus time. Initial

velocity of the bogie, calculated from the pressure tape switch data, was then used to determine the bogie velocity, and the calculated velocity trace was integrated to find the bogie's displacement. This displacement is also the displacement of the beam or post. Combining the previous results, a force vs. deflection curve was plotted for each test. Finally, integration of the force vs. deflection curve provided the energy vs. deflection curve for each test.

6.5 Results

The information desired from the bogie tests was the relation between the applied force and deflection of the beam or post at the impact location. This data was then used to find total energy (the area under the force versus deflection curve) dissipated during each test.

Although the acceleration data was applied to the impact location, the data came from the center of gravity of the bogie. Error was added to the data since the bogie was not perfectly rigid and sustained vibrations. The bogie may have also rotated during impact, causing differences in accelerations between the bogie center of mass and the bogie impact head. While these issues may affect the data, the data was still deemed valid. Filtering procedures were applied to the data to smooth out vibrations, and the rotations of the bogie during test were minor. One useful aspect of using accelerometer data was that it included influences of the post inertia on the reaction force. This fact was important as the mass of the post may affect barrier performance as well as test results.

The values described herein were calculated from the EDR-3 data curves. Although the DTS transducers produced similar results, the EDR-3 has historically provided accurate results. Test results for both transducers are provided in Appendix E.

7 DYNAMIC COMPONENT TESTING – MISSING TRANSITION POSTS

7.1 Purpose

Bogie tests were undertaken on horizontal steel beams (i.e., surrogate posts) attached to a concrete parapet, via four adhesive anchors, to determine the dynamic behavior of the retrofit design configured to replace missing posts adjacent to the bridge rail end. Subsequently, these dynamic test results were used to simulate the retrofit design in actual transition systems to determine its viability as a surrogate post. In particular, the performance of the retrofit was evaluated based on two parameters: (i) the ability of the beam to behave as intended and yield during impact and (ii) the ability of the anchors to restrain the post and base plate system without damaging the concrete parapet or the anchor rods.

Both retrofit designs developed for missing posts adjacent to bridge rails (e.g., blunt-end and sloped-end) were intended to behave similarly during impact events. However, the loads predicted for the anchors of the sloped-end retrofit were slightly higher than the loads predicted for blunt-end parapets. Thus, the critical design selected for dynamic component testing corresponded with sloped-end parapets. As long as the retrofit design configured for sloped-end parapets did not damage the concrete bridge rail, component testing of the retrofit design configured for blunt-end parapets would not be necessary.

7.2 Scope

Two dynamic bogie tests were performed on 57-in. (1,448-mm) long, ASTM A992 Grade 50 W6x12 (W152x17.9) steel beams (i.e., surrogate posts) mounted horizontally on a concrete parapet at a height of $27\frac{3}{8}$ in. (695 mm). For this study, the actual Wisconsin sloped-faced parapet was not replicated as it was considered outside of the scope of this project. Thus, a 40-in. (1,016-mm) tall, 15-in. (381-mm) thick vertical concrete parapet previously constructed at the testing facility was utilized. Thus, anchor placement on the surrogate concrete parapet, and

subsequently the impact height of the bogie vehicle, was selected to replicate the design anchor edge distances for the actual Wisconsin concrete parapet. A 12-in. x 20-in. x $\frac{1}{2}$ -in. (305-mm x 508-mm x 13-mm) ASTM A572 Grade 50 steel base plate was attached flush to the downstream end of each post by three fillet welds: (i) a $\frac{1}{4}$ -in. (6.4-mm) thick vertical fillet weld along the entire upstream edge of the beam-plate overlap; (ii) a $\frac{3}{16}$ -in. (4.8-mm) thick longitudinal fillet weld along the upper beam flange edge; and (iii) a $\frac{3}{16}$ -in. (4.8-mm) thick longitudinal fillet weld along the lower beam flange edge. Material specifications for these components are shown in Appendix F.

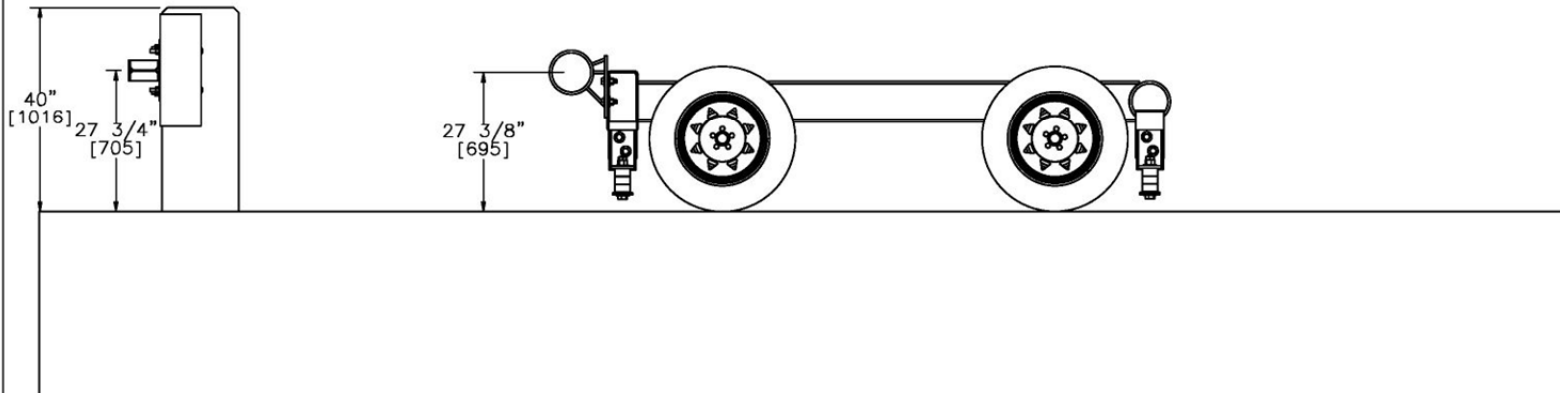
The second test that was conducted on this configuration incorporated two additional $\frac{1}{4}$ -in. (6.4-mm) thick ASTM A36 gusset plates welded to the web and flanges of the steel post. The gusset plates were positioned in plane with the upstream line of anchors.

The post and base plate component was attached to a concrete parapet by four $\frac{3}{4}$ -in. (19-mm) diameter ASTM A193 Grade B7 threaded rods. Each rod was embedded 6 in. (152 mm) into the concrete. A HITLI HIT-RE 500 chemical adhesive, with a bond strength of 1,800 psi (12.4 MPa), was used to permanently attach the anchors into the concrete. A 6-in. x 8-in. x 22-in. (152-mm x 203-mm x 559-mm) wood blockout was attached to the upstream end of each steel post by two $\frac{5}{8}$ -in. (16-mm) diameter guardrail bolts and a $\frac{1}{8}$ -in. (3-mm) thick ASTM A36 steel backup plate which was spot welded to the horizontal post/beam. The blockouts were oriented perpendicular to the horizontal posts and were utilized to transfer the applied load from the bogie head to the post.

The target impact conditions for both tests consisted of a speed of 15 mph (24 km/h) and an angle of 0 degrees, thus creating strong-axis bending in the steel post. The test setup and configuration details are shown in Figures 34 through 41.

Test No.	Test Quantity	Target Speed	Impact Orientation	Bogie No.
WAGT MP-1	1	15 mph [24.1]	Normal to the Barrier	3
WAGT MP-4	1	15 mph [24.1]	Normal to the Barrier	3

106




 Midwest Roadside Safety Facility	WSDOT AGT Missing Post	SHEET: 1 of 8
	Impact	DATE: 3/27/2012
DWG. NAME: WAGT-MP4_R4	SCALE: 1:30 UNITS: in.[mm]	DRAWN BY: JGP/MDM
		REV. BY: ERJ

Figure 34. WAGTMP Bogie Testing Matrix and Setup – Elevation View

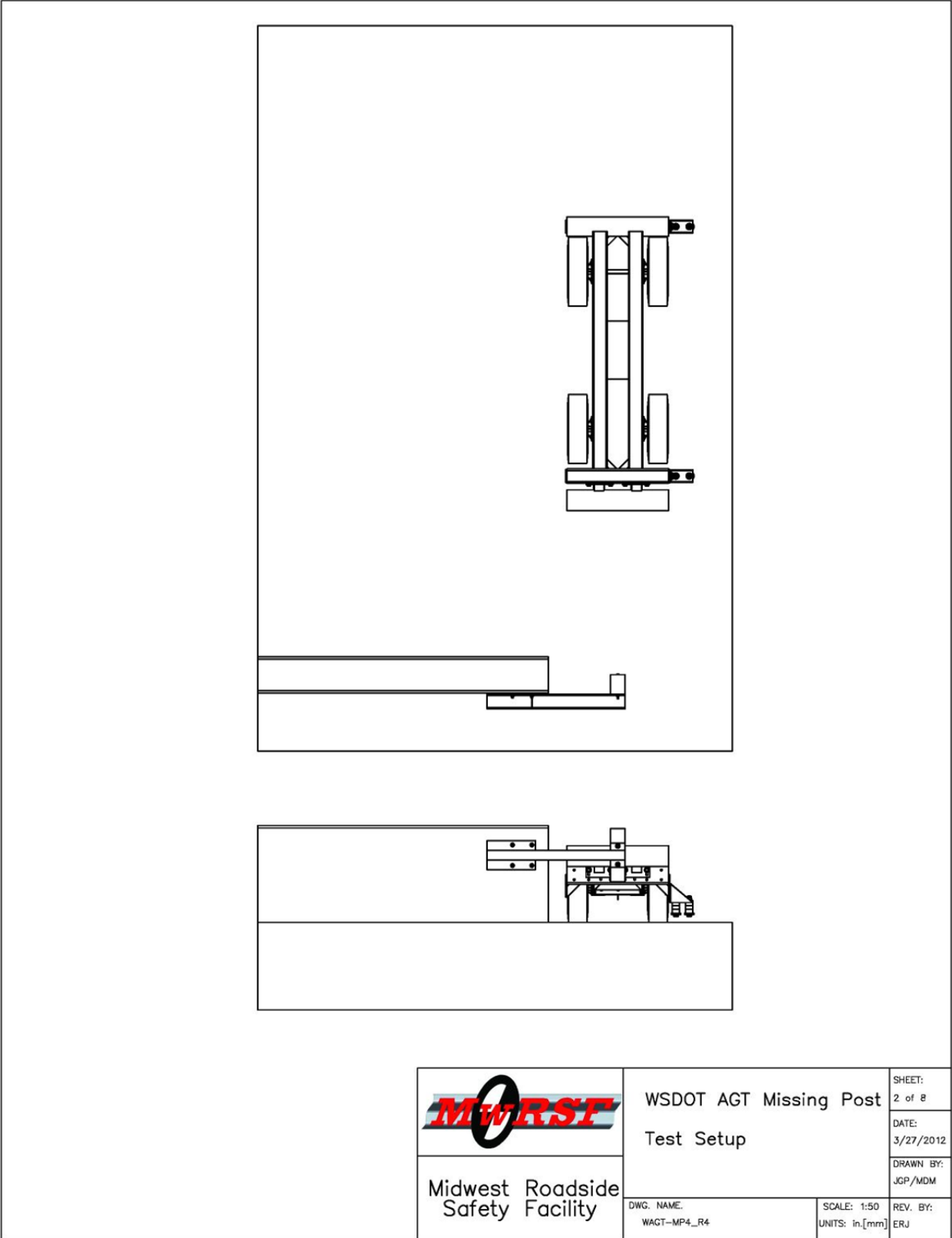


Figure 35. WAGTMP Bogie Testing Setup – Plan View

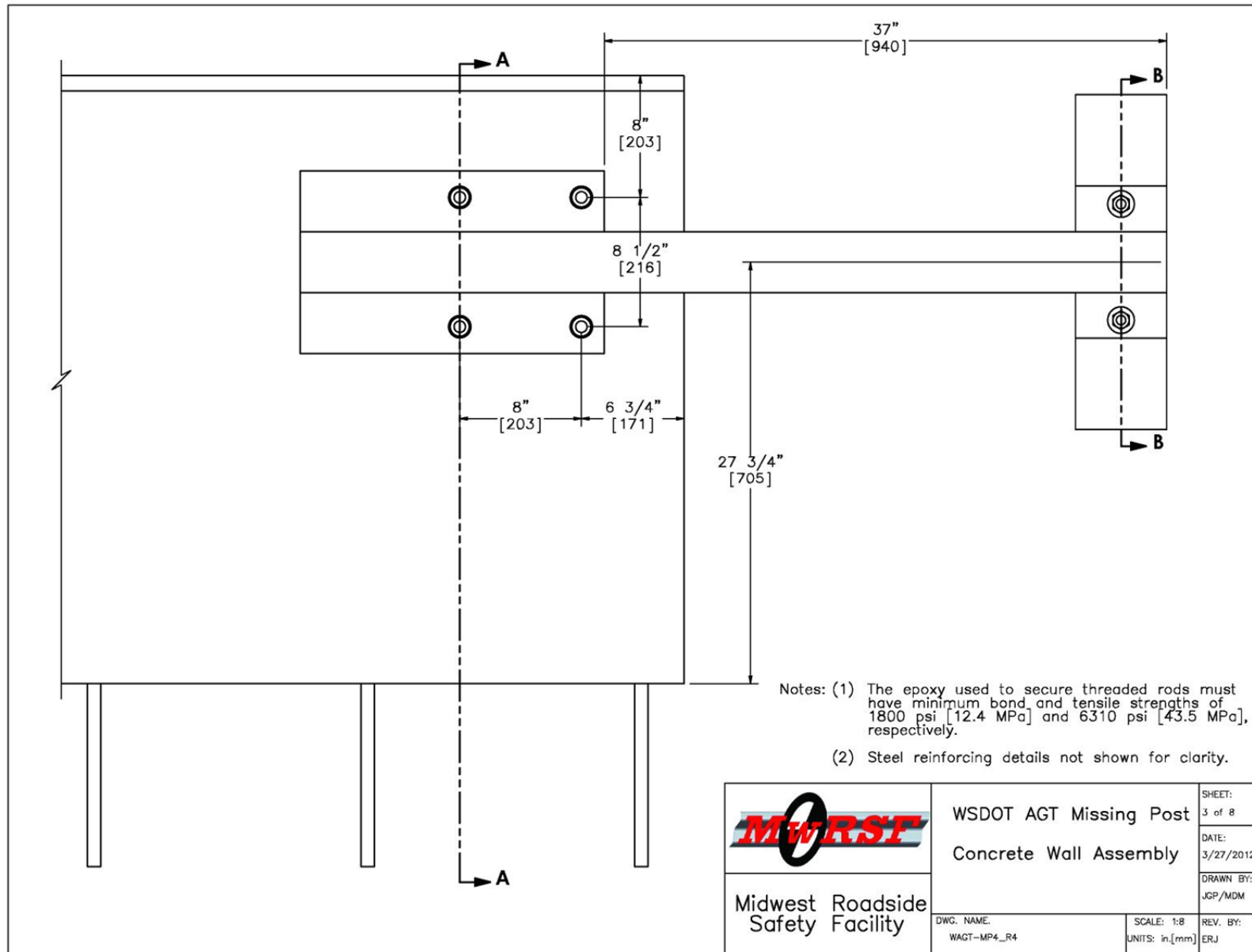


Figure 36. WAGTMP Bogie Testing Concrete Wall Assembly – Back View

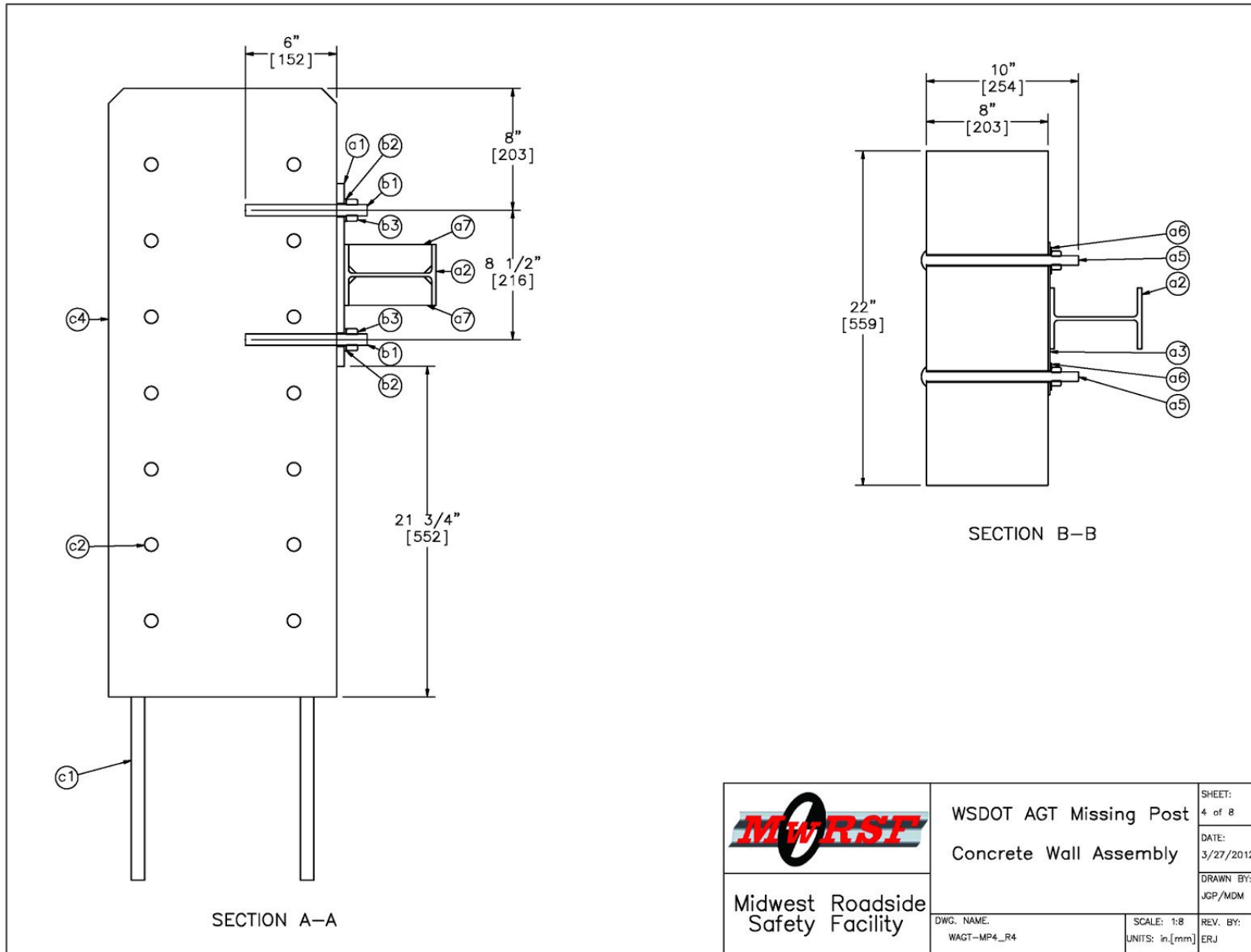


Figure 37. WAGTMP Bogie Testing Concrete Wall Assembly – Side View

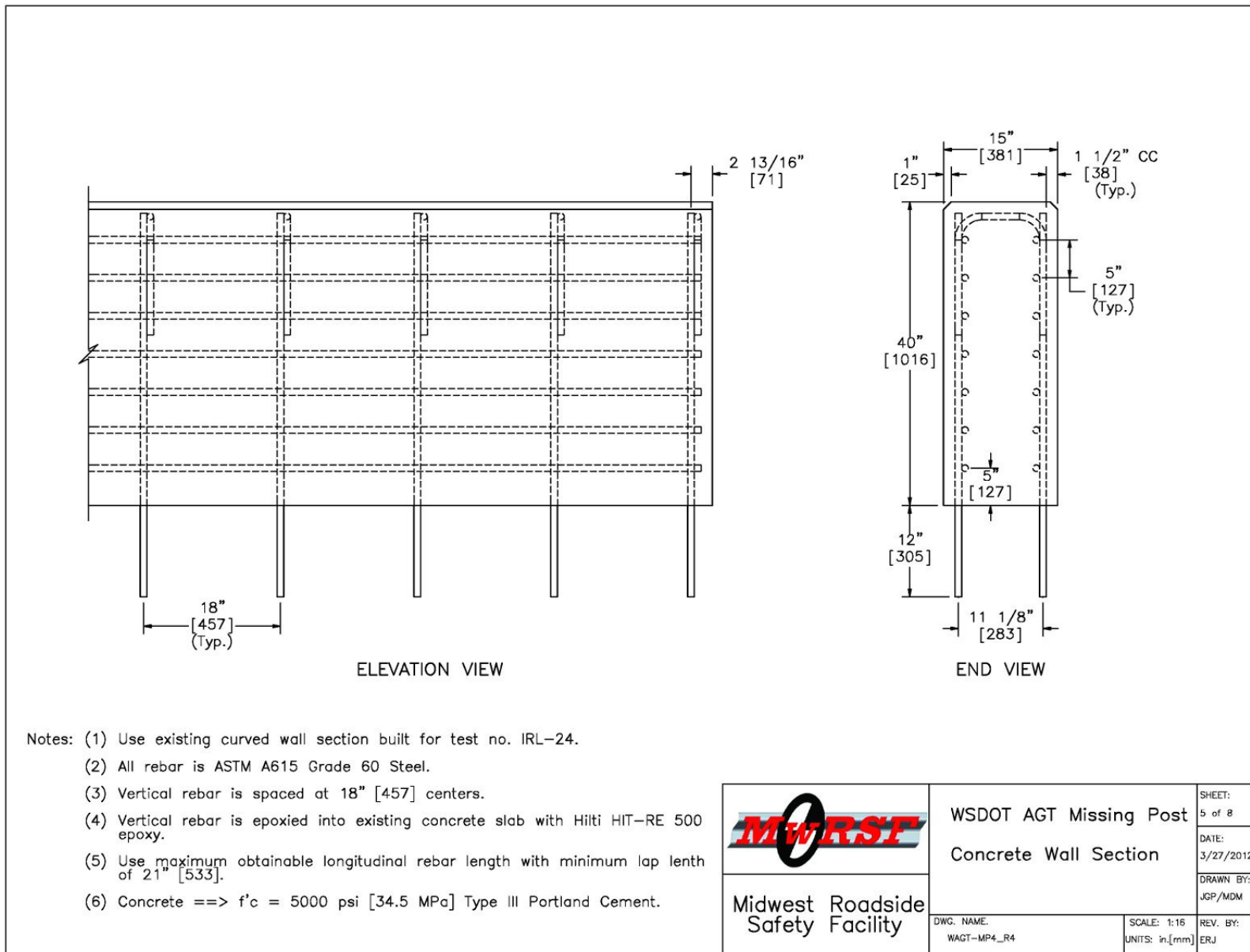


Figure 38. WAGTMP Bogie Testing Concrete Wall Reinforcement Layout

111

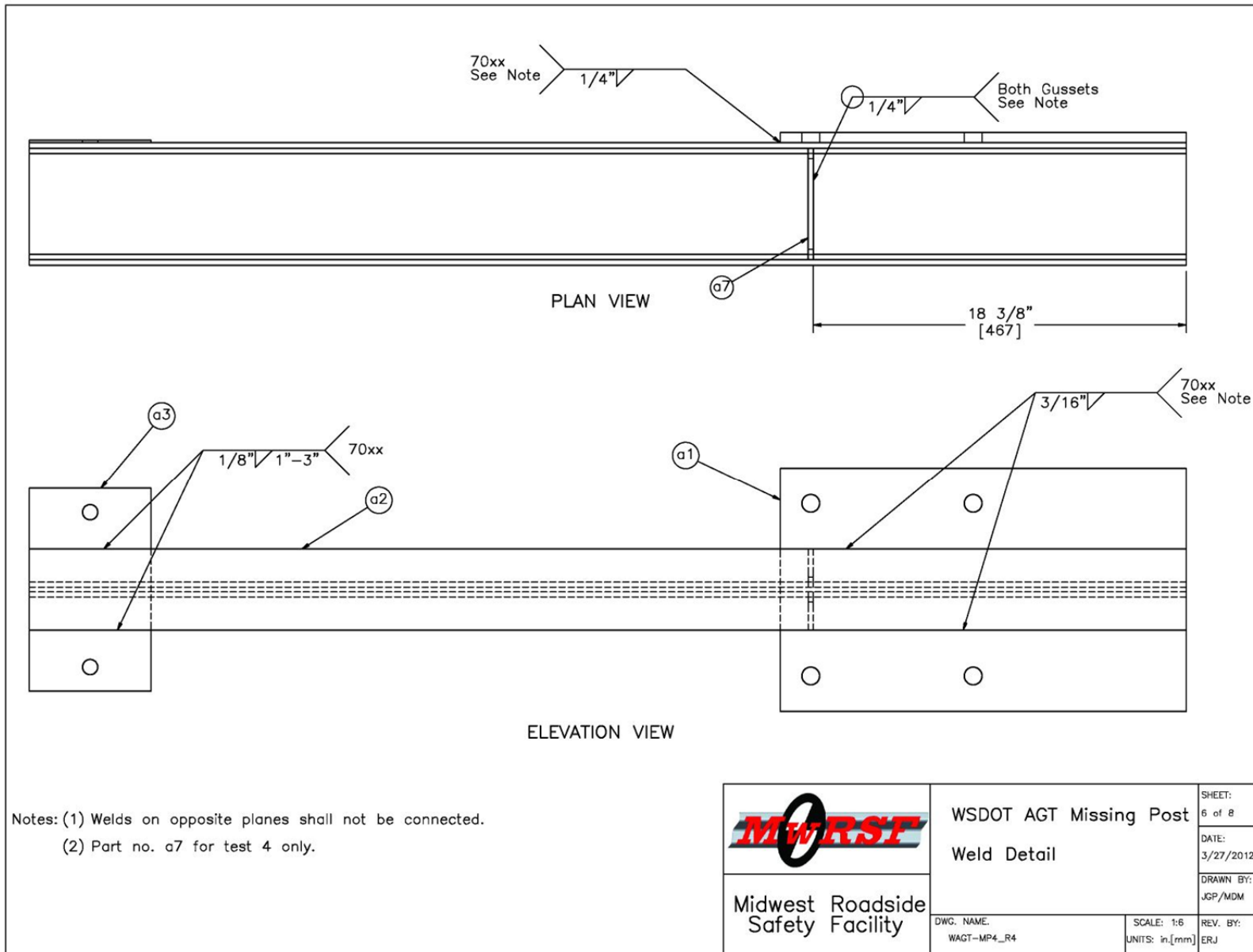


Figure 39. WAGTMP Bogie Testing Weld Details

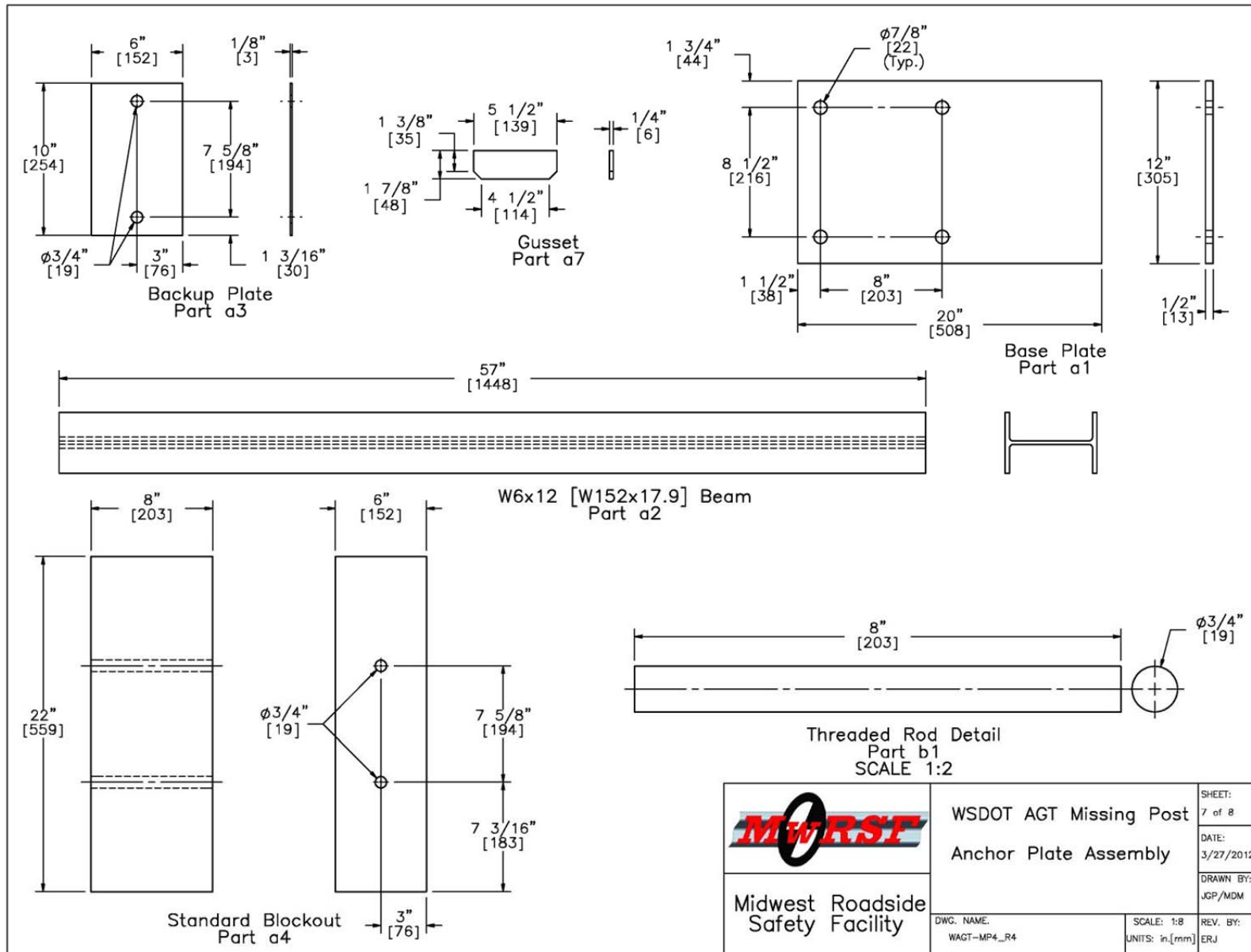



Figure 40. WAGTMP Bogie Testing Anchor Plate Assembly

	WSDOT AGT Missing Post		SHEET: 7 of 8
	Anchor Plate Assembly		DATE: 3/27/2012
Midwest Roadside Safety Facility	DWC. NAME: WAGT-MP4_R4	SCALE: 1:8 UNITS: in.[mm]	DRAWN BY: JGP/MDM
			REV. BY: ERJ

WAGTMP-4 Bill of Materials				
Item No.	QTY.	Description	Material Specification	Comments
a1	1	20"x12"x1/2" [508x305x13] Base Plate	ASTM A572 Gr. 50	-
a2	1	57" [1448] Long W6x12 [W152x17.9] Beam	ASTM A992 Gr. 50	-
a3	1	6"x10"x1/8" [152x254x3] Backup Plate	ASTM A36	Use ASTM A36 or any 50 ksi steel, which ever is more cost efficient
a4	1	6"x8"x22" [152x203x559] Blockout	SYP Grade No. 1 or better	-
a5	2	5/8" [16] Dia. x 10" [254] Long Guardrail Bolt and Nut	ASTM A307	FBB03
a6	2	5/8" [16] Dia. Flat Washer	Grade 5	-
a7	2	5 1/2"x1 7/8"x1/4" [140x48x6] Gusset	ASTM A36	
b1	4	3/4" [19] Dia. x 8" [203] Long Threaded Rod	ASTM A193 type B7	-
b2	4	3/4" [19] Dia. Flat Washer	ASTM F436	-
b3	4	3/4" [19] Dia. Heavy Hex Nut	ASTM A563	-
c1	14	Concrete Wall Vertical Reinforcement - No. 7 Rebar	Grade 60	-
c2	14	Concrete Wall Longitudinal Reinforcement - No. 7 Rebar - Upstream	Grade 60	Total Length = 118" x 14 = 1,652" (Use 21" Lap Length)
c3	7	Concrete Wall Stirrup Reinforcement - No. 7 Rebar	Grade 60	-
c4	1	Concrete - Concrete Wall	f'c = 5000 psi	-


 Midwest Roadside Safety Facility	WSDOT AGT Missing Post Bill of Materials	SHEET: 8 of 8
	DWG. NAME: WAGT-MP4_R4	SCALE: None UNITS: in./mm
		DRAWN BY: JGP/MDM
		REV. BY: ERJ

Figure 41. WAGTMP Bogie Testing Bill of Materials

7.3 Bogie Testing and Results

7.3.1 Test No. WAGTMP-1

During test no. WAGTMP-1, the bogie head impacted the 6-in. x 8-in. x 22-in. (152-mm x 203-mm x 559-mm) wood blockout at a speed of 15.4 mph (24.8 km/h), thus causing strong-axis bending in the W6x12 (W152x17.9) steel post. Initially the horizontal post deflected straight backward, but at 0.010 seconds the rear flange of the horizontal post began to buckle in compression, creating a hinge point just upstream from the base plate. The local flange buckling caused the upstream end of the post to deflect downward. As the free end of the post deflected down, the blockout began to pitch away from the bogie, creating torsion in the post. At 0.064 seconds, the orientation of the deformed post had allowed the bogie head to contact the front flange of the post. This subsequent impact further deflected the end of the post downward and also caused the front end of the bogie to pitch upward. By 0.176 seconds, the post had reached a maximum lateral deflection of 16.2 in. (411 mm) and had begun to recoil as the front end of the bogie lifted into the air and redirected away from the post.

Force vs. deflection and energy vs. deflection curves were created from the accelerometer data and are shown in Figure 42. Initially, inertial effects resulted in a peak force of 12.5 kips (55.6 kN). Soon after this inertial spike, the resistive force level again peaked at 20.9 kips (93.0 kN) around 2.7 in. (69 mm) of deflection. This second force spike caused the post to yield and buckle. Following yielding of the post, the force began to gradually decrease as the bogie was redirected, and its speed was reduced. The 12.5-kip (55.6-kN) peak force observed at 13.5 in. (343 mm) of deflection was attributed to the bogie head contacting the front flange of the post. The horizontal post had absorbed 164.5 kip-in. (19.3 kJ) of energy through combined bending and twisting. Time-sequential photographs of the impact event are shown in Figure 43.

The post assembly experienced severe plastic deformations, resulting from twisting and bending of the post, as shown in Figure 44. The post bent both backward and downward away from the bogie and had also slightly twisted about its horizontal axis. Localized buckling was found on the rear post flange near the upstream edge of the base plate. Also, a small notch corresponding to the direct bogie-post impact was found on the front post flange. The base plate experienced minor prying action along its upstream edge. The vertical weld between the post and the base plate had partially fractured during impact. However, both the top and bottom horizontal welds remained intact. The concrete parapet and anchors sustained no visible damage during the impact event, as shown in Figure 45.

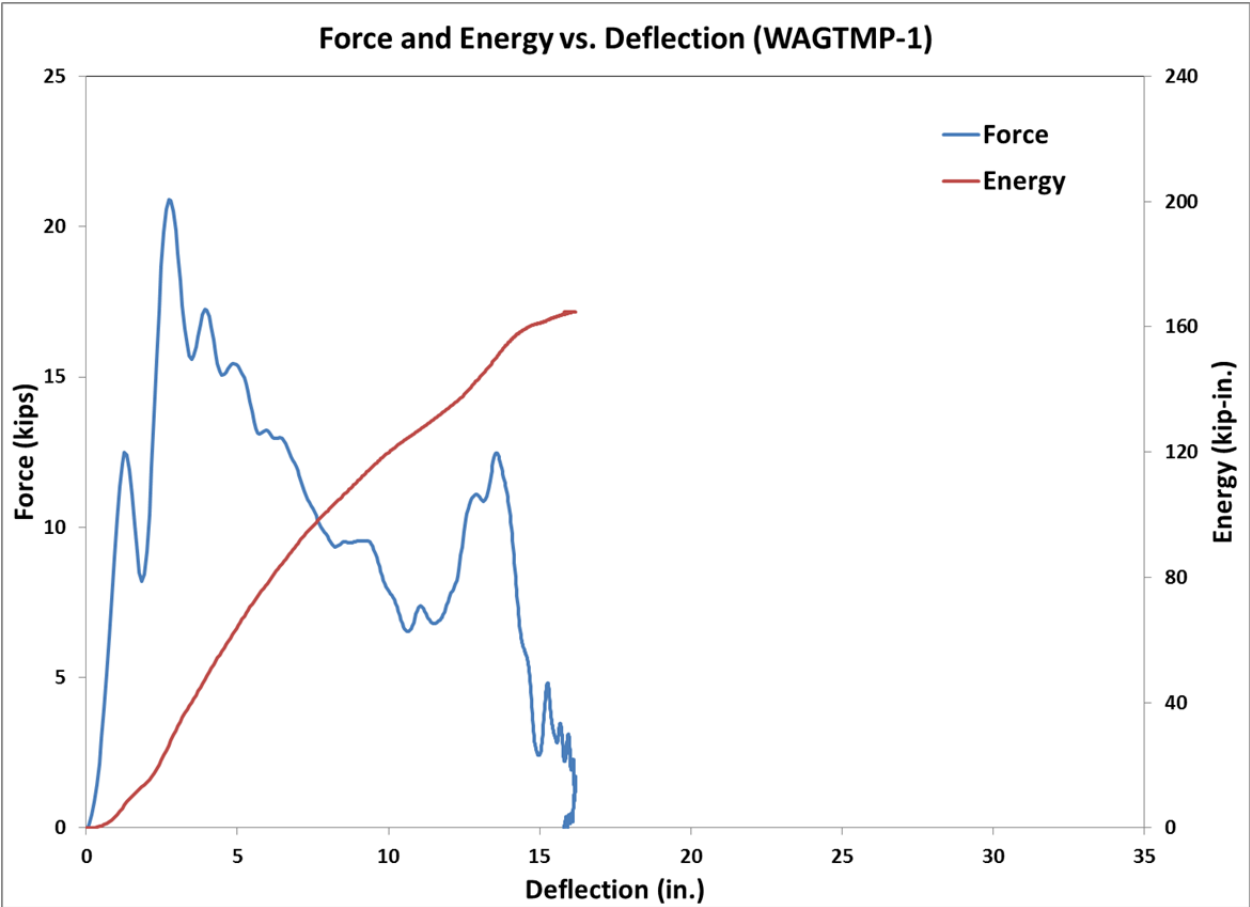
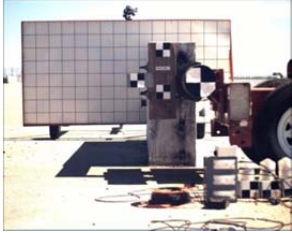


Figure 42. Force vs. Deflection and Energy vs. Deflection, Test No. WAGTMP-1



IMPACT



0.030 sec



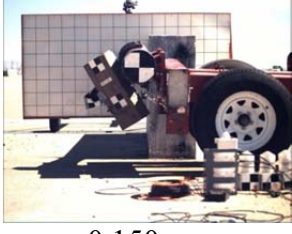
0.060 sec



0.090 sec



0.120 sec



0.150 sec



IMPACT



0.030 sec



0.060 sec



0.090 sec



0.120 sec



0.150 sec

Figure 43. Time Sequential Photographs, Test No. WAGTMP-1



Figure 44. Post Assembly Damage, Test No. WAGTMP-1



Figure 45. Anchor and Parapet Damage, Test No. WAGTMP-1

7.3.1.1 Discussion

The horizontally-mounted post was able to sustain a peak impact force consistent with design loading conditions during initial deflection. However, the resistive force quickly dropped off as post deflections increased. This drop in force was attributed to higher than expected plastic deformations experienced by the post during the early phases of the test. The post yielded as intended, but instead of deflecting back in a uniform manner, the compression flange of the post immediately began to buckle and twist.

Nonetheless, the horizontal post assembly was able to successfully reach its peak design load without causing any damage to the anchors and surrounding concrete. Various forces imparted to the post, as shown in Figure 46, were used to approximate the resistive forces in each vertical anchor pair for further investigation. This analysis was accomplished through a simple summation of moments about the downstream end of the post, as shown in Equation 6. The two anchor pairs were treated as individual constraints, with the pair farthest downstream, R_2 , limited to only one half of the resistance of the upstream pair, R_1 , as shown in Equation 7. This

assumption was based on the predicted anchor loading illustrated in Table 19. A summation of forces was also considered to satisfy equilibrium of the post, as shown in Equation 8. The location of the compressive force, C, imparted onto the post from the concrete parapet was approximated from a linear interpolation of the distribution of forces in the base plate, as shown in Figure 47. Solving for C in Equation 8 and simultaneously substituting it and Equation 7 into Equation 6 approximated the anchor loadings in terms of the applied load. These test results were plotted with corresponding anchor loading data (test nos. WEAB-11 and WEAB-12) obtained by Dickey *et al.* [30-31], as shown in Figure 48. The curves in Figure 48 demonstrate that the anchor loads were well within their predicted capacities.

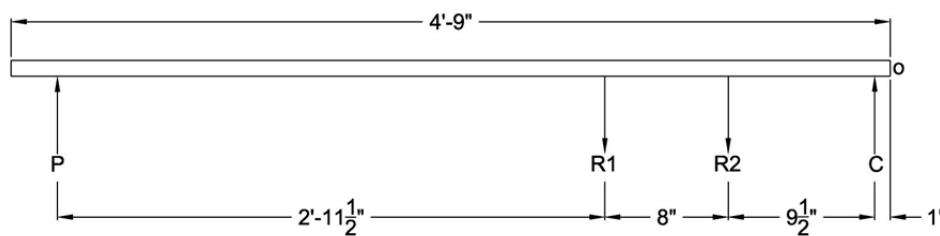


Figure 46. Horizontal Post Loading

$$\sum M_o = 0 = -54P + 18.5R_1 + 10.5R_2 - 1C \quad (6)$$

$$0.5R_1 = R_2 \quad (7)$$

$$\sum F_y = 0 = P - R_1 - R_2 + C \quad (8)$$

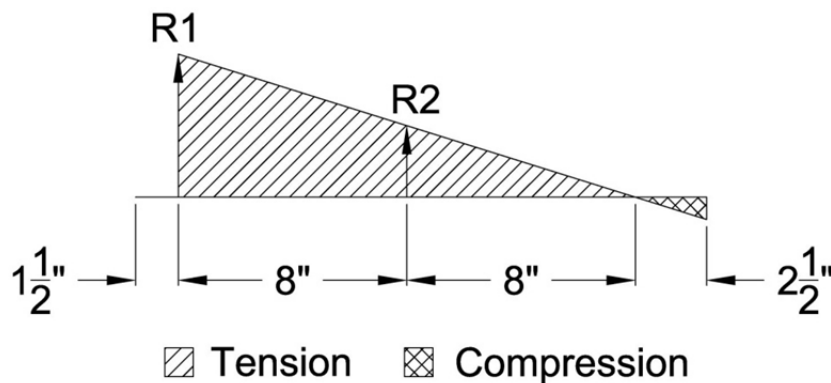


Figure 47. Distribution of Forces in the Base Plate

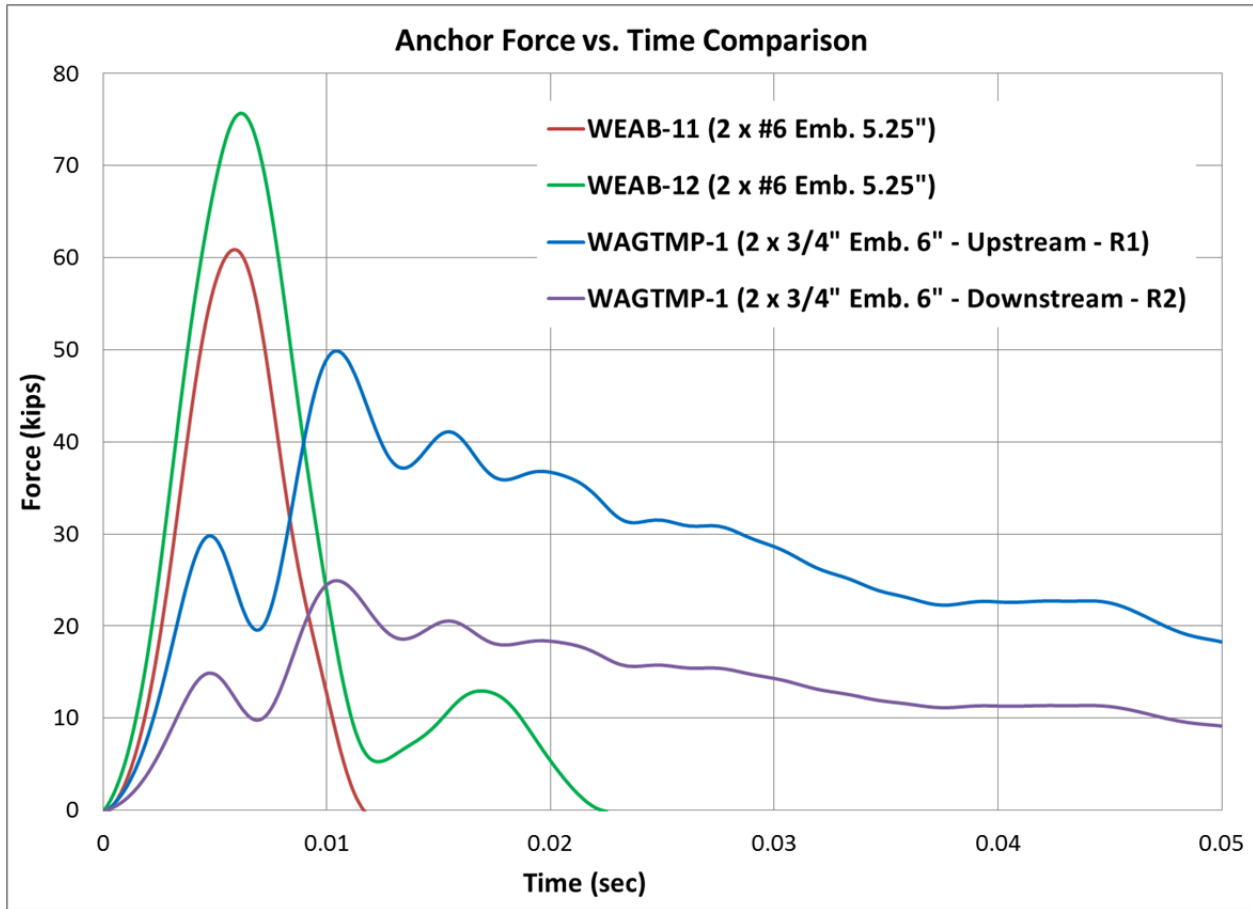


Figure 48. Anchor Force vs. Time Comparison

Following the investigation and analysis, the research team felt that the plastic deformation in the post that was experienced early in the event warranted further testing. Therefore, another test was conducted on a nearly-identical component configuration to improve the performance observed in test no. WAGTMP-1. For the subsequent test, one $\frac{1}{4}$ -in. (6-mm) thick gusset plate was welded to each side of the web. The gussets were placed in plane with the upstream line of anchors near the location where buckling of the post was observed. The gussets were intended to resist post buckling and subsequent torsion in order to increase energy dissipation.

Weld fabrication errors in the beam-to-base plate assembly resulted in two defective component tests, test nos. WAGTMP-2 and WAGTMP-3. The results from those two tests were ultimately neglected.

7.3.2 Test No. WAGTMP-4

During test no. WAGTMP-4, the bogie head impacted the 6-in. x 8-in. x 22-in. (152-mm x 203-mm x 559-mm) wood blockout at a speed of 17.9 mph (28.8 km/h), thus causing strong-axis bending in the W6x12 (W152x17.9) steel post. Initially, the horizontal post deflected straight backward. At 0.012 seconds, the rear flange of the post began to buckle in compression, creating a hinge point just upstream from the edge of the base plate. The local flange buckling caused the upstream end of the post to deflect upward. As the free end of the post deflected upward, the blockout began to pitch toward the bogie, thus creating torsion in the post. By 0.244 seconds, the rotated orientation of the deformed post had allowed the bogie head to completely pass underneath the post and blockout configuration. Thus, the vehicle passed beneath the post without redirection.

Force vs. deflection and energy vs. deflection curves were created from the accelerometer data and are shown in Figure 49. Initially, inertial effects resulted in a peak force of 13.6 kips (60.3 kN). Soon after this inertial spike, the resistive force peaked at 21.7 kips (96.3 kN) around 3.4 in. (86 mm) of deflection. This second force spike caused the post to yield and buckle. Following yielding of the post, the force began to gradually decrease as the post twisted and lost contact with the bogie head. The post had absorbed 202.7 kip-in. (22.9 kJ) of energy through combined bending and twisting. Time-sequential photographs of the impact event are shown in Figure 50.

The horizontal post assembly experienced severe plastic deformations, resulting from twisting and bending of the post, as shown in Figure 51. The post bent both backward and

upward away from the bogie and had also slightly twisted about its horizontal axis. Localized buckling was found on the rear post flange near the upstream edge of the base plate. The base plate experienced minor prying action along its upstream edge. No damage was observed in any of the post-to-base plate welded connections. The concrete parapet and anchors sustained no visible damage during the impact event, as shown in Figure 52.

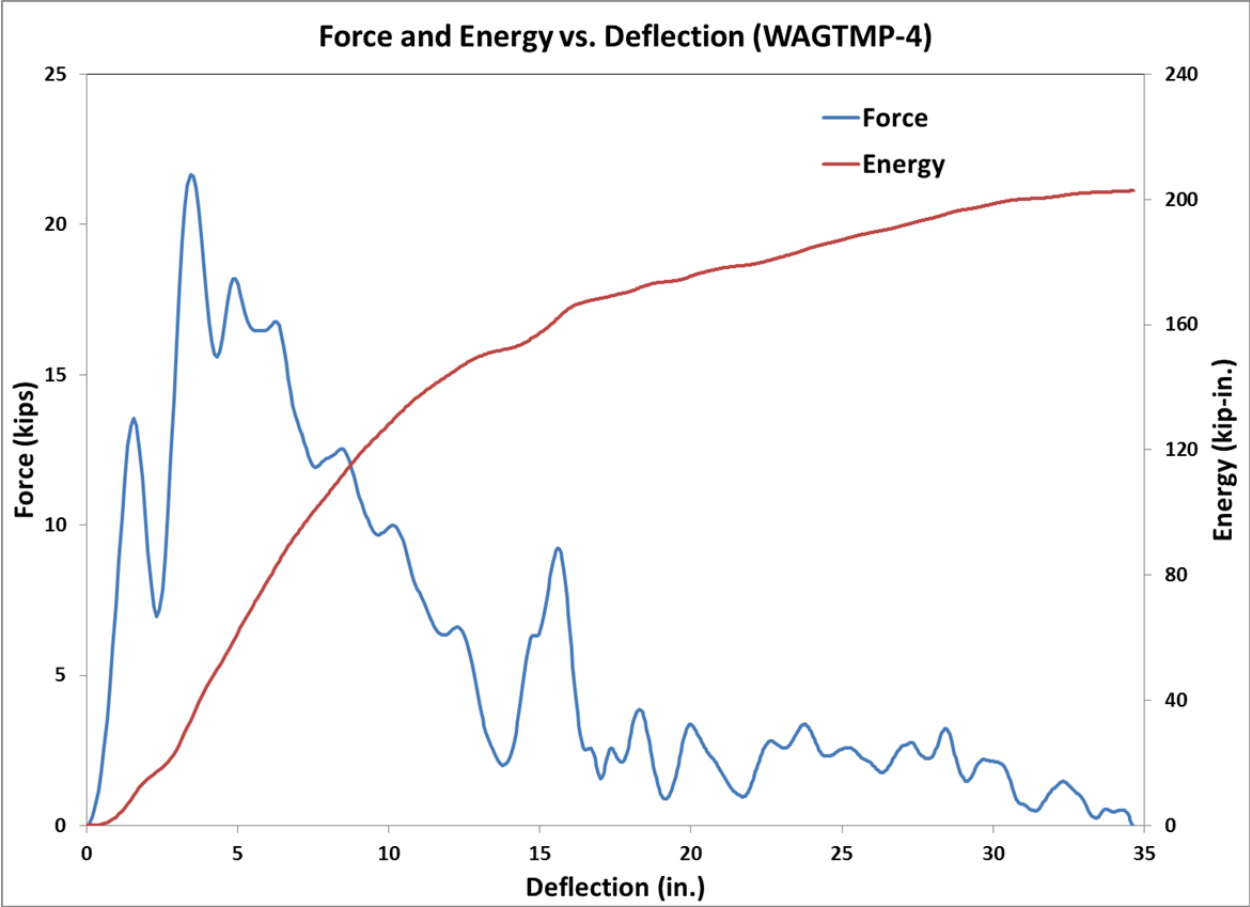
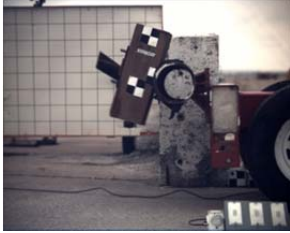


Figure 49. Force vs. Deflection and Energy vs. Deflection, Test No. WAGTMP-4



IMPACT



0.030 sec



0.060 sec



0.090 sec



0.120 sec



0.150 sec



IMPACT



0.030 sec



0.060 sec



0.090 sec



0.120 sec



0.150 sec

Figure 50. Time Sequential Photographs, Test No. WAGTMP-4



Figure 51. Post Assembly Damage, Test No. WAGTMP-4



Figure 52. Anchor and Parapet Damage, Test No. WAGTMP-4

7.3.2.1 Discussion

The horizontally-mounted post with gusset plates was able to sustain a peak impact force consistent with design loading conditions during initial deflection. However, like test no. WAGTMP-1, the resistive force quickly dropped off as post deflections increased. Again, this drop in force was attributed to higher than expected plastic deformations experienced by the post in the early phases of the test. Nonetheless, the post assembly was able to successfully reach its peak design load without causing any damage to the anchors and surrounding concrete. Peak anchor loads for the upstream and downstream anchor pairs were still well within their predicted capacities, at 51.7 kips (230 kN) and 25.8 kips (115 kN), respectively.

7.4 Analysis

The retrofit configuration that was developed for missing posts adjacent to sloped-end parapets was chosen for dynamic component testing because it represented a critical loading condition for the chemical-adhesive anchors. It was shown through testing that the anchor configuration was able to withstand peak design loading conditions without causing any damage

to the parapet or anchors. Further, the addition of gusset plates used in test no. WAGTMP-4 did not significantly improve the performance of the retrofit design and were deemed unnecessary. Results from the two bogie tests are summarized in Table 22. Inertial peak forces and average resistive forces sustained by the retrofit were similar for both tests. As shown in Figure 53, the force vs. deflection curves were also similar for the two tests. The energy absorbed in test no. WAGTMP-4 was slightly higher than that absorbed in test no. WAGTMP-1, but this difference was possibly attributed to a higher impact speed in test no. WAGTMP-4. Further, the difference in energy dissipation was insignificant over the first 15 in. (381 mm) of deflection, as shown in Figure 54.

Table 22. Bogie Testing Results – W6x12 Horizontal Retrofit Design

Test No.	Component Description	Impact Velocity (mph)	Bogie Weight (lbs)	Average Force (kips)			Peak Force (kips)	Maximum Deflection (in.)	Total Energy (k-in.)	Failure Mode
				@ 5"	@ 10"	@ 15"				
WAGTMP-1	W6x12 horizontal transition post without stiffeners	15.4	1,722	12.7	12.0	10.7	20.9	16.2	164.8	Yielding/Buckling
WAGTMP-4	W6x12 horizontal transition post with stiffeners	17.9	1,730	12.0	12.8	10.5	21.7	34.6	202.7	Yielding/Buckling

During both tests, the retrofit post experienced significant twisting regardless of whether or not gusset plates were present. The researchers concluded that the twisting observed during testing was not a substantial concern for several reasons. First, the torsion which induced this twisting was most likely caused by slight eccentricities between the bogie head and the center of the post rather than an error in design. A calculation pertaining to the unbraced length of a W6x12 (W152x17.9) member required to cause lateral torsional buckling during bending confirmed this notion. According to methods presented in the *Steel Construction Manual* [51], W6x12 (W152x17.9) ASTM A992 Grade 50 members undergoing pure bending can be unbraced for lengths up to approximately 39 in. (991 mm) before significant reductions in strength are

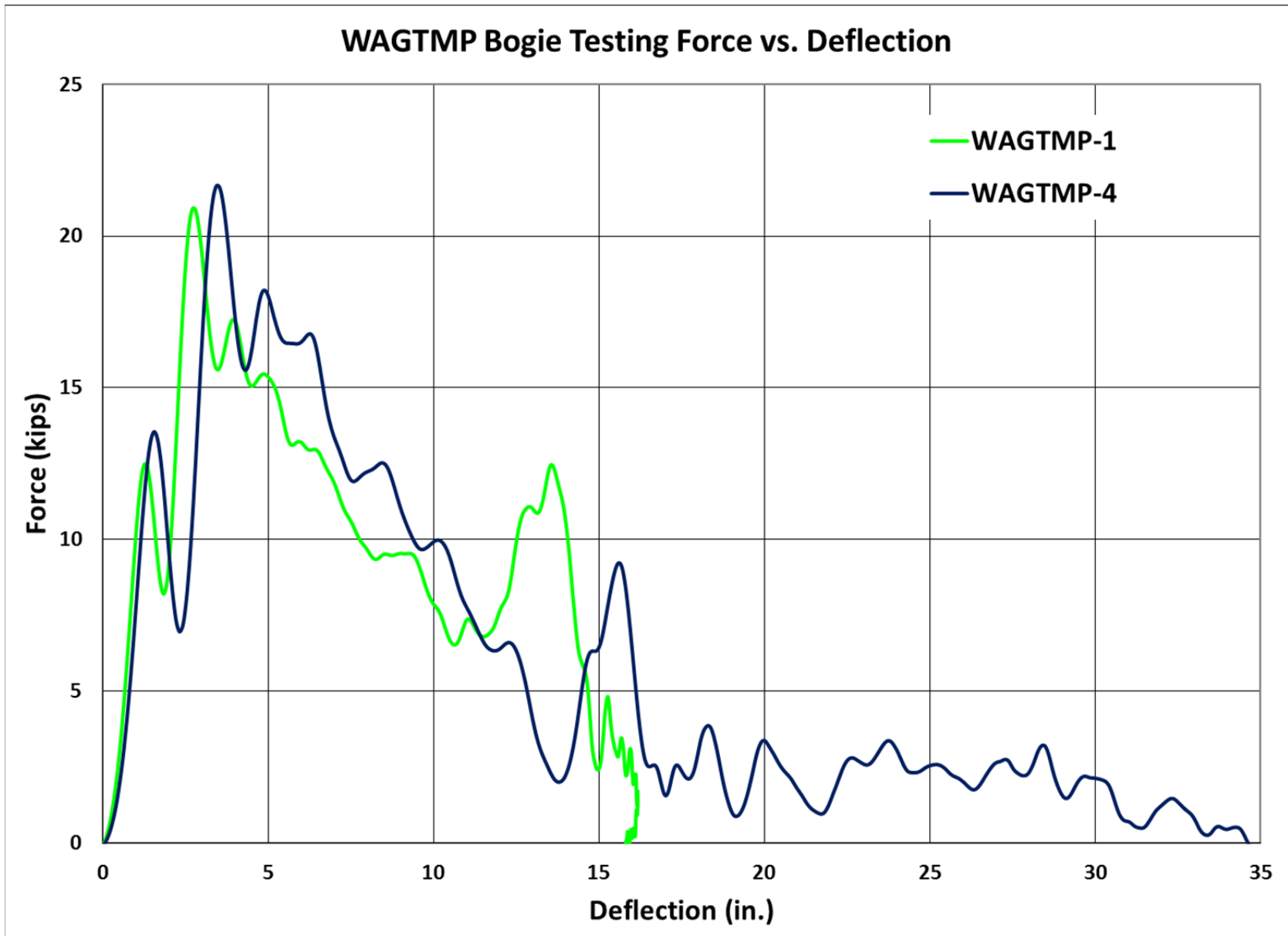


Figure 53. Force vs. Deflection Results, WAGTMP Bogie Testing

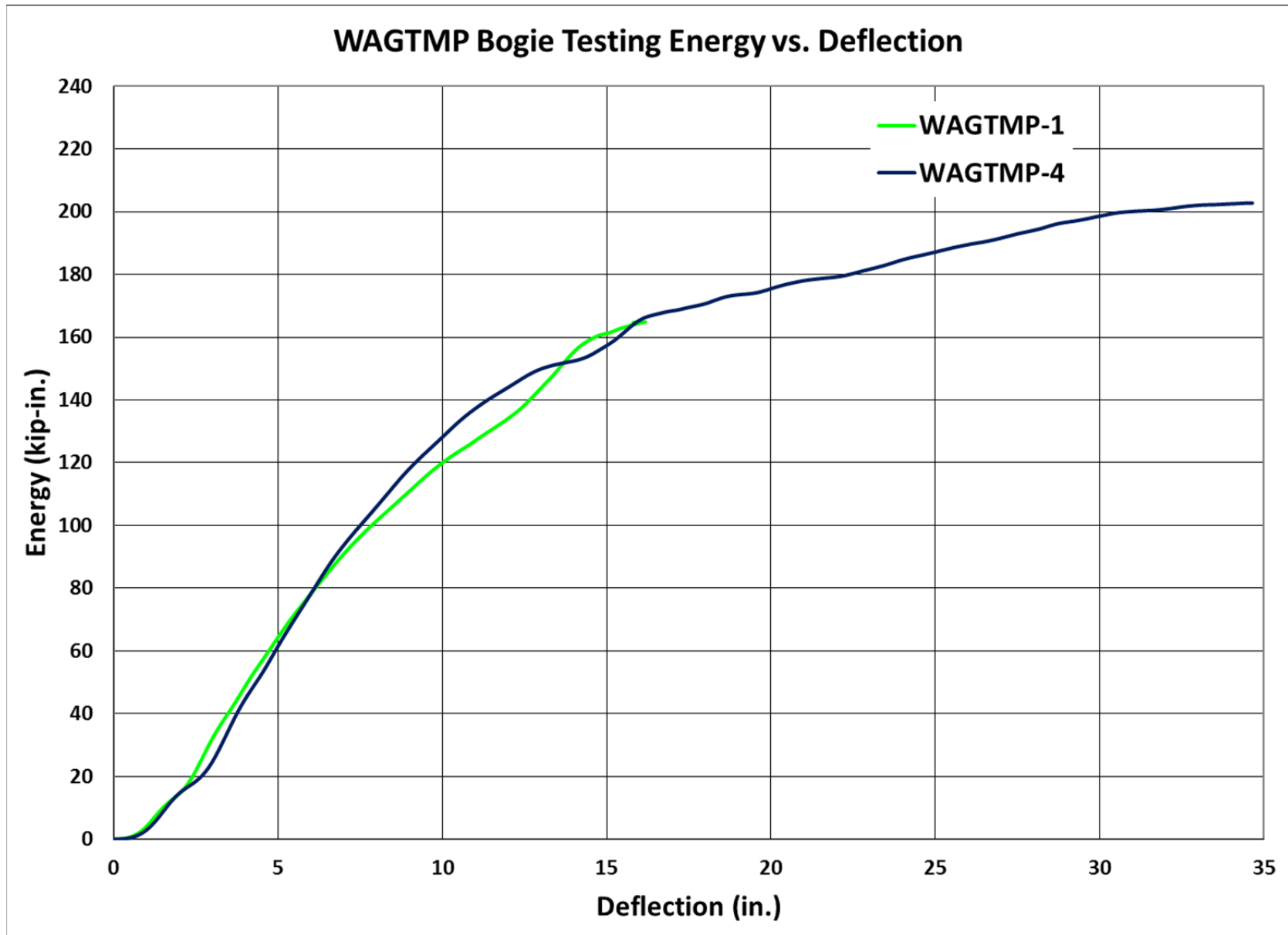


Figure 54. Energy vs. Deflection Results, WAGTMP Bogie Testing

expected. The cantilever (i.e., unbraced) section of the retrofit design was only 35.5 in. (902 mm).

Furthermore, the horizontal post did not experience any twisting over the first 5 in. (127 mm) of deflection, and it actually performed quite well over this amount of deflection. In particular, 5 in. (127 mm) of deflection represented the maximum anticipated post deflection for post no. 1. In fact, a review of successful crash tests on the 18-ft 9-in. (5.7-m) long transition system, test no. ITNJ-2 and ITNJ-4, indicated that the post nearest the bridge rail never dynamically deflected more than 4 in. (102 mm). In addition, installation of this retrofit design in existing transition systems would require the post and blockout to be directly attached to the thrie beam by two guardrail bolts, rather than left unsupported as installed in the component tests. As such, the stiffness and strength of the nested thrie beam rail would directly contribute to the torsional resistance of the post and limit subsequent twisting during impact events.

Nonetheless, the retrofit design was further examined to determine whether it's as-tested rigidity, without the anticipated support of the thrie beam rail against torsion, would still compensate for the reduced resistance in a transition system created by a missing post at this location. BARRIER VII computer simulations were conducted to replicate vehicular impacts into the 18-ft 9-in. (5.7-m) long transition system and the 31-ft 3-in. (9.5-m) long transition system utilizing the dynamic behavior observed in test no. WAGTMP-1. Force vs. deflection data obtained from that test was used to derive the input parameters shown in Table 23. The average force was 12.0 kips (53.4 kN) over 10 in. (254 mm) of deflection, which provided the basis for strong-axis resistance used in the BARRIER VII model. Utilizing an impact height of 21.65 in. (550 mm), the strong-axis bending moment, M_A , was calculated to be 260 k-in. (29.4 kN-m). A post stiffness, K_B , of 9.6 kip/in. (1.7 kN/mm) was approximated from force vs. deflection curves of the two component tests.

Table 23. Input Properties for BARRIER VII W6x12 Retrofit

Revised BARRIER VII Input Parameters		Horizontal Retrofit (W6x12)
Load Height	in.	21.65
K _B - Strong-Axis Post Stiffness	kips/in.	9.6
M _A - Strong-Axis Bending Moment	kip-in.	260
δ _{FB} - Strong Axis Displacement Failure	in.	10

Simulations were performed with a 4,409-lb (2,000-kg) pickup truck impacting at a speed of 62.1 mph (100 km/h) and at an angle of 25 degrees. Each model was iteratively impacted at 9³/₈-in. (238-mm) intervals along the system to determine values for wheel rim snag on the upstream end of the bridge rail (e.g., the reason for predicted failure, as described in Chapter 5). According to data shown in Tables 15 and 16, missing posts in positions 1 through 3 did not result in excessive dynamic deflections or vehicle pocketing angles. Thus, these parameters were not considered. A total 24 runs and 40 runs were conducted to evaluate barrier performance with the retrofit design placed in the 18-ft 9-in. (5.7-m) long transition system and the 31-ft 3-in. (9.5-m) long transition system. Comprehensive results from these additional runs can be found in Appendix D. Shown in Table 24 are the maximum values corresponding to wheel rim snag on the upstream end of the bridge rail.

The retrofit design, even without the anticipated support of the thrie beam rail against torsion, was able to significantly reduce vehicle snag on the bridge rail end, and nearly match that observed in the baseline simulations. In fact, the predicted values for wheel rim snag were reduced by almost 30 percent for each system as compared to the corresponding position with a missing post. Further, the amount of wheel rim snag predicted for both the 18-ft 9-in. (5.7-m)

long transition system and the 31-ft 3-in. (9.5-m) long transition system was well below the 2-in. (51-mm) evaluation limit. Therefore, the lateral resistance provided by a horizontally-mounted W6x12 (W152x17.9) ASTM A992 Grade 50 steel post was deemed adequate to replace missing transition posts (post no. 1) at locations adjacent to sloped-end parapets for both the 18-ft 9-in. (5.7-m) long and the 31-ft 3-in. (9.5-m) long transition systems.

Table 24. Summary of Simulation Results for W6x12 Retrofit Design

Model Description	Maximum Wheel Rim Snag	
	18-ft 9-in. Transition (in.)	31-ft 3-in. Transition (in.)
Missing Post #1	2.32	2.36
Retrofitted Post #1	1.67	1.72
Baseline	1.58	1.61

Recall, both retrofit designs developed for missing posts adjacent to bridge rails (e.g., blunt-end and sloped-end parapets) were intended to behave similarly during impact events. Since the sloped-end retrofit design did not cause any damage to the concrete bridge rail or anchors during impact events, component testing and subsequent validation for the blunt-end retrofit design was not deemed necessary. As such, a horizontally-mounted W6x9 (W152x13.4) ASTM A992 Grade 50 steel beam (i.e., surrogate post) was deemed adequate to replace missing transition posts (post no. 1) at locations adjacent to blunt-end parapets for both the 18-ft 9-in. (5.7-m) long and the 31-ft 3-in. (9.5-m) long transition systems.

8 SUMMARY, CONCLUSIONS, AND RECOMMENDATIONS – MISSING TRANSITION POSTS

8.1 Summary and Conclusions

Survey data provided by the Wisconsin DOT indicated that the proper installation of transition posts was most affected in the region directly adjacent to bridge rail ends and a region slightly farther upstream from the bridge rail end. A total of 344 BARRIER VII computer simulations were conducted to predict the consequences associated with the occurrence of a missing post in each of the positions within these regions. Simulation results demonstrated that even a single post inside the transition region caused either excessive dynamic deflection of the barrier system or an increased propensity for the vehicle to snag on the upstream end of the bridge rail.

The most desirable option for repairing a guardrail system with a missing or severely damaged post was to re-install an appropriate post in the prescribed location as intended in the original design. However, this alternative is not always possible due to various below or above grade obstructions at the location where the post should be installed. As a result, removal or relocation of the obstruction should be considered as to allow for proper installation of the transition post. When removal or relocation of an obstruction is not possible, additional blockouts should be attached to the affected post to laterally shift the post beyond the obstruction. However, combined blockout depths should not exceed 24 in. (610 mm). Thus, this alternative is not always feasible. Finally, when no other option remains, a surrogate post of sufficient stiffness and strength should be installed to replace the missing post at a given location.

In this study, three surrogate post retrofit designs were developed to satisfy all missing transition post locations: (i) one retrofit for the region directly adjacent to blunt-end parapet bridge rails; (ii) one retrofit for the region directly adjacent to sloped-end parapet bridge rails; and (iii) one retrofit for all post positions not directly adjacent to the bridge rail.

Two dynamic component tests were conducted to evaluate the performance of the device designed for positions adjacent to sloped-end bridge rails. The device was able to withstand a peak force consistent with design loading conditions and allowed the beam to yield without causing any damage to the concrete bridge rail or the chemically-bonded anchor rods. Thus, when utilized in an actual transition system, only the horizontal post and base plate of the retrofit component would be affected during a vehicular impact. This portion of the design could be easily removed and replaced with a new post and base plate component attached to the parapet utilizing the existing anchors. The retrofit design that was developed for blunt-end bridge rails was intended to behave similarly during impact to the retrofit design for sloped-end parapets. Thus, additional testing on the retrofit device for blunt-end parapets was deemed unnecessary.

The dynamic structural properties for the sloped-end retrofit were used for 64 additional computer simulations to examine whether the device was stiff enough to alleviate deficiencies caused by a missing post adjacent to a bridge rail. Results demonstrated that these retrofit devices could reduce vehicle wheel rim snag on the upstream edge of the bridge rail by nearly 30 percent as compared to the corresponding position with a missing post. Further, these retrofit devices only demonstrated a 6 percent increase above baseline values for wheel rim snag on the upstream end of the bridge rail.

Two retrofit designs were developed for all other post positions not directly adjacent to the bridge rail end. These retrofit systems consisted of a combination of post and beam members which have been subjected to significant dynamic testing over the years. The retrofit systems were configured to provide comparable stiffness and strength when either positioned on level terrain or nearby a slope break point of a 2H:1V fill slope. In either case, the combined resistance of the supporting components should match that of a 6-in. x 8-in. x 7-ft (152-mm x 203-mm x 2.1-m) long

wood guardrail posts embedded 52 in. (1,321 mm) on level terrain. Thus, additional component testing and computer simulation was deemed unnecessary. Fabrication and installation details regarding each of the retrofit devices are provided in the following sections.

8.1.1 Retrofit 1 – Missing Transition Post Adjacent to Sloped-End Parapets

The surrogate-post retrofit design for a missing post adjacent to sloped-end parapets consisted of a 55-in. (1,397-mm) long, W6x12 (W152x17.9) ASTM A992 Grade 50 steel beam (i.e., surrogate post) welded to a 12-in. x 20-in. x $\frac{1}{2}$ -in. (305-mm x 508-mm x 13-mm) ASTM A572 Grade 50 steel base plate. Three fillet welds comprise the welded joint between the beam and base plate: (i) a $\frac{1}{4}$ -in. (6.4-mm) thick vertical fillet weld along the entire 4-in. (102-mm) upstream edge of the beam-plate overlap; (ii) a $\frac{3}{16}$ -in. (4.8-mm) thick longitudinal fillet weld along the entire 20-in. (508-mm) upper beam flange edge; and (iii) a $\frac{3}{16}$ -in. (4.8-mm) thick longitudinal fillet weld along the entire 20-in. (508-mm) lower beam flange edge.

The beam and base plate component is oriented parallel to the ground (i.e., horizontal) and attaches to the sloped-end concrete parapet with four $\frac{3}{4}$ -in. (19-mm) diameter ASTM A193 Grade B7 threaded rods, each passing through a $\frac{7}{8}$ -in. (22-mm) diameter hole in the base plate and embedded 6 in. (152 mm) into the concrete. A chemical adhesive, with a bond strength of at least 1,800 psi (12.4 MPa), shall be used to anchor the threaded rods in the concrete. An adequately-sized wood blockout was used to attach to the upstream end of the steel post to the thrie beam rail with two $\frac{5}{8}$ -in. (16-mm) diameter guardrail bolts and a $\frac{1}{8}$ -in. (3-mm) thick ASTM A36 steel support plate which is spot welded to the horizontal post. In addition, any existing thrie beam end shoe through-bolts that impede upon the placement of this retrofit component should be replaced by a shorter, epoxied bolt or insert. The final retrofit design and the location of anchor placement on the sloped-end parapet are shown in Figures 55 through 59.

8.1.2 Retrofit 2 – Missing Transition Posts Adjacent to Blunt-End Parapets

The surrogate-post (i.e., horizontal beam) retrofit design for a missing post adjacent to blunt-end parapets utilized the same general concept as used for sloped-end parapets with the following exceptions:

1. The beam type was changed to a W6x9 (W152x13.4) ASTM A992 Grade 50 steel section.
2. The beam length was decreased to 38 in. (965 mm).
3. The base plate length was decreased to 16 in. (406 mm).
4. Three structurally-adequate steel tubes were required to be tack welded to the base plate to accommodate the chamfer on the back side of the concrete parapet – one steel tube to surround each of the two exposed anchors and one steel tube at the downstream edge of the base plate to compensate for missing contact pressure. Other options to fill this gap include washers, wood blocks, and other steel shapes.

The final retrofit design and the location of anchor placement on the blunt-end parapet are shown in Figures 60 through 64.

8.1.3 Retrofit 3 – Missing Transition Posts Not Adjacent to Bridge Rail

The surrogate-post retrofit design for missing posts not directly adjacent to a bridge rail end consisted of two W6x9 (W152x13.4) ASTM A992 Grade 50 steel posts placed in parallel. The two posts in parallel are spaced at 3 ft (0.91 m) on center and connected by a 40-in. (1,016-mm) long, W6x9 (W152x13.4) A992 Grade 50 steel post. Two standard guardrail bolts attach each support post to the horizontal beam. Three 6-in. x 8-in. x 22-in. (152-mm x 203-mm x 559-mm) wood blockouts offset the surrogate post system away from the thrie beam rail elements. The blockouts attach at the center of the horizontal beam with two $\frac{5}{8}$ -in. (16-mm) diameter guardrail bolts and a $\frac{1}{8}$ -in. (3-mm) thick ASTM A36 steel backup plate which is spot welded to the post.

Two design options were developed for the surrogate posts to satisfy placement on various terrains. Adequate lateral barrier resistance will be provided for each terrain situation, whether or not the steel posts yield at ground line.

8.1.3.1 Retrofit 3A – Applications on Level Terrain

Surrogate posts are comprised of two 6-ft (1.8-m) long, W6x9 (W152x13.4) ASTM A992 Grade 50 steel sections embedded 43 in. (1,092 mm) into the soil. The final component design for the level terrain application is shown in Figures 65 through 68.

8.1.3.2 Retrofit 3B – Applications Near a 2H:1V Fill Slope

Surrogate posts are comprised of two 9-ft (2.1-m) long, W6x9 (W152x13.4) ASTM A992 Grade 50 steel sections embedded 76 in. (1,930 mm) into the soil. The final component design for the 2H:1V fill slope application is shown in Figures 69 through 72.

8.2 Recommendations

The surrogate-post retrofit designs were developed herein for specific locations within the transition region of the 18-ft 9-in. (5.7-m) long and the 31-ft 3-in. (9.5-m) long transition systems. As such, any instance where installation of a specific surrogate post is warranted must first meet certain criteria. Failure to abide by these criteria may result in degraded safety performance of a transition system as well as overall failure.

The horizontal-beam (i.e., surrogate-post) retrofit designs (i.e., sloped-end and blunt-end) were only configured to replace missing posts in the first position upstream from the bridge rail end. Therefore, the horizontal-beam retrofit design should not connect to other post positions. Any change in the expected loading to the retrofit design may cause the system to perform poorly. In addition, only concrete bridge rails with geometries similar to that shown in Appendix A should be considered. Care must be taken to install the adhesive anchors according to the manufacturers'

specifications. Further, the chemical-adhesive anchors must be embedded within concrete which is in good condition and properly prepared prior to anchor placement. Poor concrete conditions (e.g., cracking, spalling, low strength, etc.) may lead to premature failure of the chemical-adhesive anchors.

For the two horizontal beam retrofit designs, it may be desirable to incorporate slots in the blackout backup plate as well as in the concrete parapet base plate. These slots would allow for some adjustment when attaching the horizontal beam retrofit to the thrie beam via a wood blackout as well as to the back side of the concrete parapet. For the steel backup plate, two $\frac{3}{4}$ -in. x $1\frac{1}{4}$ -in. (19-mm x 32-mm) vertical slots could be used in lieu of the two $\frac{3}{4}$ -in. (19-mm) diameter standard holes. However, the steel backup plate should be extended vertically from 10 in. (254 mm) to 11 in. (279 mm) long to provide adequate distance from the center of the slot to the edge of the plate.

For the concrete parapet base plate, two plate sizes were configured to account for attachment to either sloped ends or blunt ends. The base plate for the sloped parapet measured 20 in. (508 mm) long and utilized four $\frac{7}{8}$ -in. (22-mm) diameter standard holes. For the steel base plate, four $\frac{7}{8}$ -in. x $1\frac{1}{8}$ -in. (22-mm x 48-mm) horizontal slots could be used in lieu of the four $\frac{7}{8}$ -in. (22-mm) diameter standard holes. However, the base plate should be extended horizontally from 20 in. (508 mm) to 21 in. (533 mm) to provide adequate distance from the center of the slot to the edge of the plate. The center of the first two slots would be positioned approximately $2\frac{1}{2}$ in. (64 mm) from the edge of the plate. Larger plate washers should be used in combination with the slotted base plate.

The base plate for the blunt parapet measured 16 in. (406 mm) long and utilized four $\frac{7}{8}$ -in. (22-mm) diameter standard holes. Similarly, four $\frac{7}{8}$ -in. x $1\frac{1}{8}$ -in. (22-mm x 48-mm) horizontal slots could be used in lieu of the four $\frac{7}{8}$ -in. (22-mm) diameter standard holes. However, the base plate

should be extended horizontally from 16 in. (406 mm) to 17 in. (432 mm) to provide adequate distance from the center of the slot to the edge of the plate. Once again, the center of the first two slots would be positioned approximately 2½ in. (64 mm) from the edge of the plate. Again, larger plate washers should be used in combination with the slotted base plate.

The “straddle” post retrofit design was configured for any post location in the transition region. Design options were specifically configured for level terrain applications or applications with at least 2 ft (0.6 m) of level grading behind the existing transition posts as well as for applications with steel posts adjacent to a 2H:1V fill slope. Without this grading, the 21.65-in. (550-mm) impact height assumption cannot be made. Further, the surrogate posts must be triple blocked to offset the horizontal beam away from adjacent posts. Without this lateral offset, an errant vehicle may strike and snag upon the retrofit design, encounter vehicle pocketing, and/or encounter vehicular instabilities at the excessively stiffened region.

In some cases and as noted in prior sections, alternative dual-post retrofit designs may be desired beyond those provided for level terrain and 2H:1V fill slope applications. For example, specific alternatives may be desired for steel posts placed at or near 3H:1V or 4H:1V fill slopes. Based on the best available information, limited bogie testing data, and engineering judgment, it would seem reasonable to utilize lengths of 6.5 ft (1,981 mm) and 7 ft (2,100 mm) in combination with embedment depths of 46 in. (1,168 mm) and 52 in. (1,321 mm) for steel posts located at or near the slope break point of 4H:1V and 3H:1V fill slopes, respectively.

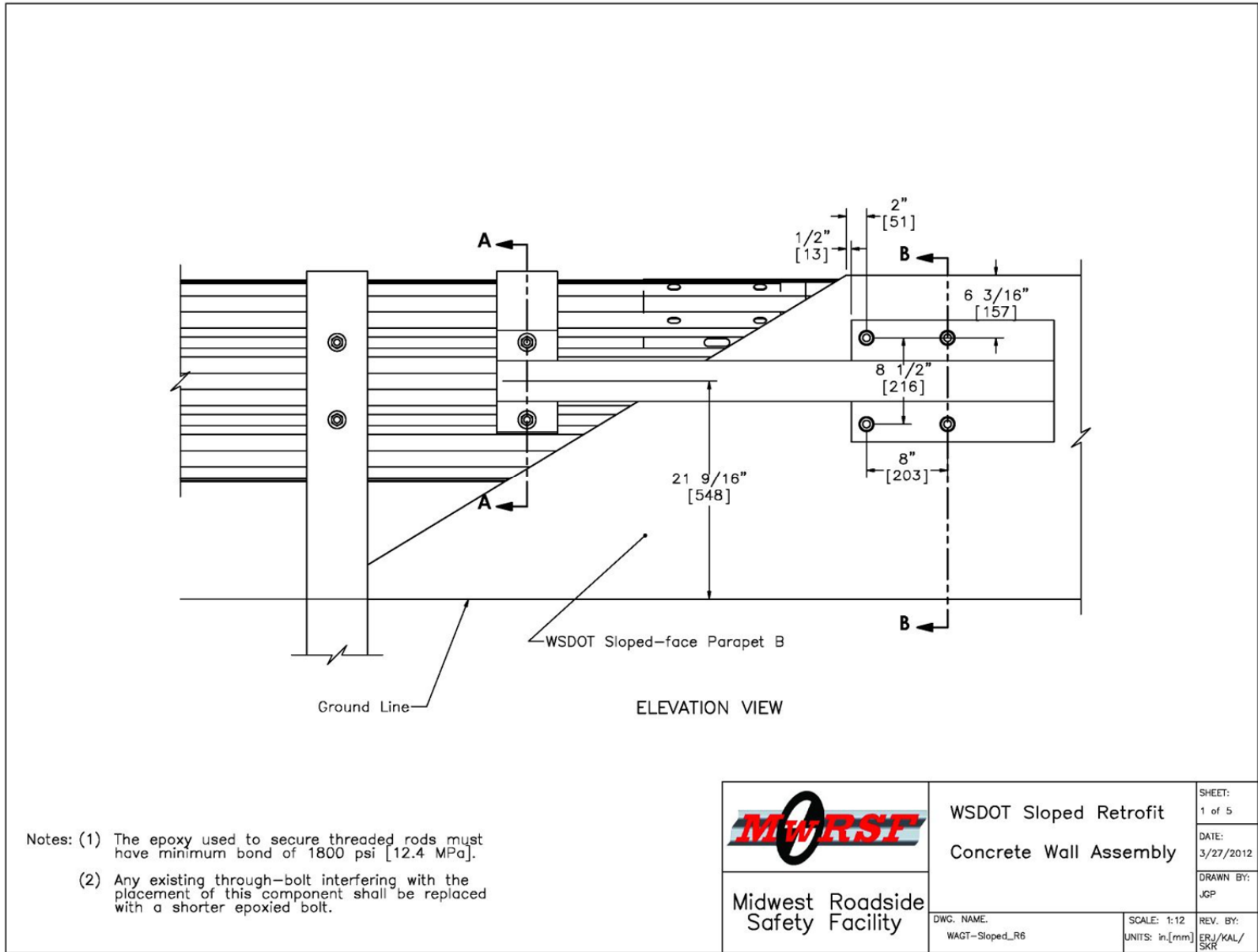


Figure 55. Retrofit 1 – Sloped-End Concrete Wall Assembly – Back View

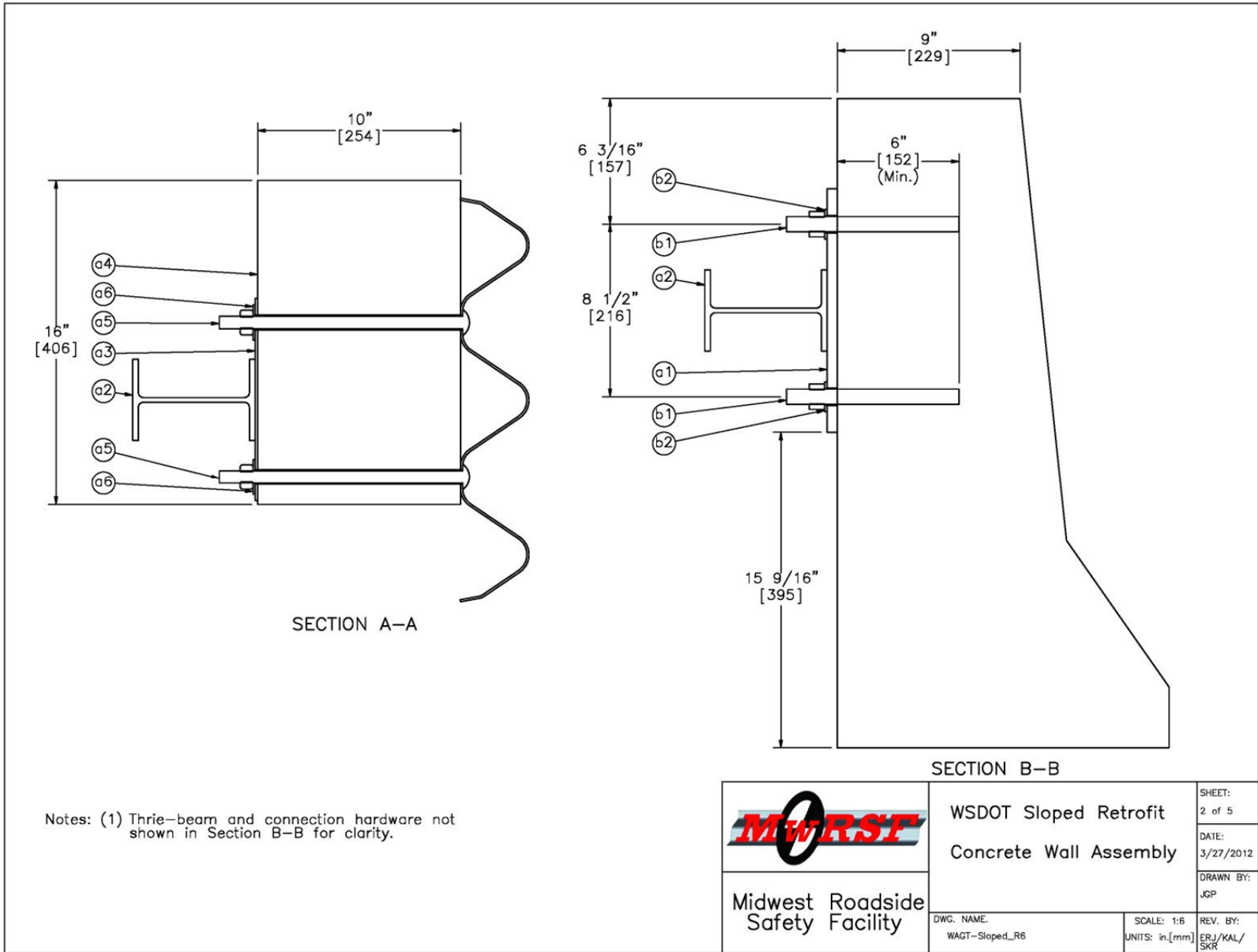


Figure 56. Retrofit 1 – Sloped-End Concrete Wall Assembly – Side View

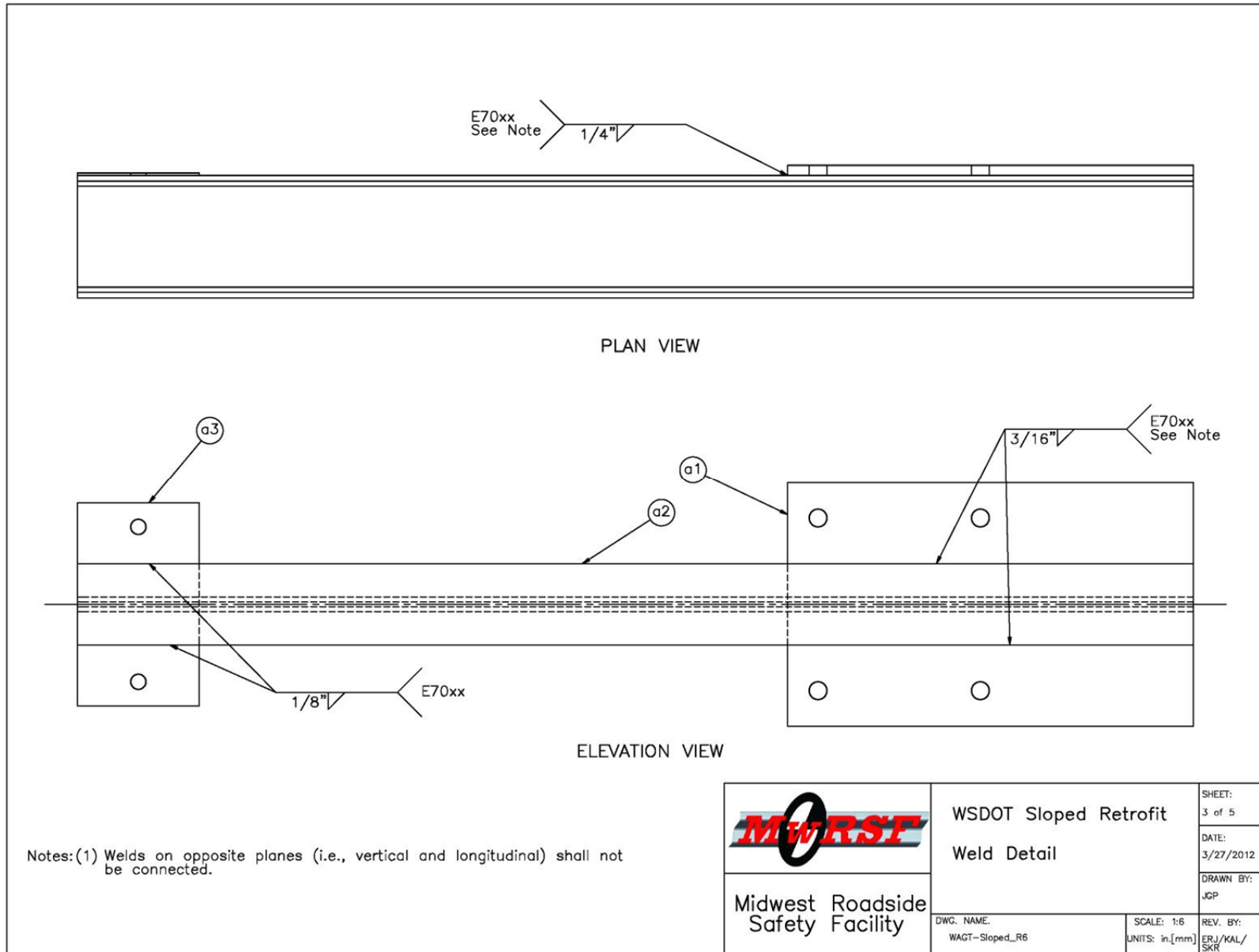


Figure 57. Retrofit 1 – Sloped-End Weld Detail

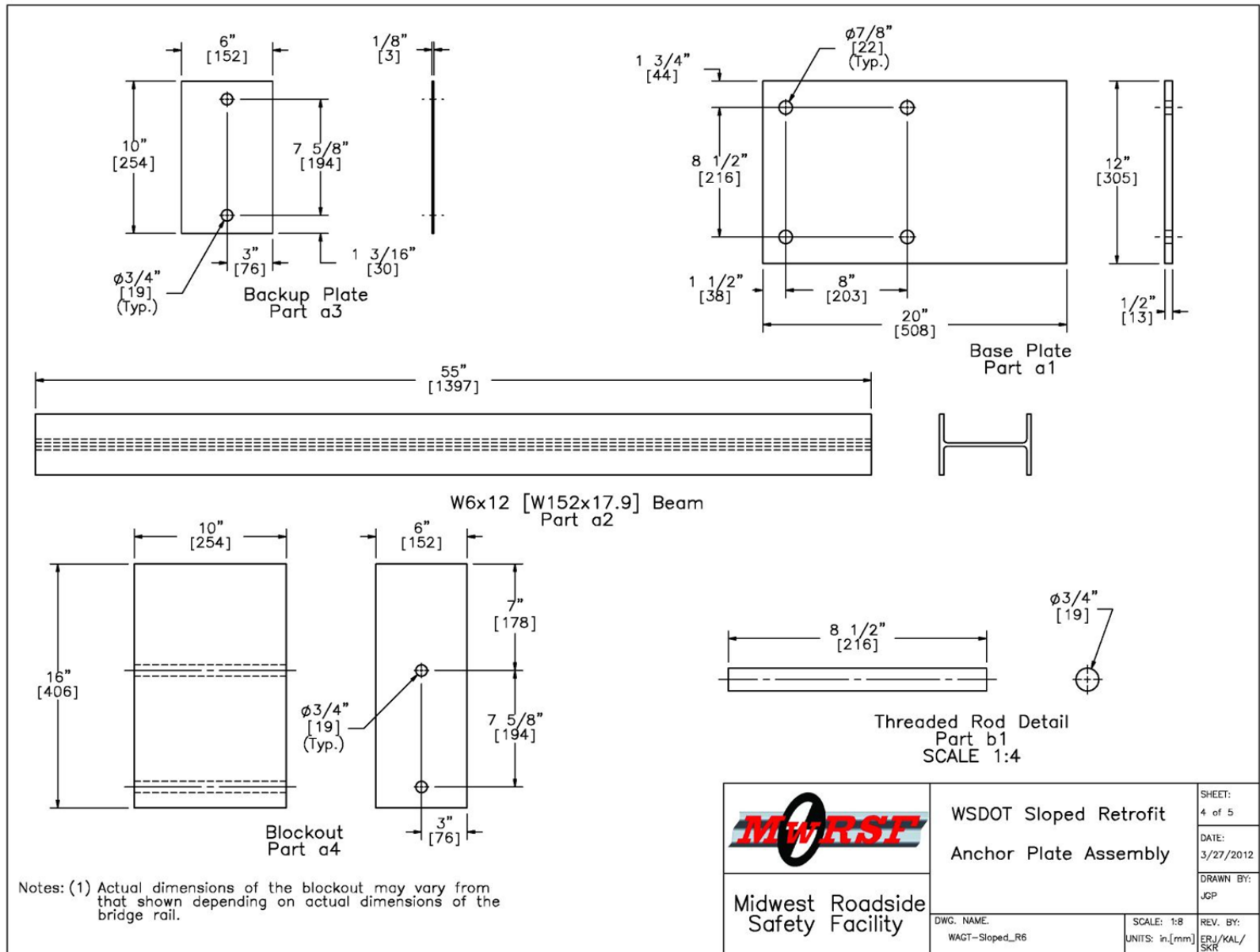


Figure 58. Retrofit 1 – Sloped-End Anchor Plate Assembly

WSDOT Sloped Faced Parapet B Retrofit Bill of Materials				
Item No.	QTY.	Description	Material Specification	Comments
a1	1	20"x12"x1/2" [508x305x13] Base Plate	ASTM A572 Gr. 50	—
a2	1	55" [1397] Long W6x12 [W152x17.9] Beam	ASTM A992 Gr. 50	—
a3	1	6"x10"x1/8" [152x254x3] Backup Plate	ASTM A36	Use ASTM A36 or any 50 ksi steel, which ever is more cost efficient
a4	1	6"x10"x16" [152x279x406] Blockout	SYP Grade No. 1 or better	—
a5	2	12" [305] Long, Dia. 5/8" [16] – 11 UNC Guardrail Bolt and Nut	SAE J429 Grade 2/ASTM A307 Grade C/ASTM F1554 Grade 36	—
a6	2	5/8" [16] Dia. Flat Washer	Grade 5	—
b1	4	8 1/2" [216] Long, Dia. 3/4" [19] – 10 UNC Threaded Rod	ASTM A193 type B7	—
b2	4	3/4" [19] Dia. Flat Washer	ASTM F436	—
b3	4	Dia. 3/4" [19] – 10 UNC Heavy Hex Nut	ASTM A563	—


	WSDOT Sloped Retrofit	SHEET: 5 of 5
	Bill of Materials	DATE: 3/27/2012
Midwest Roadside Safety Facility	DWG. NAME: WAGT-Sloped_R6	DRAWN BY: JGP
	SCALE: None UNITS: in,[mm]	REV. BY: EPJ/KAL/SKR

Figure 59. Retrofit 1 – Sloped-End Bill of Materials

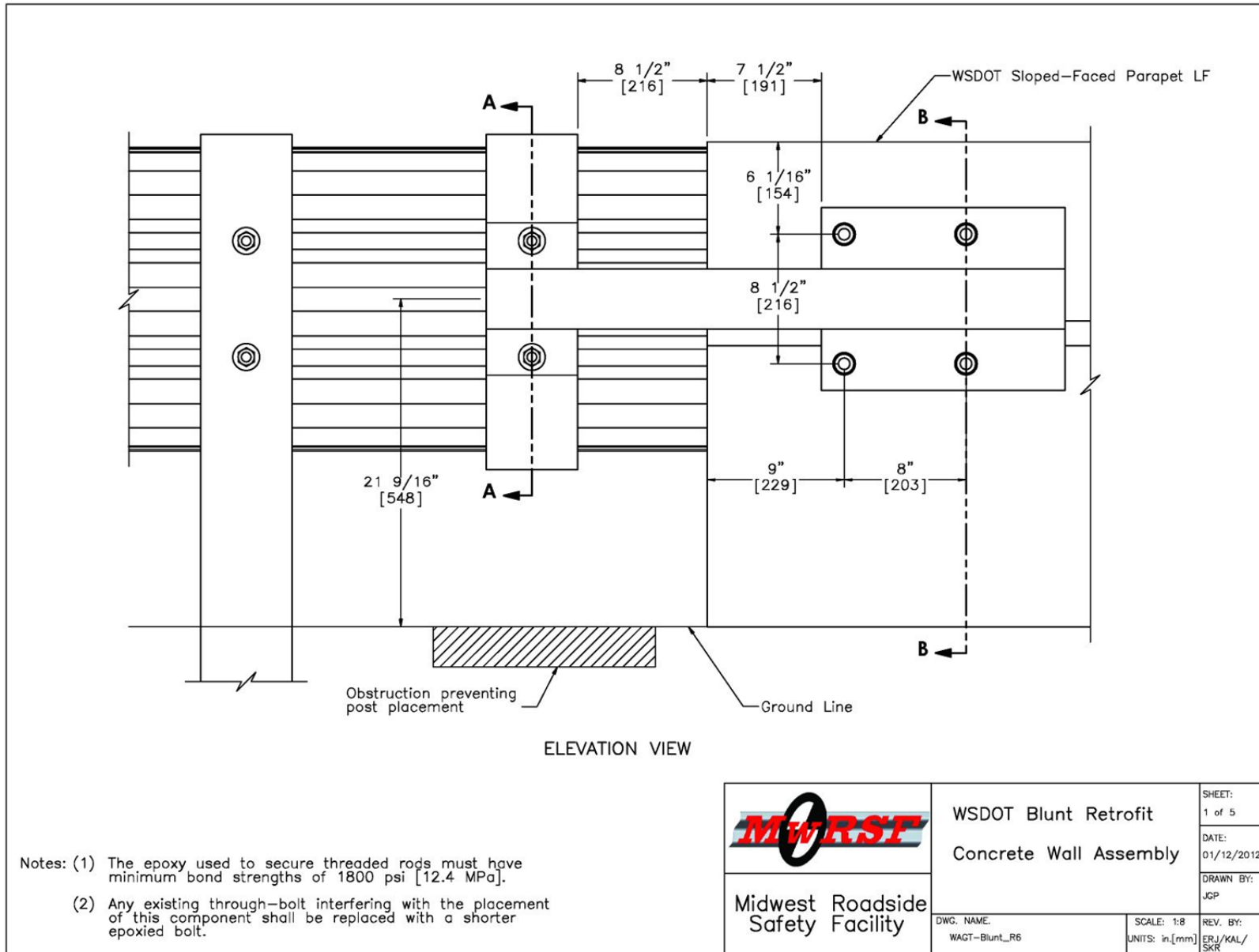


Figure 60. Retrofit 2 – Blunt-End Concrete Wall Assembly – Back View

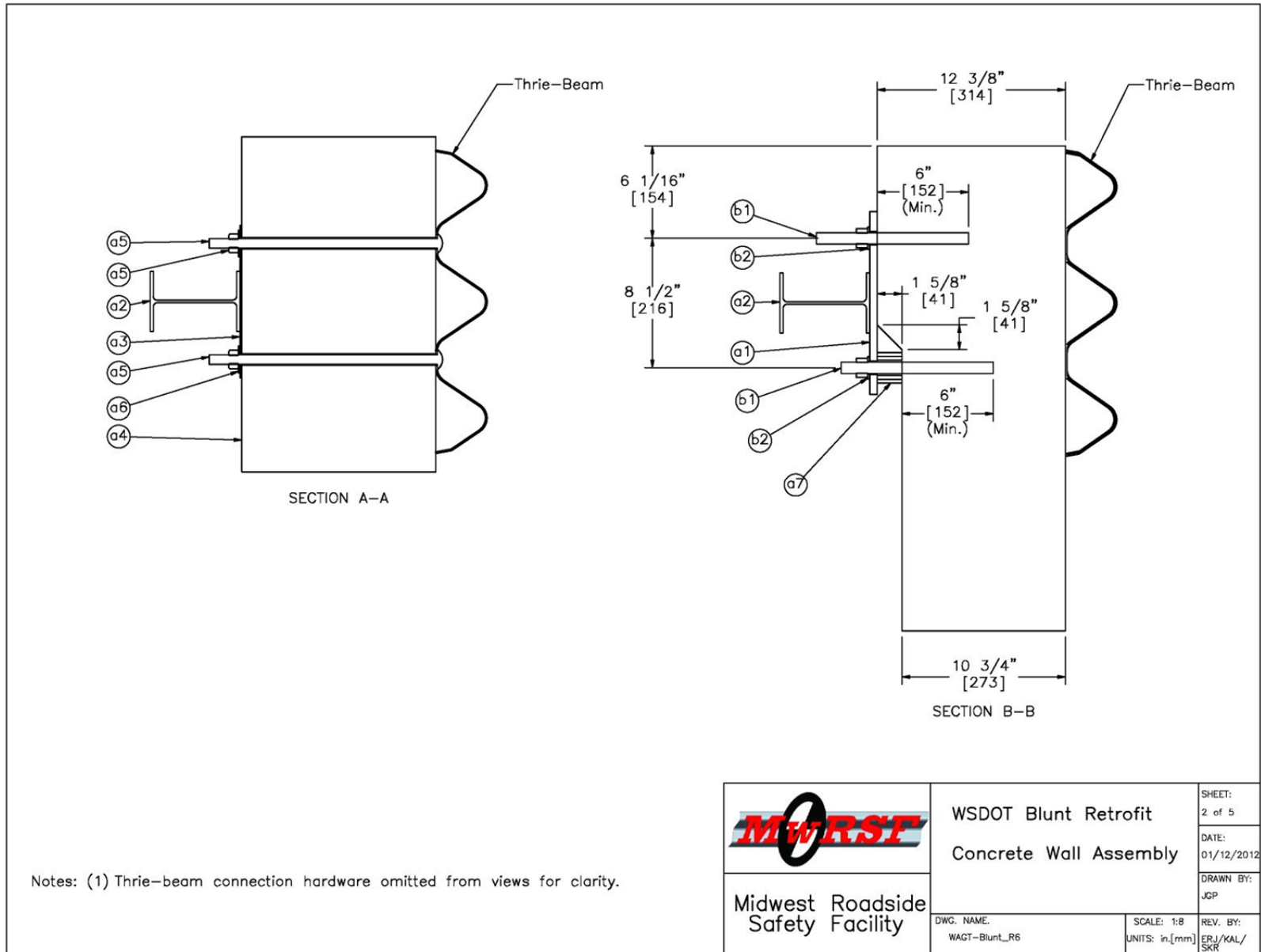


Figure 61. Retrofit 2 – Blunt-End Concrete Wall Assembly – Side View

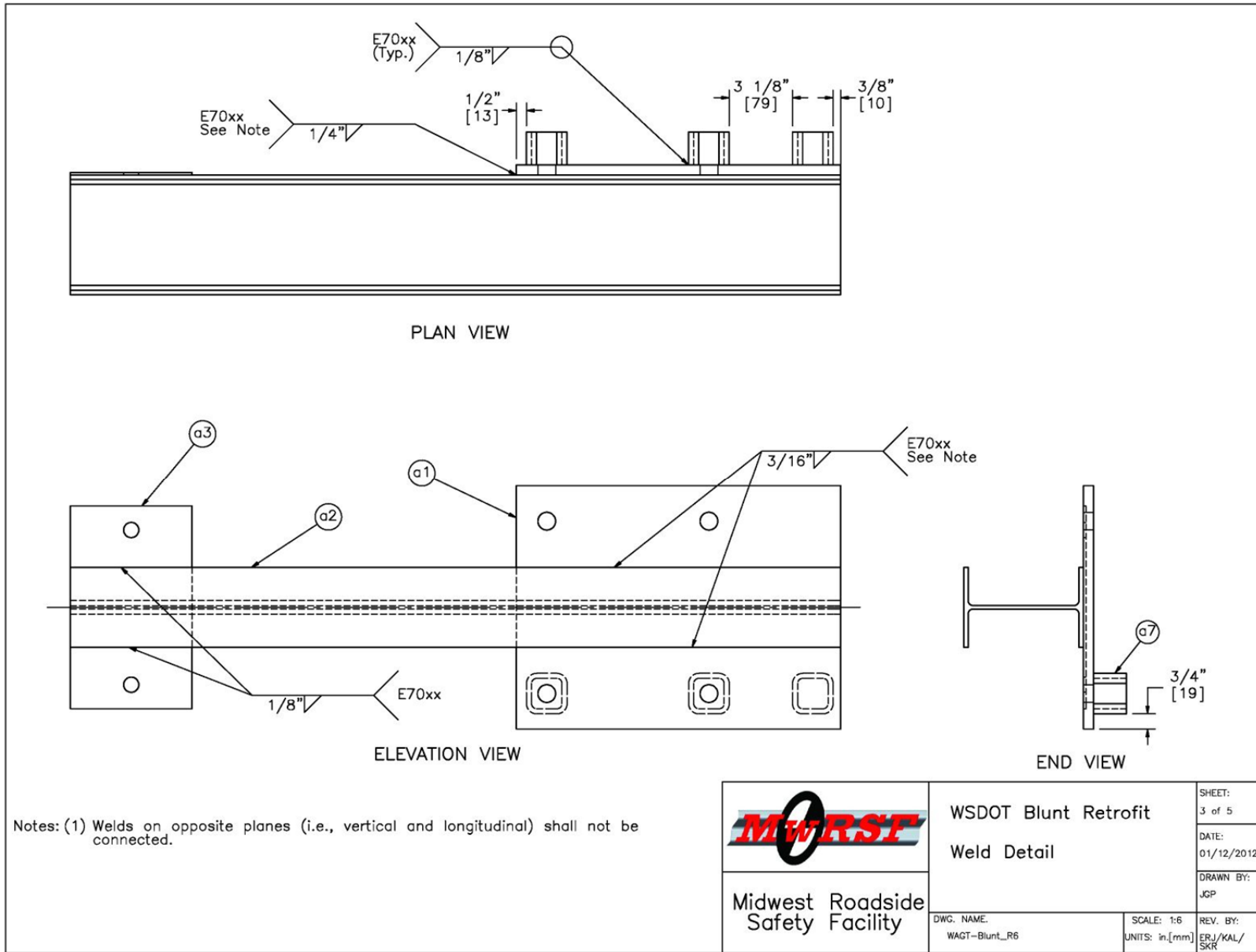


Figure 62. Retrofit 2 – Blunt-End Weld Detail

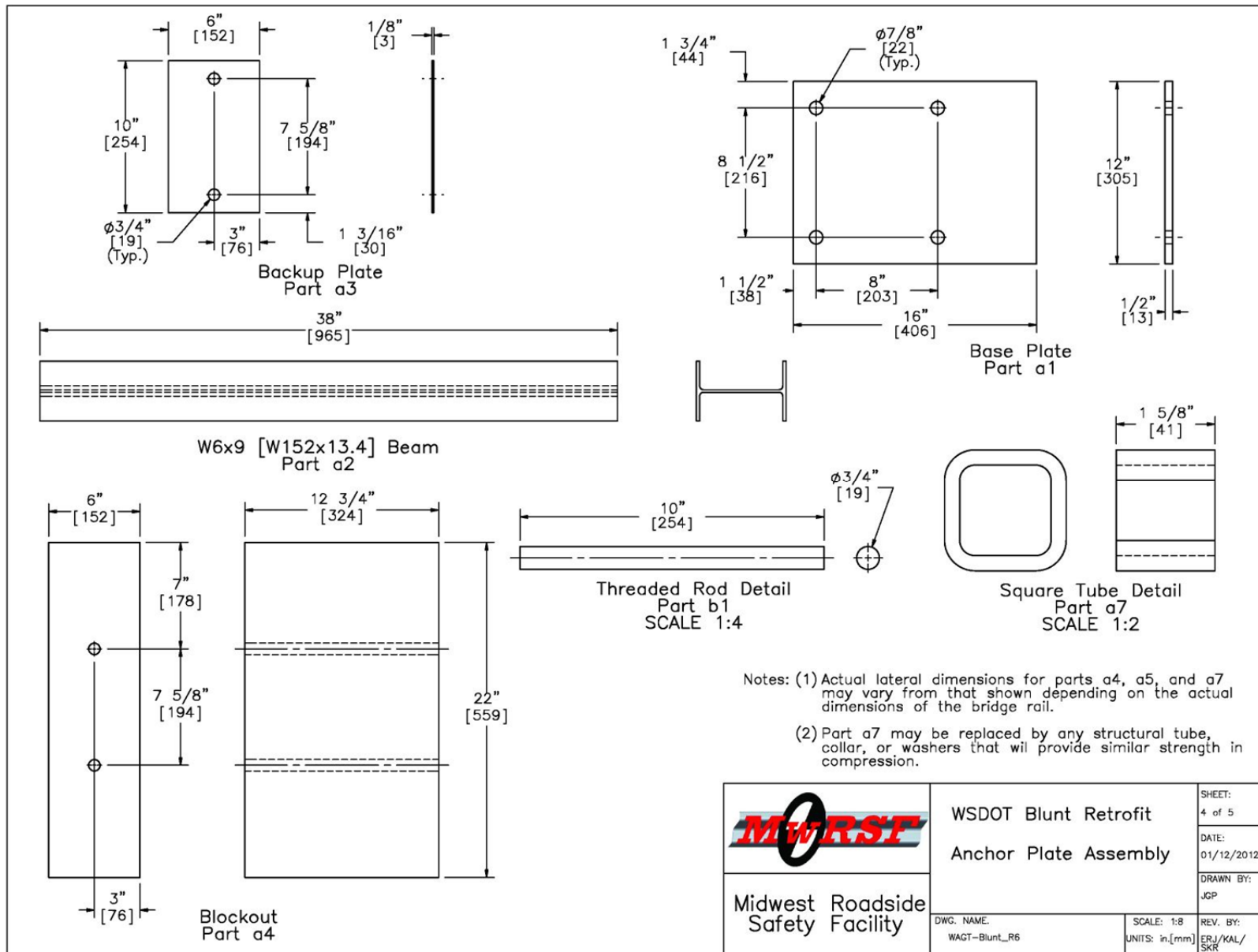


Figure 63. Retrofit 2 – Blunt-End Anchor Plate Assembly

WSDOT Sloped Faced Parapet LF Retrofit Bill of Materials				
Item No.	QTY.	Description	Material Specification	Comments
a1	1	16"x12"x1/2" [406x305x13] Base Plate	ASTM A572 Gr. 50	—
a2	1	38" [965] Long W6x9 [W152x13.4] Beam	ASTM A992 Gr. 50	—
a3	1	6"x10"x1/8" [152x254x3] Backup Plate	ASTM A36	Use ASTM A36 or any 50 ksi steel, which ever is more cost efficient
a4	1	6"x12.75"x22" [152x324x559] Blockout	SYP Grade No. 1 or better	—
a5	2	15" [381] Long, Dia. 5/8" [16] – 11 UNC Guardrail Bolt and Nut	SAE J429 Grade 2/ASTM A307 Grade C/ASTM F1554 Grade 36	—
a6	2	5/8" [16] Dia. Flat Washer	Grade 5	—
a7	3	2"x2"x1/4" [51x51x6] Square Tube 1 5/8" [41] Long	ASTM A36	—
b1	4	10" [254] Long, Dia. 3/4" [19] – 10 UNC Threaded Rod	ASTM A193 type B7	—
b2	4	3/4" [19] Dia. Flat Washer	ASTM F436	—
b3	4	Dia. 3/4" [19] – 10 UNC Heavy Hex Nut	ASTM A563	—


	WSDOT Blunt Retrofit Bill of Materials	SHEET: 5 of 5
	Midwest Roadside Safety Facility	DATE: 01/12/2012
DWG. NAME: WAGT-Blunt_R6	SCALE: None UNITS: in,[mm]	DRAWN BY: JGP
		REV. BY: EPJ/KAL/ SKR

Figure 64. Retrofit 2 – Blunt-End Bill of Materials

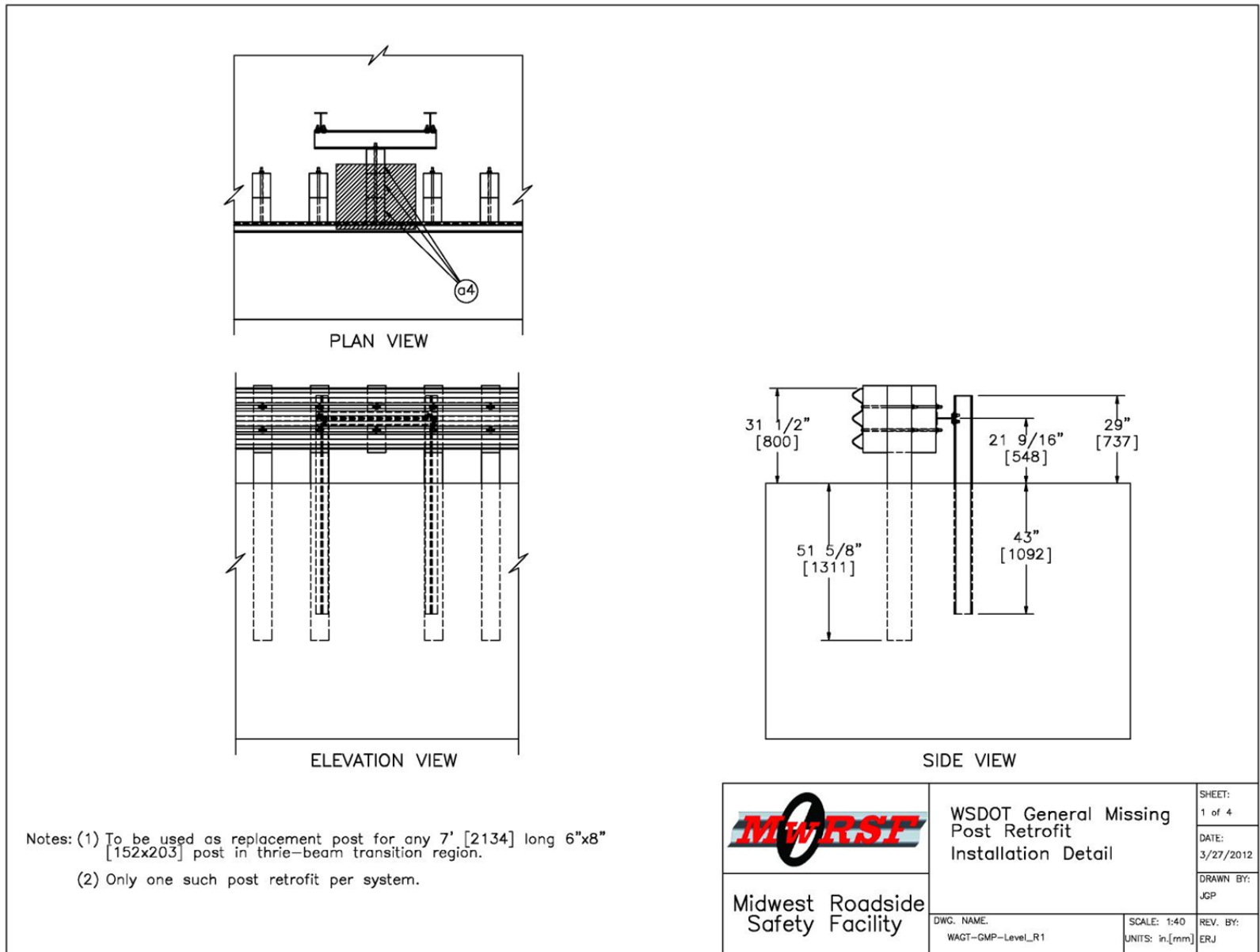


Figure 65. Retrofit 3A – General Missing Post Installation Detail

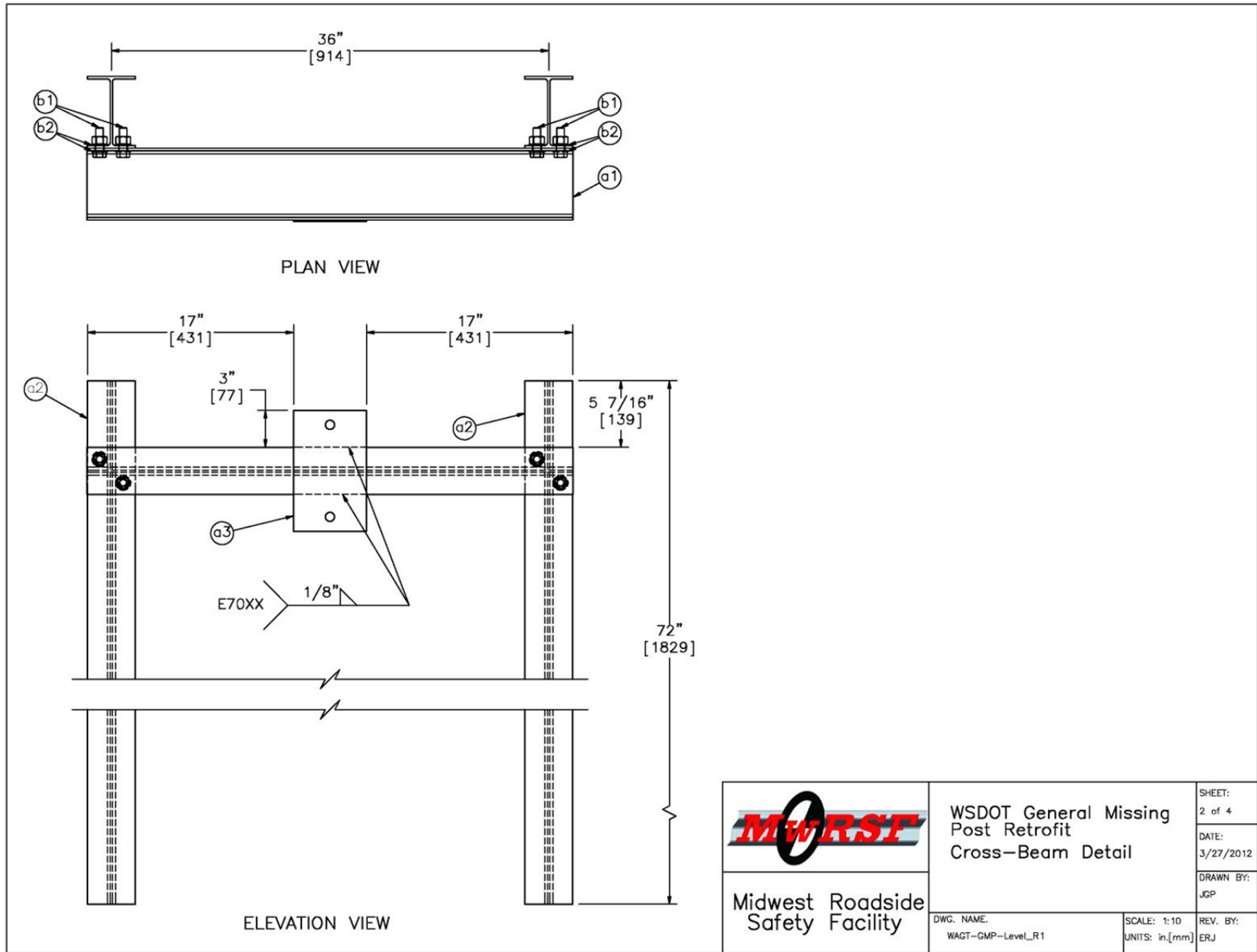


Figure 66. Retrofit 3A – General Missing Post Cross-Beam Detail

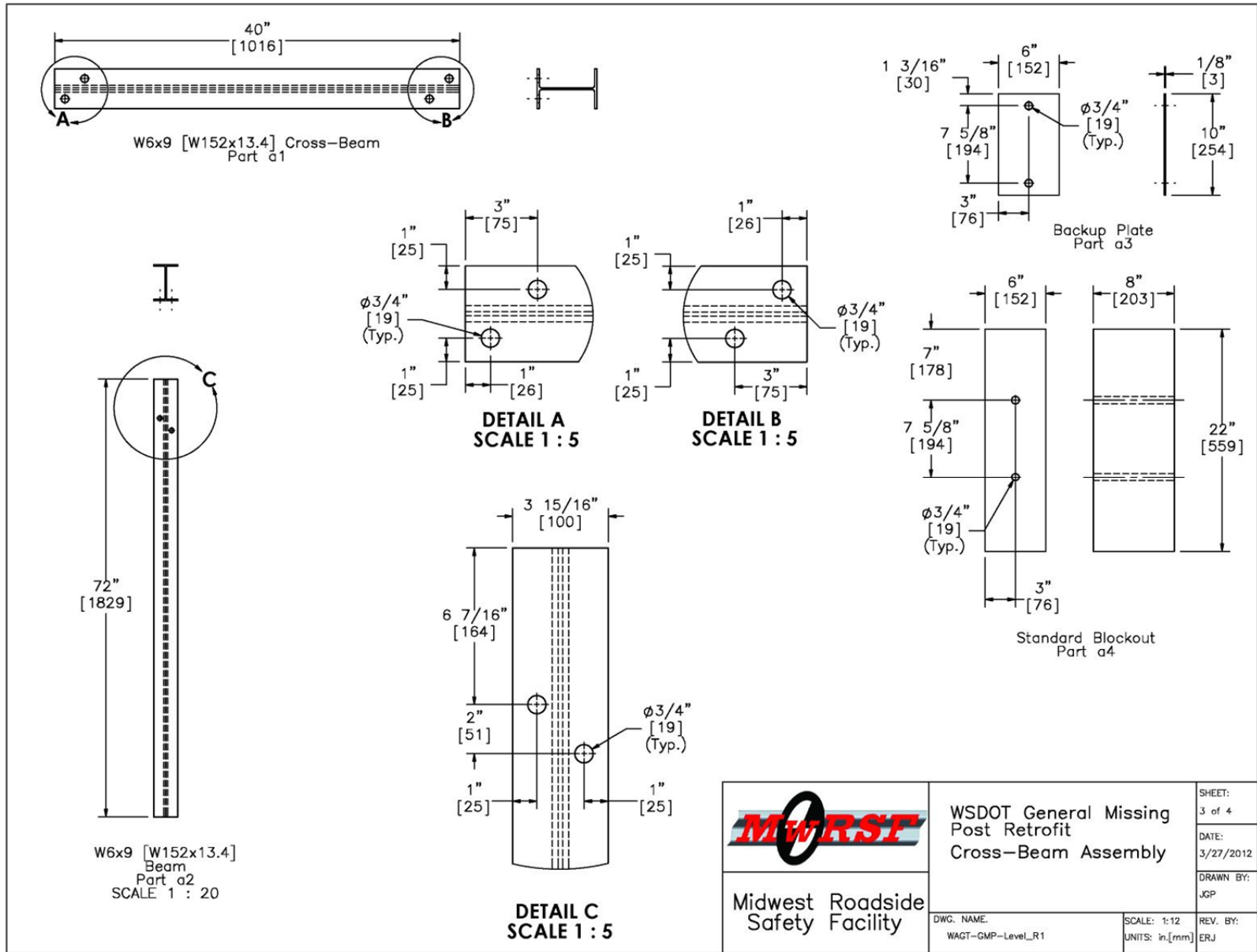


Figure 67. Retrofit 3A – General Missing Post Cross-Beam Assembly

WSDOT General Missing Post Retrofit Bill of Materials				
Item No.	QTY.	Description	Material Specification	Comment
a1	1	40" [1016] Long W6x9 [W152x13.4] Cross-Beam	ASTM A992 Gr. 50	-
a2	2	72" [1829] Long W6x9 [W152x13.4] Post	ASTM A992 Gr. 50	-
a3	1	6"x10"x1/8" [152x254x3] Backup Plate	ASTM A36	Use ASTM A36 or any 50 ksi steel, which ever is more cost efficient
a4	3	6"x8"x22" [152x203x559] Blockout	SYP Grade No. 1 or better	PDB02
b1	4	2" [51] long x Dia. 5/8" [16] - 11 UNC Hex Head Bolt	Bolt ASTM A307 or Grade 2 Steel/ Nut ASTM A563 A	FBX16a
b2	8	5/8" [16] Dia. Narrow Flat Washer	ASTM F436	-
b3	2	26" [660] Long, Dia. 5/8" [16] - 11 UNC Guardrail Bolt and Nut	SAE J429 Grade 2/ASTM A307 Grade C/ASTM F1554 Grade 36	-
b4	2	5/8" [16] Dia. Plain Round Washer	ASTM F844 or Grade 2 Steel	FWC16a


	WSDOT General Missing Post Retrofit Bill of Materials	SHEET: 4 of 4
	Midwest Roadside Safety Facility	DATE: 3/27/2012
DWG. NAME: WAGT-GMP-Level_R1	SCALE: None UNITS: in,[mm]	DRAWN BY: JGP
		REV. BY: ERJ

Figure 68. Retrofit 3A – General Missing Post Bill of Materials

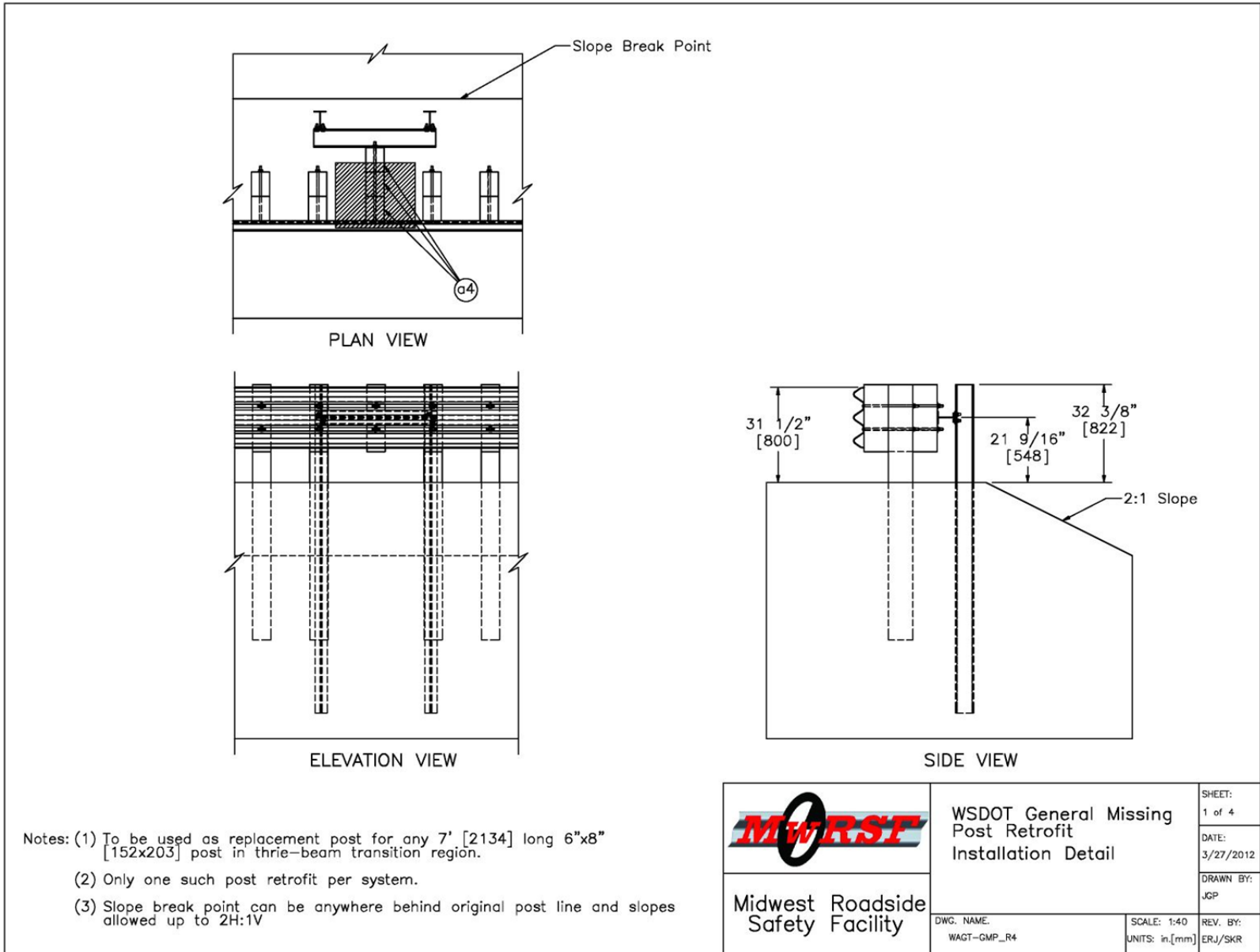


Figure 69. Retrofit 3B – General Missing Post Installation Detail

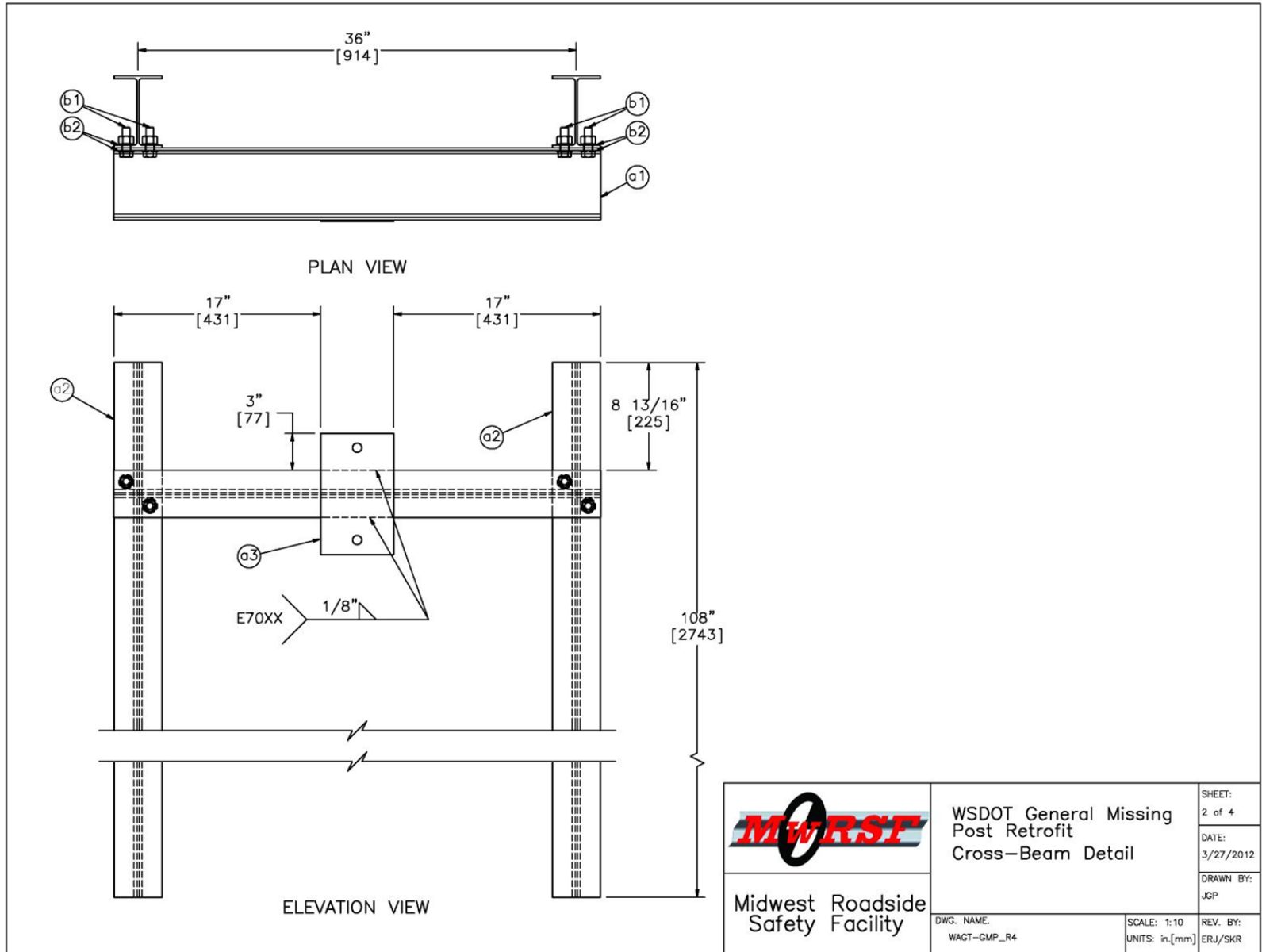


Figure 70. Retrofit 3B – General Missing Post Cross-Beam Detail

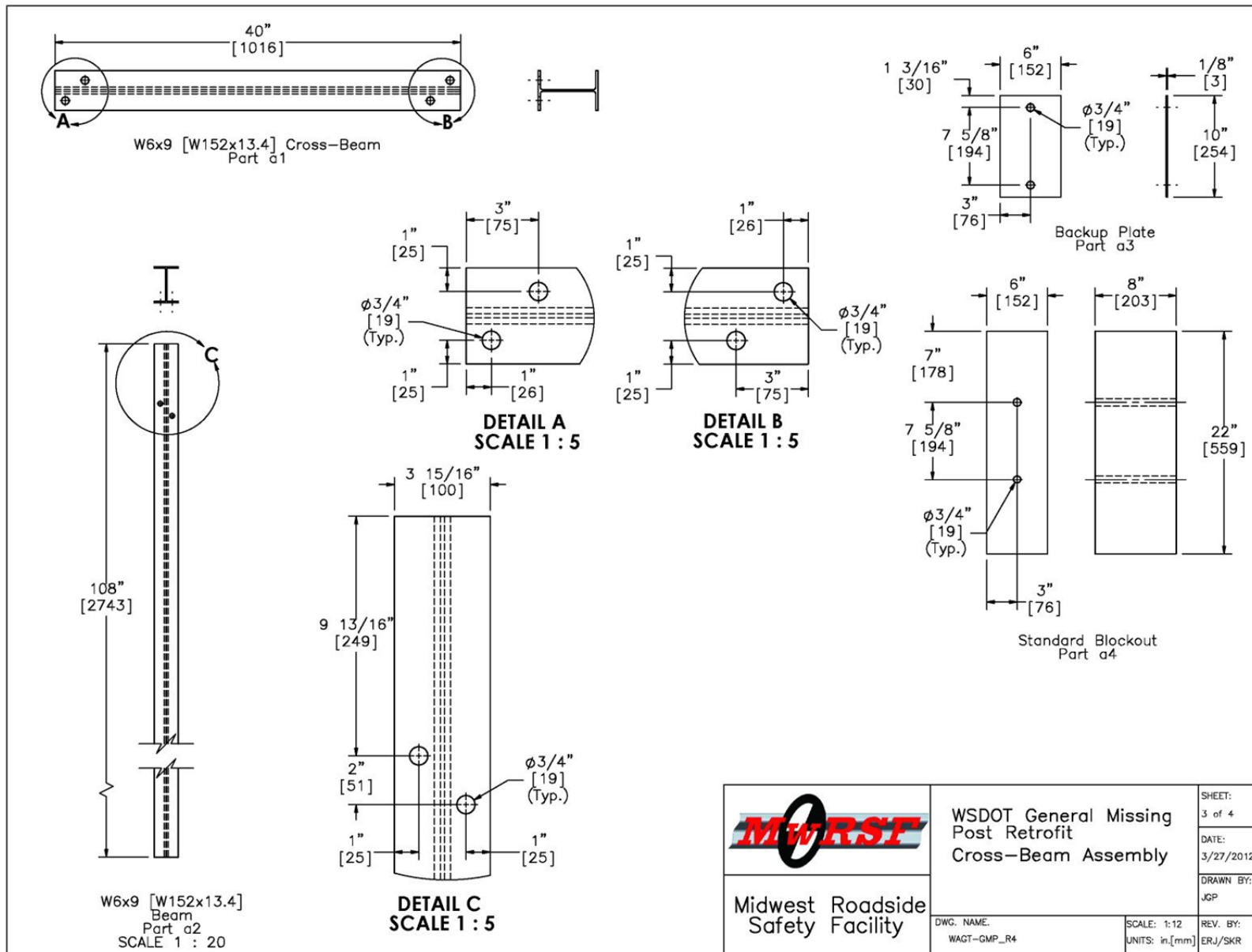


Figure 71. Retrofit 3B – General Missing Post Cross-Beam Assembly




WSDOT General Missing Post Retrofit Bill of Materials															
Item No.	QTY.	Description	Material Specification	Comment											
a1	1	40" [1016] Long W6x9 [W152x13.4] Cross-Beam	ASTM A992 Gr. 50	-											
a2	2	108" [2591] Long W6x9 [W152x13.4] Post	ASTM A992 Gr. 50	-											
a3	1	6"x10"x1/8" [152x254x3] Backup Plate	ASTM A36	Use ASTM A36 or any 50 ksi steel, which ever is more cost efficient											
a4	3	6"x8"x22" [152x203x559] Blockout	SYP Grade No. 1 or better	PDB02											
b1	4	2" [51] long x Dia. 5/8" [16] - 11 UNC Hex Head Bolt	Bolt ASTM A307 or Grade 2 Steel/ Nut ASTM A563 A	FBX16a											
b2	8	5/8" [16] Dia. Narrow Flat Washer	ASTM F436	-											
b3	2	26" [660] Long, Dia. 5/8" [16] - 11 UNC Guardrail Bolt and Nut	SAE J429 Grade 2/ASTM A307 Grade C/ASTM F1554 Grade 36	-											
b4	2	5/8" [16] Dia. Plain Round Washer	ASTM F844 or Grade 2 Steel	FWC16a											
<table border="1"> <tr> <td rowspan="2">  Midwest Roadside Safety Facility </td> <td rowspan="2"> WSDOT General Missing Post Retrofit Bill of Materials </td> <td>SHEET: 4 of 4</td> </tr> <tr> <td>DATE: 3/27/2012</td> </tr> <tr> <td rowspan="2"></td> <td rowspan="2"></td> <td>DRAWN BY: JGP</td> </tr> <tr> <td>REV. BY: ERJ/SKR</td> </tr> <tr> <td colspan="2">DWG. NAME: WAGT-GMP_R4</td> <td>SCALE: None UNITS: in,[mm]</td> </tr> </table>					 Midwest Roadside Safety Facility	WSDOT General Missing Post Retrofit Bill of Materials	SHEET: 4 of 4	DATE: 3/27/2012			DRAWN BY: JGP	REV. BY: ERJ/SKR	DWG. NAME: WAGT-GMP_R4		SCALE: None UNITS: in,[mm]
 Midwest Roadside Safety Facility	WSDOT General Missing Post Retrofit Bill of Materials	SHEET: 4 of 4													
		DATE: 3/27/2012													
		DRAWN BY: JGP													
		REV. BY: ERJ/SKR													
DWG. NAME: WAGT-GMP_R4		SCALE: None UNITS: in,[mm]													

Figure 72. Retrofit 3B – General Missing Post Bill of Materials

9 TRANSITION POSTS INSTALLED NEAR OR AT SLOPE BREAK POINT OF FILL SLOPES

9.1 Overview

As denoted in Section 3.2, it was common in the State of Wisconsin to find approach guardrail transition installations with posts installed near or at slope break point of fill slope. This observation was true for both the 18-ft 9-in. (5.7-m) long and the 31-ft 3-in. (9.5-m) long transition systems. In particular, insufficient level terrain behind the guardrail transitions had the potential to cause excessive barrier deflections, vehicle pocketing, as well as allow a vehicle to snag on the upstream end of the bridge rail. Therefore, two dynamic component tests were conducted to determine dynamic properties associated with 6-in. x 8-in. (152-mm x 203-mm) SYP wood posts installed at the slope break point of a 2H:1V fill slope. Subsequently, these post properties were used to create BARRIER VII computer models representing transition posts positioned on or nearby sloped terrain. Each transition system with posts on or near sloped terrain was analyzed and/or investigated to determine whether barrier performance was excessively degraded. Several alternatives were considered to alleviate any noted deficiencies resulting from posts installed near or at the slope break point of fill slopes.

It should be noted that the research and development as well as the successful component and full-scale crash testing of the original Iowa three beam approach guardrail transition system utilized SYP wood posts [32]. As such, this Wisconsin DOT research project also utilized SYP wood posts to serve as the baseline condition for the investigation and evaluation of degraded post and barrier performance when install near or at the slope break point of fill slopes.

The State of Wisconsin has significant native wood species (i.e., White Pine and Red Pine) that are desired for the fabrication of 6-in. x 8-in. (152-mm x 203-mm) line posts for W-beam guardrail systems. However, these native wood species have structural properties that are

moderately reduced from those structural properties exhibited by guardrail posts that are manufactured from the Southern Yellow Pine or Douglas Fir wood species. As such, guardrail posts manufactured from these reduced-strength, native wood species have not been recommended for use approach guardrail transitions unless successful safety performance has been demonstrated through full-scale vehicle crash testing or the cross-section has been appropriately resized.

9.2 Dynamic Component Testing

9.2.1 Scope

In previous research, MwRSF has conducted numerous dynamic bogie tests of 6-in. x 8-in. (152-mm x 203-mm) wood posts placed on various terrain [7-9, 32-36]. Although data obtained from those tests provided a valuable database for the expected post-soil resistance of 6-in. x 8-in. (152-mm x 203-mm) wood posts, none of the tests directly matched the parameters necessary for the current analysis. The research team determined that extrapolating resistances based on test data corresponding to different impact heights and embedment depths created some uncertainty. Specifically, the dynamic performance of 6-in. x 8-in. x 84-in. (152-mm x 203-mm x 2,134-mm) long wood posts was desired when embedded 52 in. (1,321 mm) into soil at the slope break point of a 2H:1V fill slope and impacted 21.65 in. (550 mm) above ground line. A 2H:1V fill slope was selected because it represented a conservatively severe slope (i.e., critical condition).

Two identical dynamic bogie tests were performed with 6-in.x 8-in. x 84-in. (152-mm x 203-mm x 2,134-mm) long SYP wood posts embedded 52 in. (1,321 mm) at the slope break point of a 2H:1V fill slope. The soil consisted of compacted, coarse, crushed limestone material that met AASHTO standard soil designation M147 Grade B, as recommended by MASH [14]. The target impact conditions consisted of a speed of 15 mph (24 km/h) and an angle of 0

degrees, creating a classical “head-on” or full frontal impact which results in strong-axis bending. The posts were impacted 21.65 in. (550 mm) above the ground line and perpendicular to the front face of the post. The following guidelines were established to define the end of test time using the high-speed video of the crash test. The first occurrence of any one of the following three events was used to determine the end of the test: (1) the test article fractures; (2) the surrogate vehicle overrides/loses contact with the test article; or (3) a maximum post rotation of 45 degrees. All other testing conditions, methods, and equipment remained consistent with those described in Chapter 6. The test setup and post details are shown in Figures 73 and 74. Dimensions and properties of the wood posts utilized in the tests are shown in Table 25.

Table 25. Wood Post Properties – WITB Testing Series

Test No.	Post Dimensions in. x in. (mm x mm)			Post Length in. (mm)	Weight lb (kg)	Ring Density rings/in. (rings/cm)
	At Top	At Groundline	At Bottom			
WITB-1	6 x 8 ¹ / ₈ (152 x 206)	6 x 8 ⁵ / ₁₆ (152 x 211)	6 x 8 ⁵ / ₁₆ (152 x 211)	84 ¹ / ₄ (2,140)	97.8 (44.4)	3.5 (1.4)
WITB-2	6 x 8 ³ / ₁₆ (152 x 208)	6 x 8 ¹ / ₄ (152 x 210)	6 x 8 ¹ / ₈ (152 x 206)	84 ³ / ₁₆ (2,138)	102.2 (46.4)	2 (0.8)

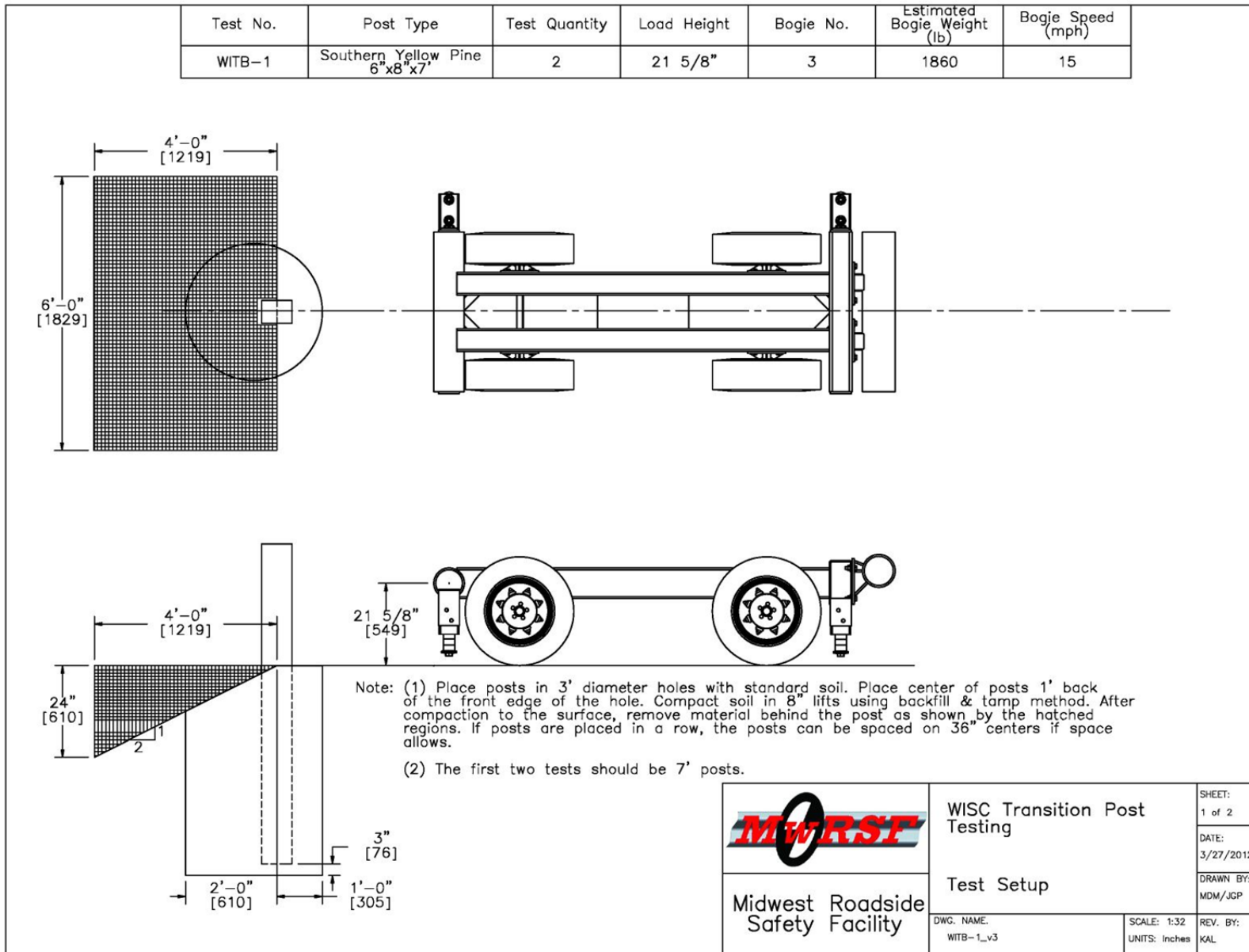


Figure 73. WITB Bogie Testing Matrix and Setup

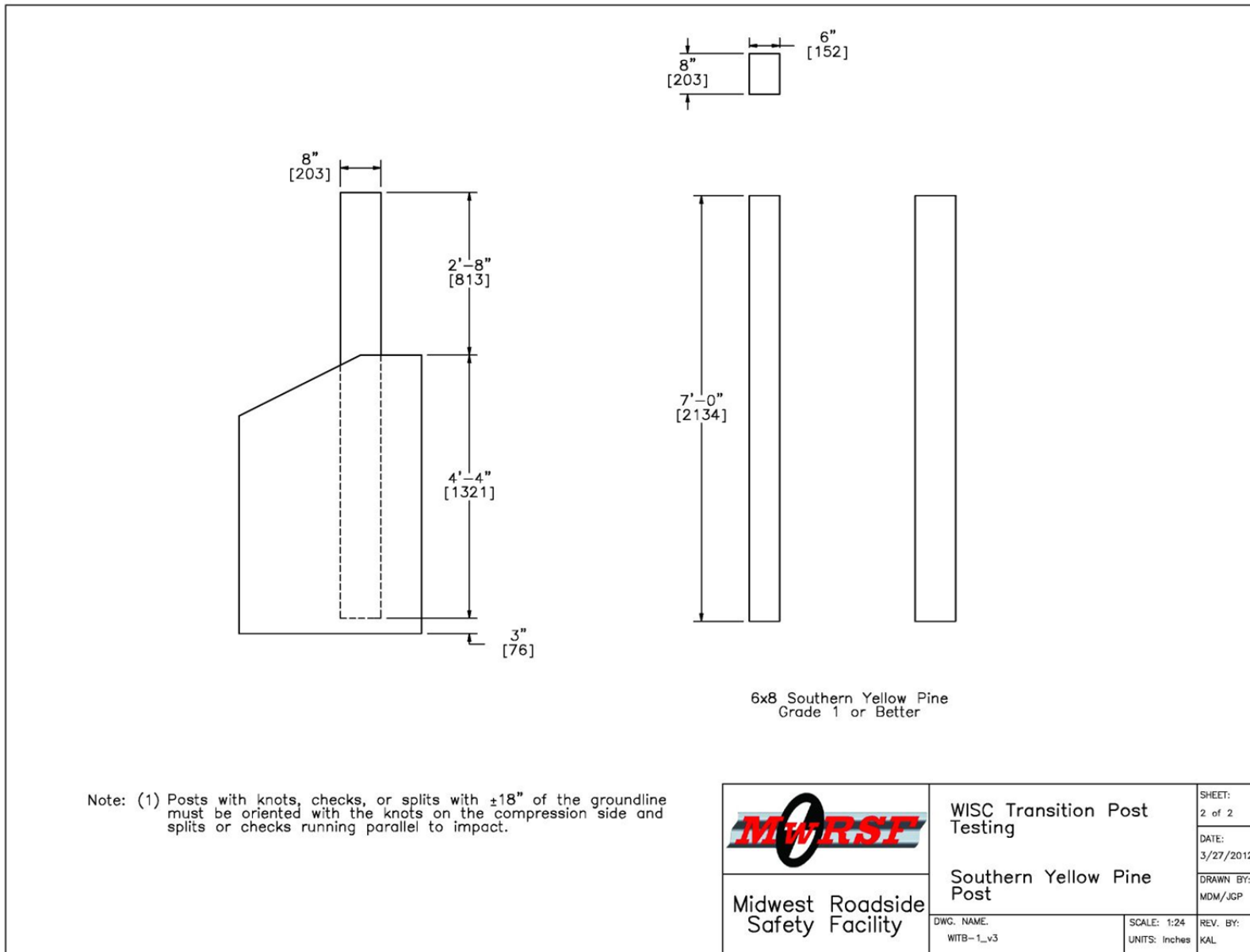


Figure 74. WITB Bogie Testing Post Details

9.2.2 Bogie Testing and Results

9.2.2.1 Test No. WITB-1

During test no. WITB-1, the bogie impacted a 6-in. x 8-in. x 84-in. (152-mm x 203-mm x 2,134-mm) long wood post at the slope break point of a 2H:1V fill slope at a speed of 15.7 mph (25.3 km/h), causing strong-axis post bending. The post rotated through the soil to a peak deflection of 26.7 in. (678 mm), showing no signs of fracture. The bogie impact head lost contact with the post after 0.376 seconds as the bogie was brought to a stop and rebounded backward.

Force vs. deflection and energy vs. deflection curves were created from the accelerometer data and are shown in Figure 75. Initially, inertial effects resulted in a peak force of 9.8 kips (43.6 kN) over the first few inches of deflection. Starting at approximately 4 in. (102 mm) of deflection, the force gradually began to decrease until approximately a deflection of 13 in. (330 mm), where a relatively steady force of around 6 kips (27 kN) was observed for the rest of the impact event. The post rotating through the soil absorbed 170.9 kip-in. (19.3 kJ) of energy. Time-sequential photographs and post-impact photographs are shown in Figure 76.

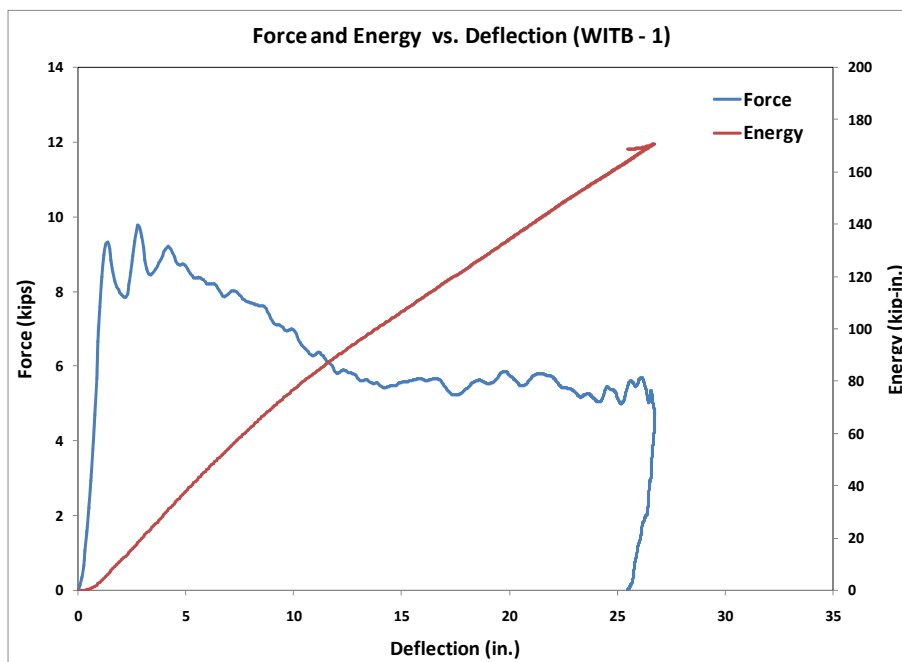


Figure 75. Force vs. Deflection and Energy vs. Deflection, Test No. WITB-1



Post After Impact – Side view



Post After Impact – Soil Displacement

Figure 76. Time-Sequential and Post-Impact Photographs, Test No. WITB-1

9.2.2.2 Test No. WITB-2

During test no. WITB-2, the bogie impacted a 6-in. x 8-in. x 84-in. (152-mm x 203-mm x 2,134-mm) long wood post at the slope break point of a 2H:1V fill slope at a speed of 15.1 mph (24.3 km/h), causing strong-axis post bending. The post rotated through the soil to a peak deflection of 26.7 in. (678 mm), showing no signs of fracture. The bogie impact head lost contact with the post after 0.366 seconds as the bogie was brought to a stop and rebound backward.

Force vs. deflection and energy vs. deflection curves were created from the accelerometer data and are shown in Figure 77. Initially, inertial effects resulted in a peak force of 9.1 kips (40.5 kN) over the first few inches of deflection. Starting at approximately 4 in. (102 mm) of deflection, the force gradually began to decrease until a deflection of approximately 15 in. (381 mm), where a relatively steady force of around 5 kips (22 kN) was observed for the rest of the impact event. The post rotating through the soil absorbed 158.2 kip-in. (17.9 kJ) of energy. Time-sequential photographs and post-impact photographs are shown in Figure 78.

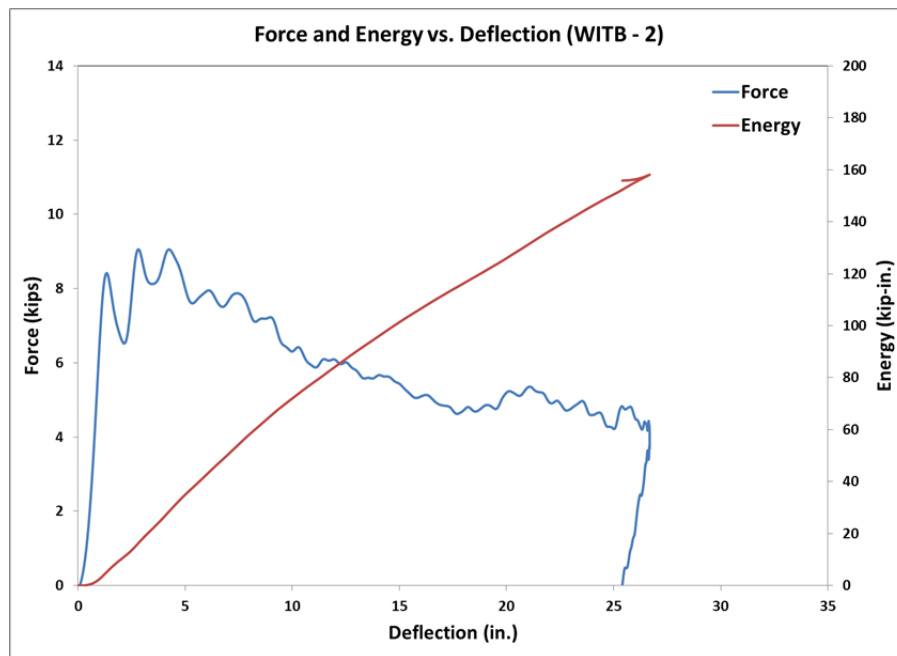
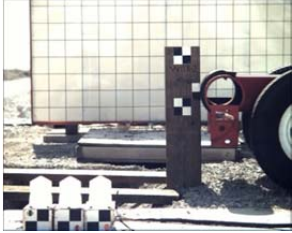


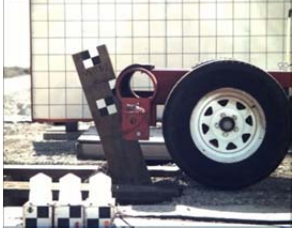
Figure 77. Force vs. Deflection and Energy vs. Deflection, Test No. WITB-2



IMPACT



0.050 sec



0.100 sec



0.150 sec



0.200 sec



0.250 sec



Post After Impact – Side view



Post After Impact – Soil Displacement

Figure 78. Time-Sequential and Post-Impact Photographs, Test No. WITB-2

9.2.3 Discussion

Results from the two bogie tests are summarized in Table 26. Force vs. deflection curves for the two tests, as shown in Figure 79, were similar throughout the test durations. In fact, both posts experienced identical maximum deflections. Likewise, inertial peak forces and average resistive forces between tests were consistent, both in terms of magnitude and duration. The peak energy absorbed in WITB-1 was slightly higher than that of WITB-2, but it was largely due to a slightly higher impact velocity. The similarities in absorbed energy between the two test setups can be seen in the energy vs. deflection comparison plot shown in Figure 80. The consistency in test results demonstrated that an accurate estimate was obtained for the dynamic post-soil behavior of 6-in. x 8-in. (152-mm x 203-mm) wood posts embedded 52 in. (1,321 mm) at the slope break point of a 2H:1V fill slope and loaded 21.65 in. (550 mm) above grade.

Table 26. Testing Results – 6-in. x 8-in. Wood Posts Embedded 52 in. on 2H:1V Fill Slope

Test No.	Impact Velocity (mph)	Peak Force		Average Force			Absorbed Energy			Maximum Deflection (in.)	Total Energy (kip-in.)	Failure Type
		Deflection (in.)	Force (kips)	@ 5 in. (kips)	@ 10 in. (kips)	@ 15 in. (kips)	@ 5 in. (kip-in.)	@ 10 in. (kip-in.)	@ 15 in. (kip-in.)			
WITB-1	15.7	2.8	9.8	7.5	7.7	7.1	38.0	77.2	106.5	26.7	170.9	Rotation in Soil
WITB-2	15.1	4.2	9.1	7.0	7.2	6.8	35.5	72.2	101.5	26.7	158.2	Rotation in Soil
Series Average			9.4	7.2	7.4	6.9	36.8	74.7	104.0			

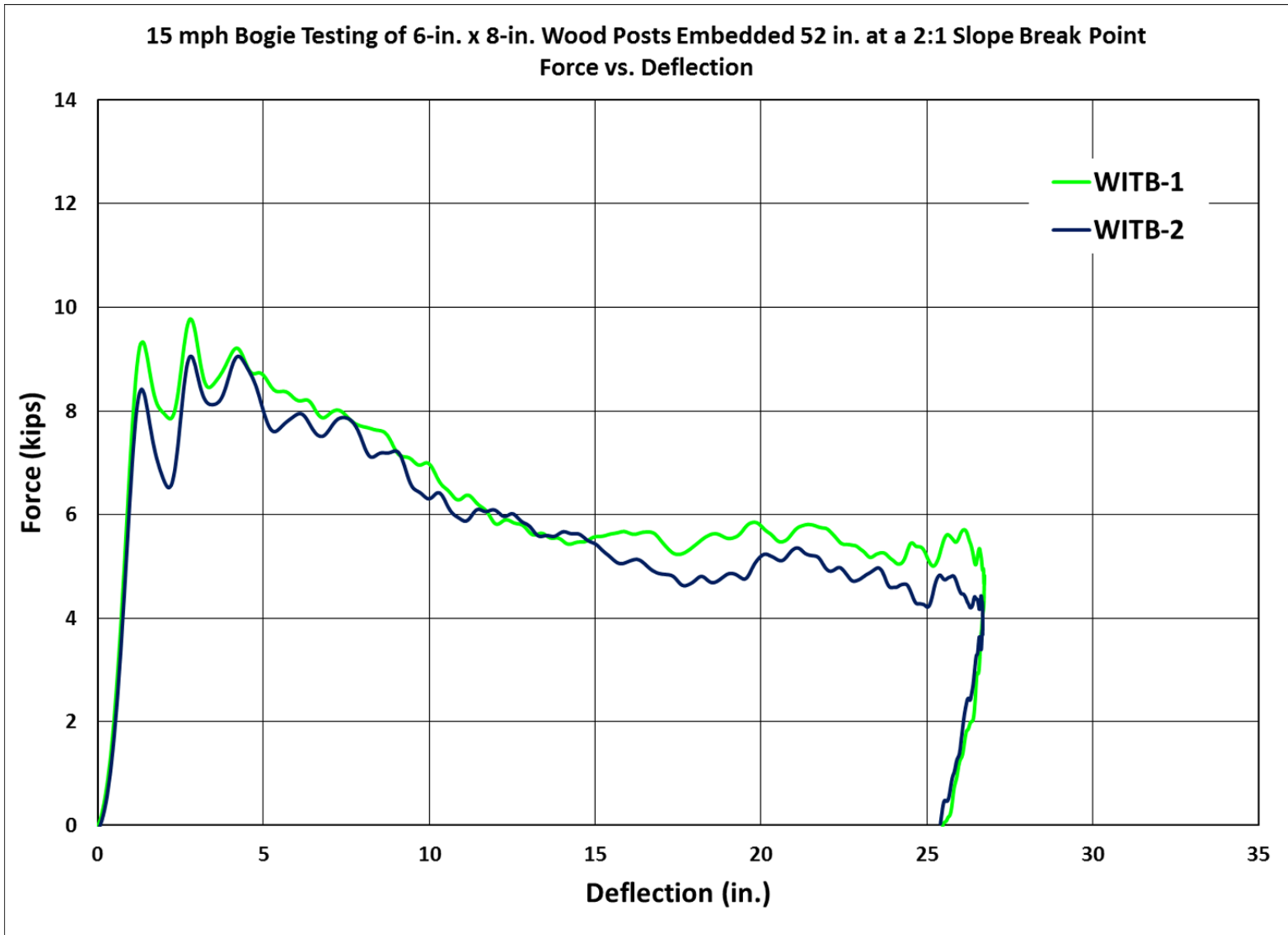


Figure 79. Force vs. Deflection Comparison Plot, WITB Bogie Testing

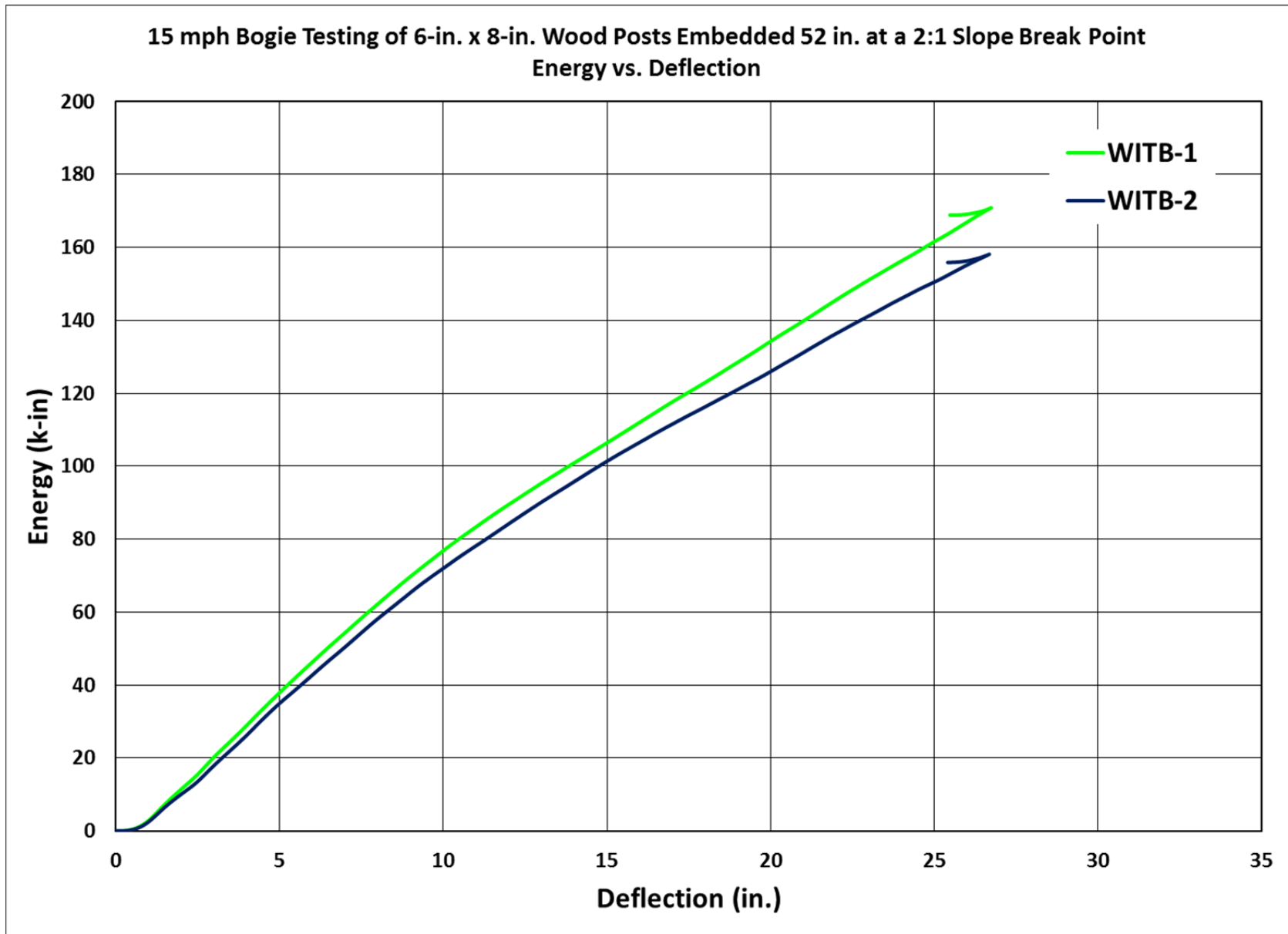


Figure 80. Energy vs. Deflection Comparison Plot, WITB Bogie Testing

9.3 BARRIER VII Analysis

BARRIER VII computer simulations were conducted to replicate vehicular impacts with both the 18-ft 9-in. (5.7-m) long transition system and the 31-ft 3-in. (9.5-m) long transition system positioned at or nearby sloped terrain. Each post located within the nested thrie beam section of the transition utilized the stiffness and strength of 6-in. x 8-in. x 84-in. (152-mm x 203-mm x 2,134-mm) long wood posts embedded 52 in. (1,321 mm) into the soil at the slope break point of a 2H:1V fill slope. Force vs. deflection results obtained from test nos. WITB-1 and WITB-2 were used to derive the BARRIER VII input parameters, as shown in Table 27. The average force of 7.4 kips (32.9 kN) over 10 in. (254 mm) of deflection provided the basis for strong-axis resistance for the BARRIER VII model. Utilizing an impact height of 21.65 in. (550 mm), the strong-axis bending moment, M_A , was calculated to be 160 k-in. (18.1 kN-m). A post stiffness, K_B , of 7 kips/in. (1.2 kN/mm) was approximated from the force vs. deflection curves of the two component tests.

Table 27. Input Properties – 6 in. x 8 in. Wood Posts Embedded 52 in. on 2H:1V Fill Slope

BARRIER VII Parameters		Wood Post at 2H:1V Fill Slope	Wood Post on Level Terrain
Load Height	in.	21.65	21.65
K_B - Strong-Axis Post Stiffness	kips/in.	7	8
M_A - Strong-Axis Bending Moment	kip-in.	160	476
δ_{FB} - Strong-Axis Displacement Failure	in.	15	15

The computer simulations consisted of a 4,409-lb (2,000-kg) pickup truck impacting at a speed of 62.1 mph (100 km/h) and at an angle of 25 degrees. Each barrier model was iteratively impacted at 9³/₈-in. (238-mm) intervals along the transition system to determine values for dynamic deflection and vehicle pocketing angles within the nested thrie beam section of the

barrier and vehicle wheel rim snag on the upstream end of the bridge rail. A total of 24 and 40 simulations were conducted to evaluate the 18-ft 9-in. (5.7-m) long system and the 31-ft 3-in. (9.5-m) long system, respectively. Comprehensive results from these simulation runs can be found in Appendix D. As shown in Table 28, the maximum values corresponding to dynamic barrier deflection and vehicle wheel rim snag on the upstream end of the bridge rail were determined.

Table 28. Summary of Simulation Results for 2H:1V Fill Slopes

BARRIER VII Evaluation Parameter		18-ft 9-in. Transition	31-ft 3-in. Transition
Dynamic	Maximum Value (in.)	10.55	10.61
Deflection	Corresponding Baseline Value (in.)	6.22	8.14
Wheel Rim	Maximum Value (in.)	3.45	3.82
Snag	Evaluation Limit (in.)	2.00	2.00
Pocketing	Maximum Value (deg)	13.5	14.0
Anlge	Corresponding Baseline Value (deg)	8.3	8.8

The barrier model which represented the highest propensity for vehicle wheel rim snag on the rigid bridge rail end was the 31-ft 3-in. (9.5-m) long transition system positioned on a 2H:1V fill slope. Nonetheless, both models predicted a value for vehicle wheel rim snag significantly greater than the 2-in. (51-mm) evaluation limit. In fact, the predicted values for vehicle wheel rim snag reached nearly twice the respective baseline value for the longer transition system. Further, the maximum dynamic deflection and maximum vehicle pocketing angle of both systems were also significantly increased from the corresponding baseline simulated deflections and pocketing angles. Thus, a retrofit was indeed required to increase the stiffness and strength of either Wisconsin transition system located on a 2H:1V fill slope.

9.4 Retrofit Development

Four unique solutions were considered to resolve the deficiency created by transition systems with steep-sloped terrain located behind the posts: (i) supplement the terrain with additional backfill to flatten the fill slope; (ii) utilize extra driven posts on slope and behind existing posts with increased strength characteristics (e.g., shape, embedment depth, etc.); (iii) remove existing posts and replace with new stronger and longer posts; or (iv) utilize an additional beam along the back side of the system with or without a new, upstream end post, as shown in Figure 81. The first three options focused on restoring lost post-soil resistance, while the fourth option focused on the dissipation of energy through additional post stiffening and rail bending.

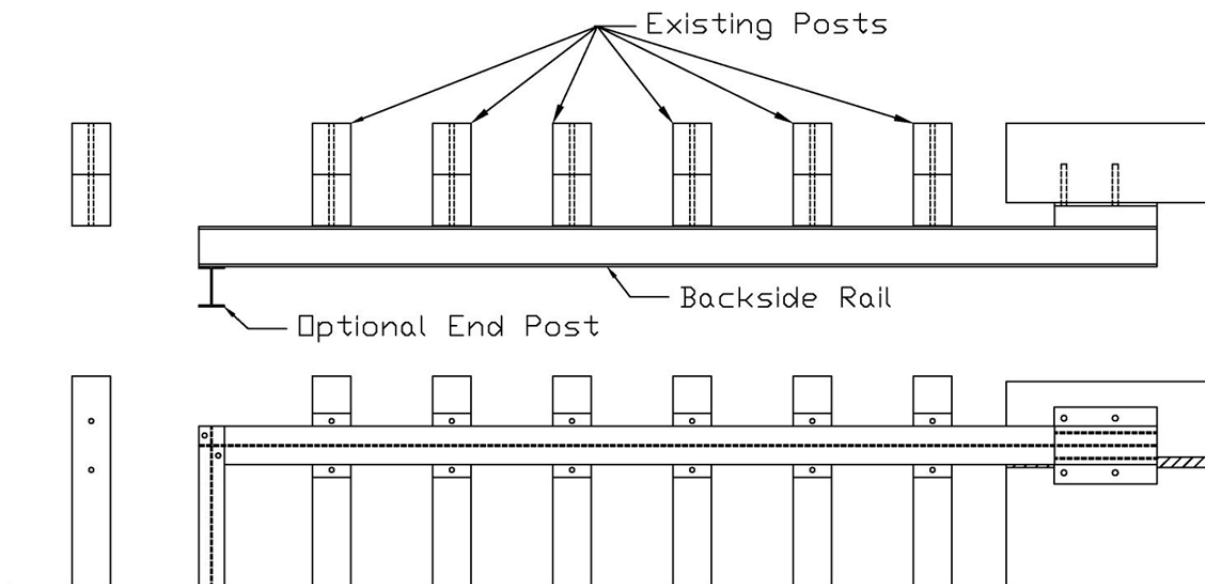


Figure 81. Backside Beam Concept

Each option presented a potential solution; however, the first and third options initially appeared to be more cost and labor intensive. Supplementing the terrain with adequate backfill could require large amounts of compacted soil, the addition of a retaining wall (depending on slope), and also utilize significant labor to implement. Similarly, the removal of existing wood

posts and replacement with completely new steel posts would require significant labor and site work to adjust post-hole dimensions prior to post placement. With either of these two methods, dirt work would be necessary and may prove very costly.

In contrast, the second and fourth options presented low-cost and minimal effort solutions. Driving new posts behind the existing 6-in. x 8-in. x 7-ft (152-mm x 203-mm x 2.1-m) long wood posts would be relatively easy and would not require any site work to adjust post-hole dimensions. Similarly, the addition of a support beam, which attached to the back side of the transition system, could be fabricated off site and installed in a relatively short period of time. Further, this option would not require dirt work or significant site labor to install. Additionally, several studies have utilized a backside rail to increase the stiffness of a transition system [22-23]. As such, extra driven posts and a backside support beam were chosen for further development and evaluation.

9.4.1 Extra Driven Steel Post Concept

Steel posts were selected for retrofitting the wood posts, supplementing post strength, and attaching to the existing 6-in. x 8-in. x 7-ft (152-mm x 203-mm x 2.1-m) long wood posts. Steel posts can be easily driven into the ground and can plastically deform below grade with deep embedment depths rather than fracture like wood posts. The ability for the supplemental steel posts to deform plastically was essential; because, it enabled the research team to base design calculations on a plastic hinge condition in the post rather than on the post-soil resistance provided by the sloped terrain.

Each supplemental post would be driven into the soil with a sufficient embedment depth to ensure that a plastic hinge would develop in the steel section before rotation in soil could occur. This condition represented a cantilever beam restrained in a 'rigid sleeve.' Further, each existing wood post, which attached to an extra driven steel post, was assumed to simultaneously

fracture with the onset of yielding in the posts. A fractured wood post with shallow embedment would provide very little additional post-soil resistance beyond that provided by the attached steel post. Previous test data, which investigated post behavior on sloped terrain, was examined to determine various post-soil resistances and investigate the depth below ground line where a hinge would occur in a steel post.

Results from tests conducted on W6x9 (W152x13.4) steel posts embedded 76 in. (1,930 mm) at the slope break point of a 2H:1V fill slope and impacted $24\frac{7}{8}$ in. (632 mm) above ground line (test nos. MGS221PT-27 and MGS221PT-28 [7]) demonstrated an average post-soil resistance of 8.65 kips (38.5 kN) over the first 15 in. (381 mm) of deflection and a hinge point approximately 14 in. (356 mm) below ground line. Results from tests conducted on W6x9 (W152x13.4) steel posts embedded 52 in. (1,321 mm) at the slope break point of a 3H:1V fill slope and impacted $24\frac{7}{8}$ in. (632 mm) above ground line (test nos. GWR5-1 and GWR5-2 [8]) demonstrated an average post-soil resistance of 11.0 kips (48.9 kN) over the first 15 in. (381 mm) of deflection and a hinge point approximately 8 in. (203 mm) below ground line. At the time of this study, only test data pertaining to posts located on 2H:1V and 3H:1V fill slopes was available.

These post-soil resistances were adjusted for an impact height of 21.65 in. (550 mm), as shown previously in Equation 4, which resulted in post-soil resistances of 9.9 kips (44.0 kN) [W6x9 (W152x13.5), 2H:1V, and 76 in. (1,930 mm) embedment] and 12.6 kips (56.0 kN) [W6x9 (W152x13.5), 3H:1V, and 52 in. (1,321 mm) embedment], respectively. Further, these resistances were used to determine at what embedment depths a 22.0-kip (97.9-kN) post-soil resistance could be expected, as shown previously in Equation 1. This analysis resulted in embedment depths of approximately 113 in. (2,870 mm) and 69 in. (1,753 mm) for 2H:1V and 3H:1V fill slopes, respectively. These embedment depths were added to the post length above

ground (i.e., 32 in. (813 mm)) to obtain the required post lengths of 12 ft (3.7 m) and 8.5 ft (2.6 m) for 2H:1V and 3H:1V fill slopes, respectively. These steel-post lengths would be necessary to ensure the sufficient post-soil resistance for supporting the wood-post transition systems found on fill slopes.

Adding the noted distances to the hinge points to an impact height of 21.65 in. (550 mm) produced the expected moment arms, L , for steel posts located on sloped terrain, 35.65 in. (906 mm) and 29.65 in. (753 mm) for 2H:1V and 3H:1V fill slopes, respectively. Multiplying L by a design load, P , of 22.0 kips (97.9 kN), as determined previously in Section 4.2.2, produced the bending moment required by steel posts located at the slope break point of 2H:1V and 3H:1V fill slopes, or 784 k-in. (88.6 kN-m) and 652 k-in (73.7 kN-m), respectively.

Using these moment values for the desired flexural capacity of a beam, as shown previously in Equation 2, the plastic section modulus could be used to identify the appropriate post section required for a specific sloped terrain. Dynamic increase factors for posts positioned in soil are difficult to determine and are typically not utilized in design other than for more rigid foundation conditions. However, researchers assumed that the steel post would more quickly yield and create a hinge before excessively rotating in soil. Thus, a dynamic impact factor of 1.5 was utilized, similar to Equation 3 previously used to determine the dynamic, flexural capacity of a steel beam. Assuming Grade 50 steel, this calculation resulted in a required plastic section moduli of 10.5 in.³ (172 cm³) and 8.7 in.³ (143 cm³) for 2H:1V and 3H:1V fill slopes, respectively. The closest steel shapes which matched these criteria were W6x16 (W152x23.8) and W6x12 (W152x17.9) steel posts, respectively. These two shapes had plastic section moduli of 11.7 in.³ (192 cm³) and 8.3 in.³ (136 cm³), respectively. These additional steel posts would be driven directly behind the wood posts and installed on the sloped terrain and lag screwed into the back side of the wood posts. Two lag bolts or screws per post would seem reasonable to attach a

steel post to a wood post. It may be possible to utilize lag bolt or screw lengths of 1½ to 2 in. (38 to 51 mm) and diameters of ¾ to ½ in. (9.5 to 12.7 mm). The recommended post sections, post lengths, and embedment depths for the 2H:1V and 3H:1V fill slopes were W6x16 (W152x23.8), 12 ft (3.7 m), and 113 in. (2,870 mm), and W6x12 (W152x17.9), 8.5 ft (2.6 m), and 69 in. (1,753 mm), respectively. This retrofit design is depicted in Figure 82.

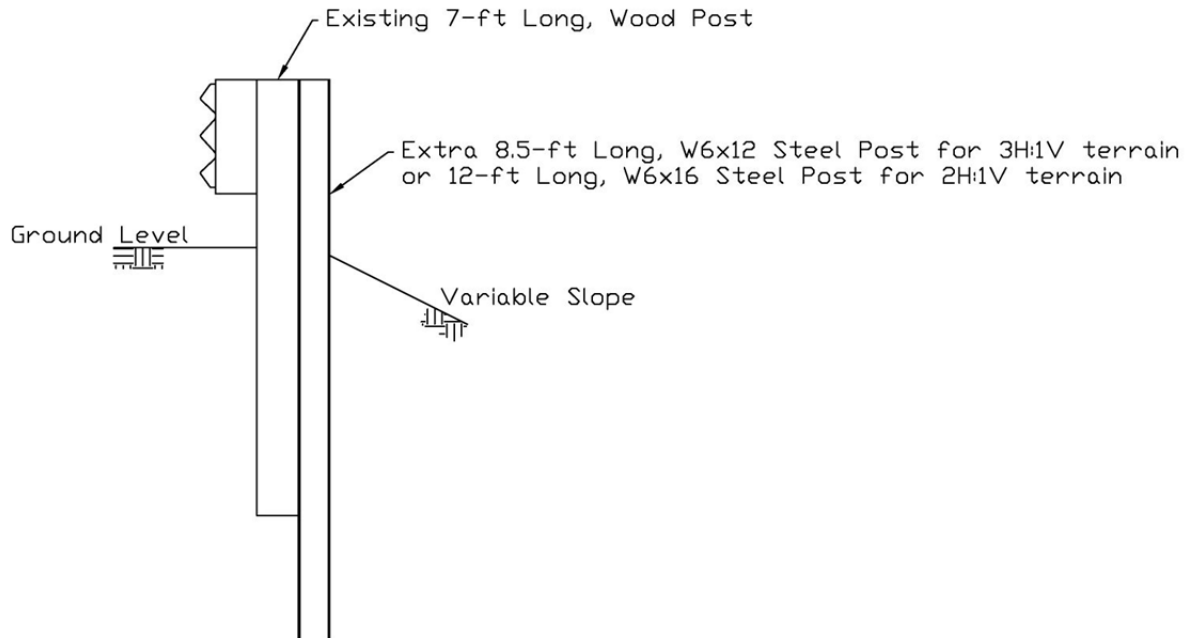


Figure 82. Extra Driven Steel Post Concept

9.4.2 Backside Beam Concept

BARRIER VII computer simulation was employed to determine the additional rail stiffness and strength required for a support beam to eliminate the propensity for vehicle wheel rim snag on the upstream end of the bridge rail. From prior simulations described in Section 9.3, this mode of failure presented a more extreme violation than excessive dynamic deflection and vehicle pocketing. The 31-ft 3-in. (9.5-m) long transition system positioned on a 2H:1V slope was selected for further investigation and analysis; since, this system had higher predicted values

for vehicle wheel rim snag on the upstream end of the bridge rail as compared to the 18-ft 9-in. (5.7-m) long transition system.

The computer simulations consisted of a 4,409-lb (2,000-kg) pickup truck impacting at a speed of 62.1 mph (100 km/h) and at an angle of 25 degrees. The barrier model was iteratively impacted at 9³/₈-in. (238-mm) intervals along the transition system. The support beam was modeled as a strengthened thrie beam along the nested thrie section of system. No optional upstream end post was utilized. Mechanical properties of the thrie beam were incrementally increased until the predicted value for vehicle wheel rim snag fell below the 2-in. (51-mm) evaluation limit. Input properties utilized for the simulation runs are shown in Table 29.

Table 29. Input Properties for BARRIER VII – Backside Beam

BARRIER VII Parameters		12-Gauge Nested Thrie Beam	12-Gauge Nested Thrie Beam + Increase	Required Increase	Percent Increase
I - Second Moment of Area	in. ⁴	7.52	30.08	22.56	300
S - Section Modulus	in. ³	4.38	17.52	13.14	300
M _y - Yield Moment	kip-in.	219	876	657	300

Results from the computer simulation effort indicated that the section modulus of the nested thrie beam required a 300 percent increase in magnitude to reduce vehicle wheel rim snag below the 2-in. (51-mm) evaluation limit. The most efficient standard shape that satisfied this condition was a W6x20 (W152x29.8) Grade 50 steel member, which has a section modulus of 13.4 in.³ (220 cm³). However, the research team was skeptical of a backside beam design which utilized a large structural member to stiffen and strengthen the thrie beam rail and supporting posts as it may cause severe vehicle pocketing and/or snag at its upstream end. Further, the large

structural member would require a robust anchoring mechanism on the backside of the concrete parapet as well as attachment to each supporting post to properly transfer the impact loads. MwRSF researchers believed that the use of a large backside beam would also require full-scale vehicle crash testing in order to evaluate its effectiveness and risks of degrading barrier performance near its upstream end. Since full-scale vehicle crash testing was outside of the scope of this project and would be required to completely evaluate the retrofit design, further development of the backside beam concept was abandoned.

9.5 Summary and Conclusions

Survey data provided by Wisconsin DOT personnel indicated that the installation of transitions along sloped terrain was a frequent problem in the State of Wisconsin. Two dynamic component tests and a total of 64 computer simulations were conducted to investigate and evaluate whether barrier performance was excessively degraded when placed on or nearby steep slopes. The simulation results demonstrated that the transitions were significantly weakened when located on sloped terrain, thus leading to concerns for excessive dynamic barrier deflections, increased propensity for a vehicle to snag on the upstream end of the bridge rail, as well as an increased potential for vehicle pocketing.

Four unique solutions were considered to resolve the deficiencies created by transition systems located on sloped terrain. The first option consisted of supplementing the terrain with additional backfill to create the proper grading required in the original design specifications. From a safety standpoint, this option was ideal. However, the anticipated soil work and associated costs made this option impractical. The second option consisted of driving extra steel posts with increased strength characteristics behind the existing wood posts. Larger and longer steel posts could be utilized to restore the resistive capacity of the system without requiring any dirt work, thus making this option economically appealing. The third option consisted of

removing the existing wood posts and replacing them with new, stronger, and longer steel posts. However, this method would require the removal and replacement of existing wood posts, which could become costly and time consuming, as well as filling and compacting soil material in holes prior to driving new steel posts. The final option consisted of attaching an additional support beam to the backside of the system. This option was initially deemed ideal from an economic standpoint, because the component could be fabricated offsite and installed in a relatively short period of time without needing soil fill and grading. Further, limited proof of the successful utilization of this general retrofit concept was available, although not in combination with sloped terrain.

For the driven post option, an analysis was conducted to determine the size and length of an extra strong steel post that was required to supplement existing 6-in. x 8-in. x 7-ft (152-mm x 203-mm x 2.1-m) long wood posts located on or nearby fill slopes. The analytical results indicated that affected wood posts positioned on a 2H:1V sloped terrain should be supplemented with 8.5-ft (2.6-m) long, W6x16 (W152x23.8) steel posts. Further, affected posts positioned on a 3H:1V sloped terrain should be supplemented with 12-ft (3.7-m) long, W6x12 (W152x17.9) steel posts. Slopes flatter than 3H:1V were not considered in this study.

For the backside beam option, BARRIER VII computer simulations were conducted to determine the size of backside beam that was required to stiffen and strengthen the thrie beam rail and support posts as well as offset the reduction in lateral resistive forces created by the sloped terrain. The simulation results indicated that a W6x20 (W152x29.8) steel beam adequately limited dynamic barrier deflections and wheel rim snag to acceptable levels at the upstream end of the bridge rail. However, concerns arose regarding the potential for vehicle pocketing and vehicle snag on the upstream end of the large backside beam as well as regarding the utilization of a robust anchoring system to attach the backside beam to the concrete parapet

and each supporting post. In addition, it was believed that full-scale crash testing would be required to evaluate the safety performance of the backside beam concept. Thus, further development of the backside beam concept was abandoned, and no additional computer simulations were performed near the upstream end of the horizontal steel member.

9.6 Recommendations

Due to the limited scope of this study, the extra post sizes mentioned above represent the best available solution for approach guardrail transition systems located on sloped terrain. It is important to note that these steel posts are attached to the existing wood posts with lag screws and sufficiently embedded into the soil so as to create a rigid foundation condition. However, the large embedment depth required for W6x16 (W152x23.8) steel posts on 2H:1V sloped terrain applications may exceed the height capability of typical roadside maintenance post-driving equipment, thus potentially making this solution impractical. If that is the case, an option to supplement the terrain behind wood posts with soil backfill could be considered. This scenario is undesirable due to the high costs associated with the extensive dirt work and/or constructing an additional retaining wall structure.

Further, abandonment of the backside beam concept does not signify that the notion is infeasible. However, a larger-scale research study would be necessary to further design, analyze, simulate, and full-scale crash test the retrofit device before justifying its use.

10 TRANSITION POSTS WITH INSUFFICIENT SOIL BACKFILL/GRADING

10.1 Overview

Data from Section 3.2 indicated that transitions supported by posts which were improperly exposed above ground line were a common occurrence in the State of Wisconsin. This deficiency was relevant for both the 18-ft 9-in. (5.7-m) long and the 31-ft 3-in. (9.5-m) long transition systems. In particular, this deficiency may cause wood posts to fracture prematurely during impact events, potentially resulting in system failure. Analytical calculations were performed to examine the increased moment induced into an improperly exposed wood transition post. Subsequently, these results were utilized to determine corresponding post-soil resistances for improperly exposed wood posts. Each transition system with this deficiency was further analyzed with computer simulation to investigate whether improperly exposed posts affect barrier performance in addition to those concerns for post fracture.

10.2 Analysis

Overly-exposed posts may occur as result of inadequate soil fill placed adjacent to the roadway, inadequate soil compaction resulting in settlement over time, or excessive soil erosion due to improper drainage control. These situations can result in an elevation difference between the roadway edge and the soil behind the barrier and posts. For a barrier system that has been correctly installed relative to the road surface but shows signs of inadequate soil backfill or grading around the posts, the load application height (e.g., moment arm) relative to the ground line will be increased. This situation could potentially result in increased moments/stresses induced within the wood post as well as premature fracture with deep embedment depths. As stated previously, premature fracturing of wood posts can lead to excessive barrier deflections, vehicle pocketing, and wheel snag. Thus, the effect of exposed posts on the performance of the transition system needed to be evaluated.

The configuration utilized to calculate base moments for improperly exposed posts is shown in Figure 83. This configuration specifically corresponded to a wood transition post with an embedment depth of 52 in. (1,321 mm) and a design impact load height of 21.65 in. (550 mm).

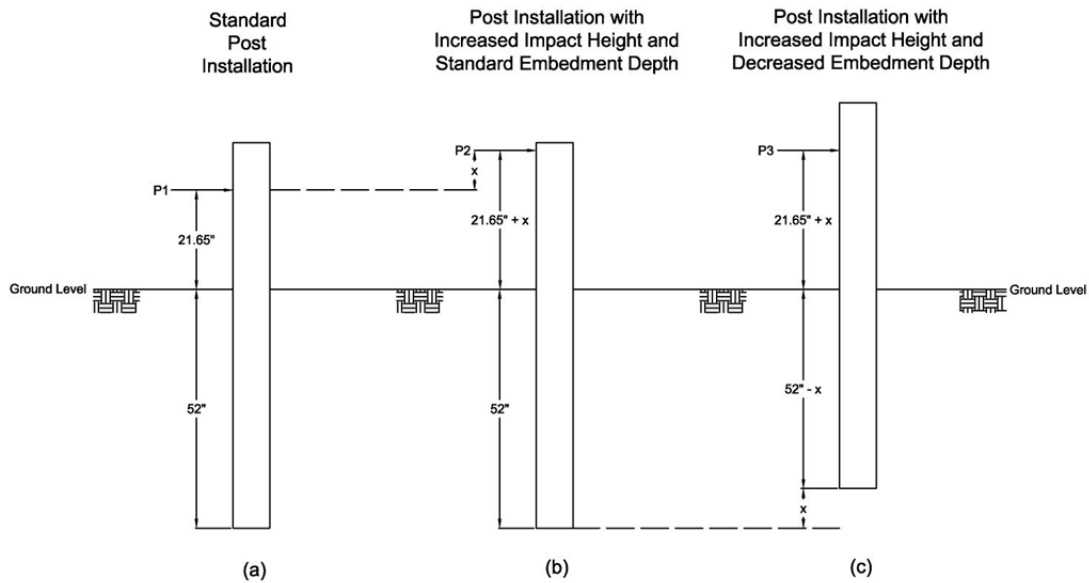


Figure 83. Base Moment Calculation – Wood Post Configuration

Although a previous study involving the dynamic testing of various wood posts at deep embedment depths on level terrain [35] demonstrated that the maximum bending moment, and consequently post fracture, occurred approximately 12 in. (305 mm) below ground level, MwRSF researchers selected ground level as the approximate location to analyze the bending moments of exposed wood posts for several reasons. First, it was believed that the distance below ground level for maximum bending would remain relatively consistent between the configurations shown in Figure 83. Thus, for each configuration, the maximum bending moment would maintain a consistent relationship with the bending moment at ground level. Second, ground level bending moment calculations were a function of the impact load height above ground level rather than a combination of height above and below ground level, thus simplifying

the analysis. Third, all calculations up to this point have been made on the assumption of post-soil yield forces at ground level.

The process from converting the estimated post-soil resistance from a standard post installation, P1, to the estimated post-soil resistance for an improperly exposed post, P3, required two steps. First, two posts with similar embedment depths but different impact heights were considered, as shown in (a) and (b) of Figure 83. As discussed previously in Section 5.3.3.1, the relationship between post-soil resistances for two posts with similar embedment depths but different impact heights can be calculated by equating soil yield moments of the posts. This derivation is shown in Equations 9 and 10, where P2(x) represents the load causing soil rotation in a wood post with a load height greater than 21.65 in. (550 mm). Recall from Section 4.2.2, a load of 22 kips (98 kN) was utilized for the average post-soil resistance/fracture limit for a 6-in. x 8-in. x 7-ft (152-mm x 203-mm x 2.1-m) long wood post with an embedment depth of 52 in. (1,321 mm) and an impact height of 21.65 in. (550 mm), which also corresponded to a standard bending moment, M1, of 476 kip-in. (53.8 kN-m).

$$M1 = P1 \times 21.65 = M2 = P2 \times (21.65 + x) \quad (9)$$

$$P2(x) = P1 \left[\frac{21.65}{21.65 + x} \right] \quad (10)$$

The next step involved converting the estimated post-soil resistance for two posts with similar impact heights but different embedment depths, as shown in (b) and (c) of Figure 83. As discussed previously in Section 4.2.2, the relationship between post-soil resistances for posts with similar impact heights but different embedment depths can be calculated as a function of the square of the embedment depth ratio, as shown previously in Equation 1. This derivation is shown in Equation 11.

$$P3(x) = P2(x) \left[\frac{52 - x}{52} \right]^2 \quad (11)$$

Substituting Equation 10 into Equation 11 provided the final relationship between the estimated post-soil resistance of a standard post installation, P1, and the estimated post-soil resistance for an improperly exposed post, P3(x). This derivation is shown in Equation 12.

$$P3(x) = P1 \left[\frac{21.65}{21.65 + x} \right] \left[\frac{52 - x}{52} \right]^2 \quad (12)$$

Finally, the estimated bending moment for various improper exposure lengths, M3(x), was calculated by multiplying Equation 12 by the corresponding increased load height, as depicted in Equations 13 and 14. Results from these calculations are summarized in Table 30 and shown graphically in Figure 84.

$$M3(x) = P3(x)[21.65 + x] \quad (13)$$

$$M3(x) = P1[21.65] \left[\frac{52 - x}{52} \right]^2 \quad (14)$$

Table 30. Calculations for Various Exposure Lengths

Improperly Exposed Length, x (in.)	Converted Post-Soil Resistance*, P3(x) (kips)	Converted Post-Soil Resistive Moment*, M3(x) (kip-in.)	Ratio of Post-Soil Resistances, P3(x)/P1	Ratio of Post-Soil Resistive Moment, M3(x)/M1
0	22.0	476	1.00	1.00
1	20.2	458	0.92	0.96
2	18.6	440	0.85	0.92
3	17.2	423	0.78	0.89
4	15.8	406	0.72	0.85
5	14.6	389	0.66	0.82
6	13.5	373	0.61	0.78

* Load converted from P1=22 kips

** Moment converted from M1=476 kip-in.

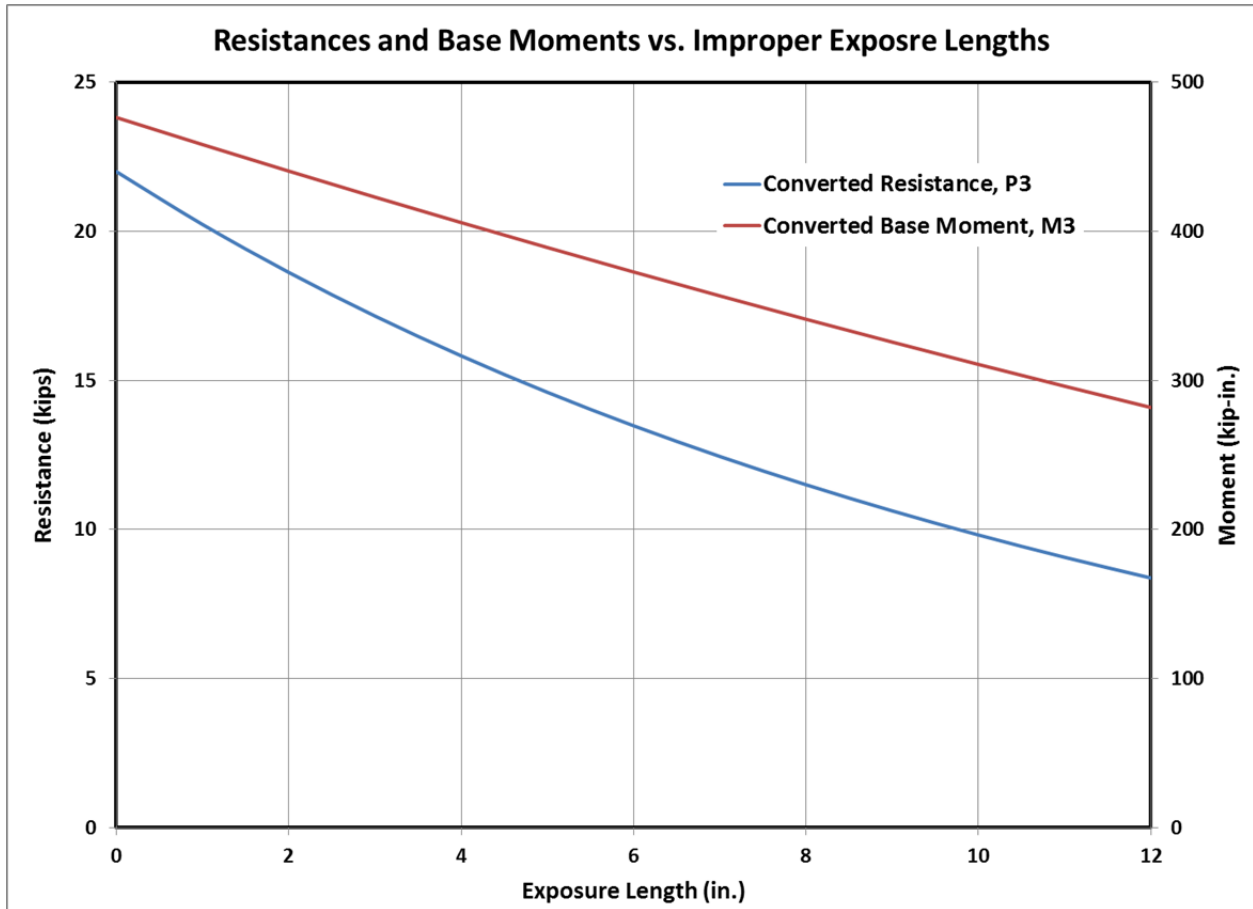


Figure 84. Resistances and Base Moments for Various Improper Exposure Lengths

As depicted in Figure 84, the post-soil resistance and resistive base moment continually decrease as the length of improper exposure increases. At 2 in. (51 mm) of improper exposure, the estimated post-soil resistance and resistive base moment would be 18.6 kips (82.7 kN) and 440 kip-in. (49.7 kN-m), respectively, or 15 and 7.5 percent less in magnitude. For a 6-in. (152-mm) improper exposure distance, the estimated post-soil resistance and resistive base moment would have dropped by 39 and 22 percent, respectively. As shown in Figure 84, a decreased post-soil resistance resulted from a decreased embedment depth and ultimately mitigated concerns for the increased load height to excessively increase the base moment. Thus, improperly exposed wood posts were no more likely to fracture than properly installed posts.

Although it was concluded that the wood transition posts were not likely to fracture due to increased exposure, the system response corresponding to a reduction in resistive forces was not fully apparent. Similar to transition posts installed on slopes, improperly exposed transition posts were expected to provide reduced resistive capacity, thus potentially leading to excessive dynamic deflections and vehicle wheel rim snag on the upstream end of the bridge rail.

BARRIER VII computer models were created to predict the critical exposure length which would result in vehicle wheel rim snag on the upstream end of the rigid bridge rail for both the 18-ft 9-in. (5.7-m) long transition system and the 31-ft 3-in. (9.5-m) long transition system. Each post located within the nested thrie beam section of the transition utilized the stiffness and strength of a 6-in. x 8-in. x 84-in. (152-mm x 203-mm x 2,134-mm) long wood post with a given amount of improper exposure. Values corresponding to the strong-axis bending moment of each improper exposure length were derived from the values shown in Table 30. The load heights for the posts were also increased by the increased exposure. Further, the strong-axis stiffness of posts with improper exposure lengths were extrapolated based on the corresponding reduction in strong-axis bending moment of posts properly embedded at 52 in. (1,321 mm). BARRIER VII input parameters for posts with various exposures distances are shown in Table 31.

Table 31. Input Properties for BARRIER VII Improperly Exposed Posts

BARRIER VII Parameters		Average Improper Exposure Distance				
		0 in.	1 in.	2 in.	3 in.	4 in.
Load Height	in.	21.65	22.65	23.65	24.65	25.65
K_B - Strong-Axis Post Stiffness	kips/in.	8.0	7.7	7.4	7.1	6.8
M_A - Strong-Axis Bending Moment	kip-in.	476	458	440	423	406
δ_{FB} - Strong-Axis Displacement Failure	in.	15	15	15	15	15

Computer simulations consisted of a 4,409-lb (2,000-kg) pickup truck impacting at a speed of 62.1 mph (100 km/h) and at an angle of 25 degrees. Based on previous simulation results, each model was impacted 95⁷/₈ in. (2,435 mm) upstream from the bridge rail end. This location corresponded to impacts which produced the maximum vehicle wheel rim snag on the upstream end of the bridge rail. A total of 4 simulations were performed on each transition system to reach the 2-in. (51-mm) critical limit. The results from these 8 simulation runs are shown in Table 32.

Table 32. Maximum Wheel Rim Snag for Improperly Exposed Posts

Average Improper Exposure (in.)	Maximum Wheel Rim Snag	
	18-ft 9-in. Transition (in.)	31-ft 3-in. Transition (in.)
0 (Baseline)	1.58	1.61
1	1.67	1.70
2	1.74	1.78
3	1.84	1.89
4	1.96	2.00

The propensity for vehicle snag on the upstream end of a bridge rail became an issue when the average exposure length along the *entire* nested thrie beam rail exceeded 4 in. (102 mm). An additional 46 simulations were conducted to investigate the dynamic performance of the 18-ft 9-in. (5.7-m) long transition system with 3 in. (76 mm) and 4 in. (102 mm) of improper exposure distance, while an additional 78 simulations were conducted to investigate the dynamic performance of the 31-ft 3-in. (9.5-m) long transition system with 3 in. (76 mm) and 4 in. (102 mm) of improper exposure distance. Comprehensive results from this series of simulation runs can be found in Appendix D. As shown in Table 33, maximum values for dynamic barrier

deflection, vehicle wheel rim snag on the upstream end of the bridge rail, and vehicle pocketing angles were determined.

Table 33. Summary of Simulation Results for Improperly Exposed Posts

BARRIER VII Evaluation Parameter		Improper Exposure Distance			
		3 in.		4 in.	
		18-ft 9-in. Transition	31-ft 3-in. Transition	18-ft 9-in. Transition	31-ft 3-in. Transition
Dynamic Deflection	Maximum Value (in.)	7.53	8.77	7.93	8.95
	Corresponding Baseline Value (in.)	6.22	8.14	6.22	8.14
Wheel Rim Snag	Maximum Value (in.)	1.84	1.89	1.96	2.00
	Corresponding Baseline Value (in.)	1.58	1.61	1.58	1.61
Pocketing Angle	Maximum Value (deg)	9.6	10.4	9.9	10.8
	Corresponding Baseline Value (deg)	8.3	8.8	8.3	8.8

Simulation results for both barrier models, which incorporated a 3-in. (76-mm) or 4-in. (102-mm) improper exposure distance, were found to meet the 2-in. (51-mm) evaluation limit for vehicle wheel rim snag on the upstream end of the bridge rail. Further, both barrier models, which incorporated a 3-in. (76-mm) or 4-in. (102-mm) improper exposure distance, were not found to significantly increase vehicle pocketing angles from those observed in the corresponding baseline simulations. On the other hand, both barrier models, which incorporated a 3-in. (76-mm) or 4-in. (102-mm) improper exposure distance, resulted in dynamic barrier deflections which exceeded those obtained for the baseline simulations. Recall that the dynamic deflection limits for the 18-ft 9-in. (5.7-m) long transition system and the 31-ft 3-in. (9.5-m) long transition system were 7.5 in. (191 mm) and 8.2 in. (208 mm), respectively. However, these deflection limits were believed to be somewhat subjective rather than hard failure limits. Thus, these increased dynamic barrier deflections were considered tolerable for 3 in. (76 mm) of improper post exposure and excessive for 4 in. (102 mm) of improper post exposure. In addition,

the primary concern regarding system failure (i.e., vehicle wheel rim snag) was satisfied for 3-in. (76-mm) improper exposure distances.

10.3 Summary, Conclusions, and Recommendations

Analytical calculations were utilized to demonstrate that wood transition posts with excessive exposure lengths were no more likely to fracture during impact events than properly installed posts. Further, a total of 132 BARRIER VII computer simulations were conducted on both transition systems to determine whether improper post exposure adversely affected barrier performance. The simulation results clearly demonstrated that slight post exposure distances ranging from 0 to 2 in. (0 to 51 mm) did not result in concerns for wheel snag on the upstream end of the bridge rail, excessive dynamic barrier deflections, or vehicle pocketing. Post exposure distances between 2 and 3 in. (51 and 76 mm) were found to satisfy the wheel snag criterion, moderately increase vehicle pocketing angles, and only modestly exceed acceptable limits for dynamic barrier deflections. However, an average exposure length of 4 in. (102 mm) along the entire nested three beam section of either transition system resulted in significant concerns for wheel snag on the bridge rail end as well as excessive dynamic barrier deflections which would increase the propensity for vehicular instabilities. Therefore, average improper exposure distances in excess of 3 in. (76 mm) should be retrofitted to mitigate concerns regarding degraded barrier performance. When exposure distances exceed 3 in. (76 mm), it is recommended that compacted soil backfill be utilized to upgrade the transition system and ensure that it conforms to the originally-specified post embedment depth.

11 WOOD TRANSITION POSTS EMBEDDED IN ASPHALT

11.1 Overview

Guardrail posts directly embedded in asphalt surfaces were found at numerous sites during the survey of Wisconsin approach guardrail transitions. In particular, this deficiency could hinder guardrail post rotation and cause wood posts to prematurely fracture during impact events. A literature review was conducted concerning the design and testing of mow strip configurations that were composed exclusively of asphalt (i.e., without the use of a leave out). Additionally, four dynamic component tests were conducted on 6-in. x 8-in. x 84-in. (152-mm x 203-mm x 2,134-mm) long SYP wood posts surrounded by thin asphalt layers in order to determine its propensity to degrade post behavior (e.g., premature fracture) and overall guardrail performance.

Once again, it should be noted that the research and development as well as the successful testing and evaluation of the original Iowa three beam approach guardrail transition system utilized SYP wood posts [32]. As such, this Wisconsin DOT research project also utilized SYP wood posts to serve as the baseline condition for the investigation and evaluation of degraded post and barrier performance when installed near or at the slope break point of fill slopes.

The State of Wisconsin has significant native wood species (i.e., White Pine and Red Pine) that are desired for the fabrication of 6-in. x 8-in. (152-mm x 203-mm) line posts for W-beam guardrail systems. However, these native wood species have structural properties that are moderately reduced from those structural properties exhibited by guardrail posts that are manufactured from the Southern Yellow Pine or Douglas Fir wood species. As such, guardrail posts manufactured from these reduced-strength, native wood species have not been recommended for use approach guardrail transitions unless successful safety performance has been demonstrated through full-scale vehicle crash testing or the cross-section has been appropriately resized.

11.2 Discussion on Direct Confinement of a Guardrail Post

It has been common practice for roadway engineers to encase guardrail posts with asphalt to prevent vegetation growth, reduce maintenance costs associated with mowing operations, and reduce erosion. However, if utilized improperly, this practice could increase safety risks to motorists rather than benefit maintenance operations. Compacted asphalt is much stiffer than soil and can restrict guardrail post displacements at ground line. This restriction creates a stress concentration in the post, which ultimately could lead to premature fracture of a wood post as well as degradation of barrier performance. Fractured wood posts could result in excessive dynamic barrier deflections, vehicle pocketing, and possibly wheel snag on the bridge rail end.

In 2004, researchers at TTI examined the hazards associated with wood guardrail posts encased in asphalt pavements [38]. Four dynamic component tests were conducted on 7-in. (178-mm) diameter wood posts positioned in 8-in. (203-mm) or 4-in. (102-mm) deep hand-tamped, asphalt leave-outs. Each post was embedded 44 in. (1,118 mm) into a soil foundation system and impacted at a height of 21.65 in. (550 mm) above ground line. The test results demonstrated that asphalt was too stiff for allowing the desired post rotation prior to post fracture. Consequently, researchers instead recommended the use of 4-in. (102-mm) deep, rectangular leave-outs that were filled with a low-strength grout material to comprise a guardrail mow strip installation.

Still, several parameters remained untested following the 2004 TTI guardrail confinement study [38]. First, no direct confinement with an asphalt layer less than 4 in. (102 mm) thick was considered. Thin asphalt layers may be more easily ruptured, potentially reducing the lateral resistance applied to the post near the ground line, thus allowing for proper post rotation in soil. Second, only round, 7-in. (178-mm) diameter wood guardrail posts were considered. Round, 7-in. (178-mm) diameter posts have a significantly lower section modulus than 6-in. x 8-in. (152-mm x 203-mm) rectangular posts, 64 in.^3 ($1,049 \text{ cm}^3$) as compared to 34 in.^3 (557 cm^3). Thus,

TTI researchers noted that 6-in. x 8-in. (152-mm x 203-mm) rectangular wood guardrail posts have the potential to sustain higher post-soil resistances before fracture as compared to 7-in. (178-mm) diameter posts. Third, TTI researchers only considered 44-in. (1,118-mm) post embedment depths in combination with level terrain.

Further, photographs provided in the Wisconsin DOT survey illustrated that asphalt usage was prevalent on sloped terrain as a possible method for preventing soil erosion, as shown in Figure 85. When guardrail posts were directly confined by asphalt on level terrain, TTI tests demonstrated that the asphalt was too stiff. However, an asphalt pavement placed on sloped terrain may not provide the same lateral resistance as provided by asphalt surrounding posts on level terrain. A post rotating in sloped soil fill with an asphalt layer may sufficiently weaken and rupture the overlay surfacing material through the introduction out-of-plane forces.



Figure 85. Asphalt Placement on Sloped Terrain

Due to the considerations mentioned above, further investigation, analysis, and dynamic component testing was deemed necessary to evaluate the performance of wood guardrail posts directly confined by compacted asphalt material. The dynamic component testing program would include the use of: (i) 6-in. x 8-in. (152-mm x 203-mm) wood posts; (ii) post placement at the slope break point of a 2H:1V fill slope; and (iii) complete confinement in a 2-in. (51-mm) thick, hand-tamped asphalt wearing surface. Unsatisfactory post performance under these conditions would ultimately eliminate the use of asphalt confinement around the wood posts.

11.3 Dynamic Component Testing

11.3.1 Scope – Round 1

Two identical dynamic bogie tests were performed with 6-in. x 8-in. x 84-in. (152-mm x 203-mm x 2,134-mm) long wood posts. The posts were placed at the slope break point of a 2H:1V fill slope and embedded to a depth of 50 in. (1,270 mm) in soil. The soil was compacted, coarse, crushed limestone material that met AASHTO standard soil designation M147 Grade B, as recommended by MASH [14]. Then, a 2-in. (51-mm) thick layer of asphalt was placed over the slope soil terrain to create a total post embedment depth of 52 in. (1,321 mm). The asphalt mixture was composed of a PG 64-22 binder with ³/₄-in. (19-mm) limestone and Nebraska Department of Roads (NDOR) 47B type aggregate. The asphalt was hand tamped, which produced an approximate density of 131 pcf (2,098 kg/m³). The target impact conditions consisted of a speed of 20 mph (32.2 km/h) and an angle of 0 degrees, creating a classical “head-on” or full frontal impact and strong-axis bending of the post. The wood posts were impacted 21.65 in. (550 mm) above the ground line and perpendicular to the front face of the post. The guidelines established in Chapter 9 regarding end of test determination were utilized. All other testing conditions, methods, and equipment remained consistent with those described in Chapter

6. The test setup is shown in Figures 86 and 87. Dimensions and properties of the wood posts utilized in the WIA test series are shown in Table 34.

Table 34. Wood Post Properties – WIA Testing Series

Test No.	Post Dimensions in. x in. (mm x mm)			Post Length in. (mm)	Weight lb (kg)	Ring Density rings/in. (rings/cm)
	At Top	At Groundline	At Bottom			
WIA-1 & WIA-3*	6 x 7 ¹⁵ / ₁₆ (152 x 202)	6 x 7 ¹⁵ / ₁₆ (152 x 202)	6 ¹ / ₈ x 7 ¹⁵ / ₁₆ (156 x 202)	84 ¹ / ₈ (2,137)	100 (45.4)	4 (1.6)
WIA-2 & WIA-4*	5 ¹⁵ / ₁₆ x 8 (151 x 203)	5 ¹⁵ / ₁₆ x 8 ¹ / ₁₆ (151 x 205)	5 ⁷ / ₈ x 8 ¹ / ₁₆ (149 x 205)	84 ⁵ / ₁₆ (2,142)	86 (39)	3.3 (1.3)

*Undamaged posts were re-used between corresponding tests.

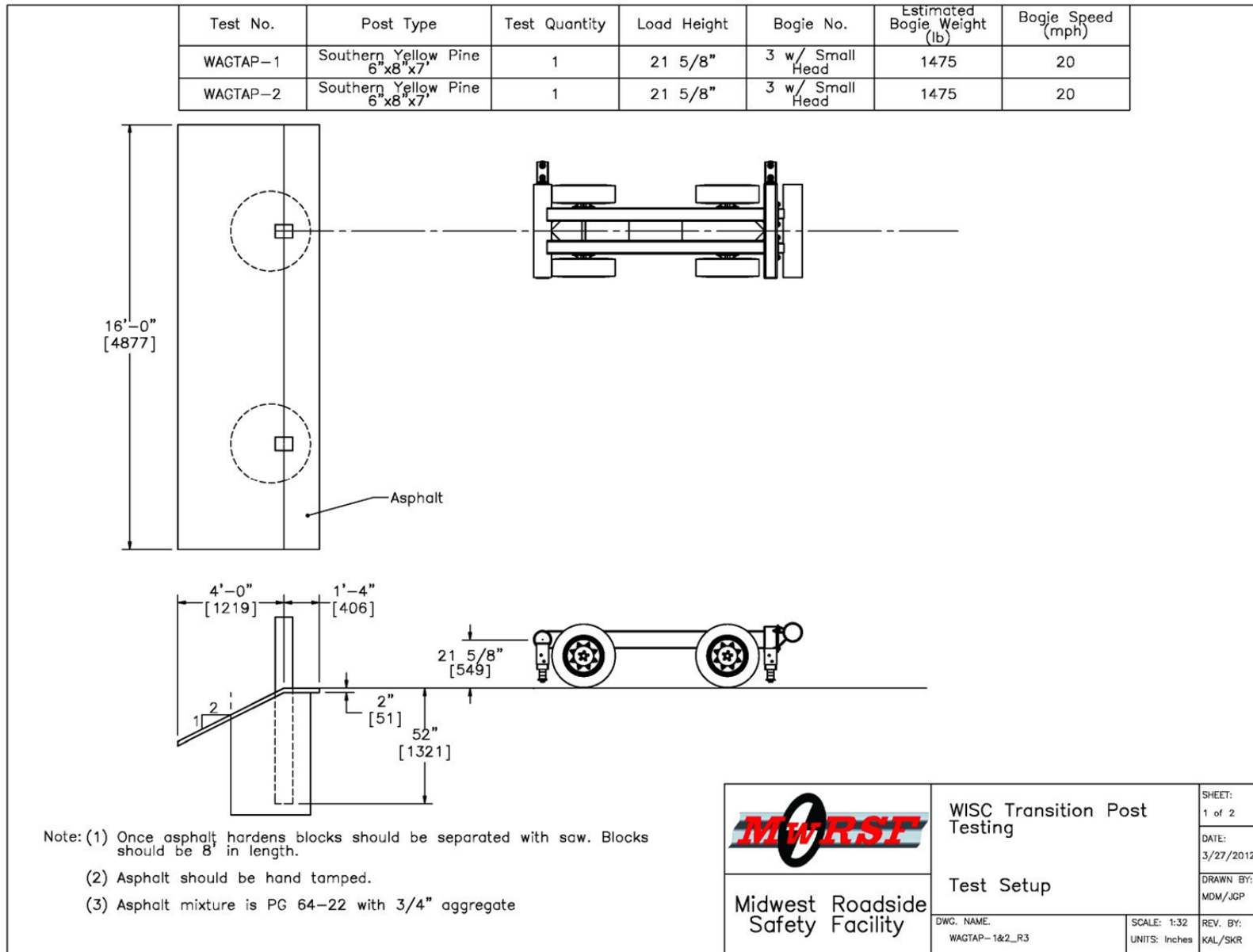


Figure 86. WIA Bogie Testing Matrix and Setup – Round 1

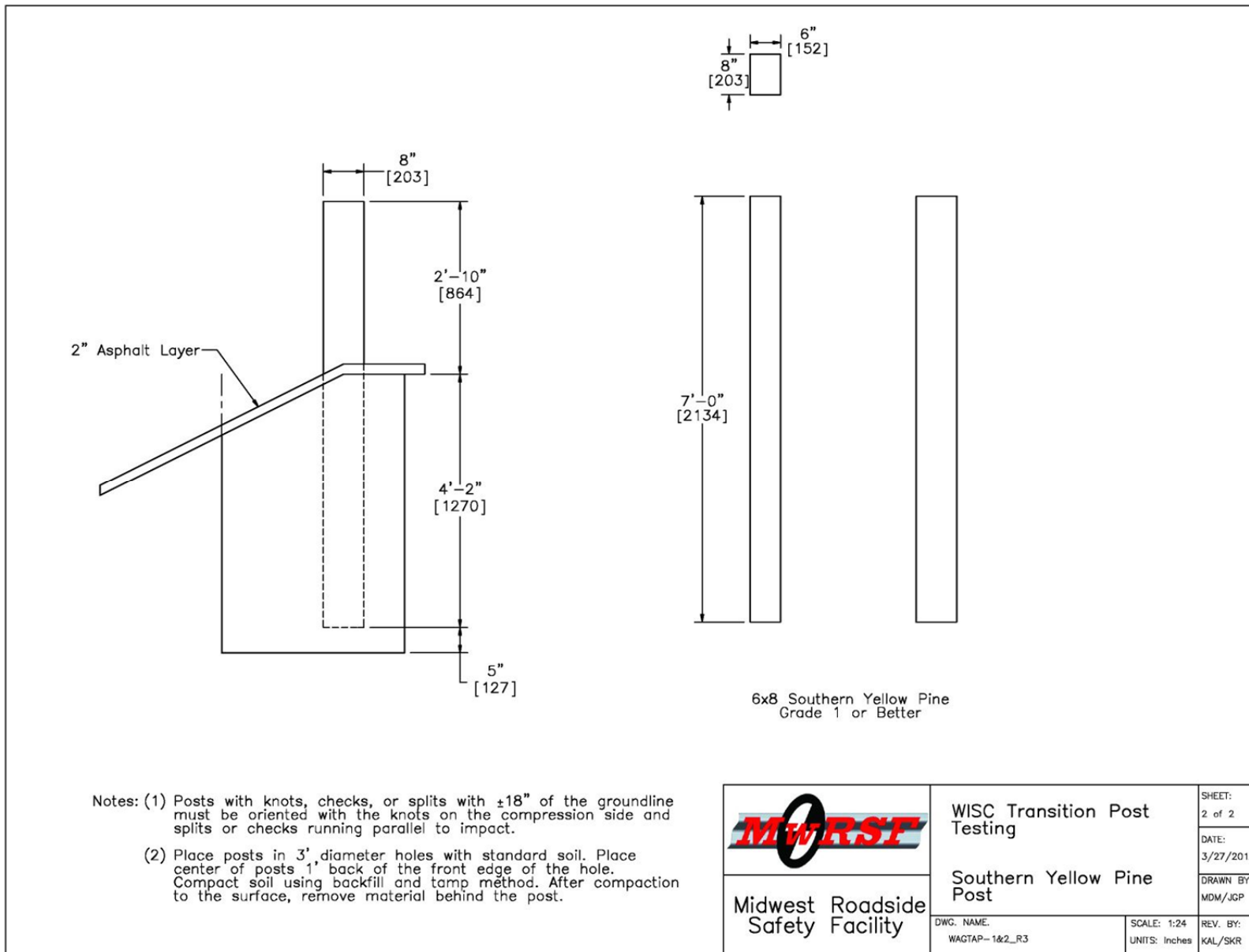


Figure 87. WIA Bogie Testing Post Detail – Round 1

11.3.2 Bogie Testing and Results – Round 1

11.3.2.1 Test No. WIA-1

During test no. WIA-1, the bogie impacted the 6-in. x 8-in. x 84-in. (152-mm x 203-mm x 2,134-mm) long wood post positioned at the slope break point of a 2H:1V fill slope at a speed of 20.2 mph (32.6 km/h), thus causing strong-axis bending in the post. The asphalt directly behind the post was immediately forced upward and began cracking, allowing the post to deflect backward. Subsequently, the deflection and rotation of the post caused the underlying soils to create an outward pressure on the asphalt. This pressure formed a bulge in the asphalt behind the post, which ultimately led to complete fracture of the asphalt by 0.100 seconds. Large sections of asphalt began to break away as the post continued to rotate through the soil to a maximum deflection of 48.3 in. (1,227 mm). The wood post showed no signs of fracture when examined after the impact event. The bogie impact head remained in contact with the post throughout the entire test, and the forward movement of the vehicle was stopped approximately 0.330 seconds after impact.

Force vs. deflection and energy vs. deflection curves were created from the accelerometer data and are shown in Figure 88. Initially, inertial effects resulted in a peak force of 12.5 kips (55.4 kN) at 1.7 in. (43 mm) of deflection. After a brief rebound, the resistive force again peaked at 13.5 kips (60.2 kN) around 3.4 in. (86 mm) of deflection. At approximately 6 in. (152 mm) of deflection, the lateral resistive force began to steadily decrease until approximately 25 in. (635 mm) of deflection. Subsequently, a relatively steady force of around 2 kips (8.9 kN) was observed for the rest of the impact event. The post rotating through the soil and breaking through the layer of asphalt had absorbed 242.8 kip-in. (27.4 kJ) of energy. Time-sequential photographs and post-impact photographs are shown in Figure 89.

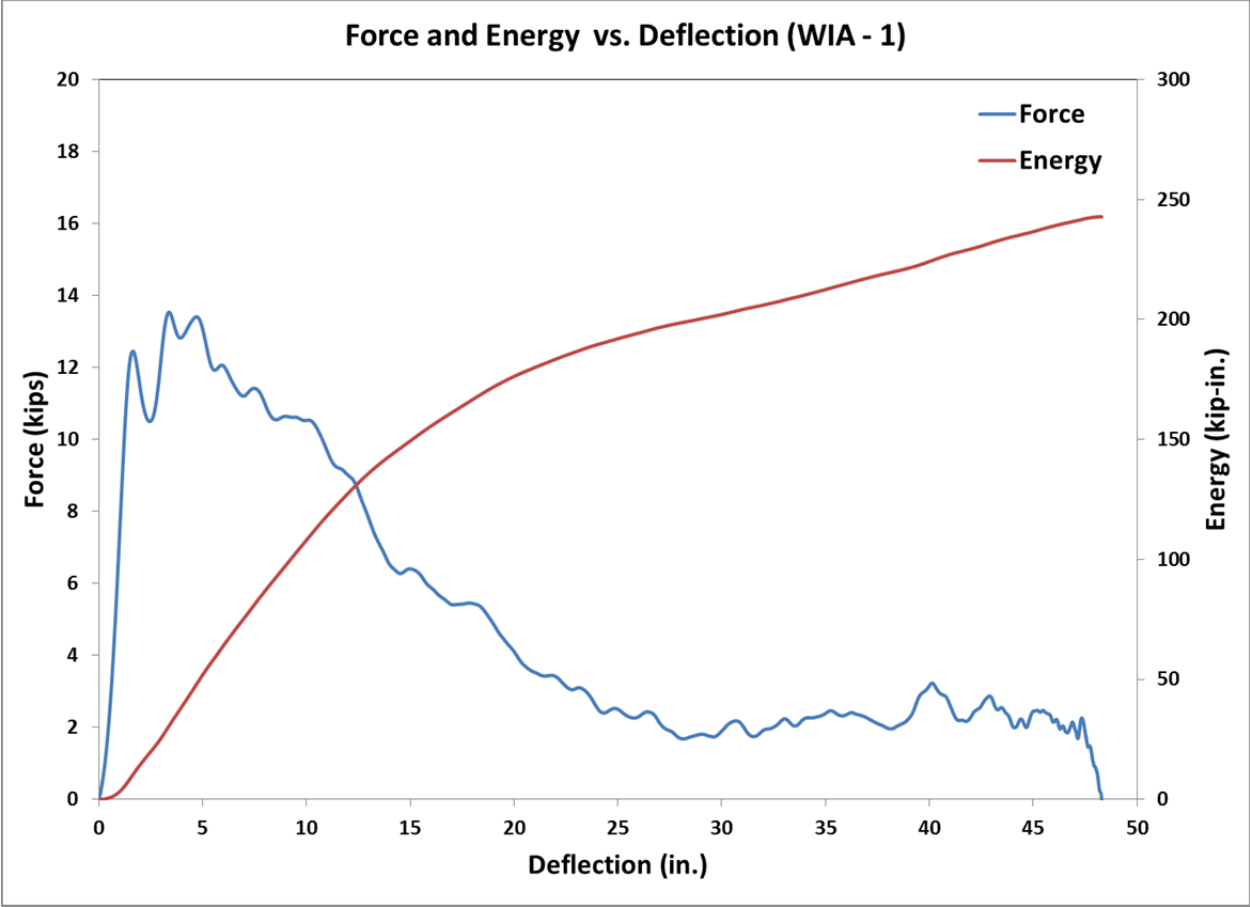
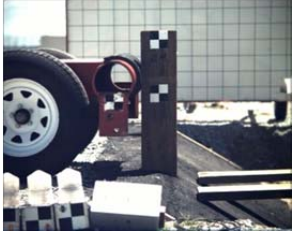


Figure 88. Force vs. Deflection and Energy vs. Deflection, Test No. WIA-1



Post After Impact – Side view



Post After Impact – Asphalt Displacement

Figure 89. Time-Sequential and Post-Impact Photographs, Test No. WIA-1

11.3.2.2 Test No. WIA-2

During test no. WIA-2, the bogie impacted the 6-in. x 8-in. x 84-in. (152-mm x 203-mm x 2,134-mm) long wood post positioned at the slope break point of a 2H:1V fill slope at a speed of 20.6 mph (33.1 km/h), thus causing strong-axis bending in the post. The asphalt directly behind the post was immediately forced upward and began to crack, allowing the post to deflect backward. Subsequently, the deflection and rotation of the post caused the underlying soils to create an outward pressure on the asphalt. This pressure formed a bulge in the asphalt behind the post, which ultimately led to complete fracture of the asphalt by 0.070 seconds. Large sections of asphalt began to break away as the post continued to rotate through the soil to a maximum deflection of 46.9 in. (1,191 mm). The wood post showed no signs of fracture when examined after the impact event. The bogie impact head remained in contact with the post throughout the entire test, and the forward movement of the vehicle was stopped approximately 0.400 seconds after impact.

Force vs. deflection and energy vs. deflection curves were created from the accelerometer data and are shown in Figure 90. Early on, the forces quickly increased to a peak force of 16.7 kips (74.3 kN) at 3.3 in. (84 mm) of deflection. After this peak was reached, the resistive force steadily decreased until approximately 23 in. (584 mm) of deflection. Subsequently, a relatively steady lateral resistive force of around 2 kips (8.9 kN) was observed for the rest of the impact event. The post rotating through the soil and breaking through the layer of asphalt had absorbed 251.5 kip-in. (28.4 kJ) of energy. Time-sequential photographs and post-impact photographs are shown in Figure 91.

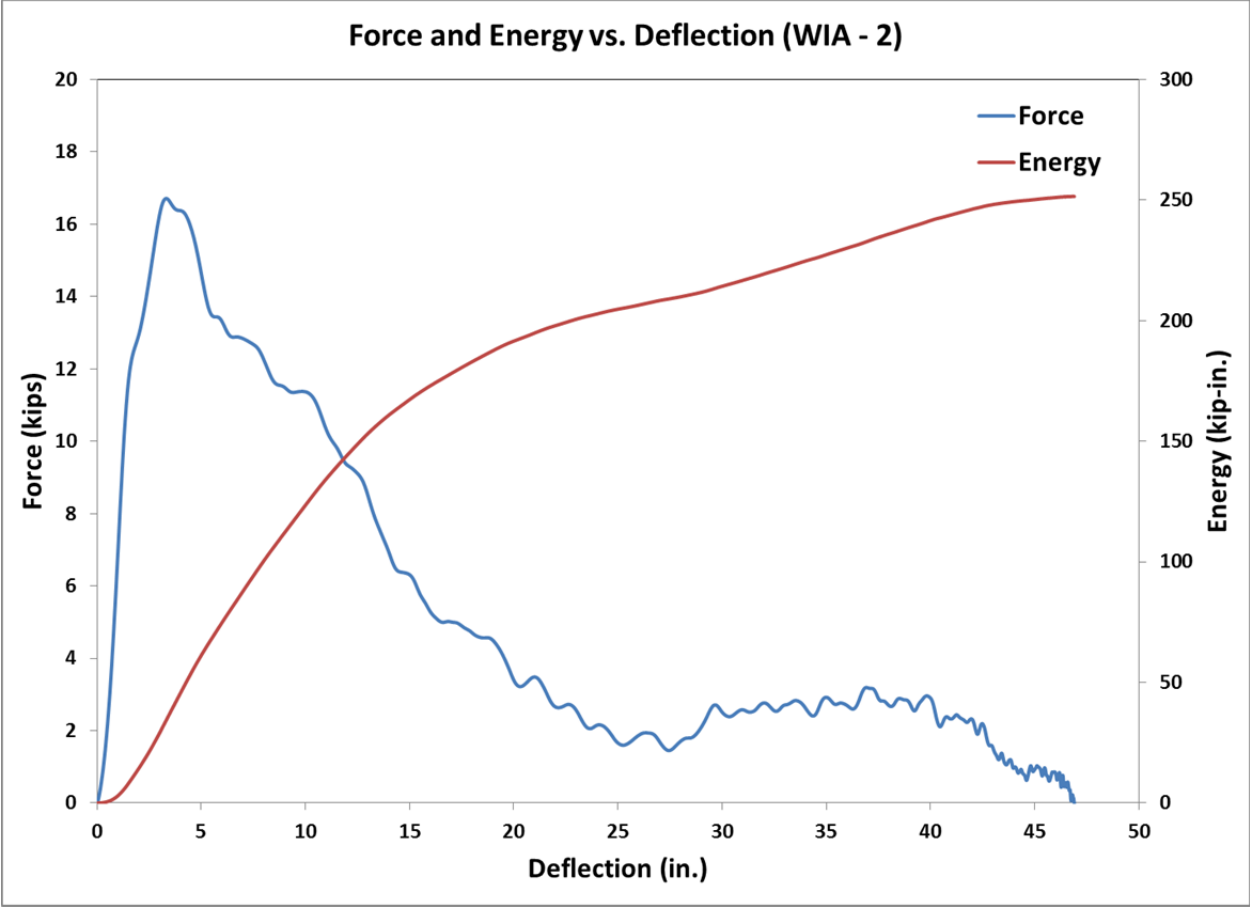


Figure 90. Force vs. Deflection and Energy vs. Deflection, Test No. WIA-2



Post After Impact – Side view



Post After Impact – Asphalt Displacement

Figure 91. Time-Sequential and Post-Impact Photographs, Test No. WIA-2

11.3.3 Scope – Round 2

It was observed during the first round of testing that 6-in. x 8-in. x 84-in. (152-mm x 203-mm x 2,134-mm) long wood posts embedded 50 in. (1,270 mm) at the slope break point of a 2H:1V fill slope and confined by a 2-in. (51-mm) thick layer of hand-tamped asphalt were not likely to fracture during impact. Thus, it was necessary to expand upon the investigation of wood transition posts directly confined by asphalt to determine the range of slopes in which the 2-in. (51-mm) thick asphalt layer would allow for adequate post rotation. Therefore, two additional bogie tests were conducted under identical impact conditions and using identical confining materials, except the posts were placed on the slope break point of a 4H:1V fill slope.

11.3.4 Bogie Testing and Results – Round 2

11.3.4.1 Test No. WIA-3

During test no. WIA-3, the bogie impacted the 6-in. x 8-in. x 84-in. (152-mm x 203-mm x 2,134-mm) long wood post positioned at the slope break point of a 4H:1V fill slope at a speed of 21.5 mph (34.5 km/h), thus causing strong-axis bending in the post. As the post began to deflect backward, it broke through the confining layer of asphalt similar to test nos. WIA-1 and WIA-2. However, at approximately 0.023 seconds after impact, a shear crack formed in the asphalt and parallel to the impact face of the post. This crack continued to propagate along the asphalt until it reached the edge of the pavement surface. At approximately 0.058 seconds after impact, the asphaltic pavement surrounding the post had separated into three sections, one in front of the post and one behind the post to either side of the post. At this point, the two sections of asphalt pavement located behind the post were each translating freely with the post. By 0.200 seconds, the post had reached a maximum lateral deflection of 28.5 in. (724 mm) as the bogie rebounded away from the post. The post showed no signs of fracture when examined after the impact event.

Force vs. deflection and energy vs. deflection curves were created from the accelerometer data and are shown in Figure 92. Initially, inertial effects resulted in a peak force of 12.5 kips (55.6 kN) at 1.9 in. (48 mm) of deflection. After a brief rebound, the resistive force again peaked at 18.1 kips (80.4 kN) at around 6.4 in. (163 mm) of deflection. After this peak, the lateral resistive force steadily decreased until approximately 22 in. (559 mm). Subsequently, a relatively steady force of around 3.5 kips (15.6 kN) was observed for the rest of the impact event. The post rotating through the soil and breaking through the layer of asphalt had absorbed 271.7 kip-in. (30.7 kJ) of energy. Time-sequential photographs and post-impact photographs are shown in Figure 93.

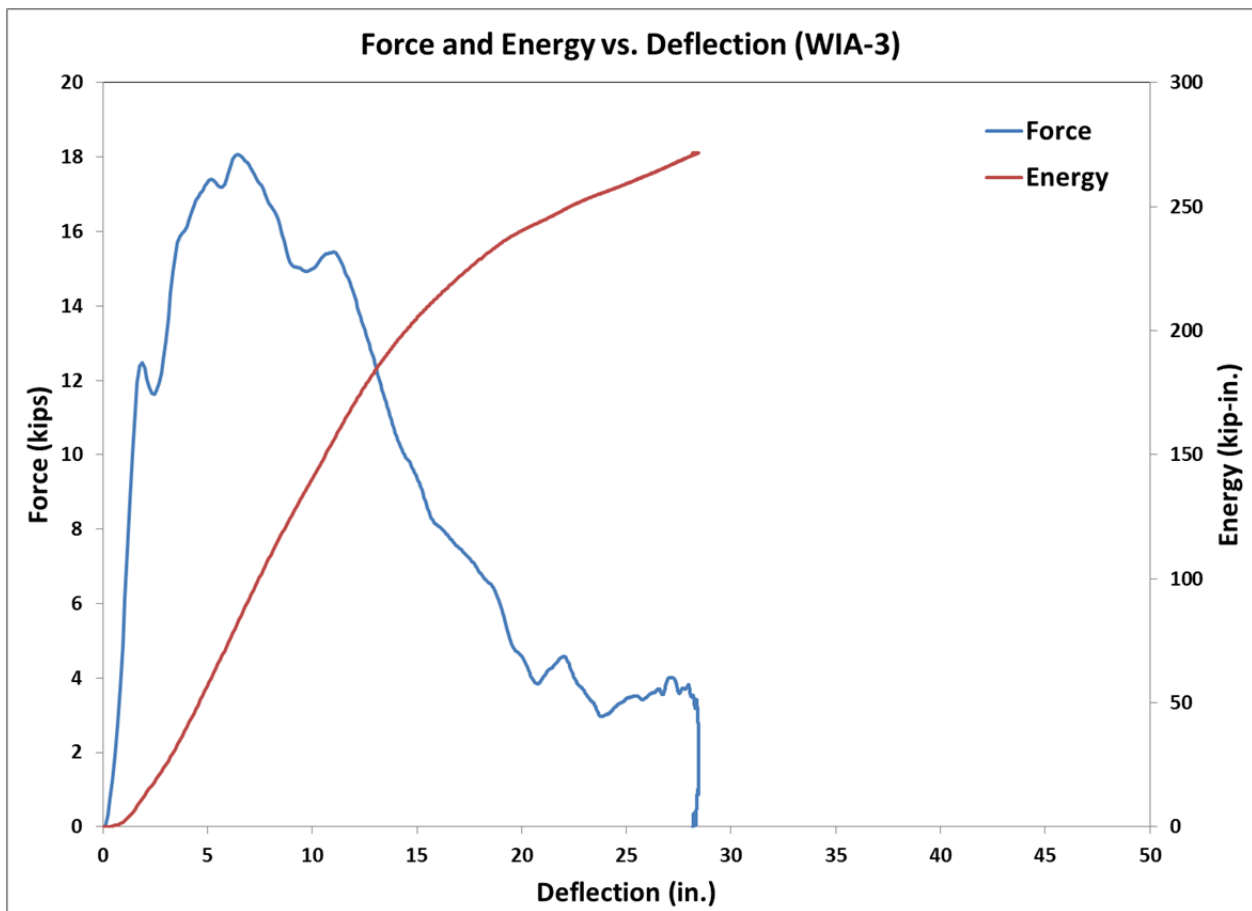


Figure 92. Force vs. Deflection and Energy vs. Deflection, Test No. WIA-3



IMPACT



0.030 sec



0.060 sec



0.090 sec



0.120 sec



0.150 sec



Post After Impact – Side view



Post After Impact – Back View

Figure 93. Time-Sequential and Post-Impact Photographs, Test No. WIA-3

11.3.4.2 Test No. WIA-4

During test no. WIA-4, the bogie impacted the 6-in. x 8-in. x 84-in. (152-mm x 203-mm x 2,134-mm) long wood post positioned at the slope break point of a 4H:1V fill slope at a speed of 19.9 mph (32.0 km/h), thus causing strong-axis bending in the post. Initially, the post began to deflect backward with the bogie head. However, by 0.010 seconds, the post had begun to fracture, allowing the upper portion of the post to rapidly deflect. Between 0.014 seconds and 0.044 seconds, the bogie head actually lost contact with the post as it was rotating backward faster than the bogie head was traveling forward. Ultimately, the bogie overrode the fractured post without redirection. No visible damage was observed in the asphalt pavement after the test.

Force vs. deflection and energy vs. deflection curves were created from the accelerometer data and are shown in Figure 94. The post reached a peak force of 17.9 kips (79.5 kN) at 2.6 in. (66 mm) of deflection. At this point, the post began to fracture and the lateral resistive force quickly declined. The post only absorbed 41.4 kip-in. (4.7 kJ) of energy before fracture. Time-sequential photographs and post-impact photographs are shown in Figure 95.

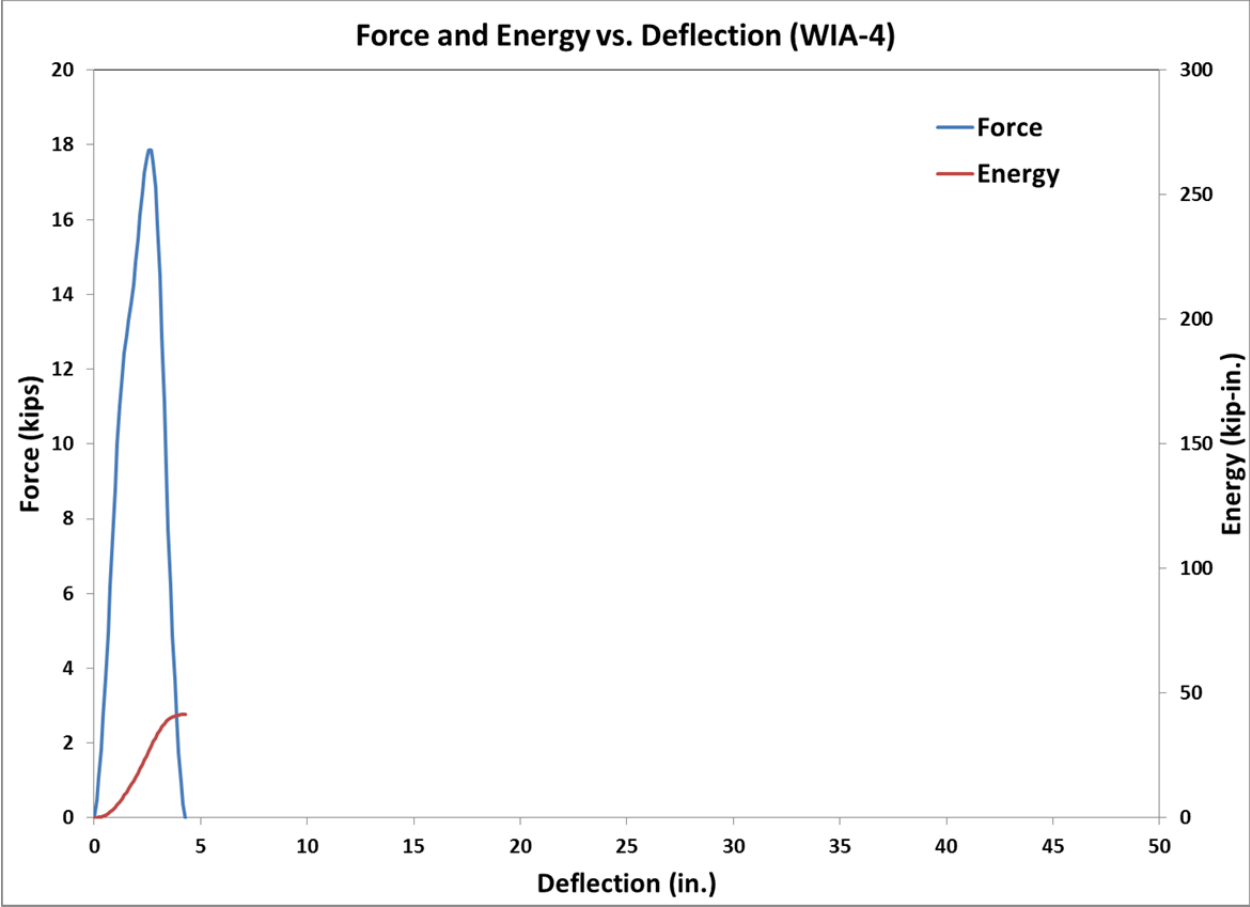


Figure 94. Force vs. Deflection and Energy vs. Deflection, Test No. WIA-4



IMPACT



0.030 sec



0.060 sec



0.090 sec



0.120 sec



0.150 sec



Post After Impact – Front view



Post After Impact – Fracture surface

Figure 95. Time-Sequential and Post-Impact Photographs, Test No. WIA-4

11.3.5 Discussion

The results from all four bogie tests are tabulated in Table 35, while force vs. deflection curves are compared and shown graphically in Figure 96. Inertial peak forces and average resistive forces sustained by the posts in the Round 1 testing program (test nos. WIA-1 and WIA-2) were similar. Further, the results from Round 1 demonstrated a definite increase in lateral resistive forces from those observed for similar tests without direct asphalt confinement, as shown in Figure 97. In fact, the 2-in. (51-mm) thick layer of asphalt increased the maximum resistive force and average resistive force at 10 in. (254 mm) of deflection by approximately 60 percent and 57 percent, respectively. As a result, the 2-in. (51-mm) thick layer of asphalt increased the energy dissipated by 56 percent through 10 in. (254 mm) of deflection, as shown in Figure 98. It should be noted that test nos. WITB-1 and WITB-2 were conducted at a speed of 15 mph (24.1 km/h) as compared to 20 mph (32.2 km/h) for test nos. WIA-1 and WIA-2. Thus, the maximum deflections observed during test nos. WITB-1 and WITB-2 were significantly less than those observed during test nos. WIA-1 and WIA-2.

When the fill slope was flattened from 2H:1V in Round 1 to 4H:1V in Round 2, a definite increase in the lateral resistive force was observed. In fact, the flatter slope increased the peak forces by approximately 19 percent and ultimately caused the post to fracture shortly after impact in test no. WIA-4. Further, the post in test no. WIA-3 sustained an average resistive force at 10 in. (254 mm) of deflection that was 20 percent higher than observed in the Round 1 tests. As a result, energy absorption through 10 in. (254 mm) of deflection was 20 percent greater than observed in the Round 1 tests, as shown in Figure 99.

Three key observations were made from these four tests. First, an increase in lateral post-soil resistance can be expected when a guardrail post is confined by a 2-in. (51-mm) thick layer of hand-tamped asphalt placed on sloped terrain. Second, this increased resistance did not

substantially restrict the rotation of a 6-in. x 8-in. x 84-in. (152-mm x 203-mm x 2,134-mm) long SYP wood post located at the slope break point of a 2H:1V fill slope. Alternatively, a 2-in. (51-mm) thick layer of asphalt on a 4H:1V fill slope demonstrated the potential to restrict post rotation and farther increase post-soil forces above those observed in similar testing on 2H:1V fill slopes. In fact, this additional restriction has the potential to cause premature post fracture, as observed in test no. WIA-4. Third, the forces observed during test no. WIA-3 confirmed the notion that 6-in. x 8-in. (152-mm x 203-mm) wood posts can resist peak lateral loads much greater than 12.1 kips (53.8 kN) and closer to the 22-kip (98-kN) peak load assumed in Section 4.2.2.

Table 35. Bogie Testing Results – Wood Posts Confined by 2-in. Thick Asphalt Layer

Test No.	Terrain (H:V)	Impact Velocity (mph)	Peak Force		Average Force			Absorbed Energy			Maximum Deflection (in.)	Total Energy (kip-in.)	Failure Type	
			Deflection (in.)	Force (kips)	@ 5 in. (kips)	@ 10 in. (kips)	@ 15 in. (kips)	@ 5 in. (kip-in.)	@ 10 in. (kip-in.)	@ 15 in. (kip-in.)				
WIA-1	2:1	20.2	3.4	13.5	10.4	10.8	10.0	53.0	108.8	149.7	48.3	242.8	Rotation in Soil	
WIA-2	2:1	20.6	3.3	16.7	12.1	12.3	11.1	61.8	124.0	167.5	46.9	251.5	Rotation in Soil	
Series Average				15.1	11.2	11.6	10.5	57.4	116.4	158.6				
WIA-3	4:1	21.4	6.4	18.1	11.3	13.9	13.6	58.4	140.6	205.2	28.5	271.7	Rotation in Soil	
WIA-4	4:1	19.9	2.6	17.9	-	-	-	-	-	-	4.3	41.4	Post Fracture	
Series Average				18.0	11.3	13.9	13.6	58.4	140.6	205.2				

11.4 Summary, Conclusions, and Recommendations

Two component testing configurations were developed to analyze 6-in. x 8-in. (152-mm x 203-mm) SYP wood guardrail posts directly confined by asphalt and installed on a slope break point. The first configuration consisted of wood guardrail posts embedded 50 in. (1,270 mm) at the slope break point of a 2H:1V fill slope and directly confined by a 2-in. (51-mm) thick layer of hand-tamped asphalt. Two dynamic component tests were conducted on this configuration.

The test results demonstrated that a 6-in. x 8-in. x 84-in. (152-mm x 203-mm x 2,134-mm) long wood posts could rotate backward with a significant increase in post-soil resistance as compared to tests conducted without the asphalt confinement.

The second configuration consisted of wood guardrail posts embedded 50 in. (1,270 mm) at the slope break point of a 4H:1V fill slope and directly confined by a 2-in. (51-mm) thick layer of hand-tamped asphalt. Two dynamic component tests were also conducted on this configuration. The test results demonstrated that a 6-in. x 8-in. x 84-in. (152-mm x 203-mm x 2,134-mm) long wood transition post could be negatively affected under these conditions.

For wood posts positioned on a 2H:1V fill slope, a 2-in. (51-mm) thick asphalt confinement was not shown to negatively affect post behavior. Thus, wood transition posts subjected to such confinements would only have modest increased risk for post fracture. However, the forces observed in test nos. WIA-1 and WIA-2 did not reach the design force used for Wisconsin approach guardrail transition systems. Therefore, any wood transition post positioned on a 2H:1V fill slope and surrounded with 2-in. (51-mm) thick asphalt pavement should be supplemented with an additional steel post as per the design recommendations denoted in Chapter 9.

For wood posts positioned on a 4H:1V fill slope, a 2-in. (51-mm) thick asphalt confinement was shown to negatively affect post behavior. Thus, any wood transition post positioned on a 4H:1V fill slope should not be completely surrounded by asphalt pavement. Due to the limited scope of this study, the lateral post-soil resistance of 6-in. x 8-in. x 84-in. (152-mm x 203-mm x 2,134-mm) long SYP wood posts placed at the slope break point of a 4H:1V fill slope and embedded 52 in. (1,321 mm) in soil was not determined. Further, no recommendations regarding the installation of an approach guardrail transition system on a 4H:1V or flatter fill

slope were available. Thus, approach guardrail transition should not be installed on a 4H:1V or flatter fill slope and surrounded by a 2-in. (51-mm) thick layer of asphalt pavement.

If placement of an approach guardrail transition on a 4H:1V or flatter fill slope with a 2-in. (51-mm) thick asphalt confinement is desired, further component testing of 6-in. x 8-in. (152-mm x 203-mm) SYP wood posts under these conditions is necessary.

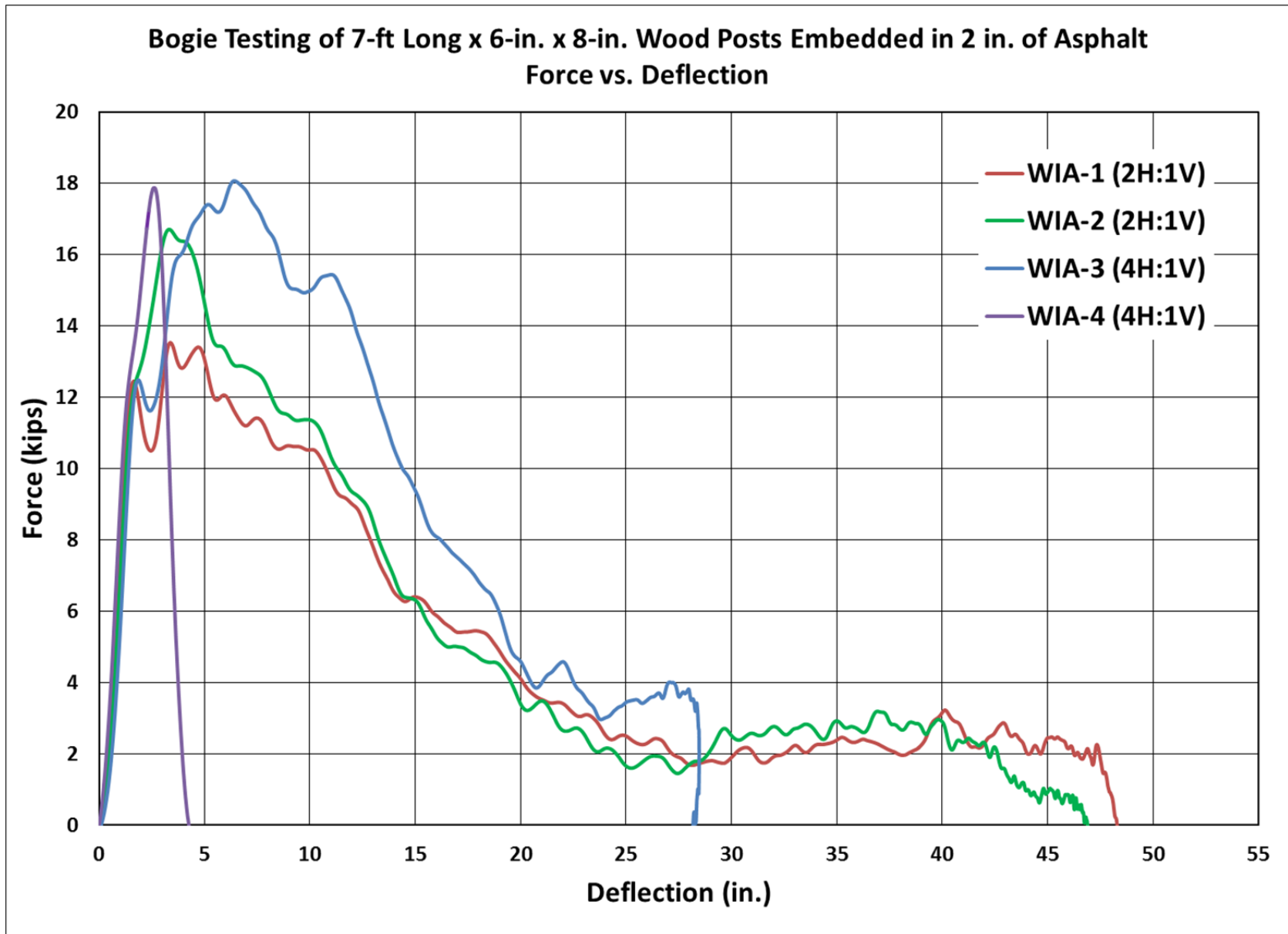


Figure 96. Force vs. Deflection Results, WIA Bogie Testing

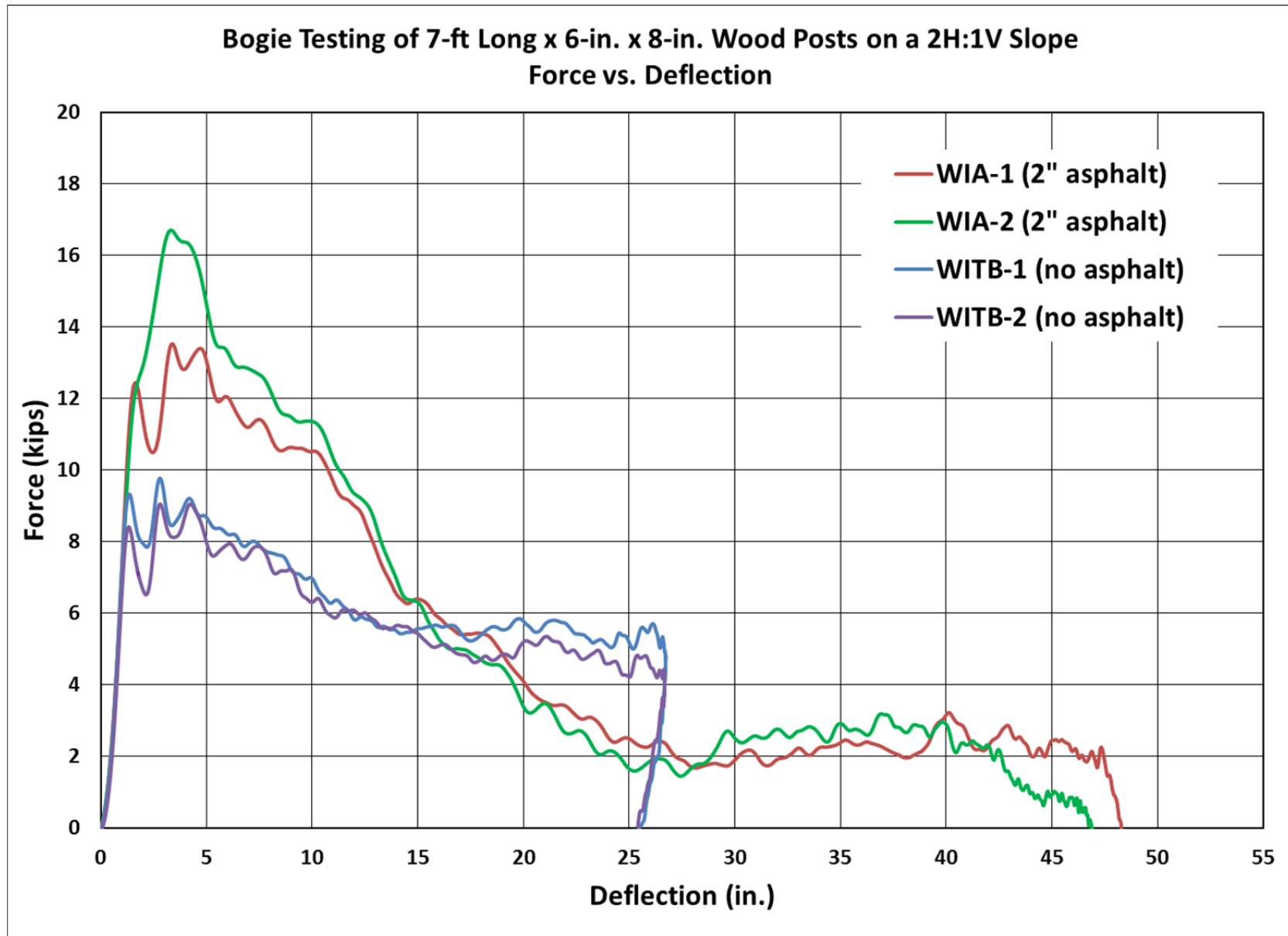


Figure 97. Force vs. Deflection Results, 2H:1V Fill Slope Bogie Testing

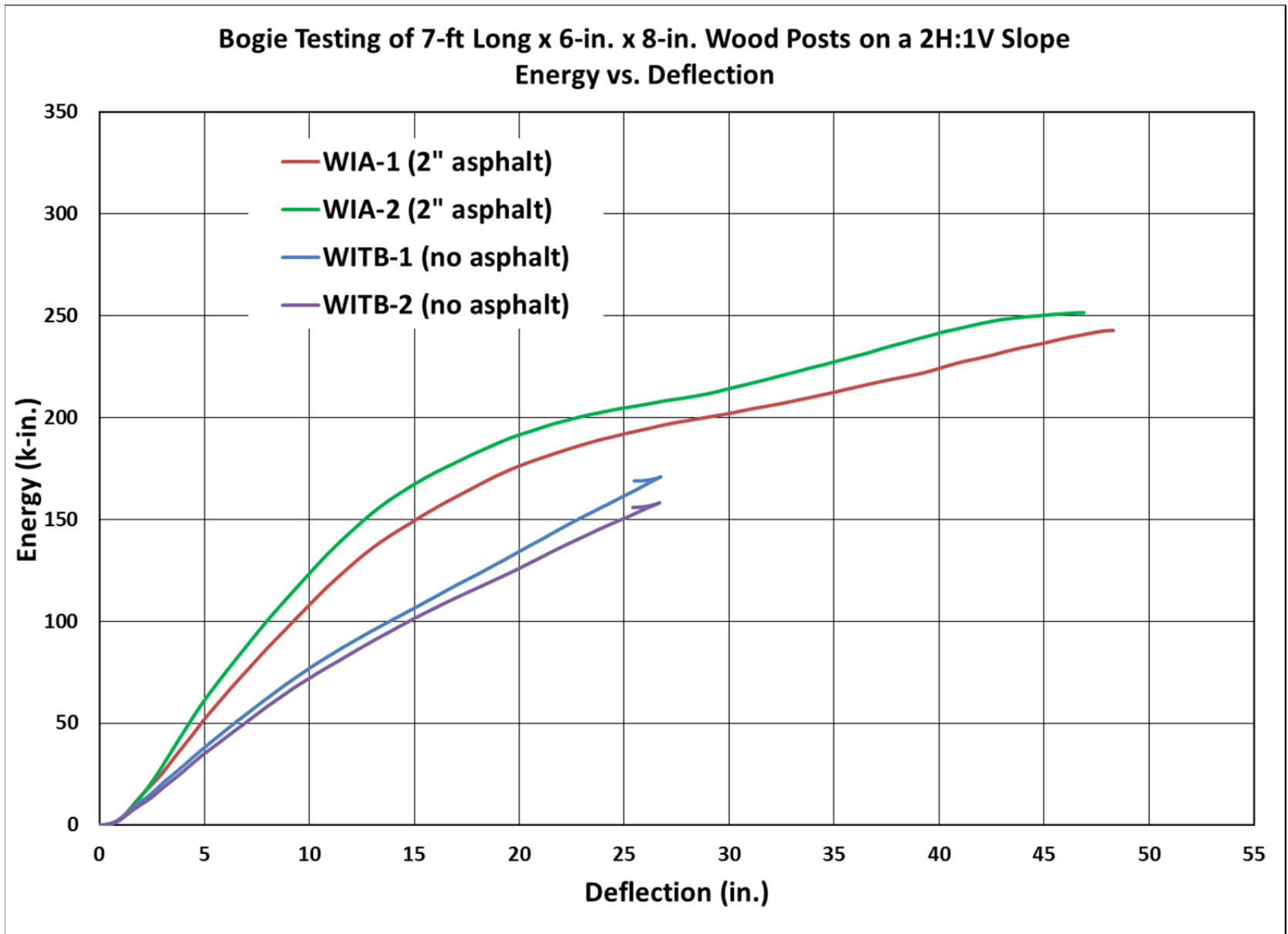


Figure 98. Energy vs. Deflection Results, 2H:1V Fill Slope Bogie Testing

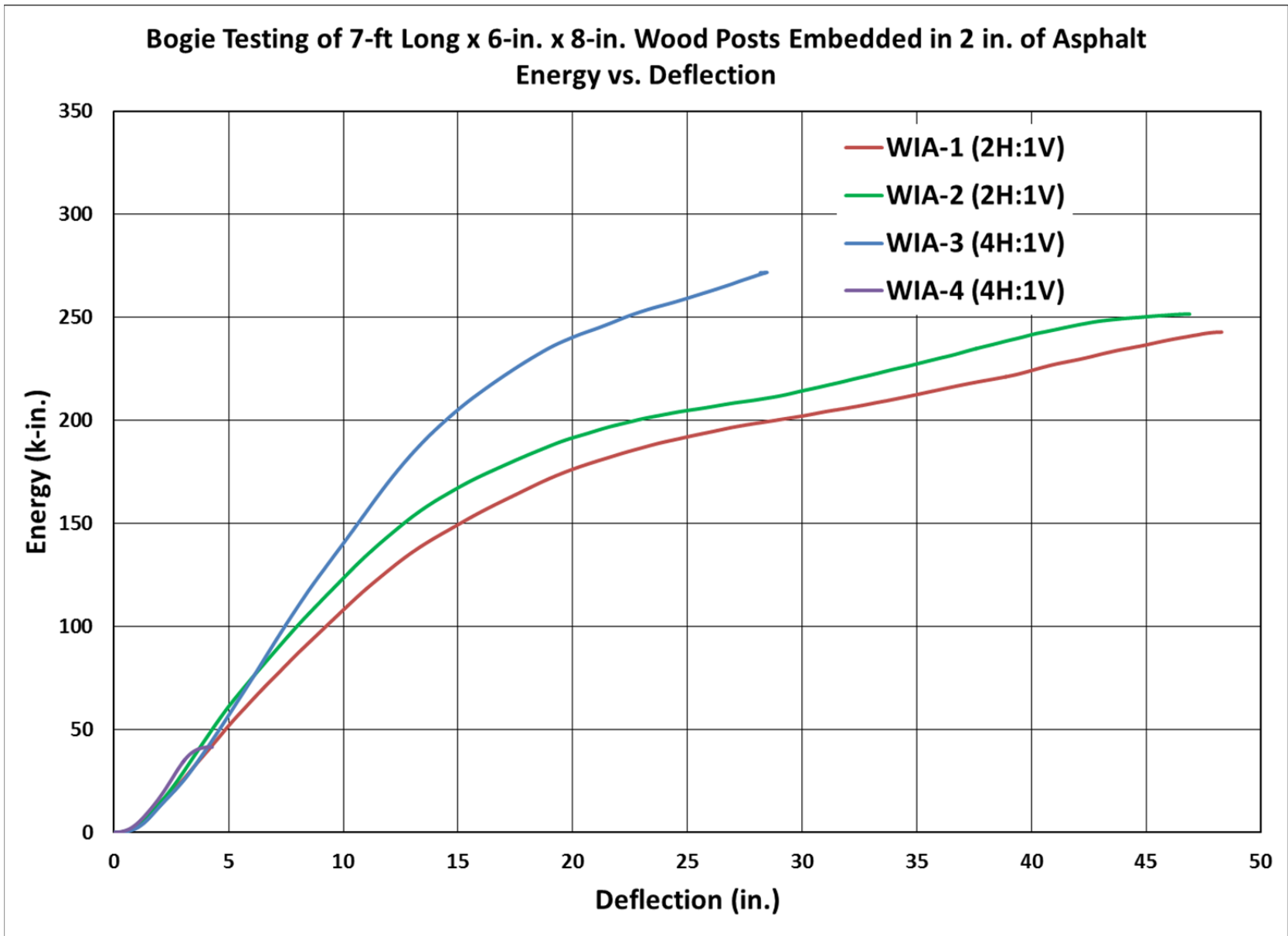


Figure 99. Energy vs. Deflection Results, WIA Bogie Testing

12 DRAINAGE STRUCTURES POSITIONED BELOW TRANSITION

12.1 Overview

Survey data from Section 3.2 indicated that lateral drainage structures (i.e., flumes) were frequently installed below both the 18-ft 9-in. (5.7-m) long transition system and the 31-ft 3-in. (9.5-m) long transition system in the State of Wisconsin. In particular, this deficiency had the potential to cause severe vehicle instabilities during vehicle containment capture and redirection of an errant vehicle. Research studies involving W-beam guardrail systems and similar approach guardrail transition systems which utilized a curb-barrier configuration were examined to determine the suitability of a lateral drainage structure (i.e., flume).

12.2 Longitudinal Curbs

According to the *Roadside Design Guide* [42], curbs may be utilized in a transition region for two reasons: (i) to control the flow of water runoff leaving the roadway and help reduce erosion along the transition system and (ii) to reduce the propensity for vehicle wheel rim snag on the upstream end of a bridge rail. However, if not designed properly, curbs and curb inlets may induce vehicle instabilities and adversely affect the crashworthiness of a transition system. For high-speed roadways where curb-barrier installation is necessary, NCHRP Report No. 537 [44] recommends the use of a 4 in. (100 mm) or shorter curb with a sloping face placed flush with the front face of the guardrail. Short, sloping curbs reduce the likelihood of causing a tire blowout, suspension damage, and/or loss of vehicle control, while placing the curb flush with the front face of the guardrail reduces concerns for a vehicle to underride or override a barrier system.

Further, curb-transition combinations that were successfully crash tested should adhere to the original design in which they were evaluated. A 2003 TTI Texas transition study [43] illustrates this notion. In that study, a previously-successful approach guardrail transition system

with a lower curb was unable to safely redirect a pickup truck when the lower curb was not incorporated below the thrie beam rail. In test no. 445643-1, the pickup truck rolled on its side, thus not satisfying the TL-3 safety criteria found in NCHRP Report No. 350. The researchers concluded that the transition system without the curb was unable to safely redirect the impacting pickup truck.

Survey data and photographs from Section 3.2 indicated that the majority of curb-transition combinations in the State of Wisconsin utilized a 6-in. (152-mm) tall, vertical curb. Although this type of curb is not prohibited, it does have an increased propensity to cause vehicular instabilities as compared to a 4-in. (102-mm) tall sloping curb. In particular, the barrier system developed in the 1998 MwRSF Iowa transition study [20] utilized a 4-in. (102-mm) tall, triangular curb, as shown previously in Figure 9. During test nos. ITNJ-2 and ITNJ-4, the test vehicles were safely contained and smoothly redirected. The wood-post version of the barrier system has not been crash-tested or evaluated without this curb. However, the steel-post version of this barrier system with some design modifications was unsuccessfully crash tested and evaluated without the curb [43]. As discussed previously, test no. 445643-1 demonstrated that the modified system without the lower curb was unable to safely redirect the impacting pickup truck. Thus, any subsequent installation of that particular transition, including the 18-ft 9-in. (5.7-m) long Wisconsin transition system, requires the use of a comparable 4-in. (102-mm) tall triangular curb below the thrie beam transition.

The 31-ft 3-in. (9.5-m) long transition system that was developed in the 1988 MwRSF Kansas transition study [21] did not utilize a curb in its original design. However, as mentioned previously, this design was not crash tested but instead simulated with BARRIER VII and compared to other crashworthy transition systems. Based on the successful crash testing of thrie beam transitions, it is believed that a 4-in. (102-mm) tall curb with a sloping face, as

recommended in NCRHP Report No. 537 for high-speed installations, could be used in combination with this barrier system to provide hydraulic drainage control and mitigate erosion behind the transition posts.

12.3 Lateral Drainage Flumes

The lateral drainage flume utilized by the Wisconsin DOT for both the 18-ft 9-in. (5.7-m) long transition system and the 31-ft 3-in. (9.5-m) long transition system, as shown in Appendix A, includes a longitudinal, 6-in. (152-mm) tall, vertical concrete curb directly below the face of the three beam rail. Between post nos. 6 and 7, the curb structure opens up, turns 90 degrees, and continues to extend laterally away from the roadway and behind the transition system. In addition, a 3-in. (76-mm) deep swell is formed below the transition rail and in the region near the lateral flume opening.

The lateral drainage-flume described above potentially presents numerous safety risks to errant motorists. First, the height and shape of the longitudinal curb is not ideal according to recommendations provided in NCHRP Report No. 537. A taller curb can lead to an increased propensity for vehicle instabilities. Second, the 6-in. (152-mm) tall curb exceeds the height originally crashed tested in the 1998 MwRSF Iowa transition study. Third, the 3-in. (76-mm) deep swell near the lateral curb opening may promote bumper or wheel snag on the corner region as vehicles wedge under the three beam rail and/or result in underride of the system. Finally, the lateral flume opening creates a significant obstruction in the wheel path of the vehicle. In essence, these curbs create multiple speed bumps during redirection, which have the potential to cause severe vehicle instabilities. Therefore, full-scale crash testing on this curb-transition structure with small cars and pickup trucks should be conducted to determine whether the lateral drainage flume with tall curb is suitable for approach guardrail transition systems found along high-speed roadways. The research team strongly recommends that no additional installations of

the Wisconsin DOT lateral drainage flume with tall curb be implemented until its safety performance has been thoroughly evaluated through full-scale vehicle crash testing.

One alternative to conducting full-scale crash testing would be to utilize large leave-outs in the concrete, as per FHWA specifications [39], and move the drainage-flume structure farther behind the transition system. This curb shift would prevent the wheel path of the vehicle from intruding upon the various hazards of the structure. Another alternative would be to utilize a drop inlet, similar to that shown in Appendix A. However, the cross-section of the longitudinal curb portion of that structure should match the recommendations presented in the previous section for longitudinal curbs.

13 SUMMARY, CONCLUSIONS, AND RECOMMENDATIONS

As part of a field investigation conducted by Wisconsin DOT personnel, it was determined that several three beam approach guardrail transition systems installed throughout the State were in a condition which substantially deviated from the standard plans and as-tested design details. The most common deviations included missing transition posts, transition posts installed near or at the slope break point of fill slopes, insufficient soil backfill/grading behind transition posts, wood posts installed in asphalt surfacing, exposed posts due to erosion, and presence of drainage structures (i.e., lateral flumes) below the three rail. The potential hazards associated with each of these five deviations found in combination with existing approach guardrail transition systems were examined in terms of dynamic barrier deflections, vehicle snag, vehicle pocketing, and vehicular instabilities.

Results from an extensive BARRIER VII computer simulation effort demonstrated that even a single missing post within the three beam transition region caused either excessive dynamic barrier deflections with increased risk for vehicular instabilities or an increased propensity for a vehicle to snag on the upstream end of the rigid bridge rail. Thus, three retrofit design concepts were developed and subjected to dynamic component testing to mitigate the degrading effects that missing transition posts had on barrier performance. Conclusions, design details, and recommendations regarding the utilization of these retrofit designs can be found in Chapter 8.

Dynamic component tests were conducted to determine the lateral post-soil resistance of 6-in. x 8-in. x 7-ft. (152-mm x 203-mm x 2.1-m) long SYP wood transition posts placed at the slope break point of a steep slope. These dynamic test results were used in combination with BARRIER VII computer simulation to demonstrate that transition systems containing posts placed on steep slopes had an increased propensity for excessive dynamic barrier deflections, an

increased propensity for a vehicle to snag on the upstream end of the bridge rail, as well as an increased potential for vehicle pocketing. One retrofit design concept, which utilized extra driven steel posts, was developed utilizing the results from previous dynamic component testing. Conclusions, design details, and recommendations regarding the utilization of this retrofit design, as well as recommendations to further investigate an alternative backside beam design can be found in Chapter 9.

Analytical calculations demonstrated that wood transition posts with insufficient soil backfill/grading and excessive exposure lengths were no more likely to fracture during impact events than properly installed transition posts. BARRIER VII computer simulation results demonstrated that no design modifications to the transition systems were deemed necessary for short exposure lengths. Conclusions and recommendations regarding the resolution of this deficiency can be found in Chapter 10.

A dynamic component testing program was conducted to determine whether SYP wood transition posts on fill slopes and directly confined by asphalt surfacing were negatively affected. Test results demonstrated that thin layers of direct asphalt confinement did not negatively affect the performance of a wood guardrail post on a 2H:1V fill slope. However, wood transition posts on a 4H:1V fill slope and confined by asphalt were more prone to premature fracture. Conclusions and recommendations regarding these findings as well as recommendations to further investigate alternate transition installations in combination with thin layers of direct asphalt confinement can be found in Chapter 11.

Conclusions and recommendations regarding the immediate modification to Wisconsin DOT lateral drainage flume with tall curb located below thrie beam transition rails can be found in Chapter 12.

Almost every aspect of this research study depended on the assumption for obtaining a very high lateral post-soil resistance for closely-spaced, 6-in. x 8-in. (152-mm x 203-mm) SYP wood transition posts embedded 52 in. (1,321 mm) into the ground. This resistance may be significantly different than what is typically observed for an individual post subjected to dynamic testing. Thus, it would be beneficial in the future to investigate the true lateral post-soil resistance of closely-spaced wood transition posts when acting collectively during impact events. Results from this investigation would likely help to validate/refute the study findings as well as help roadside design engineers with the future development of approach guardrail transition systems and/or implementation of the noted retrofits contained herein.

14 REFERENCES

1. Polivka, K.A., Faller, R.K., Sicking, D.L., Reid, J.D., Rohde, J.R., and Holloway, J.C., *Crash Testing of Missouri's W-Beam to Thrie-Beam Transition Element*, MwRSF Report No. TRP-03-94-00, Midwest Roadside Safety Facility, University of Nebraska-Lincoln, September 2000.
2. Wisconsin Department of Transportation, *Facilities Development Manual – Chapter 16: Standard Detail Drawings, Section 14b20: Vehicle Barrier Systems, Drawing 9a: Steel Thrie Beam Structure Approach*, State of Wisconsin, 2010.
3. Wisconsin Department of Transportation, *Facilities Development Manual – Chapter 16: Standard Detail Drawings, Section 14b20: Vehicle Barrier Systems, Drawing 2a: Steel Thrie Beam Structure Approach*, State of Wisconsin, 2006.
4. Gabler, H.C., Gabauer, D.J., and Hampton, C.E., *Criteria for Restoration of Longitudinal Barriers*, National Cooperative Highway Research Program (NCHRP) Report No. 656, Transportation Research Board, Washington, D.C., 2010.
5. Hampton, C.E. and Gabler, H.C., *Development of a Missing Post Repair Guideline for Longitudinal Barrier Crash Safety – Manuscript Draft*, Journal of Transportation Engineering, American Society of Civil Engineers, 2011.
6. Polivka, K.A., Faller, R.K., Sicking, D.L., Rohde, J.R., Holloway, J.C., and Keller, E.A., *Development of a W-Beam Guardrail System for Use On a 2:1 Slope*, MwRSF Report No. TRP-03-99-00, Midwest Roadside Safety Facility, University of Nebraska-Lincoln, October 2000.
7. McGhee, M.D., Lechtenberg, K.A., Bielenberg, R.W., Faller, R.K., Sicking, D.L., and Reid, J.D., *Dynamic Impact Testing of Wood Posts for the Midwest Guardrail System (MGS) Placed Adjacent to a 2H:1V Fill Slope*, MwRSF Report No. TRP-03-234-10, Midwest Roadside Safety Facility, University of Nebraska-Lincoln, December 2010.
8. Homan, D.M., Thiele, J.C., Faller, R.K., Rosenbaugh, S.K., Rohde, J.R., Arens, S.W., Lechtenberg, K.A., and Sicking, D.L., *Investigation and Dynamic Testing of Wood and Steel Posts for MGS on a Wire-Faced MSE Wall*, MwRSF Report No., TRP-03-231-11, Midwest Roadside Safety Facility, University of Nebraska-Lincoln, February 2012.
9. Meyer, C.L., Faller, R.K., Lechtenberg, K.A., Sicking, D.L., Rohde, J.R., and Reid, J.D., *Phase II Continued Investigation and Dynamic Testing of Wood Posts For Use On A Wire-Faced MSE Wall*, MwRSF Report No. TRP-03-256-12, Midwest Roadside Safety Facility, University of Nebraska-Lincoln, February 2012.
10. Powell, G.H., *BARRIER VII – A Computer Program for Evaluation of Automobile Barrier Systems*, Report No. FHWA-RD-73-51, University of California – Berkeley, Federal Highway Administration, Washington, D.C., April 1973.

11. Ross, H.E., Sicking, D.L., Zimmer, R.A., and Michie, J.D., *Recommended Procedures for the Safety Performance Evaluation of Highway Features*, National Cooperative Highway Research Program (NCHRP) Report No. 350, Transportation Research Board, Washington, D.C., 1993.
12. Michie, J.D., *Recommended Procedures for the Safety Performance Evaluation of Highway Appurtenances*, National Cooperative Highway Research Program (NCHRP) Report No. 230, Transportation Research Board, Washington, D.C., March 1981.
13. *Guide Specifications for Bridge Railings*, American Association of State Highway and Transportation Officials (AASHTO), Washington, D.C., 1989.
14. *Manual for Assessing Safety Hardware (MASH)*, American Association of State Highway and Transportation Officials (AASHTO), Washington, D.C., 2009.
15. Post, E.R., *Full-Scale Vehicle Crash Tests on Guardrail-Bridgerail Transition Designs with Special Post Spacing*, Transportation Research Report TRP-03-008-87, University of Nebraska-Lincoln, May 1987.
16. *Guardrail Transitions, Technical Advisory T 5040.26*, Federal Highway Administration (FHWA), U.S. Department of Transportation, January 1988.
17. Bligh, R.P. and Mak, K.K., *Evaluation of Tennessee Bridge Rail to Guardrail Transition Designs*, Research Report RF 7199-2, Texas Transportation Institute, College Station, TX, June 1994.
18. Pfeifer, B.G., Faller, R.K., and Reid, J.D., *NCHRP Report 350 Evaluations of the Nebraska Thrie-Beam Transition*, MwRSF Research Report No. TRP-03-70-98, Midwest Roadside Safety Facility, University of Nebraska-Lincoln, May 1998.
19. Menges, W.L., Williams, W.F., Buth, C.E., and Schoeneman, S.K., *NCHRP Report 350 Test 3-21 of the Nebraska Thrie Beam Transition*, Research Report No. 404211-7, Texas Transportation Institute, College Station, TX, May 2000.
20. Faller, R.K., Reid, J.D., Rohde, J.R., Sicking, D.L., and Keller, E.A., *Two Approach Guardrail Transitions for Concrete Safety Shape Barriers*, MwRSF Report No. TRP-03-69-98, Midwest Roadside Safety Facility, University of Nebraska-Lincoln, May 1998.
21. Tuan, C.Y., Post, E.R., Atallah, S., and Brewer, J.O., *Development of Kansas Guardrail to Bridgerail Transition Designs Using BARRIER VII*, Transportation Research Record No. 1233, Transportation Research Board, Washington, D.C., 1989.
22. Soyland, K., Faller, R.K., Sicking, D.L., and Holloway, J.C., *Development and Testing of an Approach Guardrail Transition to a Side Slope Concrete Median Barrier*, MwRSF Report No. TRP-03-47-95, Midwest Roadside Safety Facility, University of Nebraska-Lincoln, November 1995.

23. Speer, D., Peter, R., Jewell, J., and Clark, N., *Vehicular Crash Tests of a Nested Thrie Beam Transition Barrier*, Final Report No. FHWA/CA/TL-2001/09, State of California Department of Transportation, May 2002.
24. Eller, C.M., Polivka, K.A., Faller, R.K., Sicking, D.L., Rohde, J.R., Reid, J.D., Bielenberg, R.W., and Allison, E.M., *Development of the Midwest Guardrail System (MGS) W-beam to Thrie Beam Transition Element*, MwRSF Report No. TRP-03-167-07, Midwest Roadside Safety Facility, University of Nebraska-Lincoln, November 2007.
25. Rosenbaugh, S.K., Lechtenberg, K.A., Faller, R.K., Sicking, D.L., Bielenberg, R.W., and Reid, J.D., *Development of the MGS Approach Guardrail Transition Using Standardized Steel Posts*, MwRSF Report No. TRP-03-210-10, Midwest Roadside Safety Facility, University of Nebraska-Lincoln, December 2010.
26. Cook, R.A., Collins, D.M., Klingner, R.E., and Polyzois, D., *Load-Deflection Behavior of Cast-In-Place and Retrofit Anchors*, ACI Structural Journal, 89(6): 639–649, 1992.
27. Cook, R.A., Kunz, J., Fuchs, W., and Konz, R.C., *Behavior and Design of Single Adhesive Anchors Under Tensile Load in Uncracked Concrete*, ACI Structural Journal, 95(1): 9–26, 1998.
28. ACI International, 2008, *Building Code Requirements for Structural Concrete and Commentary*, ACI 318, ACI International, Farmington Hills, MI.
29. ACI International, 2008, *Building Code Requirements for Structural Concrete and Commentary – Proposed Changes to ACI – 318-08*, ACI 318, ACI International, Farmington Hills, MI.
30. Dickey, B.J., Faller, R.K., Rosenbaugh, S.K., Bielenberg, R.W., Lechtenberg, K.A., and Sicking, D.L., *Development of a Design Procedure for Concrete Traffic Barrier Attachments to Bridge Decks Utilizing Epoxy Concrete Anchors – Draft Report*, MwRSF Report No. TRP-03-264-12, Midwest Roadside Safety Facility, University of Nebraska-Lincoln, 2012, In Progress.
31. Dickey, B.J., *Development of a Design Procedure for Concrete Traffic Barrier Attachments to Bridge Decks Utilizing Epoxy Concrete Anchors*, Master's Thesis, University of Nebraska-Lincoln, Lincoln, NE, 2011.
32. Goeller, M.D., *Soil Behavior During A Guardrail Post Impact*, Master's Thesis, University of Nebraska-Lincoln, Lincoln, NE, 2000.
33. Rohde, J.R., Hascall, J.A., Polivka, K.A., Faller, R.K., and Sicking, D.L., *Dynamic Testing of Wooden Guardrail Posts – White and Red Pine Species Equivalency Study*, MwRSF Report No. TRP-03-154-04, Midwest Roadside Safety Facility, University of Nebraska-Lincoln, September 2004.

34. Rohde, J.R., Reid, J.D., and Sicking, D.L., *Evaluation of the Effect of Wood Quality on W-Beam Guardrail Performance*, MwRSF Report No. TRP-03-60-96, Midwest Roadside Safety Facility, University of Nebraska-Lincoln, November 1995.
35. Rosenbaugh, S.K., Schrum, K.D., Faller, R.K., Lechtenberg, K.A., Sicking, D.L., and Reid, J.D., *Development of Alternate Wood-Post MGS Approach Guardrail Transition*, MwRSF Report No. TRP-03-243-11, Midwest Roadside Safety Facility, University of Nebraska-Lincoln, November 2011.
36. Dey, G., Faller, R.K., Hascall, J.A., Bielenberg, R.W., Polivka, K.A., and Molacek, K., *Dynamic Impact Testing of W152x13.4 (W6X9) Steel Posts on a 2:1 Slope*, MwRSF Report No. TRP-03-165-07, Midwest Roadside Safety Facility, University of Nebraska-Lincoln, March 2007.
37. Wiebelhaus, M.J., Lechtenberg, K.A., Faller, R.K., Sicking, D.L., Bielenberg, R.W., Reid, J.D., Rohde, J.R., and Dey, G., *Development and Evaluation of the Midwest Guardrail System (MGS) Placed Adjacent to a 2:1 Fill Slope*, MwRSF Report No. TRP-03-185-10, Midwest Roadside Safety Facility, University of Nebraska-Lincoln, February 2010.
38. Bligh, R.P., Seckinger, N.R., Abu-Odeh, A.K., Roschke, P.N., and Menges, W.L., *Dynamic Response of Guardrail Systems Encased In Pavement Mow Strips*, Research Report 0-4162-2, Texas Transportation Institute, College Station, TX, January 2004.
39. Baxter, J.R., *W-Beam Guardrail Installations in Rock and in Mowing Strips*, Memorandum HAS-10/B64-B, Federal Highway Administration, U.S. Department of Transportation, March 2004.
40. Arrington, D.R., Bligh, R.P., and Menges, W.L., *Alternative Design of Guardrail Posts in Asphalt or Concrete Mowing Pads*, Research Report 405160-14-1, Texas Transportation Institute, College Station, TX, May 2009.
41. Herr, J.E., Rohde, J.R., Sicking, D.L., Reid, J.D., Faller, R.K., Holloway, J.C., Coon, B.A., and Polivka, K.A., *Development of Standards for Placement of Steel Guardrail Posts in Rock*, MwRSF Report No. TRP-03-119-03, Midwest Roadside Safety Facility, University of Nebraska-Lincoln, May 2003.
42. AASHTO, *Roadside Design Guide*, Third Edition with Updated Chapter 6, American Association of State Highway and Transportation Officials, Washington, D.C., 2006.
43. Bligh, R.P., Menges, W.L., and Haug, R.R., *Evaluations of Guardrail to Concrete Bridge Rail Transitions*, Research Report 4564-1, Texas Transportation Institute, College Station, TX, October 2003.
44. Plaxico, C.A., Ray, M.H., Weir, J.A., Orengo, F., Tiso, P., McGhee, H., Council, F., and Eccles, K., *Recommended Guidelines for Curb and Curb-Barrier Installations*, National Cooperative Highway Research Program (NCHRP) Report No 537, Transportation Research Board, Washington, D.C., 2005.

45. Wisconsin Department of Transportation, *Highway Structures – English Standard Details – Chapter 30: Railings – Section 12: Sloped Face Parapet “LF,”* State of Wisconsin, 2006.
46. Wisconsin Department of Transportation, *Highway Structures – English Standard Details – Chapter 30: Railings – Voided Detail Drawings,* State of Wisconsin, 1990.
47. Wisconsin Department of Transportation, *Facilities Development Manual – Chapter 16: Standard Detail Drawings, Section 8d2: Concrete Surface Drains Flume Type at Structures,* State of Wisconsin, 2010.
48. Wisconsin Department of Transportation, *Facilities Development Manual – Chapter 16: Standard Detail Drawings, Section 8d3: Concrete Surface Drains Drop Inlet Type at Structure,* State of Wisconsin, 2010.
49. Bligh, R.P and Sicking, D.L., *Applications of BARRIER VII in Design of Flexible Barriers,* Transportation Research Record No. 1233, Transportation Research Board, Washington, D.C., 1989.
50. Hilti Profis Anchor 2.1.2, Hilti Corporation, Schaun, LI, 2010.
51. American Institute of Steel Construction, 2005, *Steel Construction Manual,* American Institute of Steel Construction, Chicago, IL.
52. Malvar, L.J., *Review of Static and Dynamic Properties of Steel Reinforcing Bars,* ACI Materials Journal, Technical Paper No. 95-M59, American Concrete Institute, Detroit, MI, October 1998.
53. Wisconsin Department of Transportation, *Facilities Development Manual – Chapter 16: Standard Detail Drawings, Section 14b15: Steel Plate Beam Guard, Class “A,” Installation Elements, Drawing c,* State of Wisconsin, 2010.
54. Society of Automotive Engineers (SAE), *Instrumentation for Impact Test – Part 1 – Electronic Instrumentation,* SAE J211/1 MAR95, New York City, NY, July 2007.

15 APPENDICES

Appendix A. Wisconsin Detailed Drawings

The standards currently utilized by the State of Wisconsin for various structures examined herein are provided in this section.

Figure A-1. Wisconsin Sloped Face Parapet “LF” [45]

Figure A-2. Wisconsin Sloped Face Parapet “B” (Voided) [46]

Figure A-3. Wisconsin Concrete Surface Drains Flume Type at Structures [47]

Figure A-4. Wisconsin Concrete Surface Drains Drop Inlet Type at Structures [48]

Figure A-5. Wisconsin Double and Triple Blocked-Out Guardrails [53]

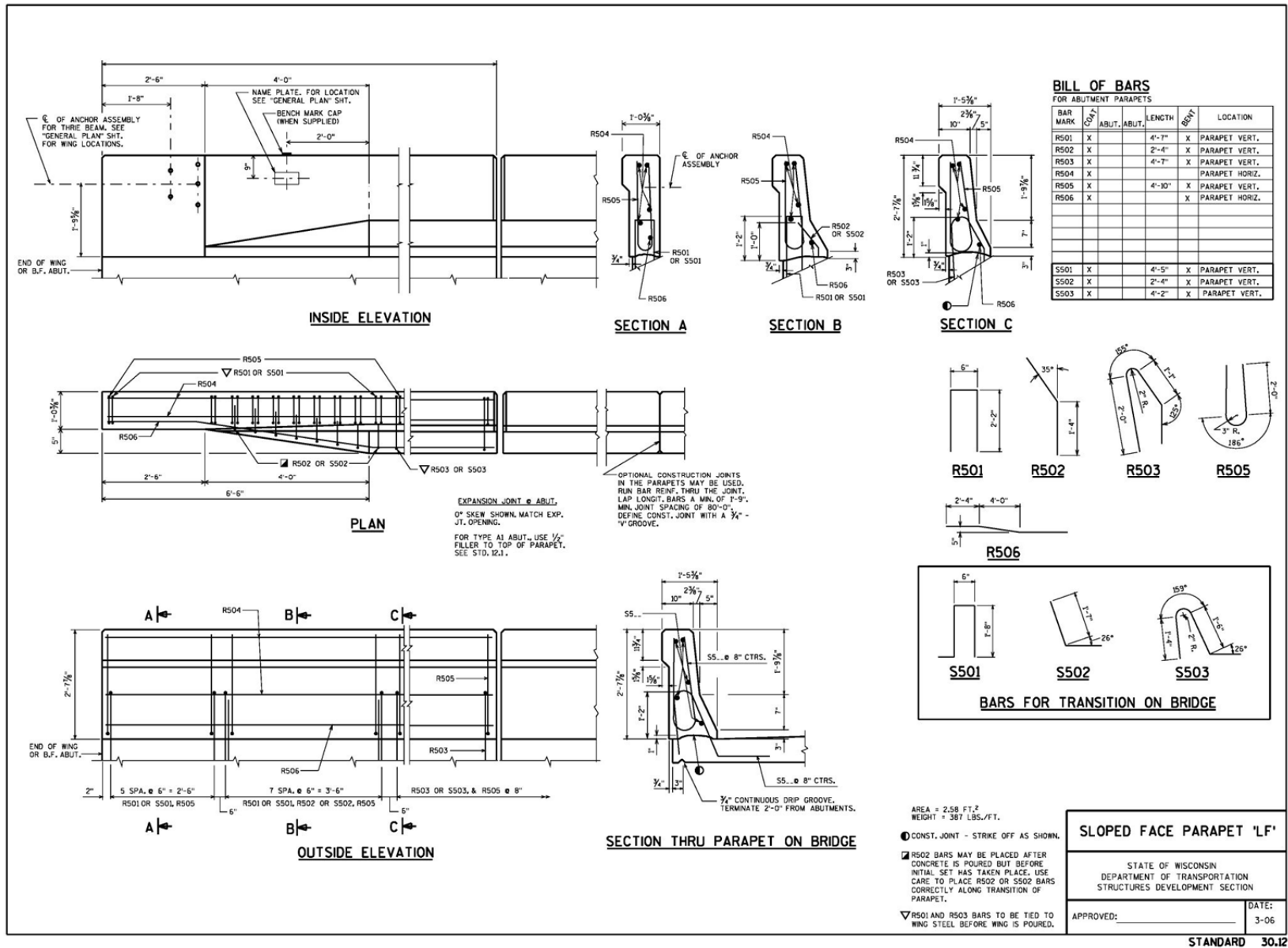


Figure A-1. Wisconsin Sloped Face Parapet "LF" [45]

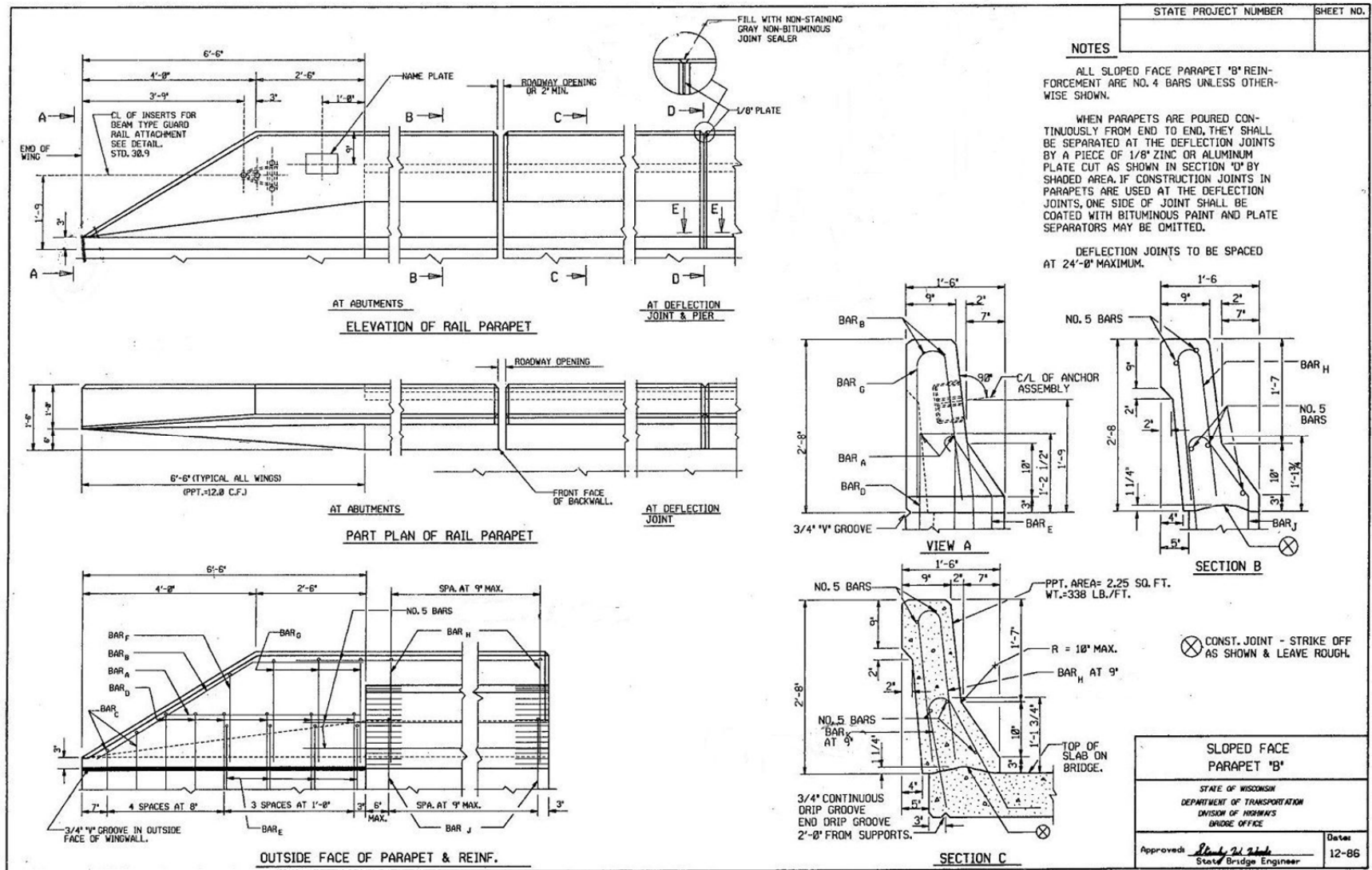


Figure A-2. Wisconsin Sloped Face Parapet "B" (Voided) [46]

8D2: Concrete Surface Drains Flume Type at Structures

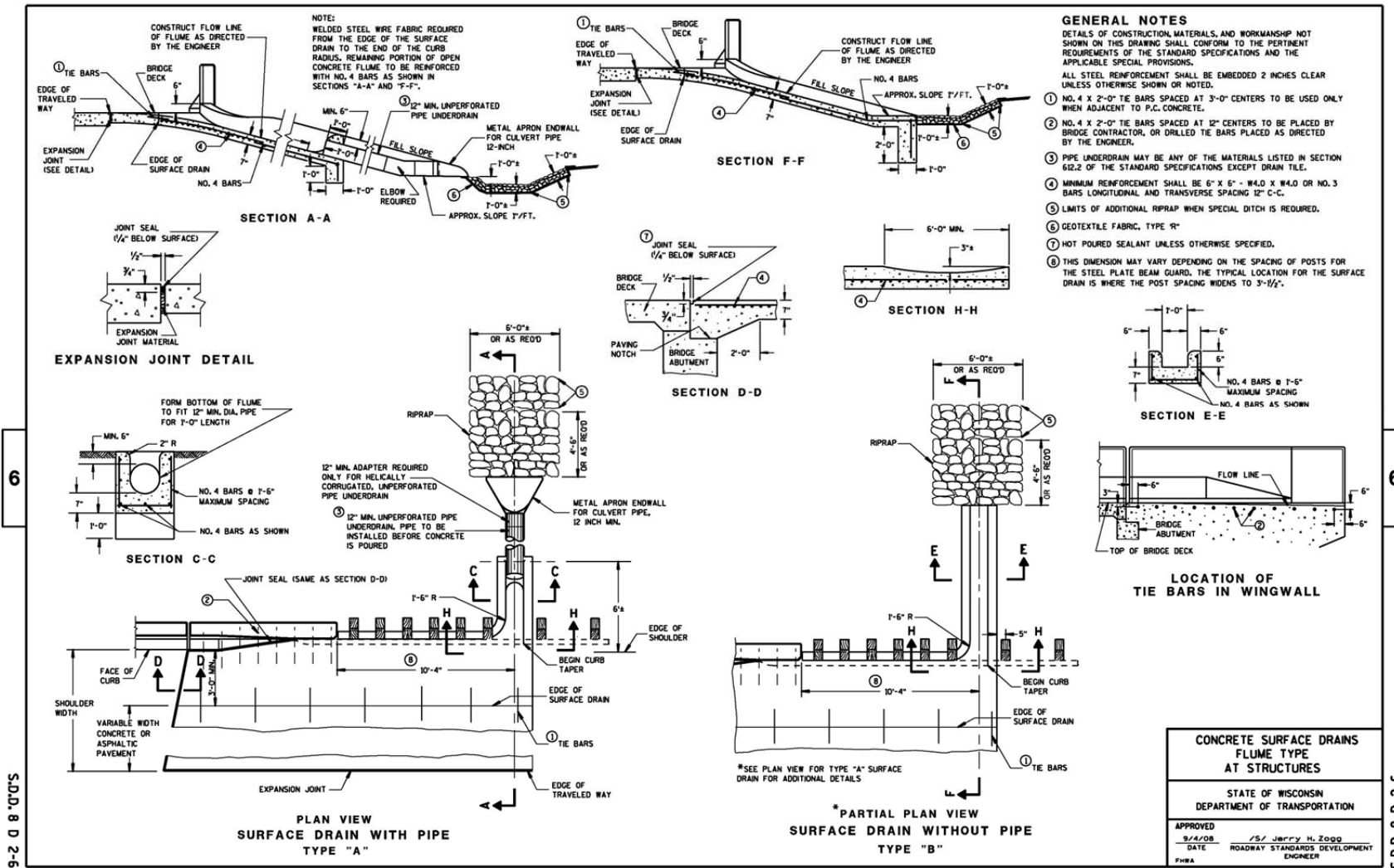
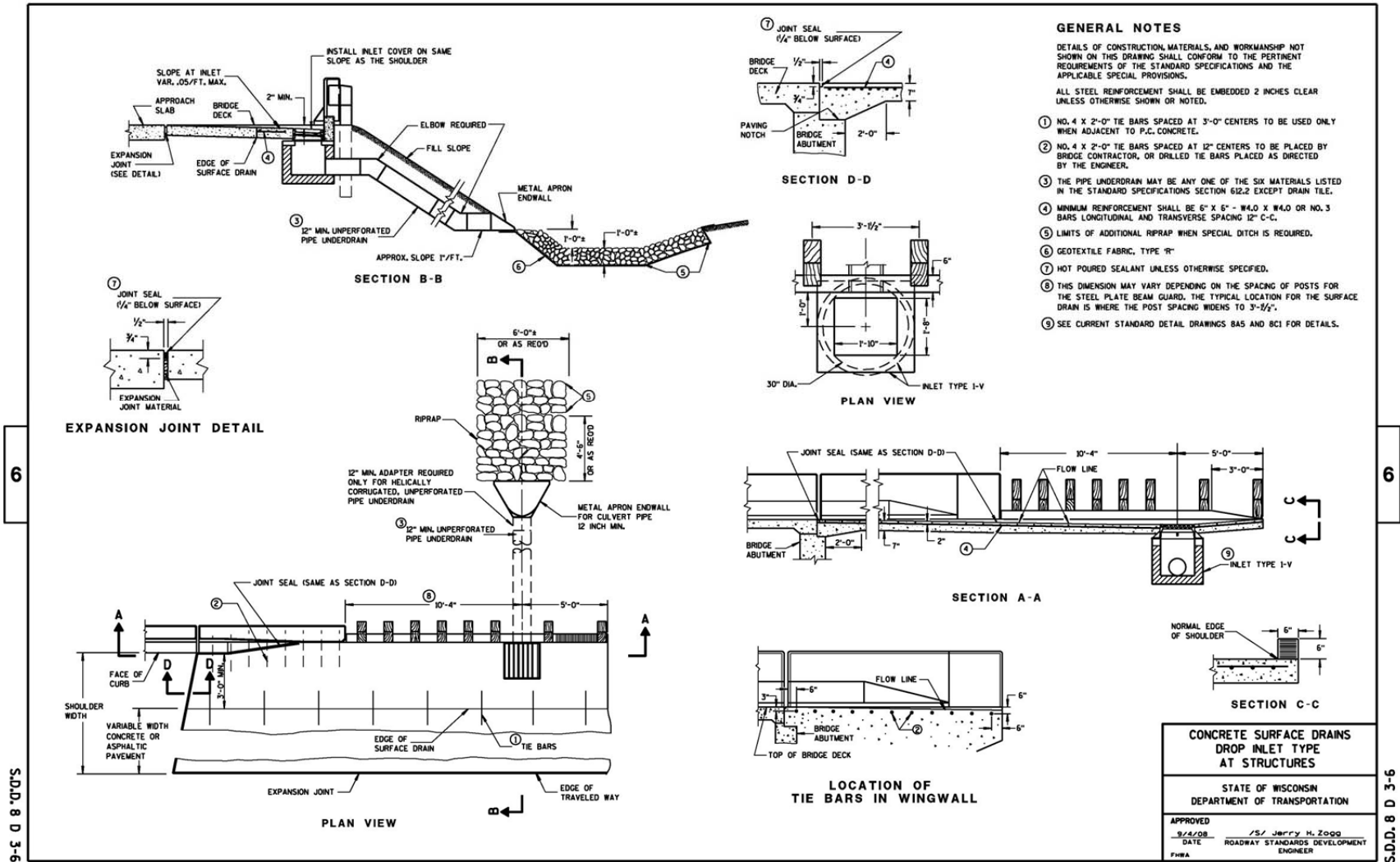


Figure A-3. Wisconsin Concrete Surface Drains Flume Type at Structures [47]

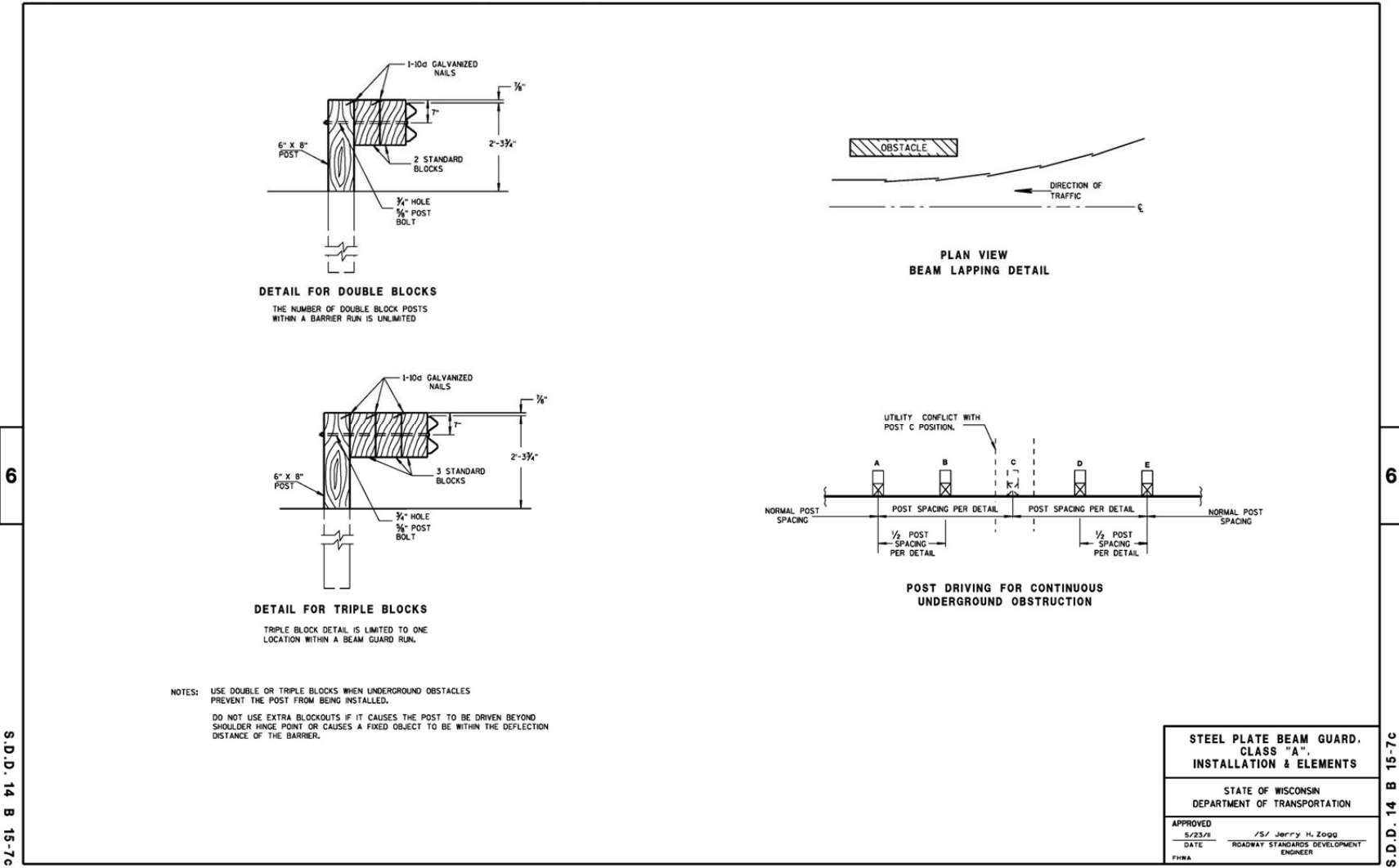
8D3: Concrete Surface Drains Drop Inlet Type at Structures



233

Figure A-4. Wisconsin Concrete Surface Drains Drop Inlet Type at Structures [48]

14B15 sheet c: Steel Plate Beam Guard, Class "A", Installation and Elements



234

6

6

S.D.D. 14 B 15-7c

S.D.D. 14 B 15-7c

Figure A-5. Wisconsin Double and Triple Blocked-Out Guardrails [53]

Appendix B. BARRIER VII Input Data

A typical input deck and visual representation for each transition system used in computer simulation is provided in this section.

Figure B-1. BARRIER VII Model Deck for the 18-ft 9-in. Long System

Figure B-2. BARRIER VII Model Deck for the 18-ft 9-in. Long System – Cont.

Figure B-3. BARRIER VII Model Deck for the 18-ft 9-in. Long System – Cont.

Figure B-4. BARRIER VII CAD Drawing of the 18-ft 9-in. Long System

Figure B-5. BARRIER VII Model Deck for the 31-ft 3-in. Long System

Figure B-6. BARRIER VII Model Deck for the 31-ft 3-in. Long System – Cont.

Figure B-7. BARRIER VII Model Deck for the 31-ft 3-in. Long System – Cont.

Figure B-8. BARRIER VII CAD Drawing of the 31-ft 3-in. Long System

18-ft - 9-in. Long Wisconsin Transition (Iowa Design) - Baseline 20T.b7

165	4	3	1	191	29	2	0			
	0.0001		0.0001		0.75	3000	0	1	1	
10	50	50	50	10	500	10				
1		0		0						
127		1181.25		0						
129		1192.75		0						
165		1530.25		0						
1	127	125	1		0					
127	129	1	1		0					
129	165	35	1		0					
1	165		0.25							
165	164	163	162	161	160	159	158	157	156	
155	154	153	152	151	150	149	148	147	146	
145	144	143	142	141	140	139	138	137	136	
135	134	133	132	131	130	129	128	127	126	
125	124	123	122	121	120	119	118	117	116	
115	114	113	112	111	110	109	108	107	106	
105	104	103	102	101	100	99	98	97	96	
95	94	93	92	91	90	89	88	87	86	
85	84	83	82	81	80	79	78	77	76	
75	74	73	72	71	70	69	68	67	66	
65	64	63	62	61	60	59	58	57	56	
55	54	53	52	51	50	49	48	47	46	
45	44	43	42	41	40	39	38	37	36	
35	34	33	32	31	30	29	28	27	26	
25	24	23	22	21	20	19	18	17	16	
15	14	13	12	11	10	9	8	7	6	
5	4	3	2	1						
100	15									
1		2.29		1.99		9.375		30000		6.92
2		3.114		2.65		9.375		30000		9.216
3		3.341		2.83		9.375		30000		9.847
4		3.569		3.01		9.375		30000		10.478
5		3.796		3.19		9.375		30000		11.109
6		4.024		3.37		9.375		30000		11.741
7		4.251		3.55		9.375		30000		12.372
8		4.479		3.73		9.375		30000		13.003
9		4.706		3.91		9.375		30000		13.634
10		3.76		3.1		9.375		30000		10.81
11		7.52		6.2		9.375		30000		21.62
12		99.99		99.99		9.375		99999.9		99.999
13		7.52		3.1		5.75		30000		21.62
14		xxx		xxx		9.375		30000		xxx
15		xxx		xxx		5.75		30000		xxx
300		7								
1		21.65		0		6		6		100
	100		100		15		15			675
2		21.65		0		3		3		100
	50		50		15		15			150
3		21.65		0		11		6		84
	25		25		6		15			368
4		21.65		0		14		8		98
	25		25		4.5		15			400
5		21.65		0		999		999		999
	999		999		999		999		999.99	999.99
6		21.65		0		0.1		0.1		1
	0.1		0.1		0.1		0.1			1
7		21.65		0		xxx		xxx		98
	xxx		xxx		4.5		15		xxx	xxx

Figure B-1. BARRIER VII Model Deck for the 18-ft 9-in. Long System

1	1	2	104	1	101	0	0	0		
105	105	106		1	102	0	0	0		
106	106	107		1	103	0	0	0		
107	107	108		1	104	0	0	0		
108	108	109		1	105	0	0	0		
109	109	110		1	106	0	0	0		
110	110	111		1	107	0	0	0		
111	111	112		1	108	0	0	0		
112	112	113		1	109	0	0	0		
113	113	114	116	1	111	0	0	0		
117	117	118	118	1	111	0	0	0		
119	119	120	120	1	111	0	0	0		
121	121	122	122	1	111	0	0	0		
123	123	124	124	1	111	0	0	0		
125	125	126	126	1	111	0	0	0		
127	127	128	128	1	113	0	0	0		
129	129	130	164	1	112	0	0	0		
165	1				301	0	0	0	0	0
166	9				302	0	0	0	0	0
167	17		176	8	303	0	0	0	0	0
177	97				303	0	0	0	0	0
178	105		180	4	304	0	0	0	0	0
181	117				304	0	0	0	0	0
182	119				304	0	0	0	0	0
183	121				304	0	0	0	0	0
184	123				304	0	0	0	0	0
185	125				304	0	0	0	0	0
186	127				304	0	0	0	0	0
187	129		191	8	305	0	0	0	0	0
4409.25			47400	20	6	4	0	25		
1	0.055		0.12			6		17		
2	0.057		0.15			7		18		
3	0.062		0.18			10		12		
4	0.11		0.35			12		6		
5	0.35		0.45			6		5		
6	1.45		1.5			15		1		
1	90		13.25	1		12	1	0	0	0
2	90		25.25	1		12	1	0	0	0
3	90		37.25	2		12	1	0	0	0
4	78		37.25	2		12	1	0	0	0
5	66		37.25	2		12	1	0	0	0
6	54		37.25	2		12	1	0	0	0
7	42		37.25	2		12	1	0	0	0
8	30		37.25	2		12	1	0	0	0
9	18		37.25	2		12	1	0	0	0
10	6		37.25	2		12	1	0	0	0
11	-28		37.25	3		12	1	0	0	0
12	-48		37.25	3		12	1	0	0	0
13	-68		37.25	3		12	1	0	0	0
14	-88		37.25	3		12	1	0	0	0
15	-108		37.25	3		12	1	0	0	0
16	-128		37.25	4		12	1	0	0	0
17	-128		-37.25	4		12	0	0	0	0
18	90		-37.25	1		12	0	0	0	0
19	55		36.125	5		1	1	0	0	0
20	-76.5		36.125	6		1	1	0	0	0
1	55		31.375		0			639.3		
2	55		-31.375		0			639.3		
3	-75.5		31.375		0			463		
4	-75.5		-31.375		0			463		

Figure B-2. BARRIER VII Model Deck for the 18-ft 9-in. Long System – Cont.

1	90	37.25						
2	-128	37.25						
3	-128	-37.25						
4	90	-37.25						
5	5	2.5						
6	5	-2.5						
7	-5	-2.5						
8	-5	2.5						
9	70.85	36						
10	70.85	26.75						
11	39.15	26.75						
12	39.15	36						
13	70.85	-26.75						
14	70.85	-36						
15	39.15	-36						
16	39.15	-26.75						
17	-60.65	36						
18	-60.65	26.75						
19	-92.35	26.75						
20	-92.35	36						
21	-60.65	-26.75						
22	-60.65	-36						
23	-92.35	-36						
24	-92.35	-26.75						
25	0	0						
3	1096.875	0	25	62.14	0	0	1	

Figure B-3. BARRIER VII Model Deck for the 18-ft 9-in. Long System – Cont.

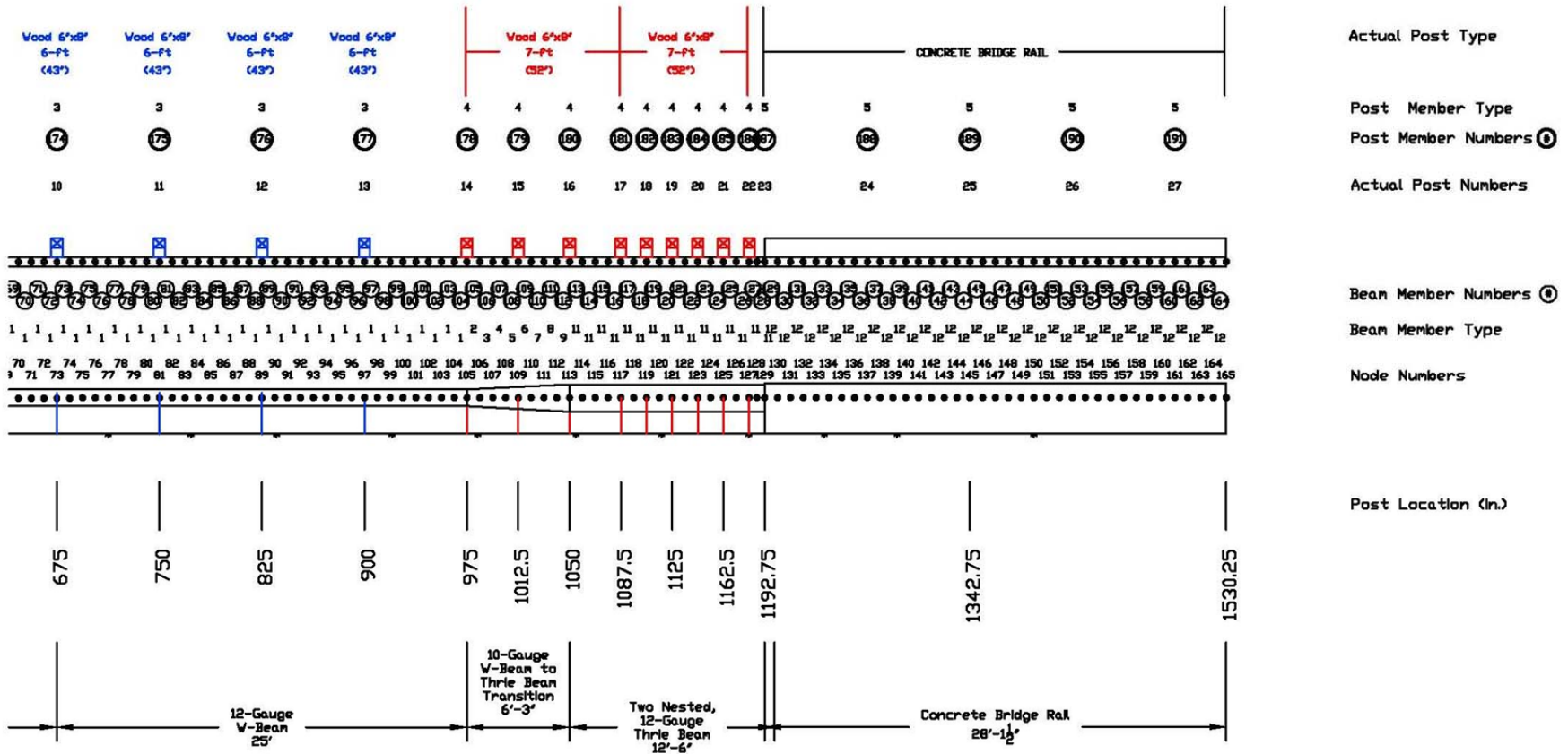


Figure B-4. BARRIER VII CAD Drawing of the 18-ft 9-in. Long System

31-ft - 3-in. Long Wisconsin Transition (Kansas Design) - Baseline 30T.b7

165	4	3	1	191	32	2	0													
	0.0001		0.0001		0.75	3000	0	1	1											
10	50	50	50	10	500	10														
1		0		0																
127		1181.25		0																
129		1192.75		0																
165		1530.25		0																
1	127	125	1		0															
127	129	1	1		0															
129	165	35	1		0															
1	165		0.25																	
165	164	163	162	161	160	159	158	157	156											
155	154	153	152	151	150	149	148	147	146											
145	144	143	142	141	140	139	138	137	136											
135	134	133	132	131	130	129	128	127	126											
125	124	123	122	121	120	119	118	117	116											
115	114	113	112	111	110	109	108	107	106											
105	104	103	102	101	100	99	98	97	96											
95	94	93	92	91	90	89	88	87	86											
85	84	83	82	81	80	79	78	77	76											
75	74	73	72	71	70	69	68	67	66											
65	64	63	62	61	60	59	58	57	56											
55	54	53	52	51	50	49	48	47	46											
45	44	43	42	41	40	39	38	37	36											
35	34	33	32	31	30	29	28	27	26											
25	24	23	22	21	20	19	18	17	16											
15	14	13	12	11	10	9	8	7	6											
5	4	3	2	1																
100	14																			
1		2.29		1.99		9.375		30000		6.92		99.5		68.5						0.05 12-GAUGE W-BEAM
2		2.382		2.059		9.375		30000		7.163		102.97		71.06						0.05 12-GAUGE W-BEAM TO THRIE BEAM
3		2.566		2.198		9.375		30000		7.649		109.91		76.19						0.05 12-GAUGE W-BEAM TO THRIE BEAM
4		2.749		2.337		9.375		30000		8.136		116.84		81.31						0.05 12-GAUGE W-BEAM TO THRIE BEAM
5		2.933		2.476		9.375		30000		8.622		123.78		86.44						0.05 12-GAUGE W-BEAM TO THRIE BEAM
6		3.117		2.614		9.375		30000		9.108		130.72		91.56						0.05 12-GAUGE W-BEAM TO THRIE BEAM
7		3.301		2.753		9.375		30000		9.594		137.66		96.69						0.05 12-GAUGE W-BEAM TO THRIE BEAM
8		3.484		2.892		9.375		30000		10.081		144.59		101.81						0.05 12-GAUGE W-BEAM TO THRIE BEAM
9		3.668		3.031		9.375		30000		10.567		151.53		106.94						0.05 12-GAUGE W-BEAM TO THRIE BEAM
10		3.76		3.1		9.375		30000		10.81		155		109.5						0.05 12-GAUGE THRIE BEAM
11		7.52		6.2		9.375		30000		21.62		310		219						0.05 12-GAUGE NESTED THRIE BEAM
12		99.99		99.99		9.375		99999.9		99.999		999.99		9999.9						0.05 CONCRETE BRIDGE RAIL
13		7.52		6.2		5.75		30000		21.62		310		219						0.05 12-GAUGE THRIE BEAM AT BRIDGE RAIL
14		5555		5555		9.375		30000		55555		55555		55555						0.05 NESTED THRIE + XXXX
300	7																			
1		21.65		0		6		6		100		675		675						0.05 SIMULATED STRONG ANCHOR POST
	100		100		15		15													
2		21.65		0		3		3		100		150		225						0.05 SECOND BCT POST
	50		50		15		15													
3		21.65		0		11		6		84		368		325						0.05 6"x8" 6-ft LONG WOOD POST (43" EMB.)
	25		25		6		15													
4		21.65		0		14		8		98		400		476						0.05 6"x8" 7-ft LONG WOOD POST (52" EMB.)
	25		25		4.5		15													
5		21.65		0		999		999		999		999.99		999.99						0.05 CONCRETE BRIDGE RAIL
	999		999		999		999													
6		21.65		0		0.1		0.1		1		1		1						0.05 MISSING POST
	0.1		0.1		0.1		0.1													
7		21.65		0		555		555		555		555		5555						0.05 POST WITH ISSUE
	555		555		555		555													

Figure B-5. BARRIER VII Model Deck for the 31-ft 3-in. Long System

1	1	2	88	1	101	0	0	0		
89	89	90		1	102	0	0	0		
90	90	91		1	103	0	0	0		
91	91	92		1	104	0	0	0		
92	92	93		1	105	0	0	0		
93	93	94		1	106	0	0	0		
94	94	95		1	107	0	0	0		
95	95	96		1	108	0	0	0		
96	96	97		1	109	0	0	0		
97	97	98	104	1	110	0	0	0		
105	105	106	108	1	110	0	0	0		
109	109	110	112	1	110	0	0	0		
113	113	114	116	1	111	0	0	0		
117	117	118	118	1	111	0	0	0		
119	119	120	120	1	111	0	0	0		
121	121	122	122	1	111	0	0	0		
123	123	124	124	1	111	0	0	0		
125	125	126	126	1	111	0	0	0		
127	127	128	128	1	113	0	0	0		
129	129	130	164	1	112	0	0	0		
165	1				301	0	0	0		
166	9				302	0	0	0	0	0
167	17		176	8	303	0	0	0	0	0
177	97				304	0	0	0	0	0
178	105		180	4	304	0	0	0	0	0
181	117				304	0	0	0	0	0
182	119				306	0	0	0	0	0
183	121				304	0	0	0	0	0
184	123				304	0	0	0	0	0
185	125				304	0	0	0	0	0
186	127				304	0	0	0	0	0
187	129		191	8	305	0	0	0	0	0
4409.25		47400	20	6	4	0	25			
1	0.055		0.12		6		17			
2	0.057		0.15		7		18			
3	0.062		0.18		10		12			
4	0.11		0.35		12		6			
5	0.35		0.45		6		5			
6	1.45		1.5		15		1			
1	90		13.25	1		12	1	0	0	0
2	90		25.25	1		12	1	0	0	0
3	90		37.25	2		12	1	0	0	0
4	78		37.25	2		12	1	0	0	0
5	66		37.25	2		12	1	0	0	0
6	54		37.25	2		12	1	0	0	0
7	42		37.25	2		12	1	0	0	0
8	30		37.25	2		12	1	0	0	0
9	18		37.25	2		12	1	0	0	0
10	6		37.25	2		12	1	0	0	0
11	-28		37.25	3		12	1	0	0	0
12	-48		37.25	3		12	1	0	0	0
13	-68		37.25	3		12	1	0	0	0
14	-88		37.25	3		12	1	0	0	0
15	-108		37.25	3		12	1	0	0	0
16	-128		37.25	4		12	1	0	0	0
17	-128		-37.25	4		12	0	0	0	0
18	90		-37.25	1		12	0	0	0	0
19	55		36.125	5		1	1	0	0	0
20	-76.5		36.125	6		1	1	0	0	0
1	55		31.375		0		639.3			
2	55		-31.375		0		639.3			
3	-75.5		31.375		0		463			
4	-75.5		-31.375		0		463			

Figure B-6. BARRIER VII Model Deck for the 31-ft 3-in. Long System – Cont.

1	90	37.25							
2	-128	37.25							
3	-128	-37.25							
4	90	-37.25							
5	5	2.5							
6	5	-2.5							
7	-5	-2.5							
8	-5	2.5							
9	70.85	36							
10	70.85	26.75							
11	39.15	26.75							
12	39.15	36							
13	70.85	-26.75							
14	70.85	-36							
15	39.15	-36							
16	39.15	-26.75							
17	-60.65	36							
18	-60.65	26.75							
19	-92.35	26.75							
20	-92.35	36							
21	-60.65	-26.75							
22	-60.65	-36							
23	-92.35	-36							
24	-92.35	-26.75							
25	0	0							
3	1096.875	0	25	62.14	0	0	1		

Figure B-7. BARRIER VII Model Deck for the 31-ft 3-in. Long System – Cont.

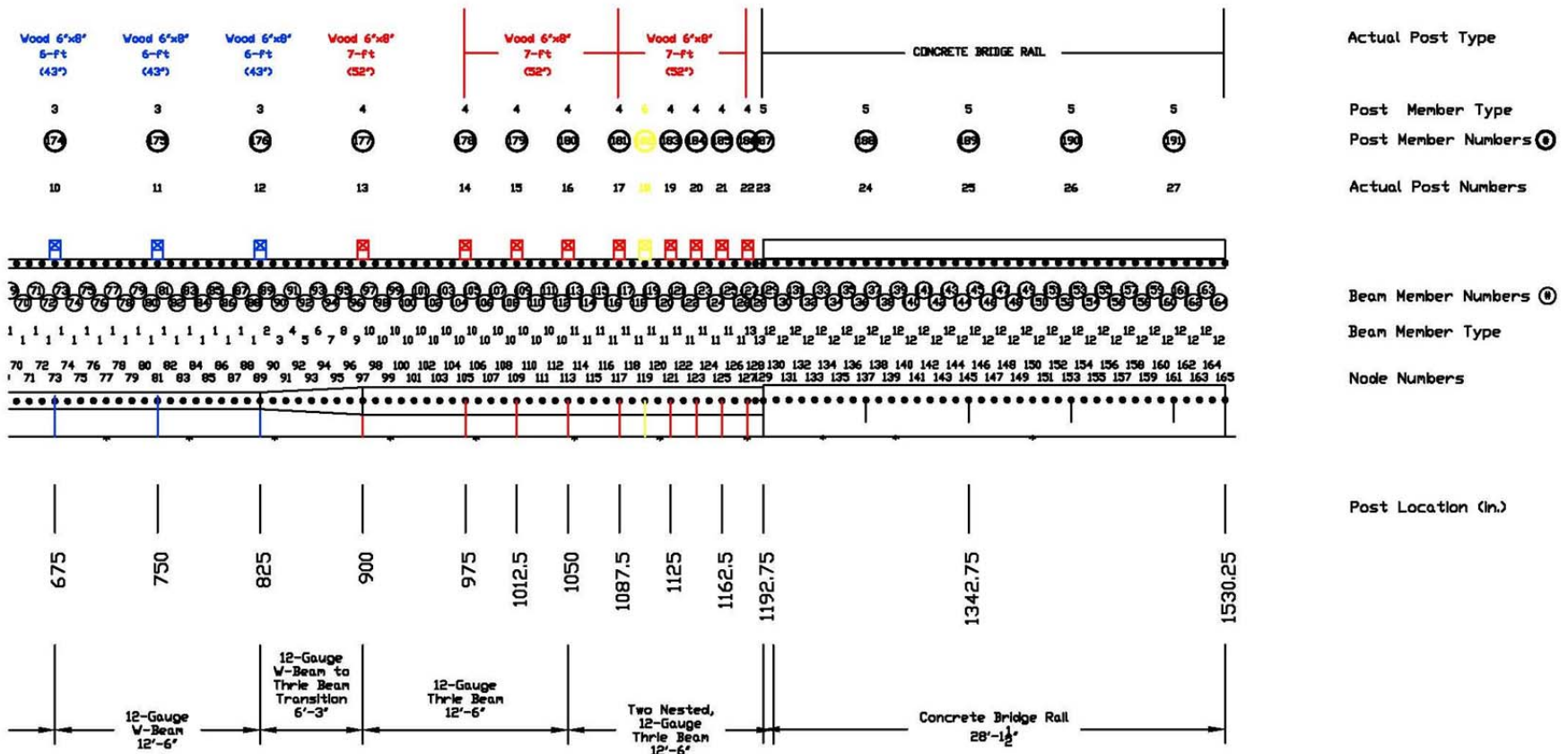


Figure B-8. BARRIER VII CAD Drawing of the 31-ft 3-in. Long System

Appendix C. BARRIER VII Execution Procedures

The codes and input decks used to execute the BARRIER VII computer program along with detailed instructions on obtaining results from output files are provided in this section. These files can be found under the following path: /mwrsf-server/active & current projects/WSDOT Retrofitting Approach Guardrail Transitions (2011-present)/Barrier VII.

Executable Codes

auto-b7-wisagt – this is a script that runs and post-processes BARRIER VII; it was used to obtain maximum dynamic barrier deflections, maximum rail tension, vehicle parallel times, and vehicle pocketing angles.

BARlrg8d – this is an alternate program that also runs and post-processes BARRIER VII; it was used to obtain wheel rim snag on the upstream end of the bridge rail.

Input Decks

Baseline Models:

wisagt20base.b7

wisagt33base.b7

Missing Transition Posts:

wisagt20mp1.b7

wisagt33mp1.b7

wisagt20mp1retro.b7

wisagt33mp1retro.b7

wisagt20mp2.b7

wisagt33mp2.b7

wisagt20mp3.b7

wisagt33mp3.b7

wisagt20mp4.b7

wisagt33mp4.b7

wisagt20mp5.b7

wisagt33mp6.b7

wisagt20mp6.b7

Transition Posts Installed on Fill Slopes:

wisagt20sloped.b7

wisagt33sloped.b7

wisagt33slopedretro.b7

Exposed Transition Posts:

wisagt20exposed3.b7

wisagt33exposed3.b7

wisagt20exposed4.b7

wisagt33exposed4.b7

Instructions to Obtain Results

1. How to run the auto-b7-wisagt code:
 - a. Locate the appropriate input deck and make any modifications necessary to represent the desired conditions, including vehicle characteristics and impact location. Note that this script requires 25 specific output data points for the vehicle.
 - b. Use the auto-b7-wisagt script to execute the simulation of the model. Successful completion of this operation will result in the creation of various output files.
2. Obtaining post-process results for the auto-b7-wisagt code:
 - a. Open the output file titled summary.results. This file contains a summary of results from the simulation.
 - b. Obtain the magnitude and location of maximum deflection. This is the maximum dynamic barrier deflection for this simulation.
 - c. Obtain the magnitude and location of maximum force. This is the maximum rail tension for this simulation.
 - d. Obtain the value for vehicle heading parallel time. This is the time until the angle of the vehicle becomes parallel with the barrier for this simulation.
 - e. Obtain the minimum value and location for the 5 node least square slope of the barrier. This is the barrier pocketing angle (radians) for this simulation.
3. How to run the BARlrg8d program:
 - a. Locate the appropriate input deck and make any modifications necessary to represent the desired conditions, including impact location.
 - b. Use the BARlrg8d program to execute the simulation of the model.
 - c. Enter appropriate names for the 3 output files (i.e., basic, vehicle, structure).
4. Obtaining post-process results for the BARlrg8d program:
 - a. Open the structure output file. This file contains the position of each barrier and vehicle node during each time interval of the entire impact event. These time intervals are based on parameters provided in the input deck and can be adjusted by the user.

- b. For each time interval, locate the second from last row. This row should contain the number 19 in the first column. This is the node that represents the front left tire of the vehicle.
- c. Observe the third column of this row. This is the longitudinal position of the front left tire along the barrier. If this value is 1178, proceed to Step 4d. Otherwise, continue to scroll down through time intervals until the third column in the second to last row reaches 1178.
- d. Observe the fourth column of this row. This is the amount of displacement of the node beyond the initial vertical plane of the barrier. If the value is positive, then document the magnitude. This represents the wheel *tire* snag on the bridge rail end. If the value is negative, then there is no predicted wheel *tire* snag for this simulation.
- e. Continue to scroll down through time intervals until the third column in the second to last row reaches a value of 1184.
- f. Observe the fourth column of this row. If this value is positive, then document the magnitude. This represents the wheel *rim* snag on the bridge rail end. If the value is negative, then there is no predicted wheel *rim* snag for this simulation.

Appendix D. BARRIER VII Simulation Results

A summary table for each BARRIER VII simulation is provided in this section. Summary tables include maximum pocketing angle, rail force, dynamic barrier deflection, and wheel snag.

Table D-1. 18-ft 9-in. Long System – Baseline

Table D-2. 18-ft 9-in. Long System – Missing Post Position 1

Table D-3. 18-ft 9-in. Long System – Retrofitted Post Position 1 (W6x12)

Table D-4. 18-ft 9-in. Long System – Missing Post Position 2

Table D-5. 18-ft 9-in. Long System – Missing Post Position 3

Table D-6. 18-ft 9-in. Long System – Missing Post Position 4

Table D-7. 18-ft 9-in. Long System – Missing Post Position 5

Table D-8. 18-ft 9-in. Long System – Missing Post Position 6

Table D-9. 18-ft 9-in. Long System – 3-in. Improper Post Exposure

Table D-10. 18-ft 9-in. Long System – 4-in. Improper Post Exposure

Table D-11. 18-ft 9-in. Long System – Break Point of a 2H:1V Fill Slope

Table D-12. 31-ft 3-in. Long System – Baseline

Table D-13. 31-ft 3-in. Long System – Missing Post Position 1

Table D-14. 31-ft 3-in. Long System – Retrofitted Post Position 1 (W6x12)

Table D-15. 31-ft 3-in. Long System – Missing Post Position 2

Table D-16. 31-ft 3-in. Long System – Missing Post Position 3

Table D-17. 31-ft 3-in. Long System – Missing Post Position 4

Table D-18. 31-ft 3-in. Long System – Missing Post Position 6

Table D-19. 31-ft 3-in. Long System – 3 in. Improper Post Exposure

Table D-20. 33-ft 3-in. Long System – 4-in. Improper Post Exposure

Table D-21. 31-ft 3-in. Long System – Break Point of a 2H:1V Fill Slope

Table D-1. 18-ft 9-in. Long System – Baseline

	Impact Point			5-Node Maximum Slope		5-Node Maximum Pocket Angle		Maximum Force		Maximum Deflection		Snag - Tire (Deformed)	Snag - Rim (Deformed)	Heading Parallel Time
	US of Bridge Rail (in.)	(in.)	Node No.	(rad)	@ Node	(deg)	@ Node	(kips)	@ Node	(in.)	@ Node	(in.)	(in.)	(sec)
W-to-Thrie Element	217.750	975.000	105	0.1665	114	9.5	114	120.09	110	10.13	112	-	-	0.204
	208.375	984.375	106	0.1739	115	9.9	115	117.30	109	9.78	112	-	-	0.204
	199.000	993.750	107	0.1707	115	9.7	115	113.24	113	9.05	114	-	-	0.205
	189.625	1003.125	108	0.1599	115	9.1	115	112.91	113	8.56	115	-	-	0.203
	180.250	1012.500	109	0.1557	116	8.8	116	105.64	113	8.44	115	-	-	0.206
	170.875	1021.875	110	0.1476	116	8.4	116	101.19	113	8.09	115	-	-	0.206
	161.500	1031.250	111	0.1300	118	7.4	118	88.06	113	7.48	116	-	-	0.205
	152.125	1040.625	112	0.1200	119	6.8	119	78.92	117	6.74	118	-	-	0.205
Nested Thrie Beam	142.750	1050.000	113	0.1161	120	6.6	120	70.74	117	6.22	118	-	-	0.203
	133.375	1059.375	114	0.1093	121	6.2	121	57.35	119	5.64	120	-	-	0.204
	124.000	1068.750	115	0.0987	122	5.6	122	56.12	119	4.91	121	-	-	0.204
	114.625	1078.125	116	0.1072	124	6.1	124	60.82	121	4.90	122	0.03	-	0.202
	105.250	1087.500	117	0.1241	125	7.1	125	65.76	123	4.80	123	1.06	0.46	0.202
	95.875	1096.875	118	0.1389	125	7.9	125	70.24	123	4.67	124	1.68	0.85	0.201
	86.500	1106.250	119	0.1410	125	8.0	125	70.20	123	4.33	124	2.17	1.22	0.203
	77.125	1115.625	120	0.1244	125	7.1	125	58.59	123	3.67	125	2.24	1.44	0.210
	67.750	1125.000	121	0.1019	125	5.8	125	43.42	123	3.03	125	2.20	1.58	0.222
	58.375	1134.375	122	0.0828	125	4.7	125	25.74	125	2.38	125	1.74	1.49	0.231
	49.000	1143.750	123	0.0533	126	3.1	126	12.76	125	1.93	126	1.31	1.21	0.230
	39.625	1153.125	124	0.0149	126	0.9	126	11.32	129	1.61	129	0.44	0.68	0.226
	30.250	1162.500	125	0.0139	134	0.8	134	10.69	129	1.44	129	0.11	0.20	0.222
	20.875	1171.875	126	0.0085	136	0.5	136	7.85	129	0.94	129	0.04	0.05	0.222
	11.500	1181.250	127	0.0075	138	0.4	138	7.01	129	0.56	132	-	-	0.222
5.750	1187.000	128	0.0053	136	0.3	136	7.01	129	0.40	134	-	-	0.222	

Table D-2. 18-ft 9-in. Long System – Missing Post Position 1

Impact Point			5-Node Maximum Slope		5-Node Maximum Pocket Angle		Maximum Force		Maximum Deflection		Snag - Tire (Deformed)	Snag - Rim (Deformed)	Heading Parallel Time	
US of Bridge Rail (in.)	(in.)	Node No.	(rad)	@ Node	(deg)	@ Node	(kips)	@ Node	(in.)	@ Node	(in.)	(in.)	(sec)	
W-to-Thrie Element	217.750	975.000	105	0.1665	114	9.5	114	120.04	110	10.13	112	-	-	0.204
	208.375	984.375	106	0.1739	115	9.9	115	117.23	109	9.78	112	-	-	0.204
	199.000	993.750	107	0.1707	115	9.7	115	113.26	113	9.06	114	-	-	0.205
	189.625	1003.125	108	0.1599	115	9.1	115	112.87	113	8.56	115	-	-	0.203
	180.250	1012.500	109	0.1563	115	8.9	115	105.65	113	8.44	115	-	-	0.206
	170.875	1021.875	110	0.1476	116	8.4	116	100.97	113	8.09	115	-	-	0.206
	161.500	1031.250	111	0.1311	118	7.5	118	87.92	113	7.47	116	-	-	0.205
	152.125	1040.625	112	0.1189	119	6.8	119	78.90	117	6.75	118	-	-	0.205
	142.750	1050.000	113	0.1150	120	6.6	120	70.20	119	6.22	118	-	-	0.203
	133.375	1059.375	114	0.1093	121	6.2	121	57.14	119	5.64	120	-	-	0.204
Nested Thrie Beam	124.000	1068.750	115	0.0954	122	5.4	122	55.52	119	4.90	121	-	-	0.205
	114.625	1078.125	116	0.1045	124	6.0	124	58.43	121	4.89	122	0.31	-	0.204
	105.250	1087.500	117	0.1331	125	7.6	125	69.98	123	4.90	123	1.30	0.79	0.202
	95.875	1096.875	118	0.1486	125	8.5	125	84.28	123	4.89	124	2.33	1.22	0.200
	86.500	1106.250	119	0.1562	125	8.9	125	86.09	125	4.62	124	2.99	1.90	0.203
	77.125	1115.625	120	0.1397	125	8.0	125	74.47	125	4.15	125	3.13	2.21	0.214
	67.750	1125.000	121	0.1181	126	6.7	126	62.02	125	3.62	126	2.94	2.32	0.228
	58.375	1134.375	122	0.0920	126	5.3	126	39.50	126	3.00	126	2.29	2.08	0.235
	49.000	1143.750	123	0.0643	126	3.7	126	23.31	125	2.61	126	1.64	1.61	0.233
	39.625	1153.125	124	0.0181	130	1.0	130	18.36	129	2.11	128	0.54	0.84	0.227
	30.250	1162.500	125	0.0160	132	0.9	132	14.20	129	1.84	129	0.10	0.22	0.224
	20.875	1171.875	126	0.0107	136	0.6	136	8.92	129	1.24	129	0.04	0.05	0.222
	11.500	1181.250	127	0.0075	139	0.4	139	7.02	129	0.65	129	-	-	0.222
	5.750	1187.000	128	0.0053	136	0.3	136	6.93	129	0.42	134	-	-	0.222

Table D-3. 18-ft 9-in. Long System – Retrofitted Post Position 1 (W6x12)

	Impact Point			5-Node Maximum Slope		5-Node Maximum Pocket Angle		Maximum Force		Maximum Deflection		Snag - Tire (Deformed)	Snag - Rim (Deformed)	Heading Parallel Time
	US of Bridge Rail (in.)	(in.)	Node No.	(rad)	@ Node	(deg)	@ Node	(kips)	@ Node	(in.)	@ Node	(in.)	(in.)	(sec)
W-to-Thrie Element	217.750	975.000	105	0.1665	114	9.5	114	120.09	110	10.13	112	-	-	0.204
	208.375	984.375	106	0.1739	115	9.9	115	117.30	109	9.78	112	-	-	0.204
	199.000	993.750	107	0.1708	115	9.7	115	113.60	113	9.05	114	-	-	0.205
	189.625	1003.125	108	0.1599	115	9.1	115	112.91	113	8.56	115	-	-	0.203
	180.250	1012.500	109	0.1557	116	8.8	116	105.64	113	8.44	115	-	-	0.206
	170.875	1021.875	110	0.1476	116	8.4	116	101.20	113	8.09	115	-	-	0.206
	161.500	1031.250	111	0.1300	118	7.4	118	88.07	113	7.48	116	-	-	0.205
	152.125	1040.625	112	0.1190	119	6.8	119	78.88	117	6.74	118	-	-	0.205
Nested Thrie Beam	142.750	1050.000	113	0.1161	120	6.6	120	70.83	119	6.22	118	-	-	0.203
	133.375	1059.375	114	0.1093	121	6.2	121	57.44	119	5.64	120	-	-	0.204
	124.000	1068.750	115	0.0986	122	5.6	122	56.08	119	4.91	121	-	-	0.204
	114.625	1078.125	116	0.1084	124	6.2	124	60.87	121	4.91	122	-	-	0.202
	105.250	1087.500	117	0.1241	125	7.1	125	65.98	123	4.79	123	1.03	0.27	0.202
	95.875	1096.875	118	0.1389	125	7.9	125	70.40	123	4.64	124	1.72	0.89	0.201
	86.500	1106.250	119	0.1399	125	8.0	125	71.62	123	4.29	124	2.29	1.33	0.203
	77.125	1115.625	120	0.1257	125	7.2	125	59.06	123	3.68	125	2.39	1.61	0.211
	67.750	1125.000	121	0.1012	125	5.8	125	42.89	123	3.00	125	2.24	1.67	0.223
	58.375	1134.375	122	0.0800	125	4.6	125	24.38	125	2.33	125	1.70	1.47	0.232
	49.000	1143.750	123	0.0522	126	3.0	126	12.14	125	1.89	126	1.26	1.17	0.230
	39.625	1153.125	124	0.0149	126	0.9	126	10.34	129	1.54	129	0.43	0.66	0.226
	30.250	1162.500	125	0.0107	134	0.6	134	10.21	129	1.37	129	0.10	0.20	0.222
	20.875	1171.875	126	0.0075	136	0.4	136	7.73	129	0.89	129	0.04	0.05	0.222
	11.500	1181.250	127	0.0053	142	0.3	142	6.99	129	0.55	132	-	-	0.222
5.750	1187.000	128	0.0053	136	0.3	136	7.01	129	0.40	134	-	-	0.222	

250

Table D-4. 18-ft 9-in. Long System – Missing Post Position 2

	Impact Point			5-Node Maximum Slope		5-Node Maximum Pocket Angle		Maximum Force		Maximum Deflection		Snag - Tire (Deformed)	Snag - Rim (Deformed)	Heading Parallel Time
	US of Bridge Rail (in.)	(in.)	Node No.	(rad)	@ Node	(deg)	@ Node	(kips)	@ Node	(in.)	@ Node	(in.)	(in.)	(sec)
W-to-Thrie Element	217.750	975.000	105	0.1665	114	9.5	114	120.00	110	10.13	112	-	-	0.204
	208.375	984.375	106	0.1739	115	9.9	115	117.32	109	9.78	112	-	-	0.204
	199.000	993.750	107	0.1707	115	9.7	115	113.17	113	9.06	114	-	-	0.205
	189.625	1003.125	108	0.1599	115	9.1	115	112.71	113	8.55	115	-	-	0.203
	180.250	1012.500	109	0.1546	116	8.8	116	105.41	113	8.44	115	-	-	0.206
	170.875	1021.875	110	0.1476	116	8.4	116	100.57	113	8.08	115	-	-	0.206
	161.500	1031.250	111	0.1301	117	7.4	117	87.71	113	7.48	116	-	-	0.205
	152.125	1040.625	112	0.1159	118	6.6	118	77.19	117	6.75	118	-	-	0.206
Nested Thrie Beam	142.750	1050.000	113	0.1075	120	6.1	120	67.54	119	6.24	118	-	-	0.205
	133.375	1059.375	114	0.0933	122	5.3	122	54.01	119	5.60	120	-	-	0.207
	124.000	1068.750	115	0.0989	124	5.6	124	61.54	121	5.07	122	0.08	-	0.208
	114.625	1078.125	116	0.1336	125	7.6	125	73.32	121	5.33	122	1.41	0.66	0.204
	105.250	1087.500	117	0.1700	125	9.6	125	106.11	123	5.73	124	2.16	1.19	0.198
	95.875	1096.875	118	0.1826	125	10.3	125	117.22	123	6.01	124	2.63	1.50	0.200
	86.500	1106.250	119	0.1826	125	10.3	125	116.05	123	5.73	124	2.86	1.91	0.205
	77.125	1115.625	120	0.1731	125	9.8	125	100.15	123	5.10	125	2.98	2.00	0.216
	67.750	1125.000	121	0.1510	125	8.6	125	81.23	123	4.48	125	2.93	2.22	0.229
	58.375	1134.375	122	0.1210	125	6.9	125	55.54	123	3.58	125	2.40	2.04	0.237
	49.000	1143.750	123	0.0775	125	4.4	125	24.15	124	2.69	126	1.77	1.52	0.234
	39.625	1153.125	124	0.0235	126	1.3	126	12.75	129	1.79	128	0.63	0.82	0.227
	30.250	1162.500	125	0.0139	132	0.8	132	11.46	129	1.59	129	0.12	0.22	0.223
	20.875	1171.875	126	0.0107	135	0.6	135	8.09	129	1.07	129	0.04	0.05	0.222
11.500	1181.250	127	0.0075	138	0.4	138	6.94	129	0.59	132	-	-	0.222	
5.750	1187.000	128	0.0053	136	0.3	136	6.93	129	0.42	134	-	-	0.222	

Table D-5. 18-ft 9-in. Long System – Missing Post Position 3

Impact Point			5-Node Maximum Slope		5-Node Maximum Pocket Angle		Maximum Force		Maximum Deflection		Snag - Tire (Deformed)	Snag - Rim (Deformed)	Heading Parallel Time	
US of Bridge Rail (in.)	(in.)	Node No.	(rad)	@ Node	(deg)	@ Node	(kips)	@ Node	(in.)	@ Node	(in.)	(in.)	(sec)	
W-to-Thrie Element	217.750	975.000	105	0.1665	114	9.5	114	119.41	109	10.11	112	-	-	0.204
	208.375	984.375	106	0.1729	115	9.8	115	117.13	109	9.79	112	-	-	0.204
	199.000	993.750	107	0.1675	115	9.5	115	112.74	113	9.07	114	-	-	0.205
	189.625	1003.125	108	0.1599	115	9.1	115	112.33	113	8.61	115	-	-	0.203
	180.250	1012.500	109	0.1563	115	8.9	115	104.42	113	8.46	115	-	-	0.207
	170.875	1021.875	110	0.1465	116	8.3	116	99.29	113	8.11	115	-	-	0.208
	161.500	1031.250	111	0.1215	116	6.9	116	84.69	113	7.54	116	-	-	0.208
	152.125	1040.625	112	0.1039	118	5.9	118	76.87	117	6.91	118	-	-	0.209
	142.750	1050.000	113	0.1103	121	6.3	121	71.24	119	6.43	119	-	-	0.208
Nested Thrie Beam	133.375	1059.375	114	0.1172	122	6.7	122	71.60	119	6.12	120	-	-	0.205
	124.000	1068.750	115	0.1270	123	7.2	123	87.26	121	6.08	122	0.44	-	0.202
	114.625	1078.125	116	0.1524	124	8.7	124	106.75	121	6.42	122	1.16	0.45	0.199
	105.250	1087.500	117	0.1547	125	8.8	125	116.30	121	6.44	123	1.68	0.78	0.200
	95.875	1096.875	118	0.1628	125	9.2	125	110.64	121	6.22	123	2.40	1.16	0.202
	86.500	1106.250	119	0.1623	125	9.2	125	98.60	121	5.49	124	2.56	1.61	0.206
	77.125	1115.625	120	0.1550	125	8.8	125	86.17	121	4.85	124	2.80	1.81	0.215
	67.750	1125.000	121	0.1286	125	7.3	125	59.14	121	3.99	124	2.62	1.98	0.227
	58.375	1134.375	122	0.0969	125	5.5	125	29.39	125	2.80	125	1.98	1.65	0.233
	49.000	1143.750	123	0.0603	126	3.5	126	13.83	125	2.12	126	1.46	1.30	0.231
	39.625	1153.125	124	0.0178	126	1.0	126	11.08	129	1.63	128	0.51	0.73	0.226
	30.250	1162.500	125	0.0139	135	0.8	135	10.49	129	1.46	129	0.11	0.21	0.222
	20.875	1171.875	126	0.0107	136	0.6	136	7.80	129	0.98	129	0.04	0.05	0.222
11.500	1181.250	127	0.0075	138	0.4	138	6.93	129	0.57	132	-	-	0.222	
5.750	1187.000	128	0.0053	136	0.3	136	6.93	129	0.42	134	-	-	0.222	

252

Table D-6. 18-ft 9-in. Long System – Missing Post Position 4

	Impact Point			5-Node Maximum Slope		5-Node Maximum Pocket Angle		Maximum Force		Maximum Deflection		Snag - Tire (Deformed)	Snag - Rim (Deformed)	Heading Parallel Time
	US of Bridge Rail (in.)	(in.)	Node No.	(rad)	@ Node	(deg)	@ Node	(kips)	@ Node	(in.)	@ Node	(in.)	(in.)	(sec)
W-to-Thrie Element	217.750	975.000	105	0.1632	114	9.3	114	118.97	110	10.16	112	-	-	0.204
	208.375	984.375	106	0.1691	115	9.6	115	116.50	109	9.85	112	-	-	0.205
	199.000	993.750	107	0.1618	115	9.2	115	109.87	113	9.14	114	-	-	0.206
	189.625	1003.125	108	0.1545	115	8.8	115	109.55	113	8.72	115	-	-	0.206
	180.250	1012.500	109	0.1474	115	8.4	115	104.92	113	8.61	115	-	-	0.209
	170.875	1021.875	110	0.1334	115	7.6	115	103.87	113	8.43	116	-	-	0.210
	161.500	1031.250	111	0.1292	120	7.4	120	88.63	113	7.83	116	-	-	0.207
	152.125	1040.625	112	0.1346	120	7.7	120	95.17	119	7.52	118	-	-	0.202
Nested Thrie Beam	142.750	1050.000	113	0.1436	121	8.2	121	101.03	119	7.52	120	-	-	0.202
	133.375	1059.375	114	0.1455	122	8.3	122	106.39	119	7.43	120	-	-	0.200
	124.000	1068.750	115	0.1444	122	8.2	122	112.62	119	7.23	121	-	-	0.202
	114.625	1078.125	116	0.1405	124	8.0	124	105.90	119	6.83	121	0.77	-	0.203
	105.250	1087.500	117	0.1565	125	8.9	125	98.55	119	6.28	122	1.46	0.65	0.201
	95.875	1096.875	118	0.1641	125	9.3	125	91.47	123	5.72	123	2.13	1.10	0.203
	86.500	1106.250	119	0.1637	125	9.3	125	76.95	123	5.26	124	2.42	1.44	0.206
	77.125	1115.625	120	0.1422	125	8.1	125	59.56	123	4.31	124	2.53	1.56	0.213
	67.750	1125.000	121	0.1087	125	6.2	125	40.93	123	3.17	125	2.23	1.68	0.223
	58.375	1134.375	122	0.0856	125	4.9	125	24.07	125	2.47	125	1.79	1.53	0.232
	49.000	1143.750	123	0.0562	126	3.2	126	12.13	125	1.95	126	1.35	1.24	0.230
	39.625	1153.125	124	0.0167	126	1.0	126	10.98	129	1.60	129	0.46	0.69	0.226
	30.250	1162.500	125	0.0139	132	0.8	132	10.36	129	1.43	129	0.10	0.20	0.222
	20.875	1171.875	126	0.0085	136	0.5	136	7.74	129	0.95	129	0.04	0.05	0.222
	11.500	1181.250	127	0.0075	138	0.4	138	6.94	129	0.56	132	-	-	0.222
5.750	1187.000	128	0.0053	136	0.3	136	6.93	129	0.42	134	-	-	0.222	

253

Table D-7. 18-ft 9-in. Long System – Missing Post Position 5

	Impact Point			5-Node Maximum Slope		5-Node Maximum Pocket Angle		Maximum Force		Maximum Deflection		Snag - Tire (Deformed)	Snag - Rim (Deformed)	Heading Parallel Time
	US of Bridge Rail (in.)	(in.)	Node No.	(rad)	@ Node	(deg)	@ Node	(kips)	@ Node	(in.)	@ Node	(in.)	(in.)	(sec)
W-to-Thrie Element	217.750	975.000	105	0.1489	113	8.5	113	115.88	109	10.28	112	-	-	0.208
	208.375	984.375	106	0.1474	114	8.4	114	114.36	109	10.02	112	-	-	0.208
	199.000	993.750	107	0.1442	115	8.2	115	112.42	113	9.59	114	-	-	0.208
	189.625	1003.125	108	0.1467	117	8.3	117	117.05	113	9.41	115	-	-	0.204
	180.250	1012.500	109	0.1573	118	8.9	118	119.48	113	9.36	116	-	-	0.201
	170.875	1021.875	110	0.1601	118	9.1	118	118.90	113	9.13	116	-	-	0.202
	161.500	1031.250	111	0.1619	119	9.2	119	115.11	117	8.76	118	-	-	0.203
	152.125	1040.625	112	0.1544	119	8.8	119	117.12	117	8.40	118	-	-	0.202
Nested Thrie Beam	142.750	1050.000	113	0.1522	120	8.7	120	113.85	117	8.15	119	-	-	0.206
	133.375	1059.375	114	0.1414	120	8.0	120	104.86	117	7.82	119	-	-	0.207
	124.000	1068.750	115	0.1344	122	7.7	122	91.72	117	7.23	120	-	-	0.205
	114.625	1078.125	116	0.1408	124	8.0	124	84.59	121	6.58	122	0.84	-	0.204
	105.250	1087.500	117	0.1560	125	8.9	125	84.66	123	6.05	122	1.58	0.77	0.201
	95.875	1096.875	118	0.1569	125	8.9	125	72.32	123	5.31	124	2.15	1.14	0.201
	86.500	1106.250	119	0.1497	125	8.5	125	68.41	123	4.57	124	2.32	1.36	0.204
	77.125	1115.625	120	0.1294	125	7.4	125	56.19	123	3.80	125	2.33	1.52	0.211
	67.750	1125.000	121	0.1049	125	6.0	125	41.07	123	3.08	125	2.16	1.62	0.222
	58.375	1134.375	122	0.0828	125	4.7	125	24.66	125	2.40	125	1.76	1.51	0.232
	49.000	1143.750	123	0.0533	126	3.1	126	12.01	125	1.93	126	1.32	1.22	0.230
	39.625	1153.125	124	0.0167	125	1.0	125	11.08	129	1.61	129	0.45	0.68	0.226
	30.250	1162.500	125	0.0139	134	0.8	134	10.53	129	1.44	129	0.10	0.20	0.222
	20.875	1171.875	126	0.0085	136	0.5	136	7.75	129	0.94	129	0.04	0.05	0.222
	11.500	1181.250	127	0.0075	138	0.4	138	6.95	129	0.56	132	-	-	0.222
5.750	1187.000	128	0.0053	136	0.3	136	6.93	129	0.42	134	-	-	0.222	

254

Table D-8. 18-ft 9-in. Long System – Missing Post Position 6

Impact Point			5-Node Maximum Slope		5-Node Maximum Pocket Angle		Maximum Force		Maximum Deflection		Snag - Tire (Deformed)	Snag - Rim (Deformed)	Heading Parallel Time	
US of Bridge Rail (in.)	(in.)	Node No.	(rad)	@ Node	(deg)	@ Node	(kips)	@ Node	(in.)	@ Node	(in.)	(in.)	(sec)	
W-to-Thrie Element	217.750	975.000	105	0.1687	115	9.6	115	119.61	113	10.53	112	-	-	0.209
	208.375	984.375	106	0.1758	115	10.0	115	126.64	113	10.38	112	-	-	0.204
	199.000	993.750	107	0.1785	116	10.1	116	131.57	113	10.15	115	-	-	0.202
	189.625	1003.125	108	0.1756	117	10.0	117	138.10	113	9.86	115	-	-	0.202
	180.250	1012.500	109	0.1777	117	10.1	117	139.35	113	9.92	116	-	-	0.202
	170.875	1021.875	110	0.1724	117	9.8	117	136.52	114	9.61	116	-	-	0.205
	161.500	1031.250	111	0.1676	117	9.5	117	128.05	114	9.20	117	-	-	0.208
	152.125	1040.625	112	0.1509	117	8.6	117	114.76	113	8.60	117	-	-	0.209
	142.750	1050.000	113	0.1364	120	7.8	120	103.18	113	8.17	118	-	-	0.208
Nested Thrie Beam	133.375	1059.375	114	0.1322	121	7.5	121	91.24	119	7.64	118	-	-	0.209
	124.000	1068.750	115	0.1344	122	7.7	122	79.26	121	6.97	120	-	-	0.205
	114.625	1078.125	116	0.1357	124	7.7	124	67.66	121	6.10	122	0.81	-	0.203
	105.250	1087.500	117	0.1379	125	7.9	125	67.47	123	5.17	123	1.22	0.50	0.202
	95.875	1096.875	118	0.1450	125	8.3	125	69.59	123	4.85	124	1.81	0.94	0.201
	86.500	1106.250	119	0.1425	125	8.1	125	68.04	123	4.44	124	2.23	1.28	0.203
	77.125	1115.625	120	0.1257	125	7.2	125	56.24	123	3.74	125	2.28	1.47	0.210
	67.750	1125.000	121	0.1049	125	6.0	125	41.22	123	3.05	125	2.22	1.60	0.222
	58.375	1134.375	122	0.0828	125	4.7	125	24.91	125	2.39	125	1.76	1.50	0.231
	49.000	1143.750	123	0.0533	126	3.1	126	12.26	125	1.93	126	1.32	1.22	0.230
	39.625	1153.125	124	0.0149	126	0.9	126	11.11	129	1.61	129	0.44	0.68	0.226
	30.250	1162.500	125	0.0139	132	0.8	132	10.47	129	1.43	129	0.10	0.20	0.222
	20.875	1171.875	126	0.0085	136	0.5	136	7.76	129	0.94	129	0.04	0.05	0.222
11.500	1181.250	127	0.0075	138	0.4	138	6.95	129	0.56	132	-	-	0.222	
5.750	1187.000	128	0.0053	136	0.3	136	6.93	129	0.42	134	-	-	0.222	

255

Table D-9. 18-ft 9-in. Long System – 3-in. Improper Post Exposure

Impact Point			5-Node Maximum Slope		5-Node Maximum Pocket Angle		Maximum Force		Maximum Deflection		Snag - Tire (Deformed)	Snag - Rim (Deformed)	Heading Parallel Time	
US of Bridge Rail (in.)	(in.)	Node No.	(rad)	@ Node	(deg)	@ Node	(kips)	@ Node	(in.)	@ Node	(in.)	(in.)	(sec)	
W40-Thrie Element	217.750	975.000	105	0.1632	114	9.3	114	118.81	109	10.18	112	-	-	0.205
	208.375	984.375	106	0.1697	115	9.6	115	118.40	109	9.97	112	-	-	0.205
	199.000	993.750	107	0.1677	115	9.5	115	114.70	113	9.44	114	-	-	0.205
	189.625	1003.125	108	0.1575	115	9.0	115	117.57	113	9.07	115	-	-	0.203
	180.250	1012.500	109	0.1599	116	9.1	116	118.00	113	9.05	115	-	-	0.207
	170.875	1021.875	110	0.1521	116	8.6	116	113.81	114	8.75	116	-	-	0.206
	161.500	1031.250	111	0.1433	118	8.2	118	103.79	113	8.33	117	-	-	0.206
	152.125	1040.625	112	0.1365	119	7.8	119	97.17	117	7.89	118	-	-	0.206
	142.750	1050.000	113	0.1346	120	7.7	120	93.68	119	7.53	119	-	-	0.205
	133.375	1059.375	114	0.1324	121	7.5	121	86.57	119	7.25	120	-	-	0.204
Nested Thrie Beam	124.000	1068.750	115	0.1301	123	7.4	123	81.51	121	6.55	121	0.07	-	0.203
	114.625	1078.125	116	0.1454	124	8.3	124	87.13	121	6.19	122	1.06	0.04	0.201
	105.250	1087.500	117	0.1611	125	9.2	125	94.47	123	6.01	123	1.72	0.85	0.200
	95.875	1096.875	118	0.1686	125	9.6	125	91.89	123	5.73	124	2.32	1.26	0.201
	86.500	1106.250	119	0.1673	125	9.5	125	84.73	123	5.29	124	2.57	1.61	0.204
	77.125	1115.625	120	0.1489	125	8.5	125	71.74	123	4.44	125	2.63	1.63	0.213
	67.750	1125.000	121	0.1190	125	6.8	125	50.50	123	3.54	125	2.54	1.84	0.225
	58.375	1134.375	122	0.0899	125	5.1	125	28.64	125	2.63	125	1.94	1.66	0.233
	49.000	1143.750	123	0.0562	126	3.2	126	13.57	125	2.08	126	1.41	1.29	0.230
	39.625	1153.125	124	0.0167	126	1.0	126	11.71	129	1.66	129	0.47	0.71	0.226
	30.250	1162.500	125	0.0139	132	0.8	132	10.73	129	1.49	129	0.10	0.20	0.222
	20.875	1171.875	126	0.0085	136	0.5	136	7.81	129	0.99	129	0.40	0.50	0.222
	11.500	1181.250	127	0.0075	138	0.4	138	6.92	129	0.57	132	-	-	0.222
	5.750	1187.000	128	0.0053	136	0.3	136	6.93	129	0.40	134	-	-	0.222

256

Table D-10. 18-ft 9-in. Long System – 4-in. Improper Post Exposure

Impact Point			5-Node Maximum Slope		5-Node Maximum Pocket Angle		Maximum Force		Maximum Deflection		Snag - Tire (Deformed)	Snag - Rim (Deformed)	Heading Parallel Time	
US of Bridge Rail (in.)	(in.)	Node No.	(rad)	@ Node	(deg)	@ Node	(kips)	@ Node	(in.)	@ Node	(in.)	(in.)	(sec)	
W40-Thrie Element	217.750	975.000	105	0.1611	114	9.2	114	119.62	109	10.29	112	-	-	0.206
	208.375	984.375	106	0.1664	115	9.4	115	118.23	109	10.01	112	-	-	0.205
	199.000	993.750	107	0.1642	115	9.3	115	115.01	113	9.52	114	-	-	0.205
	189.625	1003.125	108	0.1575	115	9.0	115	119.47	113	9.27	115	-	-	0.204
	180.250	1012.500	109	0.1599	116	9.1	116	120.19	113	9.15	115	-	-	0.207
	170.875	1021.875	110	0.1500	116	8.5	116	117.53	114	8.96	116	-	-	0.206
	161.500	1031.250	111	0.1455	118	8.3	118	108.04	113	8.59	117	-	-	0.207
	152.125	1040.625	112	0.1376	119	7.8	119	102.72	117	8.23	118	-	-	0.206
	142.750	1050.000	113	0.1379	120	7.9	120	101.74	119	7.93	119	-	-	0.206
	133.375	1059.375	114	0.1401	122	8.0	122	96.70	119	7.71	120	-	-	0.204
Nested Thrie Beam	124.000	1068.750	115	0.1421	123	8.1	123	94.32	121	7.11	121	0.60	-	0.204
	114.625	1078.125	116	0.1559	124	8.9	124	96.66	121	6.69	122	1.36	0.41	0.201
	105.250	1087.500	117	0.1693	125	9.6	125	102.32	123	6.41	123	1.92	0.98	0.200
	95.875	1096.875	118	0.1751	125	9.9	125	98.51	123	6.03	124	2.47	1.38	0.201
	86.500	1106.250	119	0.1744	125	9.9	125	89.89	123	5.59	124	2.72	1.59	0.205
	77.125	1115.625	120	0.1562	125	8.9	125	76.40	123	4.66	124	2.76	1.77	0.215
	67.750	1125.000	121	0.1286	125	7.3	125	54.72	123	3.78	125	2.69	1.96	0.226
	58.375	1134.375	122	0.0950	125	5.4	125	30.79	125	2.75	125	2.03	1.73	0.233
	49.000	1143.750	123	0.0602	126	3.4	126	14.33	125	2.13	126	1.45	1.32	0.231
	39.625	1153.125	124	0.0167	126	1.0	126	11.98	129	1.68	128	0.49	0.72	0.226
	30.250	1162.500	125	0.0139	132	0.8	132	10.79	129	1.50	129	0.10	0.20	0.223
	20.875	1171.875	126	0.0107	136	0.6	136	7.84	129	1.00	129	0.40	0.50	0.222
	11.500	1181.250	127	0.0075	138	0.4	138	6.92	129	0.57	132	-	-	0.222
	5.750	1187.000	128	0.0053	136	0.3	136	6.93	129	0.40	134	-	-	0.222

257

Table D-11. 18-ft 9-in. Long System – Break Point of a 2H:1V Fill Slope

	Impact Point			5-Node Maximum Slope		5-Node Maximum Pocket Angle		Maximum Force		Maximum Deflection		Snag - Tire (Deformed)	Snag - Rim (Deformed)	Heading Parallel Time
	US of Bridge Rail (in.)	(in.)	Node No.	(rad)	@ Node	(deg)	@ Node	(kips)	@ Node	(in.)	@ Node	(in.)	(in.)	(sec)
W-to-Thrie Element	217.750	975.000	105	0.1444	110	8.2	110	114.35	109	10.35	112	-	-	0.214
	208.375	984.375	106	0.1466	115	8.3	115	116.49	109	10.21	112	-	-	0.213
	199.000	993.750	107	0.1435	115	8.2	115	117.42	113	10.14	115	-	-	0.211
	189.625	1003.125	108	0.1423	116	8.1	116	127.03	113	10.20	116	-	-	0.210
	180.250	1012.500	109	0.1519	117	8.6	117	138.30	114	10.69	116	-	-	0.210
	170.875	1021.875	110	0.1530	119	8.7	119	141.73	117	10.93	117	-	-	0.210
	161.500	1031.250	111	0.1585	120	9.0	120	149.05	119	10.86	118	-	-	0.209
	152.125	1040.625	112	0.1673	121	9.5	121	154.19	119	10.59	119	-	-	0.207
Nested Thrie Beam	142.750	1050.000	113	0.1800	123	10.2	123	156.80	119	10.54	119	1.04	-	0.205
	133.375	1059.375	114	0.2005	124	11.3	124	160.47	121	10.55	120	2.23	0.70	0.205
	124.000	1068.750	115	0.2240	125	12.6	125	163.86	121	10.38	120	3.01	1.57	0.203
	114.625	1078.125	116	0.2356	125	13.3	125	161.12	123	10.00	121	3.88	2.30	0.204
	105.250	1087.500	117	0.2393	125	13.5	125	151.88	123	9.60	122	4.46	2.84	0.205
	95.875	1096.875	118	0.2400	125	13.5	125	141.07	123	8.73	123	4.61	3.45	0.209
	86.500	1106.250	119	0.2292	125	12.9	125	132.17	123	7.87	123	4.58	3.42	0.216
	77.125	1115.625	120	0.2174	125	12.3	125	112.66	123	7.02	124	4.21	3.17	0.227
	67.750	1125.000	121	0.1876	125	10.6	125	95.15	125	5.66	125	3.91	3.07	0.238
	58.375	1134.375	122	0.1335	125	7.6	125	58.20	125	4.33	126	3.08	2.57	0.240
	49.000	1143.750	123	0.0672	126	3.8	126	19.83	125	2.76	126	1.67	1.55	0.233
	39.625	1153.125	124	0.0167	126	1.0	126	12.26	129	1.72	128	0.48	0.72	0.227
	30.250	1162.500	125	0.0139	132	0.8	132	10.69	129	1.50	129	0.10	0.20	0.223
	20.875	1171.875	126	0.0107	136	0.6	136	7.78	129	0.99	129	0.04	0.05	0.222
	11.500	1181.250	127	0.0075	138	0.4	138	6.90	129	0.57	132	-	-	0.222
5.750	1187.000	128	0.0053	136	0.3	136	6.90	129	0.40	134	-	-	0.222	

Table D-12. 31-ft 3-in. Long System – Baseline

	Impact Point			5-Node Maximum Slope		5-Node Maximum Pocket Angle		Maximum Force		Maximum Deflection		Snag - Tire (Deformed)	Snag - Rim (Deformed)	Heading Parallel Time
	US of Bridge Rail (in.)	(in.)	Node No.	(rad)	@ Node	(deg)	@ Node	(kips)	@ Node	(in.)	@ Node	(in.)	(in.)	(sec)
W-to-Thrie Element	367.750	825.000	89	0.2505	101	14.1	101	111.69	97	15.25	99	-	-	0.221
	358.375	834.375	90	0.2567	101	14.4	101	113.95	97	15.27	100	-	-	0.220
	349.000	843.750	91	0.2599	101	14.6	101	113.94	97	15.66	100	-	-	0.218
	339.625	853.125	92	0.2587	101	14.5	101	120.25	97	15.76	101	-	-	0.216
	330.250	862.500	93	0.2463	103	13.8	103	118.40	98	15.50	102	-	-	0.215
	320.875	871.875	94	0.2387	104	13.4	104	119.48	99	15.08	102	-	-	0.214
	311.500	881.250	95	0.2242	105	12.6	105	119.33	100	14.41	103	-	-	0.215
	302.125	890.625	96	0.2012	106	11.4	106	119.24	99	13.25	103	-	-	0.213
	292.750	900.000	97	0.1943	106	11.0	106	118.88	100	12.74	104	-	-	0.213
Single Thrie Beam	283.375	909.375	98	0.1911	106	10.8	106	125.07	105	12.16	106	-	-	0.215
	274.000	918.750	99	0.2022	109	11.4	109	131.97	105	12.37	107	-	-	0.214
	264.625	928.125	100	0.1931	109	10.9	109	129.21	105	12.14	107	-	-	0.212
	255.250	937.500	101	0.1888	109	10.7	109	120.60	105	11.73	108	-	-	0.212
	245.875	946.875	102	0.1845	110	10.5	110	119.10	109	11.09	110	-	-	0.212
	236.500	956.250	103	0.1742	110	9.9	110	122.14	109	10.57	111	-	-	0.211
	227.125	965.625	104	0.1544	110	8.8	110	127.88	109	9.91	111	-	-	0.209
	217.750	975.000	105	0.1489	111	8.5	111	121.86	109	10.09	112	-	-	0.208
	208.375	984.375	106	0.1474	114	8.4	114	117.74	109	9.95	112	-	-	0.208
	199.000	993.750	107	0.1431	116	8.1	116	116.85	113	9.49	114	-	-	0.208
	189.625	1003.125	108	0.1413	117	8.0	117	119.43	113	9.20	115	-	-	0.204
	180.250	1012.500	109	0.1551	118	8.8	118	120.86	113	9.35	116	-	-	0.201
	170.875	1021.875	110	0.1573	118	8.9	118	122.05	114	9.11	116	-	-	0.202
	161.500	1031.250	111	0.1597	119	9.1	119	117.88	117	8.66	117	-	-	0.203
	152.125	1040.625	112	0.1511	119	8.6	119	120.99	117	8.29	118	-	-	0.202
	142.750	1050.000	113	0.1520	119	8.6	119	118.14	117	8.14	118	-	-	0.205
	133.375	1059.375	114	0.1411	120	8.0	120	108.88	117	7.75	119	-	-	0.207
124.000	1068.750	115	0.1344	122	7.7	122	95.08	117	7.18	120	-	-	0.205	
114.625	1078.125	116	0.1408	124	8.0	124	86.14	121	6.56	122	0.82	-	0.204	
105.250	1087.500	117	0.1547	125	8.8	125	85.65	123	6.01	122	1.56	0.77	0.201	
95.875	1096.875	118	0.1569	125	8.9	125	73.51	123	5.31	124	2.12	1.23	0.201	
86.500	1106.250	119	0.1468	125	8.4	125	69.96	123	4.55	124	2.31	1.35	0.204	
77.125	1115.625	120	0.1294	125	7.4	125	57.91	123	3.78	125	2.32	1.51	0.211	
67.750	1125.000	121	0.1049	125	6.0	125	42.32	123	3.07	125	2.15	1.61	0.222	
58.375	1134.375	122	0.0828	125	4.7	125	25.47	125	2.39	125	1.76	1.51	0.232	
49.000	1143.750	123	0.0533	126	3.1	126	12.58	125	1.93	126	1.32	1.22	0.230	
39.625	1153.125	124	0.0167	125	1.0	125	11.14	129	1.61	129	0.44	0.68	0.226	
30.250	1162.500	125	0.0139	134	0.8	134	10.63	129	1.44	129	0.10	0.20	0.222	
20.875	1171.875	126	0.0085	136	0.5	136	7.79	129	0.94	129	0.04	0.05	0.222	
11.500	1181.250	127	0.0075	138	0.4	138	6.98	129	0.56	132	-	-	0.222	
5.750	1187.000	128	0.0053	136	0.3	136	6.99	129	0.40	134	-	-	0.222	

Table D-13. 31-ft 3-in. Long System – Missing Post Position 1

	Impact Point			5-Node Maximum Slope		5-Node Maximum Pocket Angle		Maximum Force		Maximum Deflection		Snag - Tire (Deformed)	Snag - Rim (Deformed)	Heading Parallel Time
	US of Bridge Rail (in.)	(in.)	Node No.	(rad)	@ Node	(deg)	@ Node	(kips)	@ Node	(in.)	@ Node	(in.)	(in.)	(sec)
W-to-Thrie Element	367.750	825.000	89	0.2483	101	13.9	101	111.62	97	15.24	99	-	-	0.221
	358.375	834.375	90	0.2567	101	14.4	101	113.92	97	15.27	100	-	-	0.220
	349.000	843.750	91	0.2599	101	14.6	101	114.03	97	15.66	100	-	-	0.218
	339.625	853.125	92	0.2587	101	14.5	101	120.20	97	15.76	101	-	-	0.216
	330.250	862.500	93	0.2463	103	13.8	103	118.40	98	15.50	102	-	-	0.215
	320.875	871.875	94	0.2387	104	13.4	104	119.47	99	15.08	102	-	-	0.214
	311.500	881.250	95	0.2242	105	12.6	105	119.33	100	14.41	103	-	-	0.215
	302.125	890.625	96	0.2012	106	11.4	106	119.26	99	13.25	103	-	-	0.213
	292.750	900.000	97	0.1943	106	11.0	106	118.86	100	12.74	104	-	-	0.213
Single Thrie Beam	283.375	909.375	98	0.1911	106	10.8	106	125.00	105	12.17	106	-	-	0.215
	274.000	918.750	99	0.2022	109	11.4	109	132.02	105	12.37	107	-	-	0.214
	264.625	928.125	100	0.1931	109	10.9	109	129.20	105	12.14	107	-	-	0.212
	255.250	937.500	101	0.1888	109	10.7	109	120.63	105	11.73	108	-	-	0.212
	245.875	946.875	102	0.1845	110	10.5	110	119.03	109	11.09	110	-	-	0.212
	236.500	956.250	103	0.1742	110	9.9	110	122.11	109	10.57	111	-	-	0.211
	227.125	965.625	104	0.1544	110	8.8	110	127.81	109	9.91	111	-	-	0.209
	217.750	975.000	105	0.1489	111	8.5	111	121.82	109	10.09	112	-	-	0.208
	208.375	984.375	106	0.1467	115	8.3	115	116.93	109	9.92	112	-	-	0.208
	199.000	993.750	107	0.1431	116	8.1	116	116.80	113	9.49	114	-	-	0.208
	189.625	1003.125	108	0.1413	117	8.0	117	119.34	113	9.20	115	-	-	0.204
	180.250	1012.500	109	0.1551	118	8.8	118	120.96	113	9.36	116	-	-	0.201
	170.875	1021.875	110	0.1573	118	8.9	118	122.00	114	9.11	116	-	-	0.203
	161.500	1031.250	111	0.1587	119	9.0	119	117.69	117	8.66	117	-	-	0.204
	152.125	1040.625	112	0.1511	119	8.6	119	120.93	117	8.29	118	-	-	0.202
	Nested Thrie Beam	142.750	1050.000	113	0.1520	119	8.6	119	118.24	117	8.14	118	-	-
133.375		1059.375	114	0.1403	120	8.0	120	108.96	117	7.76	119	-	-	0.207
124.000		1068.750	115	0.1331	122	7.6	122	94.75	117	7.20	120	-	-	0.205
114.625		1078.125	116	0.1416	124	8.1	124	87.43	121	6.64	122	1.20	0.03	0.205
105.250		1087.500	117	0.1657	125	9.4	125	91.28	123	6.10	123	1.98	1.10	0.202
95.875		1096.875	118	0.1702	125	9.7	125	88.75	123	5.56	124	2.74	1.65	0.201
86.500		1106.250	119	0.1631	125	9.3	125	88.00	125	4.88	124	3.06	2.09	0.204
77.125		1115.625	120	0.1483	125	8.4	125	75.59	125	4.29	125	3.25	2.30	0.215
67.750		1125.000	121	0.1211	126	6.9	126	61.24	125	3.67	126	2.99	2.36	0.228
58.375		1134.375	122	0.0931	126	5.3	126	39.16	125	3.03	126	2.33	2.10	0.236
49.000		1143.750	123	0.0643	126	3.7	126	22.84	125	2.61	126	1.65	1.62	0.233
39.625		1153.125	124	0.0181	130	1.0	130	18.11	129	2.11	128	0.54	0.83	0.227
30.250		1162.500	125	0.0160	132	0.9	132	14.07	129	1.84	129	0.11	0.22	0.224
20.875		1171.875	126	0.0107	136	0.6	136	8.84	129	1.24	129	0.04	0.05	0.222
11.500		1181.250	127	0.0075	139	0.4	139	6.99	129	0.65	129	-	-	0.222
5.750		1187.000	128	0.0053	136	0.3	136	6.91	129	0.42	134	-	-	0.222

Table D-14. 31-ft 3-in. Long System – Retrofitted Post Position 1 (W6x12)

	Impact Point			Maximum Slope		Maximum Pocket Angle		Maximum Force		Maximum Deflection		Snag - Tire (Deformed)	Snag - Rim (Deformed)	Heading Parallel Time	
	US of Bridge Rail (in.)	(in.)	Node No.	(rad)	@ Node	(deg)	@ Node	(kips)	@ Node	(in.)	@ Node	(in.)	(in.)	(sec)	
W-to-Thrie Element	367.750	825.000	89	0.2505	101	14.1	101	111.69	97	15.25	99	-	-	0.221	
	358.375	834.375	90	0.2567	101	14.4	101	113.94	97	15.27	100	-	-	0.220	
	349.000	843.750	91	0.2599	101	14.6	101	113.94	97	15.66	100	-	-	0.218	
	339.625	853.125	92	0.2587	101	14.5	101	120.24	97	15.76	101	-	-	0.216	
	330.250	862.500	93	0.2463	103	13.8	103	118.40	98	15.50	102	-	-	0.215	
	320.875	871.875	94	0.2387	104	13.4	104	119.48	99	15.08	102	-	-	0.214	
	311.500	881.250	95	0.2242	105	12.6	105	119.33	100	14.41	103	-	-	0.215	
	302.125	890.625	96	0.2012	106	11.4	106	119.24	99	13.25	103	-	-	0.213	
	292.750	900.000	97	0.1943	106	11.0	106	118.88	100	12.74	104	-	-	0.213	
Single Thrie Beam	283.375	909.375	98	0.1911	106	10.8	106	125.07	105	12.16	106	-	-	0.215	
	274.000	918.750	99	0.2022	109	11.4	109	131.97	105	12.37	107	-	-	0.214	
	264.625	928.125	100	0.1931	109	10.9	109	129.21	105	12.14	107	-	-	0.212	
	255.250	937.500	101	0.1888	109	10.7	109	120.60	105	11.73	108	-	-	0.212	
	245.875	946.875	102	0.1845	110	10.5	110	119.10	109	11.09	110	-	-	0.212	
	236.500	956.250	103	0.1742	110	9.9	110	122.14	109	10.57	111	-	-	0.211	
	227.125	965.625	104	0.1544	110	8.8	110	127.88	109	9.91	111	-	-	0.209	
	217.750	975.000	105	0.1489	111	8.5	111	121.82	109	10.09	112	-	-	0.208	
	208.375	984.375	106	0.1467	115	8.3	115	116.93	109	9.92	112	-	-	0.208	
	199.000	993.750	107	0.1431	116	8.1	116	116.85	113	9.49	114	-	-	0.208	
	189.625	1003.125	108	0.1413	117	8.0	117	119.42	113	9.20	115	-	-	0.204	
	180.250	1012.500	109	0.1551	118	8.8	118	120.84	113	9.35	116	-	-	0.201	
	170.875	1021.875	110	0.1573	118	8.9	118	122.07	114	9.11	116	-	-	0.202	
	161.500	1031.250	111	0.1597	119	9.1	119	118.51	117	8.68	117	-	-	0.203	
	152.125	1040.625	112	0.1511	119	8.6	119	121.02	117	8.29	118	-	-	0.202	
	Nested Thrie Beam	142.750	1050.000	113	0.1520	119	8.6	119	118.18	117	8.14	118	-	-	0.205
		133.375	1059.375	114	0.1411	120	8.0	120	108.96	117	7.75	119	-	-	0.207
124.000		1068.750	115	0.1365	122	7.8	122	95.29	117	7.17	120	-	-	0.204	
114.625		1078.125	116	0.1408	124	8.0	124	85.79	121	6.55	122	0.78	-	0.204	
105.250		1087.500	117	0.1551	125	8.8	125	86.08	123	5.98	122	1.58	0.77	0.202	
95.875		1096.875	118	0.1606	125	9.1	125	75.29	123	5.28	124	2.26	1.23	0.201	
86.500		1106.250	119	0.1480	125	8.4	125	72.16	123	4.51	124	2.47	1.49	0.203	
77.125		1115.625	120	0.1294	125	7.4	125	58.94	123	3.79	125	2.49	1.69	0.211	
67.750		1125.000	121	0.1041	125	5.9	125	42.05	123	3.05	125	2.30	1.72	0.223	
58.375		1134.375	122	0.0815	125	4.7	125	24.35	125	2.35	125	1.72	1.49	0.232	
49.000		1143.750	123	0.0522	126	3.0	126	12.03	125	1.88	126	1.27	1.17	0.230	
39.625		1153.125	124	0.0167	125	1.0	125	10.16	129	1.54	129	0.43	0.66	0.226	
30.250		1162.500	125	0.0107	134	0.6	134	10.17	129	1.37	129	0.10	0.20	0.222	
20.875		1171.875	126	0.0075	136	0.4	136	7.67	129	0.89	129	0.04	0.05	0.222	
11.500		1181.250	127	0.0053	142	0.3	142	6.96	129	0.55	132	-	-	0.222	
5.750	1187.000	128	0.0053	139	0.3	139	6.99	129	0.40	134	-	-	0.222		

Table D-15. 31-ft 3-in. Long System – Missing Post Position 2

	Impact Point			5-Node Maximum Slope		5-Node Maximum Pocket Angle		Maximum Force		Maximum Deflection		Snag - Tire (Deformed)	Snag - Rim (Deformed)	Heading Parallel Time
	US of Bridge Rail (in.)	(in.)	Node No.	(rad)	@ Node	(deg)	@ Node	(kips)	@ Node	(in.)	@ Node	(in.)	(in.)	(sec)
W-to-Thrie Element	367.750	825.000	89	0.2483	101	13.9	101	110.04	97	15.13	99	-	-	0.221
	358.375	834.375	90	0.2567	101	14.4	101	114.00	97	15.27	100	-	-	0.220
	349.000	843.750	91	0.2599	101	14.6	101	113.99	97	15.66	100	-	-	0.218
	339.625	853.125	92	0.2587	101	14.5	101	120.20	97	15.76	101	-	-	0.216
	330.250	862.500	93	0.2463	103	13.8	103	118.38	98	15.50	102	-	-	0.215
	320.875	871.875	94	0.2387	104	13.4	104	119.48	99	15.08	102	-	-	0.214
	311.500	881.250	95	0.2242	105	12.6	105	119.37	100	14.42	103	-	-	0.215
	302.125	890.625	96	0.2012	106	11.4	106	119.26	99	13.25	103	-	-	0.213
	292.750	900.000	97	0.1943	106	11.0	106	118.85	100	12.74	104	-	-	0.213
Single Thrie Beam	283.375	909.375	98	0.1911	106	10.8	106	124.98	105	12.17	106	-	-	0.215
	274.000	918.750	99	0.2022	109	11.4	109	131.14	105	12.30	107	-	-	0.214
	264.625	928.125	100	0.1931	109	10.9	109	129.18	105	12.14	107	-	-	0.212
	255.250	937.500	101	0.1888	109	10.7	109	120.65	105	11.73	108	-	-	0.212
	245.875	946.875	102	0.1845	110	10.5	110	119.05	109	11.09	110	-	-	0.212
	236.500	956.250	103	0.1742	110	9.9	110	122.00	109	10.56	110	-	-	0.211
	227.125	965.625	104	0.1544	110	8.8	110	127.80	109	9.91	111	-	-	0.209
	217.750	975.000	105	0.1489	111	8.5	111	121.55	109	10.09	112	-	-	0.208
	208.375	984.375	106	0.1463	114	8.3	114	116.88	109	9.92	112	-	-	0.208
	199.000	993.750	107	0.1420	116	8.1	116	116.64	113	9.49	114	-	-	0.208
	189.625	1003.125	108	0.1434	117	8.2	117	119.53	113	9.24	115	-	-	0.204
	180.250	1012.500	109	0.1540	118	8.8	118	120.18	113	9.37	116	-	-	0.202
	170.875	1021.875	110	0.1541	118	8.8	118	121.15	113	9.13	116	-	-	0.203
	161.500	1031.250	111	0.1541	118	8.8	118	116.96	117	8.75	118	-	-	0.205
	152.125	1040.625	112	0.1451	119	8.3	119	119.97	117	8.39	118	-	-	0.203
	142.750	1050.000	113	0.1440	119	8.2	119	120.66	117	8.26	119	-	-	0.208
	133.375	1059.375	114	0.1301	120	7.4	120	113.16	117	8.04	119	-	-	0.210
Nested Thrie Beam	124.000	1068.750	115	0.1551	125	8.8	125	101.06	121	7.52	120	1.40	0.21	0.205
	114.625	1078.125	116	0.1864	125	10.6	125	115.59	123	7.17	122	2.03	1.08	0.200
	105.250	1087.500	117	0.2018	125	11.4	125	122.77	123	6.96	123	2.60	1.44	0.199
	95.875	1096.875	118	0.2036	125	11.5	125	121.88	123	6.76	124	3.06	1.67	0.201
	86.500	1106.250	119	0.1940	125	11.0	125	115.11	123	6.13	124	3.09	1.93	0.206
	77.125	1115.625	120	0.1797	125	10.2	125	99.16	123	5.28	125	3.07	2.07	0.217
	67.750	1125.000	121	0.1550	125	8.8	125	80.49	123	4.61	125	2.99	2.27	0.230
	58.375	1134.375	122	0.1206	125	6.9	125	53.85	123	3.63	125	2.43	2.06	0.238
	49.000	1143.750	123	0.0775	125	4.4	125	23.71	124	2.69	126	1.78	1.53	0.234
	39.625	1153.125	124	0.0235	126	1.3	126	12.64	129	1.80	128	0.63	0.82	0.227
	30.250	1162.500	125	0.0139	132	0.8	132	11.32	129	1.59	129	0.12	0.22	0.223
	20.875	1171.875	126	0.0107	136	0.6	136	8.05	129	1.08	129	0.04	0.05	0.222
	11.500	1181.250	127	0.0075	138	0.4	138	6.92	129	0.59	132	-	-	0.222
	5.750	1187.000	128	0.0053	136	0.3	136	6.99	129	0.40	134	-	-	0.222

Table D-16. 31-ft 3-in. Long System – Missing Post Position 3

	Impact Point			5-Node Maximum Slope		5-Node Maximum Pocket Angle		Maximum Force		Maximum Deflection		Snag - Tire (Deformed)	Snag - Rim (Deformed)	Heading Parallel Time
	US of Bridge Rail (in.)	(in.)	Node No.	(rad)	@ Node	(deg)	@ Node	(kips)	@ Node	(in.)	@ Node	(in.)	(in.)	(sec)
W-to-Thrie Element	367.750	825.000	89	0.2505	101	14.1	101	111.62	97	15.25	99	-	-	0.221
	358.375	834.375	90	0.2567	101	14.4	101	114.05	97	15.27	100	-	-	0.220
	349.000	843.750	91	0.2599	101	14.6	101	114.10	97	15.66	100	-	-	0.218
	339.625	853.125	92	0.2587	101	14.5	101	120.21	97	15.76	101	-	-	0.216
	330.250	862.500	93	0.2463	103	13.8	103	118.36	98	15.50	102	-	-	0.215
	320.875	871.875	94	0.2387	104	13.4	104	119.51	99	15.08	102	-	-	0.215
	311.500	881.250	95	0.2242	105	12.6	105	120.06	100	14.45	103	-	-	0.215
Single Thrie Beam	302.125	890.625	96	0.2012	106	11.4	106	119.24	99	13.25	103	-	-	0.213
	292.750	900.000	97	0.1943	106	11.0	106	118.85	100	12.74	104	-	-	0.213
	283.375	909.375	98	0.1930	107	10.9	107	124.98	105	12.18	106	-	-	0.215
	274.000	918.750	99	0.2022	109	11.4	109	131.19	105	12.31	107	-	-	0.214
	264.625	928.125	100	0.1953	109	11.1	109	129.54	105	12.21	108	-	-	0.212
	255.250	937.500	101	0.1888	109	10.7	109	121.42	105	11.84	108	-	-	0.212
	245.875	946.875	102	0.1846	110	10.5	110	119.14	109	11.10	110	-	-	0.212
	236.500	956.250	103	0.1742	110	9.9	110	121.87	109	10.57	111	-	-	0.211
	227.125	965.625	104	0.1544	110	8.8	110	127.48	109	9.92	111	-	-	0.209
	217.750	975.000	105	0.1489	111	8.5	111	120.94	109	10.09	112	-	-	0.208
	208.375	984.375	106	0.1442	114	8.2	114	118.16	109	10.02	112	-	-	0.208
	199.000	993.750	107	0.1392	115	7.9	115	115.01	113	9.50	114	-	-	0.208
	189.625	1003.125	108	0.1357	117	7.7	117	118.14	113	9.27	115	-	-	0.206
	180.250	1012.500	109	0.1389	117	7.9	117	117.60	113	9.50	116	-	-	0.204
	170.875	1021.875	110	0.1411	118	8.0	118	119.95	114	9.29	116	-	-	0.205
	161.500	1031.250	111	0.1356	119	7.7	119	118.77	117	9.18	118	-	-	0.206
	152.125	1040.625	112	0.1411	121	8.0	121	127.64	117	8.91	119	-	-	0.204
Nested Thrie Beam	142.750	1050.000	113	0.1520	122	8.6	122	130.09	117	8.83	119	-	-	0.201
	133.375	1059.375	114	0.1597	123	9.1	123	121.03	117	8.53	120	-	-	0.202
	124.000	1068.750	115	0.1719	124	9.8	124	129.03	121	8.36	120	1.20	-	0.202
	114.625	1078.125	116	0.1808	124	10.2	124	131.01	121	8.15	122	1.64	0.70	0.201
	105.250	1087.500	117	0.1811	125	10.3	125	125.74	121	7.63	122	2.20	1.09	0.202
	95.875	1096.875	118	0.1855	125	10.5	125	114.68	121	7.07	123	2.79	1.41	0.205
	86.500	1106.250	119	0.1797	125	10.2	125	98.84	121	6.20	123	2.89	1.73	0.208
	77.125	1115.625	120	0.1628	125	9.2	125	83.29	121	5.14	124	2.98	1.95	0.217
	67.750	1125.000	121	0.1323	125	7.5	125	57.04	121	4.11	124	2.70	2.06	0.228
	58.375	1134.375	122	0.0979	125	5.6	125	28.34	125	2.87	125	2.03	1.68	0.234
	49.000	1143.750	123	0.0603	126	3.5	126	13.36	125	2.11	126	1.47	1.31	0.231
	39.625	1153.125	124	0.0194	125	1.1	125	10.92	129	1.64	129	0.52	0.73	0.226
	30.250	1162.500	125	0.0139	135	0.8	135	10.34	129	1.46	129	0.12	0.21	0.222
	20.875	1171.875	126	0.0107	136	0.6	136	7.73	129	0.98	129	0.04	0.05	0.222
	11.500	1181.250	127	0.0075	138	0.4	138	6.89	129	0.57	132	-	-	0.222
5.750	1187.000	128	0.0053	136	0.3	136	6.99	129	0.40	134	-	-	0.222	

Table D-17. 31-ft 3-in. Long System – Missing Post Position 4

	Impact Point			5-Node Maximum Slope		5-Node Maximum Pocket Angle		Maximum Force		Maximum Deflection		Snag - Tire (Deformed)	Snag - Rim (Deformed)	Heading Parallel Time
	US of Bridge Rail (in.)	(in.)	Node No.	(rad)	@ Node	(deg)	@ Node	(kips)	@ Node	(in.)	@ Node	(in.)	(in.)	(sec)
W-to-Thrie Element	367.750	825.000	89	0.2483	101	13.9	101	110.28	97	15.10	99	-	-	0.221
	358.375	834.375	90	0.2567	101	14.4	101	114.05	97	15.27	100	-	-	0.220
	349.000	843.750	91	0.2599	101	14.6	101	114.13	97	15.66	100	-	-	0.218
	339.625	853.125	92	0.2587	101	14.5	101	120.22	97	15.76	101	-	-	0.216
	330.250	862.500	93	0.2463	103	13.8	103	118.36	98	15.50	102	-	-	0.215
	320.875	871.875	94	0.2387	104	13.4	104	119.63	99	15.08	102	-	-	0.214
	311.500	881.250	95	0.2242	105	12.6	105	120.18	100	14.45	103	-	-	0.215
	302.125	890.625	96	0.2012	106	11.4	106	119.20	99	13.25	103	-	-	0.213
Single Thrie Beam	292.750	900.000	97	0.1943	106	11.0	106	118.85	100	12.74	104	-	-	0.213
	283.375	909.375	98	0.1930	107	10.9	107	124.80	105	12.18	106	-	-	0.215
	274.000	918.750	99	0.2022	109	11.4	109	132.09	105	12.37	107	-	-	0.214
	264.625	928.125	100	0.1921	109	10.9	109	129.60	105	12.21	107	-	-	0.212
	255.250	937.500	101	0.1888	109	10.7	109	121.38	105	11.85	108	-	-	0.212
	245.875	946.875	102	0.1813	110	10.3	110	118.23	109	11.11	110	-	-	0.212
	236.500	956.250	103	0.1720	110	9.8	110	120.92	109	10.57	110	-	-	0.211
	227.125	965.625	104	0.1544	110	8.8	110	126.33	109	9.94	111	-	-	0.210
	217.750	975.000	105	0.1466	110	8.3	110	119.06	109	10.14	112	-	-	0.210
	208.375	984.375	106	0.1380	113	7.9	113	116.63	109	10.09	112	-	-	0.212
	199.000	993.750	107	0.1269	113	7.2	113	112.53	113	9.63	114	-	-	0.211
	189.625	1003.125	108	0.1268	118	7.2	118	115.23	113	9.43	115	-	-	0.209
	180.250	1012.500	109	0.1542	119	8.8	119	124.50	114	9.88	116	-	-	0.205
	170.875	1021.875	110	0.1607	120	9.1	120	129.49	117	9.72	118	-	-	0.202
	161.500	1031.250	111	0.1653	120	9.4	120	136.29	117	9.58	118	-	-	0.201
	152.125	1040.625	112	0.1654	121	9.4	121	145.35	117	9.41	119	-	-	0.202
Nested Thrie Beam	142.750	1050.000	113	0.1734	121	9.8	121	153.50	117	9.43	119	-	-	0.201
	133.375	1059.375	114	0.1701	121	9.7	121	143.11	117	9.05	120	-	-	0.203
	124.000	1068.750	115	0.1652	122	9.4	122	134.16	117	8.73	120	0.63	-	0.207
	114.625	1078.125	116	0.1761	124	10.0	124	123.88	119	8.29	121	1.60	0.43	0.206
	105.250	1087.500	117	0.1877	125	10.6	125	114.91	123	7.57	121	2.16	1.10	0.204
	95.875	1096.875	118	0.1894	125	10.7	125	103.39	123	6.94	122	2.60	1.44	0.206
	86.500	1106.250	119	0.1810	125	10.3	125	82.83	123	5.93	124	2.84	1.67	0.208
	77.125	1115.625	120	0.1575	125	9.0	125	62.27	123	4.83	124	2.78	1.76	0.215
	67.750	1125.000	121	0.1152	125	6.6	125	40.27	123	3.38	125	2.34	1.76	0.224
	58.375	1134.375	122	0.0865	125	4.9	125	23.98	125	2.52	125	1.82	1.55	0.233
	49.000	1143.750	123	0.0562	126	3.2	126	11.60	125	1.93	126	1.36	1.25	0.230
	39.625	1153.125	124	0.0171	125	1.0	125	10.90	129	1.61	129	0.47	0.69	0.226
	30.250	1162.500	125	0.0139	132	0.8	132	10.24	129	1.42	129	0.11	0.20	0.222
	20.875	1171.875	126	0.0085	136	0.5	136	7.66	129	0.95	129	0.04	0.05	0.222
11.500	1181.250	127	0.0075	138	0.4	138	6.91	129	0.56	132	-	-	0.222	
5.750	1187.000	128	0.0053	136	0.3	136	6.99	129	0.40	134	-	-	0.222	

Table D-18. 31-ft 3-in. Long System – Missing Post Position 6

	Impact Point			5-Node Maximum Slope		5-Node Maximum Pocket Angle		Maximum Force		Maximum Deflection		Snag - Tire (Deformed)	Snag - Rim (Deformed)	Heading Parallel Time
	US of Bridge Rail (in.)	(in.)	Node No.	(rad)	@ Node	(deg)	@ Node	(kips)	@ Node	(in.)	@ Node	(in.)	(in.)	(sec)
W-to-Thrie Element	367.750	825.000	89	0.2483	101	13.9	101	110.21	97	15.11	99	-	-	0.221
	358.375	834.375	90	0.2567	101	14.4	101	114.07	97	15.27	100	-	-	0.220
	349.000	843.750	91	0.2599	101	14.6	101	114.09	97	15.66	100	-	-	0.218
	339.625	853.125	92	0.2587	101	14.5	101	120.24	97	15.77	101	-	-	0.216
	330.250	862.500	93	0.2455	103	13.8	103	118.55	98	15.49	102	-	-	0.215
	320.875	871.875	94	0.2401	103	13.5	103	120.13	99	15.11	102	-	-	0.215
	311.500	881.250	95	0.2263	105	12.8	105	120.44	100	14.48	103	-	-	0.215
	302.125	890.625	96	0.2014	106	11.4	106	119.04	99	13.25	103	-	-	0.214
	292.750	900.000	97	0.1944	105	11.0	105	118.79	100	12.76	104	-	-	0.214
Single Thrie Beam	283.375	909.375	98	0.1889	106	10.7	106	123.19	105	12.20	106	-	-	0.215
	274.000	918.750	99	0.1888	108	10.7	108	130.70	105	12.40	107	-	-	0.217
	264.625	928.125	100	0.1811	106	10.3	106	128.88	105	12.39	108	-	-	0.216
	255.250	937.500	101	0.1730	109	9.8	109	119.09	105	12.02	108	-	-	0.217
	245.875	946.875	102	0.1687	109	9.6	109	109.17	105	11.36	110	-	-	0.217
	236.500	956.250	103	0.1585	109	9.0	109	115.50	109	11.08	111	-	-	0.216
	227.125	965.625	104	0.1432	110	8.1	110	122.43	109	10.46	112	-	-	0.215
	217.750	975.000	105	0.1431	117	8.1	117	120.91	113	10.75	112	-	-	0.214
	208.375	984.375	106	0.1687	117	9.6	117	134.01	113	10.59	114	-	-	0.211
	199.000	993.750	107	0.1755	117	10.0	117	142.70	113	10.81	115	-	-	0.204
	189.625	1003.125	108	0.1765	117	10.0	117	153.71	113	10.58	116	-	-	0.201
	180.250	1012.500	109	0.1807	118	10.2	118	155.89	114	10.85	116	-	-	0.202
	170.875	1021.875	110	0.1896	119	10.7	119	159.91	114	10.94	117	-	-	0.204
	161.500	1031.250	111	0.1896	119	10.7	119	153.26	115	10.62	118	-	-	0.205
	152.125	1040.625	112	0.1770	119	10.0	119	147.72	115	10.10	118	-	-	0.207
	Nested Thrie Beam	142.750	1050.000	113	0.1688	120	9.6	120	141.33	113	9.64	119	-	-
133.375		1059.375	114	0.1621	121	9.2	121	130.02	113	9.39	119	-	-	0.210
124.000		1068.750	115	0.1623	124	9.2	124	117.80	121	8.99	119	0.48	-	0.210
114.625		1078.125	116	0.1726	124	9.8	124	106.37	121	8.38	120	1.50	0.39	0.208
105.250		1087.500	117	0.1789	125	10.1	125	98.43	123	7.36	122	1.94	0.97	0.204
95.875		1096.875	118	0.1757	125	10.0	125	76.94	123	6.10	123	2.38	1.28	0.203
86.500		1106.250	119	0.1577	125	9.0	125	68.56	123	4.96	124	2.50	1.35	0.205
77.125		1115.625	120	0.1341	125	7.6	125	55.93	123	3.92	125	2.40	1.41	0.211
67.750		1125.000	121	0.1059	125	6.0	125	40.28	123	3.12	125	2.20	1.64	0.223
58.375		1134.375	122	0.0828	125	4.7	125	25.19	125	2.40	125	1.78	1.52	0.232
49.000		1143.750	123	0.0533	126	3.1	126	12.54	125	1.92	126	1.33	1.23	0.230
39.625		1153.125	124	0.0167	125	1.0	125	10.89	129	1.60	129	0.44	0.68	0.226
30.250		1162.500	125	0.0139	134	0.8	134	10.51	129	1.44	129	0.10	0.20	0.222
20.875		1171.875	126	0.0085	136	0.5	136	7.70	129	0.95	129	0.04	0.05	0.222
11.500		1181.250	127	0.0075	138	0.4	138	6.92	129	0.56	132	-	-	0.222
5.750	1187.000	128	0.0053	139	0.3	139	6.94	129	0.40	134	-	-	0.222	

Table D-19. 31-ft 3-in. Long System – 3 in. Improper Post Exposure

	Impact Point			Maximum Slope		Maximum Pocket Angle		Maximum Force		Maximum Deflection		Snag - Tire (Deformed)	Snag - Rim (Deformed)	Heading Parallel Time
	US of Bridge Rail (in.)	(in.)	Node No.	(rad)	@ Node	(deg)	@ Node	(kips)	@ Node	(in.)	@ Node	(in.)	(in.)	(sec)
W-to-Thrie Element	367.750	825.000	89	0.2483	101	13.9	101	111.63	97	15.24	99	-	-	0.221
	358.375	834.375	90	0.2567	101	14.4	101	113.99	97	15.27	100	-	-	0.220
	349.000	843.750	91	0.2599	101	14.6	101	114.02	97	15.66	100	-	-	0.218
	339.625	853.125	92	0.2587	101	14.5	101	120.25	97	15.76	101	-	-	0.216
	330.250	862.500	93	0.2465	103	13.8	103	118.38	98	15.50	102	-	-	0.215
	320.875	871.875	94	0.2387	104	13.4	104	119.46	99	15.08	102	-	-	0.214
	311.500	881.250	95	0.2242	105	12.6	105	119.32	100	14.41	103	-	-	0.215
	302.125	890.625	96	0.2033	106	11.5	106	119.14	99	13.26	103	-	-	0.214
	292.750	900.000	97	0.1943	106	11.0	106	118.87	100	12.74	104	-	-	0.213
Single Thrie Beam	283.375	909.375	98	0.1911	106	10.8	106	124.88	105	12.17	106	-	-	0.215
	274.000	918.750	99	0.2054	109	11.6	109	131.98	105	12.38	107	-	-	0.214
	264.625	928.125	100	0.1921	109	10.9	109	129.51	105	12.20	107	-	-	0.212
	255.250	937.500	101	0.1855	109	10.5	109	121.44	105	11.85	108	-	-	0.212
	245.875	946.875	102	0.1813	110	10.3	110	118.00	109	11.12	110	-	-	0.213
	236.500	956.250	103	0.1720	110	9.8	110	120.86	109	10.59	111	-	-	0.212
	227.125	965.625	104	0.1555	110	8.8	110	126.56	109	9.94	111	-	-	0.211
	217.750	975.000	105	0.1457	111	8.3	111	119.70	109	10.15	112	-	-	0.210
	208.375	984.375	106	0.1431	115	8.1	115	117.51	109	10.05	112	-	-	0.210
	199.000	993.750	107	0.1445	116	8.2	116	118.57	113	9.67	115	-	-	0.208
	189.625	1003.125	108	0.1443	117	8.2	117	125.04	113	9.54	115	-	-	0.204
	180.250	1012.500	109	0.1578	118	9.0	118	130.40	113	9.79	116	-	-	0.202
	170.875	1021.875	110	0.1630	119	9.3	119	130.71	114	9.61	116	-	-	0.204
	161.500	1031.250	111	0.1623	119	9.2	119	126.63	117	9.35	118	-	-	0.204
	152.125	1040.625	112	0.1544	119	8.8	119	130.95	117	8.88	118	-	-	0.204
	142.750	1050.000	113	0.1542	120	8.8	120	132.08	117	8.77	119	-	-	0.207
	133.375	1059.375	114	0.1488	122	8.5	122	125.99	117	8.60	119	-	-	0.206
124.000	1068.750	115	0.1541	123	8.8	123	111.98	117	8.23	120	0.85	-	0.207	
114.625	1078.125	116	0.1730	124	9.8	124	110.47	121	7.83	122	1.73	0.75	0.203	
105.250	1087.500	117	0.1832	125	10.4	125	107.34	123	7.26	122	2.10	1.08	0.202	
95.875	1096.875	118	0.1826	125	10.3	125	94.60	123	6.47	123	2.57	1.44	0.203	
86.500	1106.250	119	0.1815	125	10.3	125	84.31	123	5.76	124	2.85	1.69	0.206	
77.125	1115.625	120	0.1561	125	8.9	125	70.68	123	4.59	125	2.73	1.72	0.214	
67.750	1125.000	121	0.1213	125	6.9	125	50.24	123	3.65	125	2.61	1.89	0.225	
58.375	1134.375	122	0.0911	125	5.2	125	28.62	125	2.66	125	1.96	1.67	0.233	
49.000	1143.750	123	0.0562	126	3.2	126	13.58	125	2.07	126	1.42	1.30	0.231	
39.625	1153.125	124	0.0167	126	1.0	126	11.58	129	1.66	129	0.48	0.71	0.226	
30.250	1162.500	125	0.0139	132	0.8	132	10.67	129	1.49	129	0.10	0.20	0.222	
20.875	1171.875	126	0.0085	136	0.5	136	7.76	129	0.99	129	0.04	0.05	0.222	
11.500	1181.250	127	0.0075	138	0.4	138	6.91	129	0.57	132	-	-	0.222	
5.750	1187.000	128	0.0053	136	0.3	136	6.92	129	0.40	134	-	-	0.222	

Table D-20. 33-ft 3-in. Long System – 4-in. Improper Post Exposure

	Impact Point			Maximum Slope		Maximum Pocket Angle		Maximum Force		Maximum Deflection		Snag - Tire (Deformed)	Snag - Rim (Deformed)	Heading Parallel Time
	US of Bridge Rail (in.)	(in.)	Node No.	(rad)	@ Node	(deg)	@ Node	(kips)	@ Node	(in.)	@ Node	(in.)	(in.)	(sec)
W-to-Thrie Element	367.750	825.000	89	0.2483	101	13.9	101	111.63	97	15.24	99	-	-	0.221
	358.375	834.375	90	0.2567	101	14.4	101	113.99	97	15.27	100	-	-	0.220
	349.000	843.750	91	0.2599	101	14.6	101	114.02	97	15.66	100	-	-	0.218
	339.625	853.125	92	0.2587	101	14.5	101	120.25	97	15.76	101	-	-	0.216
	330.250	862.500	93	0.2465	103	13.8	103	118.38	98	15.50	102	-	-	0.215
	320.875	871.875	94	0.2387	104	13.4	104	119.46	99	15.08	102	-	-	0.214
	311.500	881.250	95	0.2242	105	12.6	105	119.32	100	14.42	103	-	-	0.215
	302.125	890.625	96	0.2033	106	11.5	106	119.14	99	13.26	103	-	-	0.214
	292.750	900.000	97	0.1943	106	11.0	106	118.87	100	12.74	104	-	-	0.213
Single Thrie Beam	283.375	909.375	98	0.1911	106	10.8	106	124.81	105	12.17	106	-	-	0.215
	274.000	918.750	99	0.2022	109	11.4	109	131.43	105	12.34	107	-	-	0.214
	264.625	928.125	100	0.1921	109	10.9	109	129.47	105	12.20	107	-	-	0.212
	255.250	937.500	101	0.1855	109	10.5	109	121.39	105	11.86	108	-	-	0.212
	245.875	946.875	102	0.1813	110	10.3	110	117.26	109	11.13	110	-	-	0.213
	236.500	956.250	103	0.1720	110	9.8	110	120.78	109	10.65	111	-	-	0.213
	227.125	965.625	104	0.1555	110	8.8	110	125.69	109	9.95	111	-	-	0.212
	217.750	975.000	105	0.1455	110	8.3	110	119.05	109	10.17	112	-	-	0.211
	208.375	984.375	106	0.1431	115	8.1	115	117.41	109	10.09	112	-	-	0.211
	199.000	993.750	107	0.1431	116	8.1	116	118.44	113	9.72	115	-	-	0.208
	189.625	1003.125	108	0.1443	117	8.2	117	126.59	113	9.65	115	-	-	0.205
	180.250	1012.500	109	0.1579	118	9.0	118	133.12	113	9.92	116	-	-	0.203
	170.875	1021.875	110	0.1609	119	9.1	119	132.67	114	9.74	116	-	-	0.204
	161.500	1031.250	111	0.1609	119	9.1	119	129.56	117	9.53	118	-	-	0.204
	152.125	1040.625	112	0.1544	119	8.8	119	134.42	117	9.10	118	-	-	0.204
	Nested Thrie Beam	142.750	1050.000	113	0.1539	120	8.7	120	137.13	117	8.95	119	-	-
133.375		1059.375	114	0.1533	122	8.7	122	127.88	117	8.76	119	-	-	0.206
124.000		1068.750	115	0.1648	124	9.4	124	117.89	121	8.51	120	1.18	-	0.206
114.625		1078.125	116	0.1812	124	10.3	124	118.11	121	8.12	121	1.95	1.00	0.203
105.250		1087.500	117	0.1897	125	10.7	125	112.83	123	7.67	122	2.35	1.25	0.202
95.875		1096.875	118	0.1909	125	10.8	125	102.66	123	6.83	123	2.81	1.65	0.203
86.500		1106.250	119	0.1882	125	10.7	125	91.12	123	6.10	124	3.06	1.93	0.207
77.125		1115.625	120	0.1669	125	9.5	125	74.97	123	4.93	124	2.92	1.91	0.216
67.750		1125.000	121	0.1323	125	7.5	125	54.26	125	3.88	125	2.75	2.00	0.227
58.375		1134.375	122	0.0946	125	5.4	125	30.62	125	2.77	125	2.05	1.75	0.233
49.000		1143.750	123	0.0602	126	3.4	126	14.38	125	2.13	126	1.46	1.33	0.231
39.625		1153.125	124	0.0171	125	1.0	125	11.89	129	1.69	129	0.49	0.73	0.226
30.250		1162.500	125	0.0139	132	0.8	132	10.72	129	1.50	129	0.10	0.20	0.223
20.875		1171.875	126	0.0107	136	0.6	136	7.78	129	1.00	129	0.04	0.05	0.222
11.500	1181.250	127	0.0075	138	0.4	138	6.90	129	0.57	132	-	-	0.222	
5.750	1187.000	128	0.0053	136	0.3	136	6.92	129	0.40	134	-	-	0.222	

Table D-21. 31-ft 3-in. Long System – Break Point of a 2H:1V Fill Slope

	Impact Point			5-Node Maximum Slope		5-Node Maximum Pocket Angle		Maximum Force		Maximum Deflection		Snag - Tire (Deformed)	Snag - Rim (Deformed)	Heading Parallel Time
	US of Bridge Rail (in.)	(in.)	Node No.	(rad)	@ Node	(deg)	@ Node	(kips)	@ Node	(in.)	@ Node	(in.)	(in.)	(sec)
W-to-Thrie Element	367.750	825.000	89	0.2483	101	13.9	101	110.30	97	15.10	99	-	-	0.221
	358.375	834.375	90	0.2567	101	14.4	101	113.98	97	15.27	100	-	-	0.220
	349.000	843.750	91	0.2599	101	14.6	101	114.02	97	15.66	100	-	-	0.218
	339.625	853.125	92	0.2587	101	14.5	101	120.25	97	15.77	101	-	-	0.216
	330.250	862.500	93	0.2463	103	13.8	103	118.60	98	15.47	102	-	-	0.215
	320.875	871.875	94	0.2387	104	13.4	104	119.45	99	15.08	102	-	-	0.214
	311.500	881.250	95	0.2242	105	12.6	105	119.32	100	14.42	103	-	-	0.215
	302.125	890.625	96	0.2033	106	11.5	106	119.13	99	13.26	103	-	-	0.214
	292.750	900.000	97	0.1943	106	11.0	106	118.87	100	12.74	104	-	-	0.213
Single Thrie Beam	283.375	909.375	98	0.1911	106	10.8	106	124.85	105	12.17	106	-	-	0.215
	274.000	918.750	99	0.2054	109	11.6	109	131.96	105	12.38	107	-	-	0.215
	264.625	928.125	100	0.1921	109	10.9	109	129.50	105	12.20	107	-	-	0.213
	255.250	937.500	101	0.1855	109	10.5	109	121.43	105	11.86	108	-	-	0.215
	245.875	946.875	102	0.1779	109	10.1	109	112.50	105	11.18	110	-	-	0.216
	236.500	956.250	103	0.1718	110	9.7	110	114.55	109	10.82	111	-	-	0.216
	227.125	965.625	104	0.1555	110	8.8	110	120.07	109	10.10	111	-	-	0.216
	217.750	975.000	105	0.1454	110	8.3	110	114.38	109	10.25	112	-	-	0.218
	208.375	984.375	106	0.1333	111	7.6	111	114.37	109	10.09	112	-	-	0.218
	199.000	993.750	107	0.1325	117	7.5	117	121.51	113	10.29	115	-	-	0.214
	189.625	1003.125	108	0.1387	118	7.9	118	136.91	114	10.54	116	-	-	0.210
	180.250	1012.500	109	0.1520	119	8.6	119	149.13	117	11.19	117	-	-	0.207
	170.875	1021.875	110	0.1621	120	9.2	120	163.16	117	11.47	118	-	-	0.206
	161.500	1031.250	111	0.1708	121	9.7	121	165.47	117	11.33	118	-	-	0.205
	152.125	1040.625	112	0.1753	121	9.9	121	165.77	117	10.89	119	-	-	0.206
	Nested Thrie Beam	142.750	1050.000	113	0.1862	121	10.5	121	166.38	117	10.61	120	1.09	-
133.375		1059.375	114	0.2129	124	12.0	124	169.70	121	10.43	121	2.35	0.98	0.206
124.000		1068.750	115	0.2373	125	13.3	125	172.90	121	10.35	120	3.28	2.01	0.205
114.625		1078.125	116	0.2477	125	13.9	125	169.69	123	10.27	121	4.19	2.57	0.206
105.250		1087.500	117	0.2502	125	14.0	125	164.49	123	10.03	122	4.89	3.26	0.208
95.875		1096.875	118	0.2409	125	13.5	125	153.67	123	9.51	122	5.13	3.82	0.212
86.500		1106.250	119	0.2392	125	13.5	125	140.01	123	8.63	123	4.85	3.70	0.220
77.125		1115.625	120	0.2309	125	13.0	125	117.41	123	7.60	124	4.56	3.51	0.231
67.750		1125.000	121	0.1977	125	11.2	125	96.01	125	6.11	124	4.12	3.26	0.241
58.375		1134.375	122	0.1402	125	8.0	125	58.82	125	4.54	126	3.21	2.67	0.241
49.000		1143.750	123	0.0672	126	3.8	126	19.46	125	2.78	126	1.68	1.57	0.233
39.625		1153.125	124	0.0167	126	1.0	126	12.22	129	1.73	128	0.48	0.72	0.227
30.250		1162.500	125	0.0139	132	0.8	132	10.65	129	1.50	129	0.10	0.20	0.223
20.875		1171.875	126	0.0085	136	0.5	136	7.74	129	0.99	129	0.04	0.05	0.222
11.500		1181.250	127	0.0075	138	0.4	138	6.88	129	0.57	132	-	-	0.222
5.750		1187.000	128	0.0053	136	0.3	136	6.90	129	0.40	134	-	-	0.222

Appendix E. Test Results

A summary sheet for each dynamic bogie test is provided in this section. Summary sheets include acceleration, velocity, and displacement versus time plots, as well as force and energy versus displacement plots.

Figure E-1. Results of Test No. WAGTMP-1 (EDR-3)

Figure E-2. Results of Test No. WAGTMP-1 (DTS)

Figure E-3. Results of Test No. WAGTMP-4 (EDR-3)

Figure E-4. Results of Test No. WAGTMP-4 (DTS)

Figure E-5. Results of Test No. WITB-1 (EDR-3)

Figure E-6. Results of Test No. WITB-1 (DTS)

Figure E-7. Results of Test No. WITB-2 (EDR-3)

Figure E-8. Results of Test No. WITB-2 (DTS)

Figure E-9. Results of Test No. WIA-1 (EDR-3)

Figure E-10. Results of Test No. WIA-1 (DTS)

Figure E-11. Results of Test No. WIA-2 (EDR-3)

Figure E-12. Results of Test No. WIA-2 (DTS)

Figure E-13. Results of Test No. WIA-3 (EDR-3)

Figure E-14. Results of Test No. WIA-3 (DTS)

Figure E-15. Results of Test No. WIA-4 (EDR-3)

Figure E-16. Results of Test No. WIA-4 (DTS)

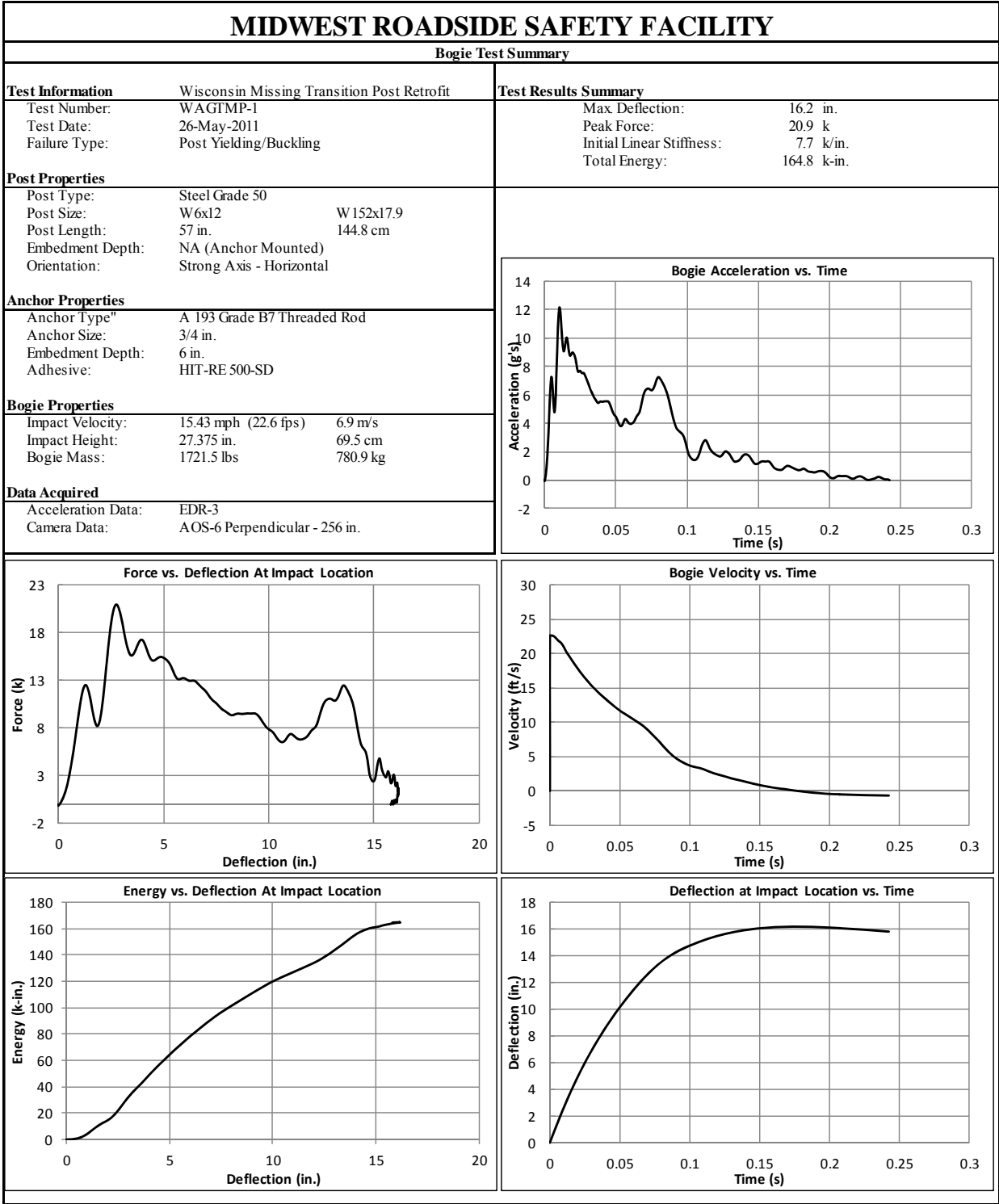


Figure E-1. Results of Test No. WAGTMP-1 (EDR-3)

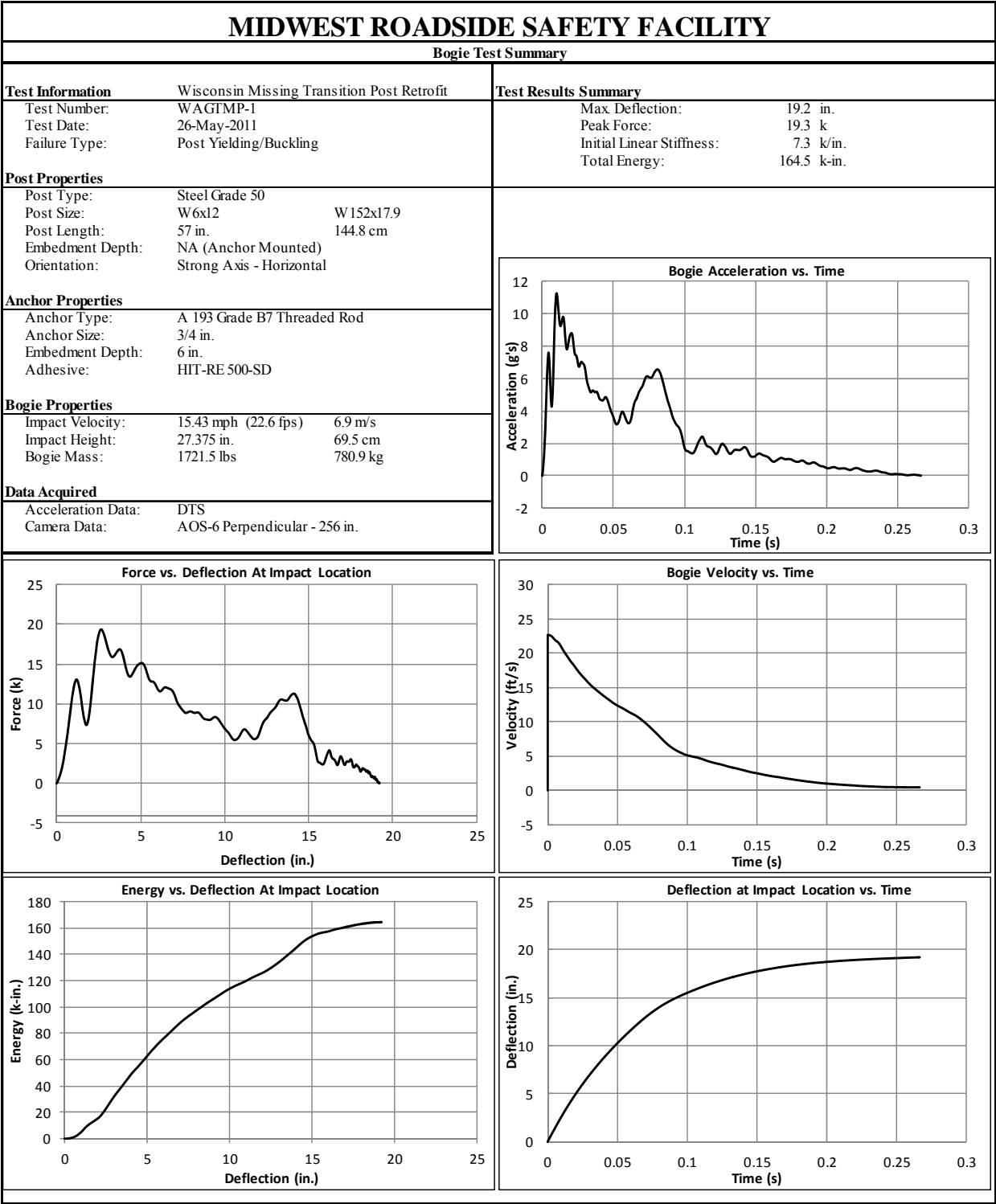


Figure E-2. Results of Test No. WAGTMP-1 (DTS)

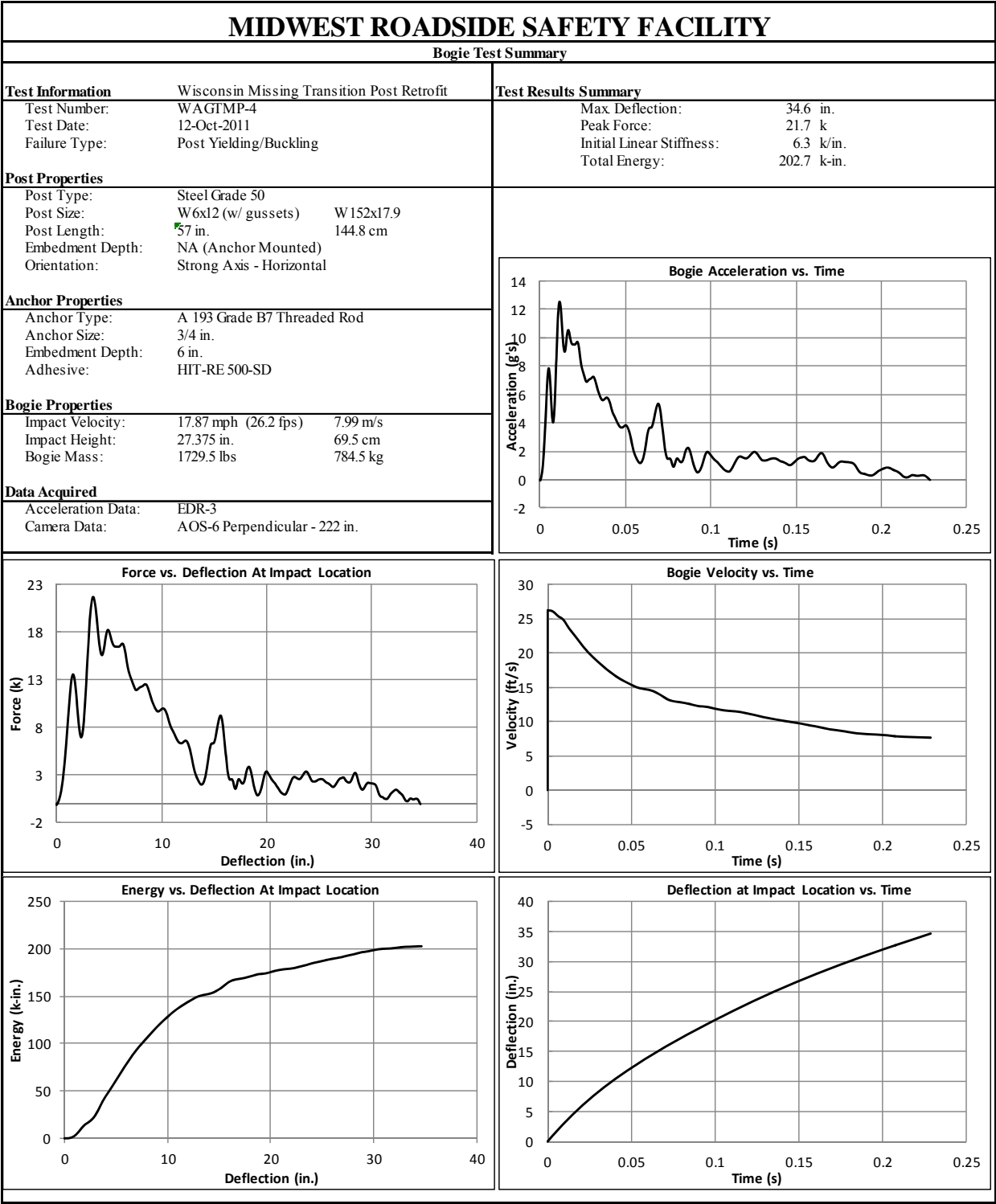


Figure E-3. Results of Test No. WAGTMP-4 (EDR-3)

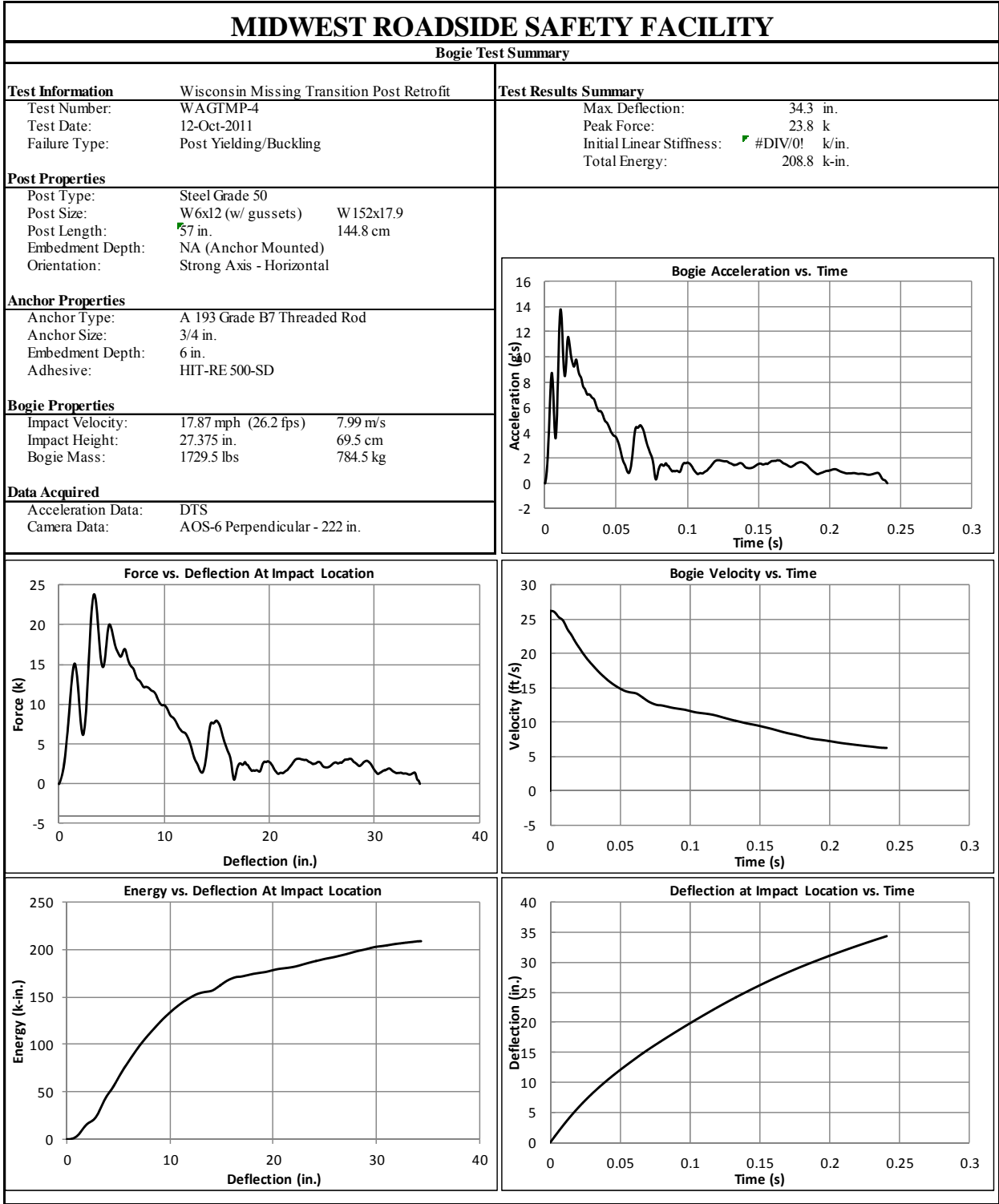


Figure E-4. Results of Test No. WAGTMP-4 (DTS)

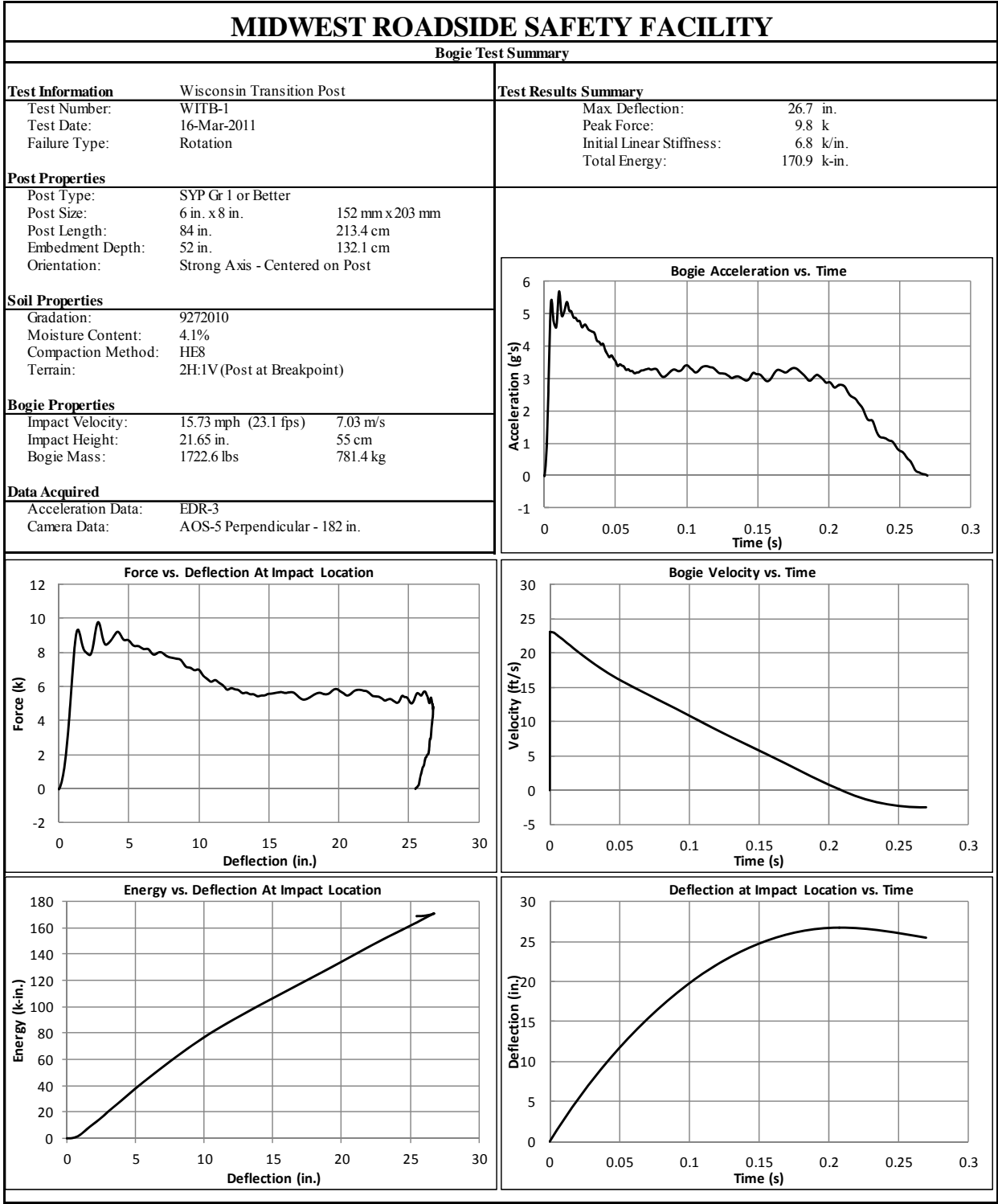


Figure E-5. Results of Test No. WITB-1 (EDR-3)

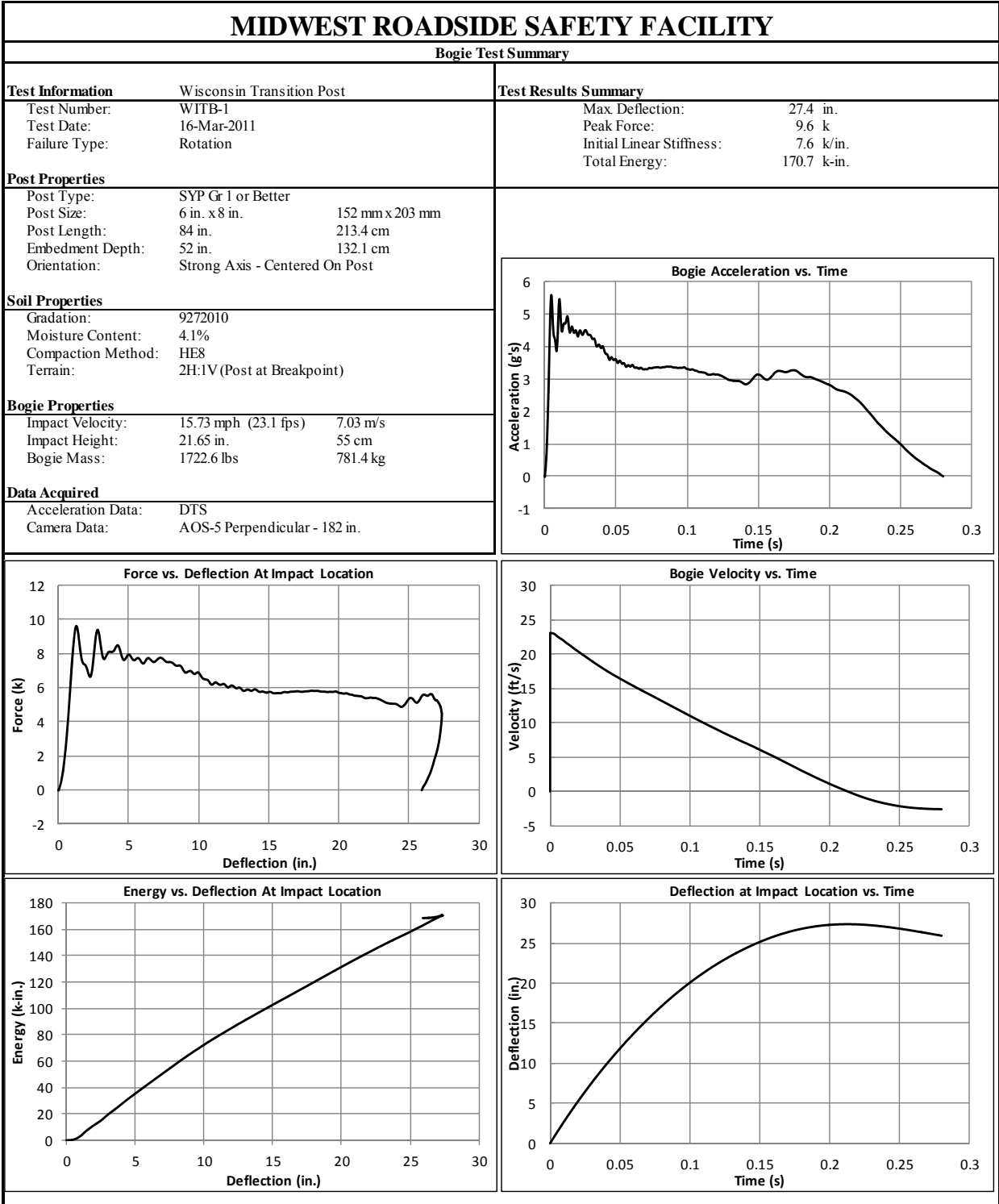


Figure E-6. Results of Test No. WITB-1 (DTS)

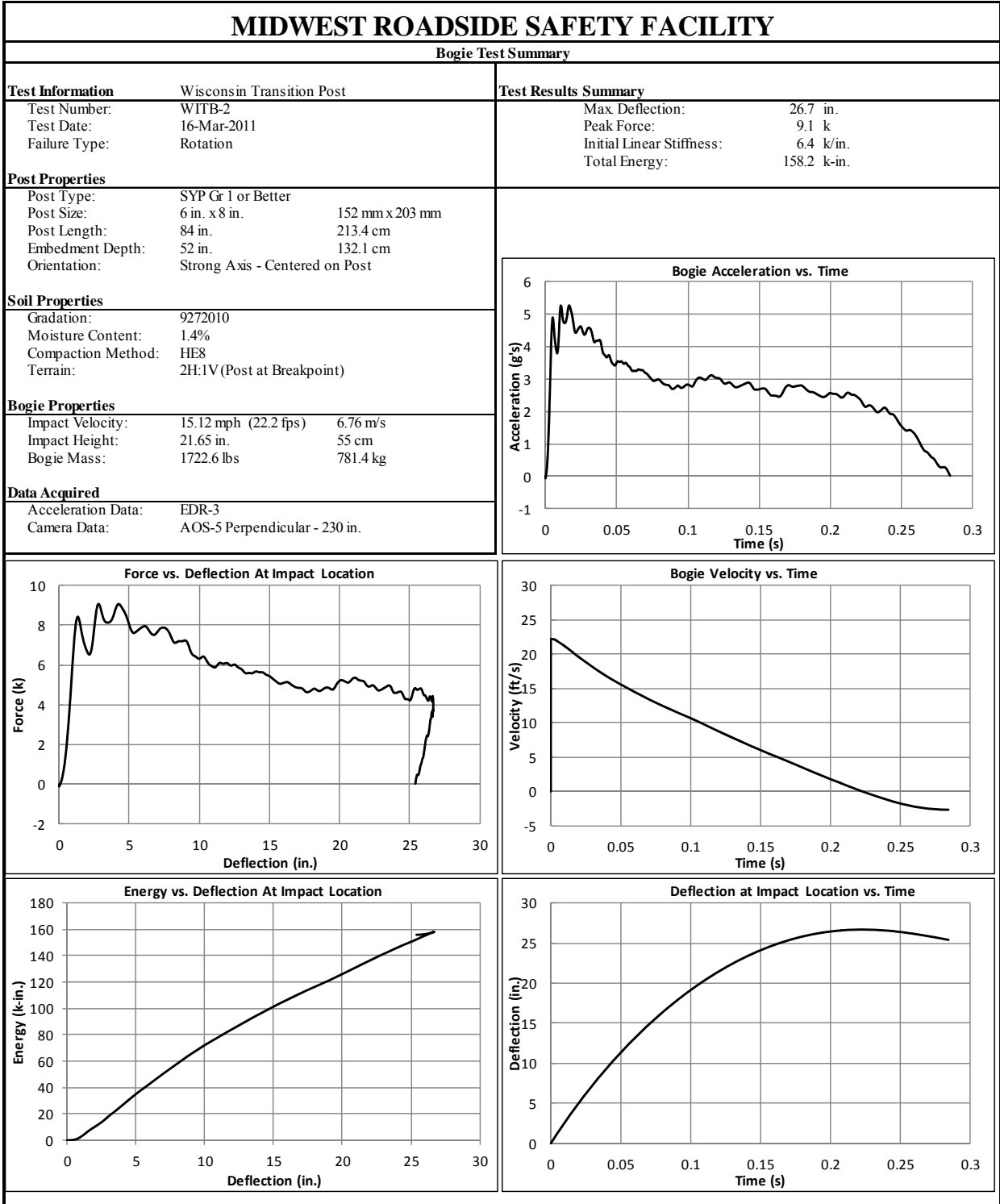


Figure E-7. Results of Test No. WITB-2 (EDR-3)

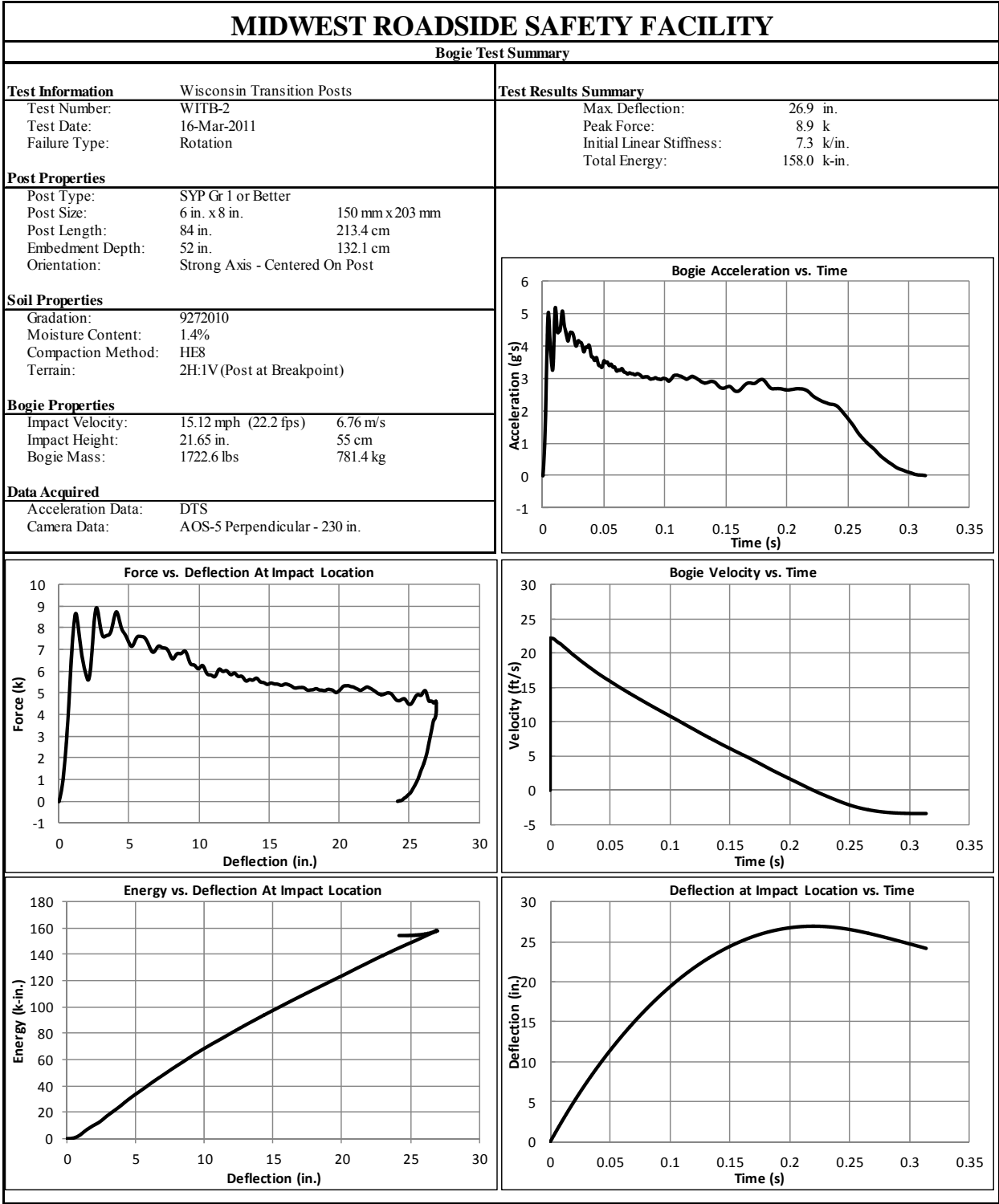


Figure E-8. Results of Test No. WITB-2 (DTS)

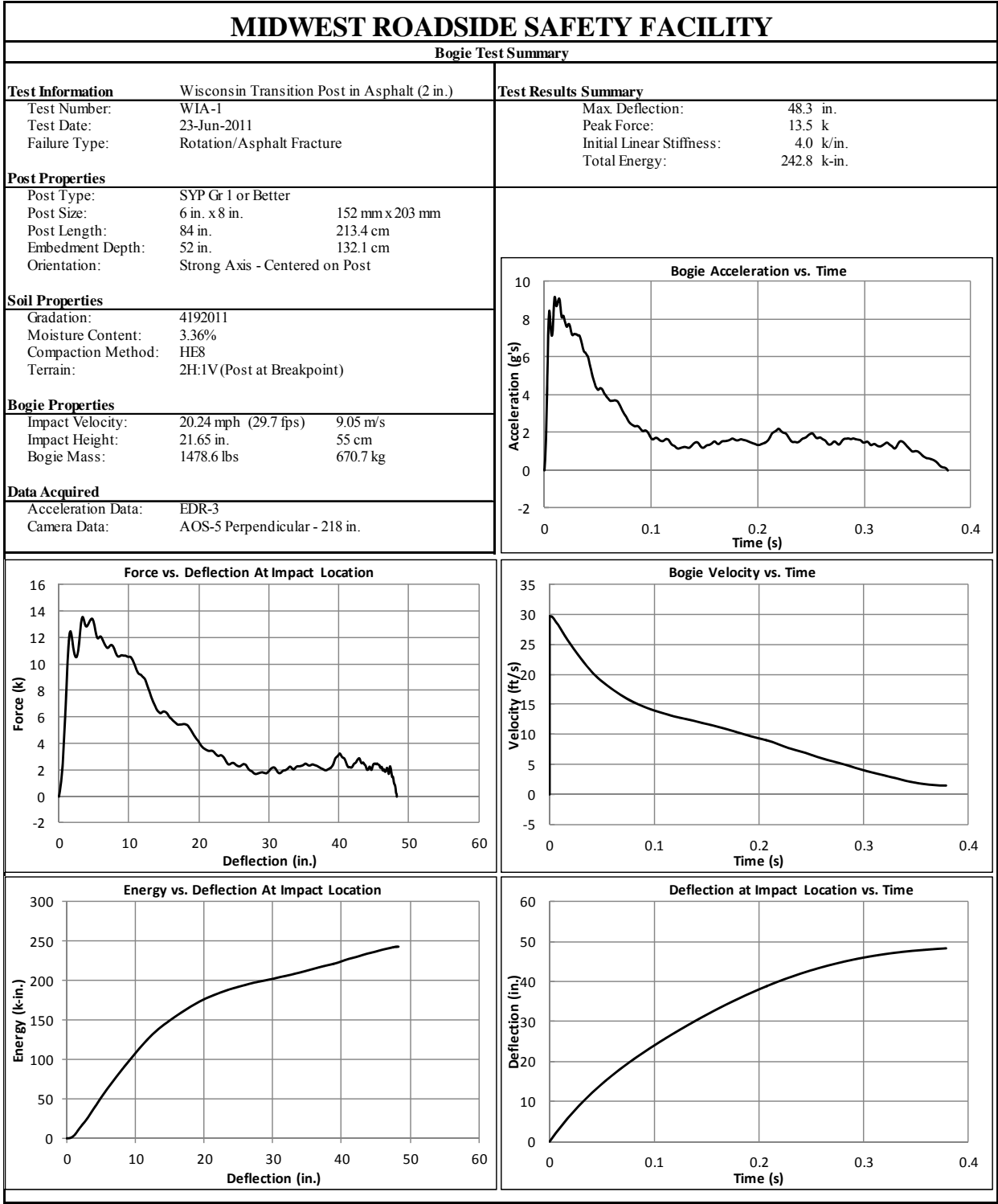


Figure E-9. Results of Test No. WIA-1 (EDR-3)

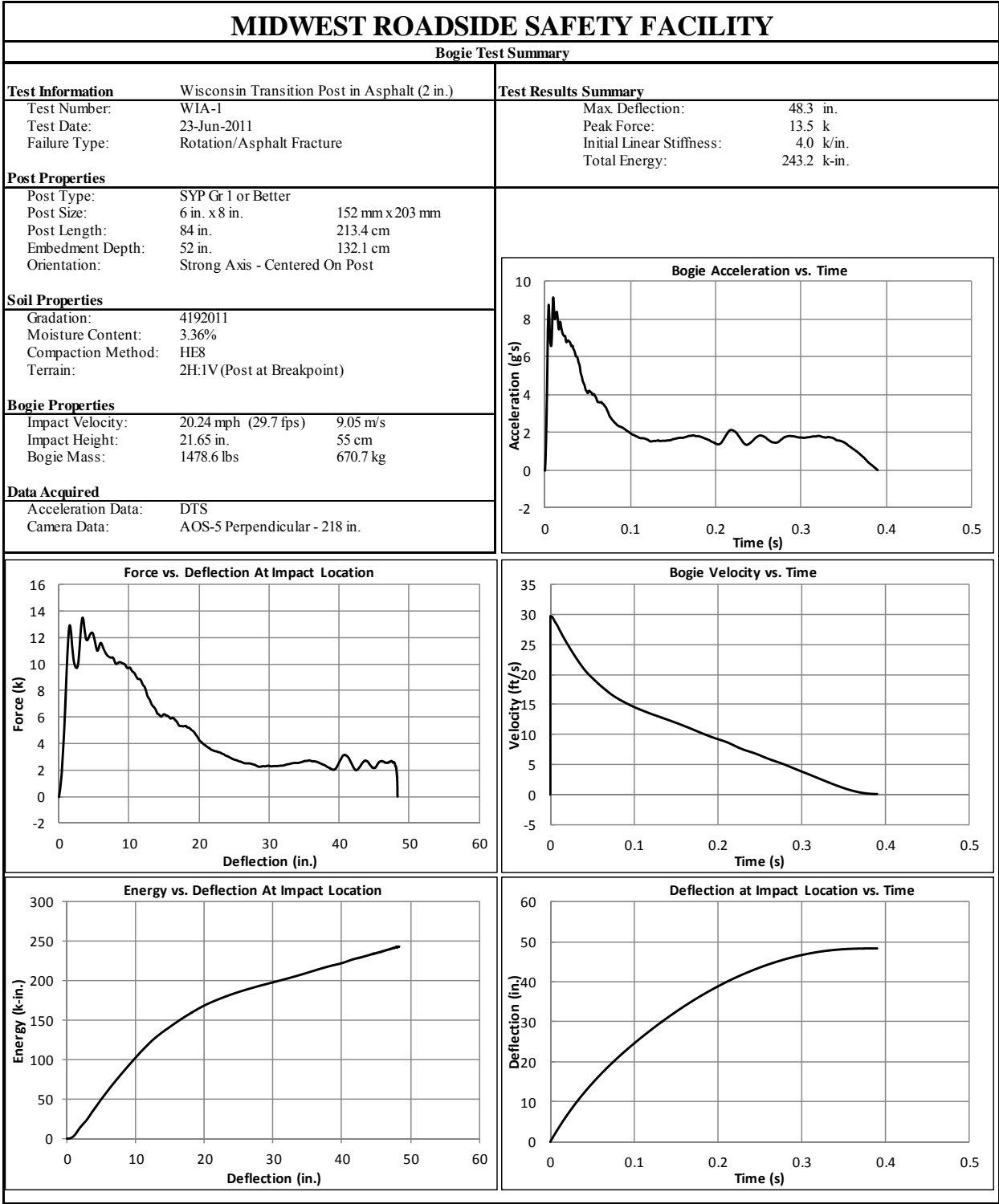


Figure E-10. Results of Test No. WIA-1 (DTS)

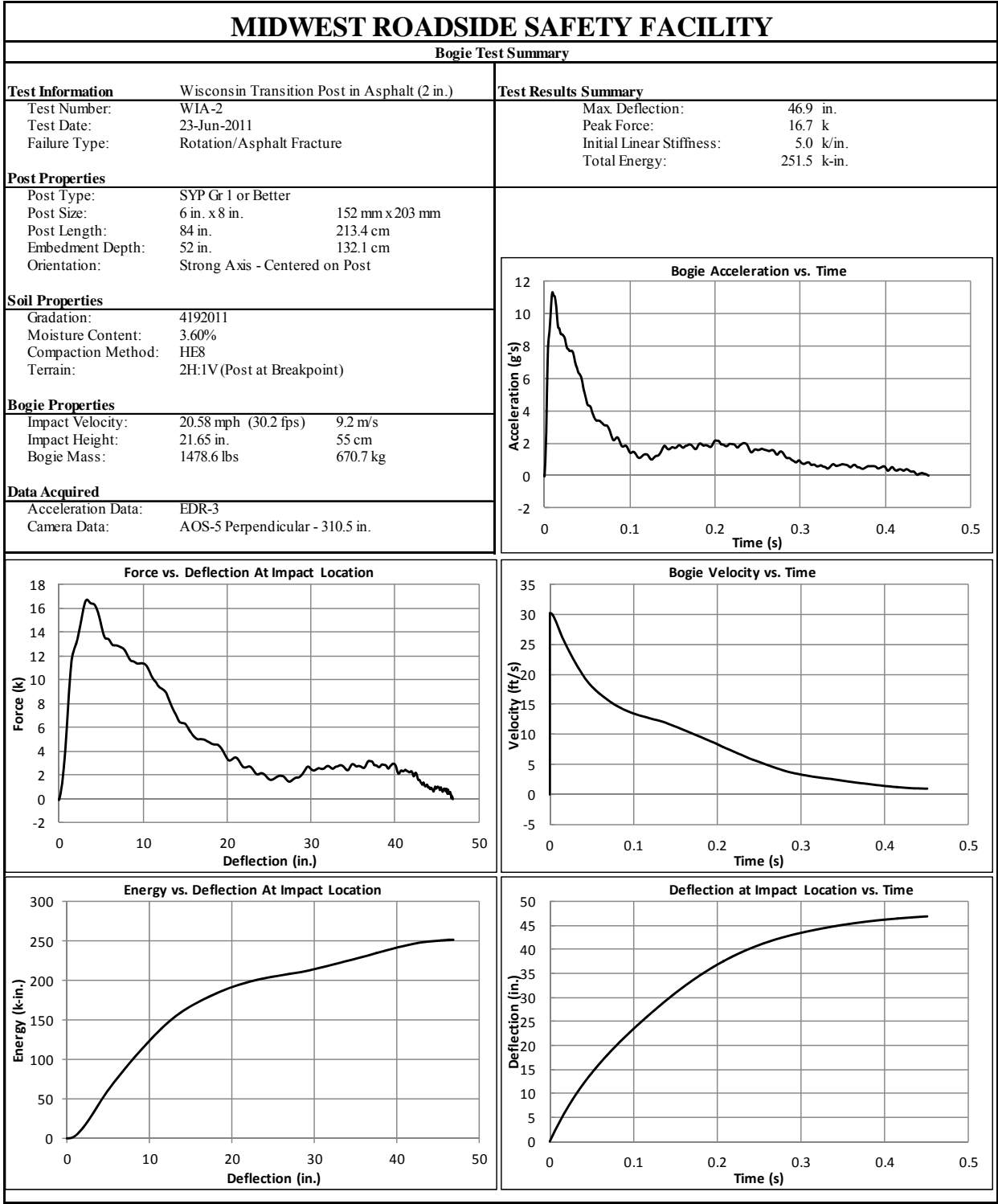


Figure E-11. Results of Test No. WIA-2 (EDR-3)

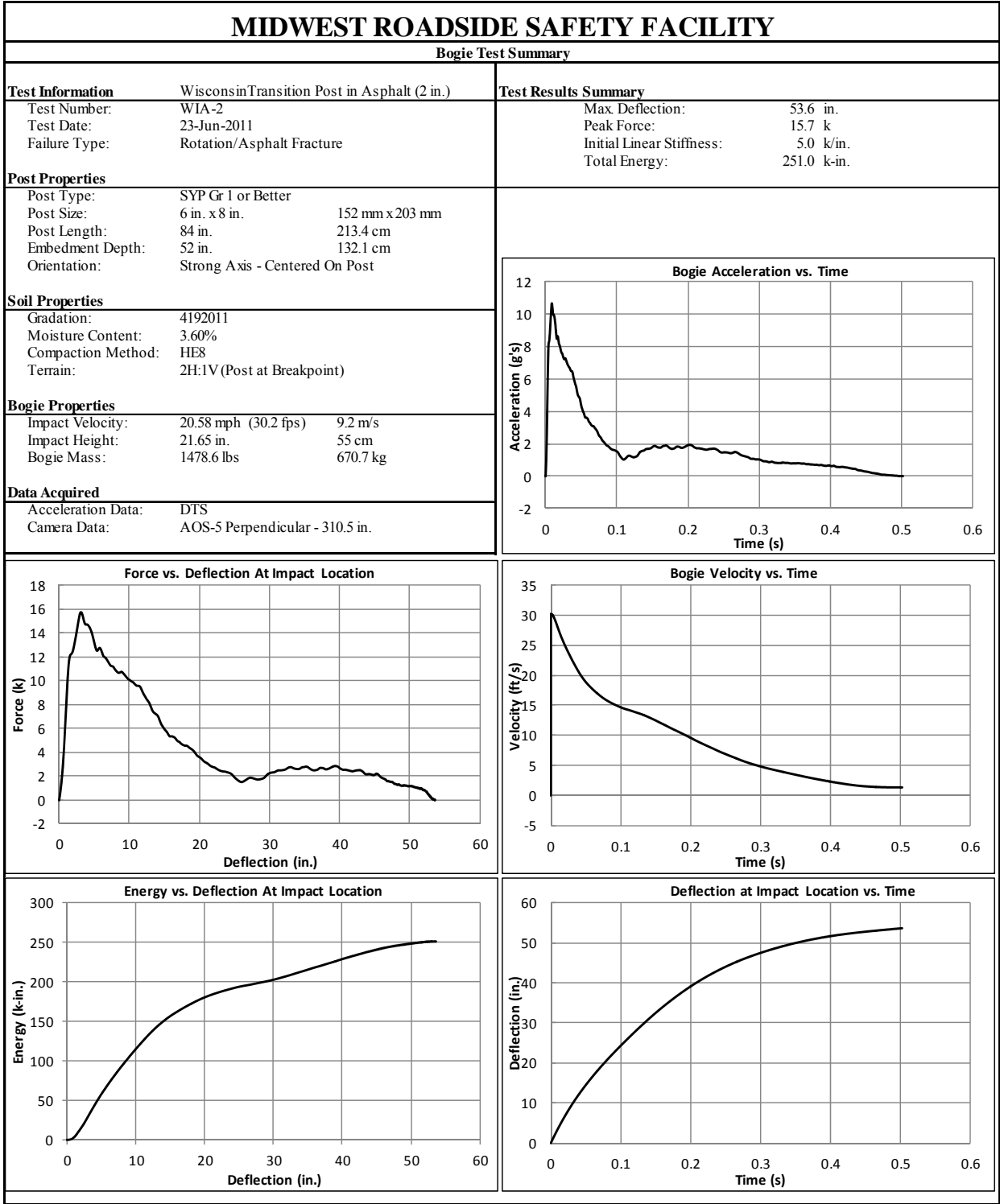


Figure E-12. Results of Test No. WIA-2 (DTS)

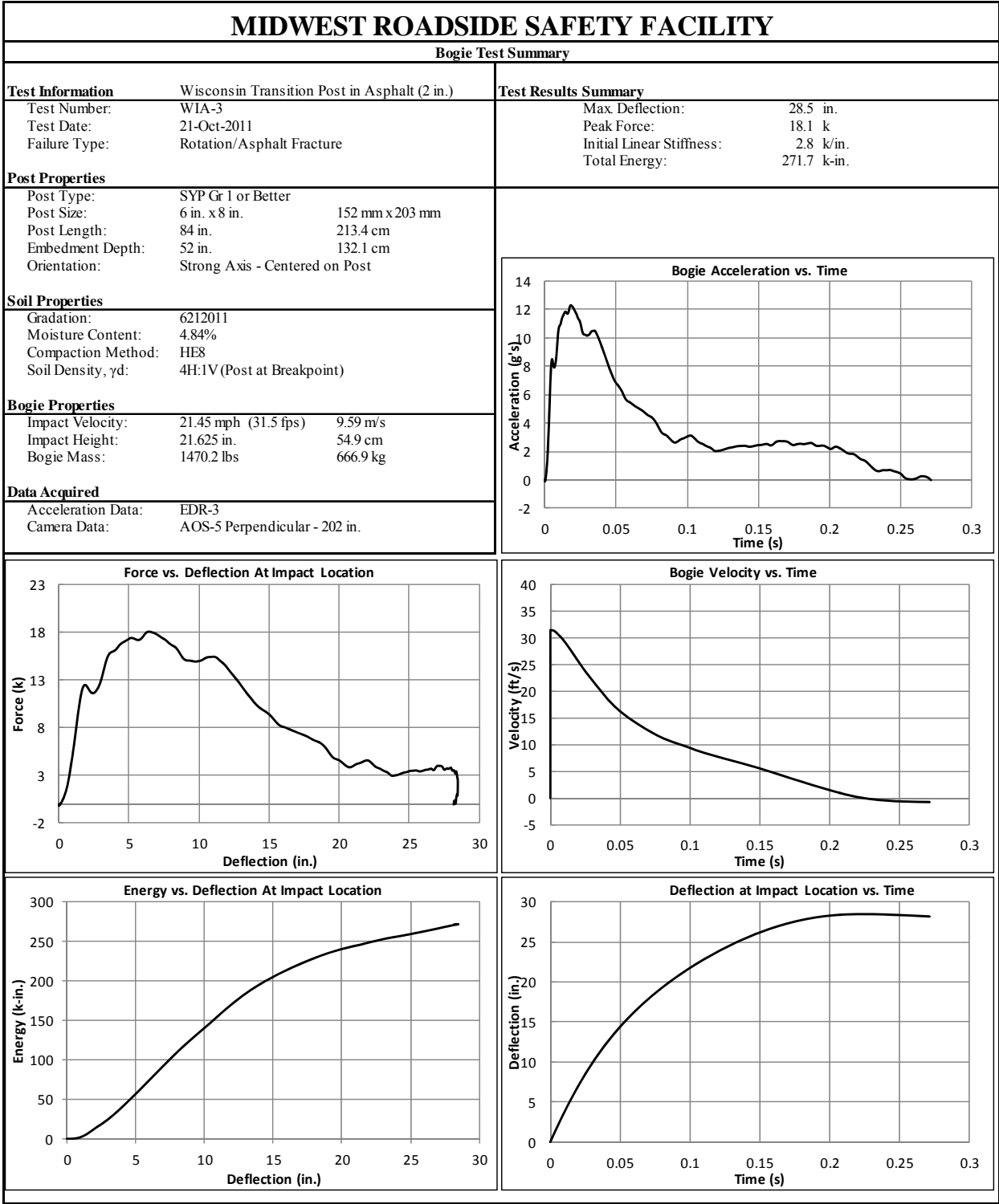


Figure E-13. Results of Test No. WIA-3 (EDR-3)

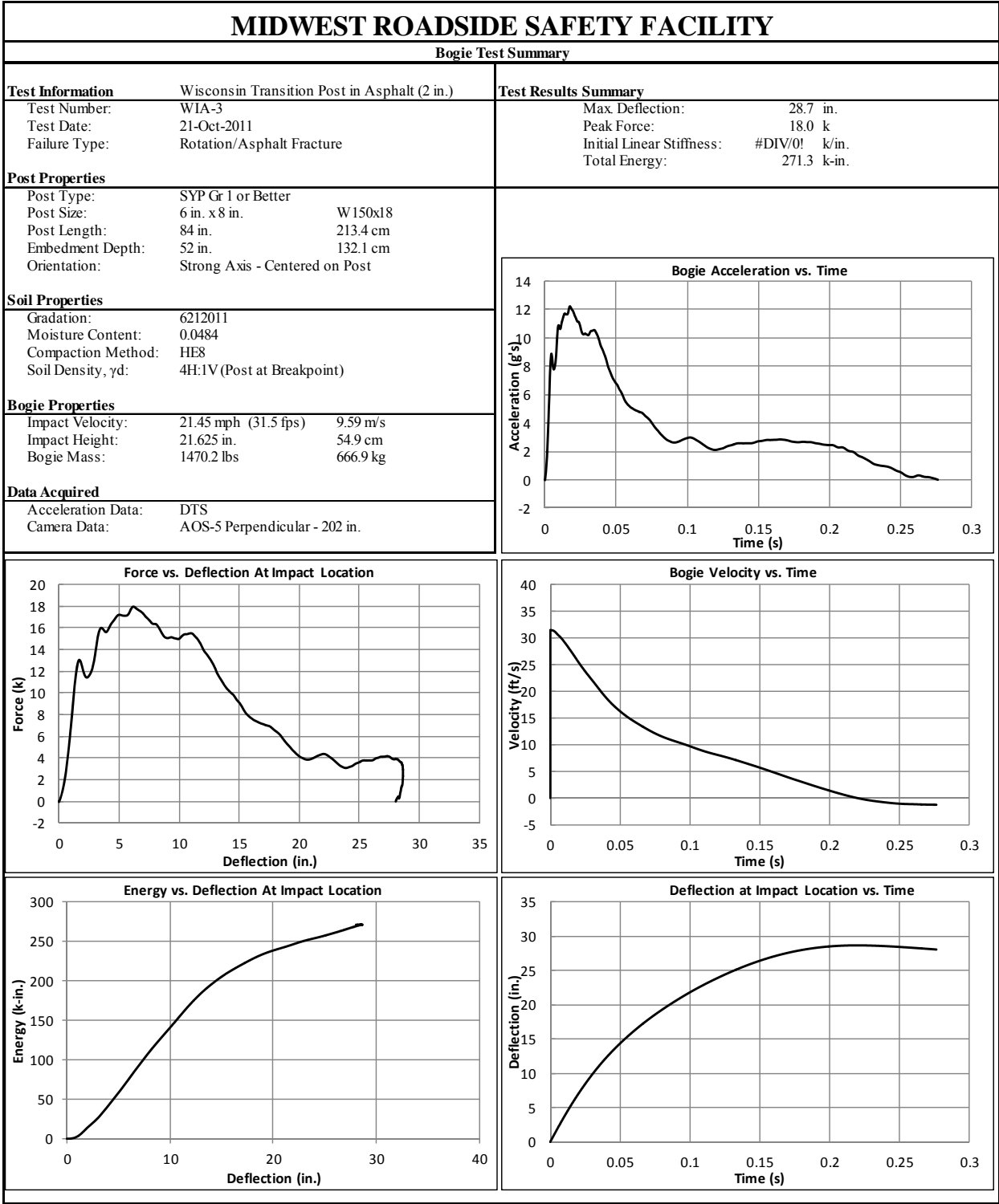


Figure E-14. Results of Test No. WIA-3 (DTS)

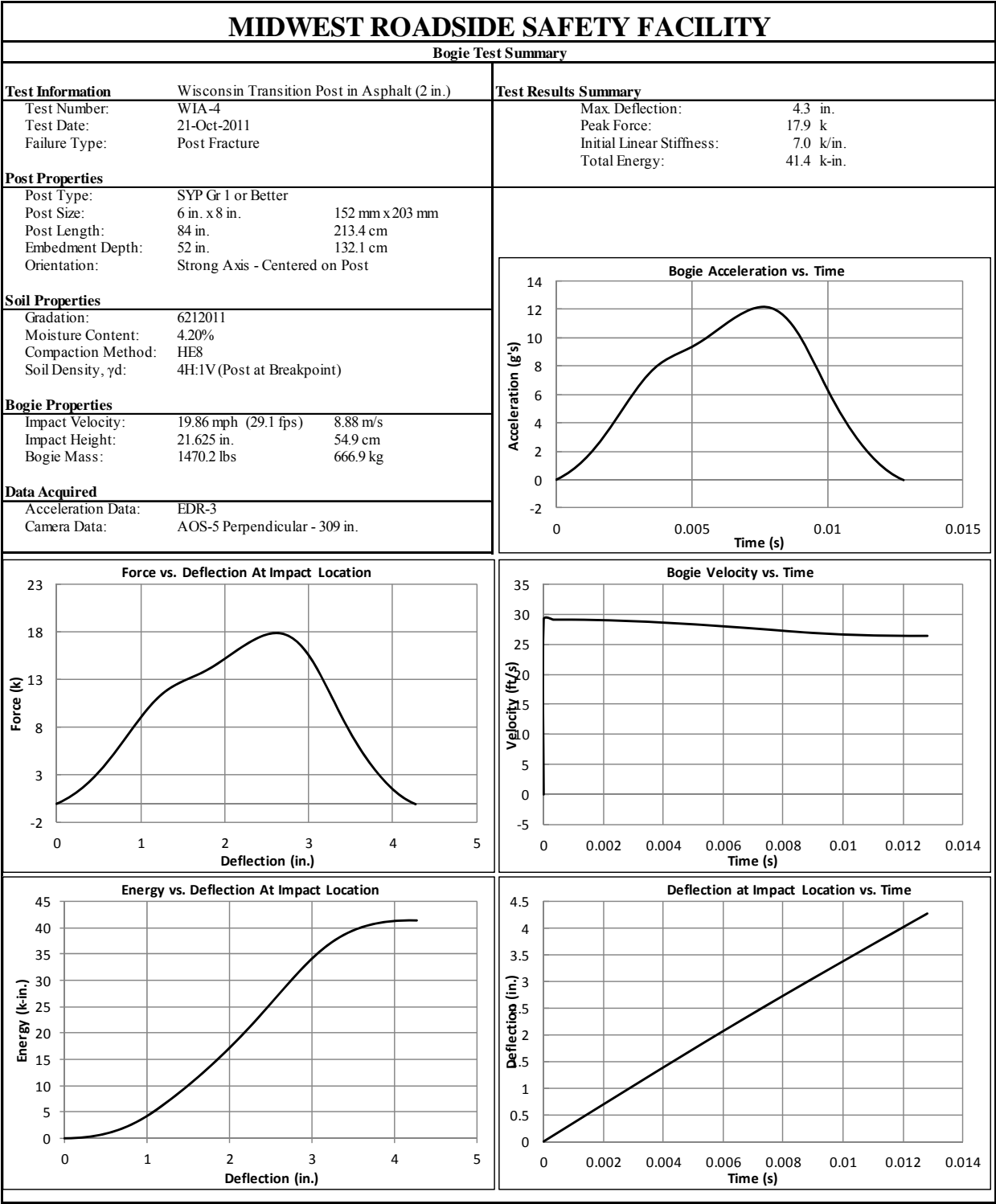


Figure E-15. Results of Test No. WIA-4 (EDR-3)

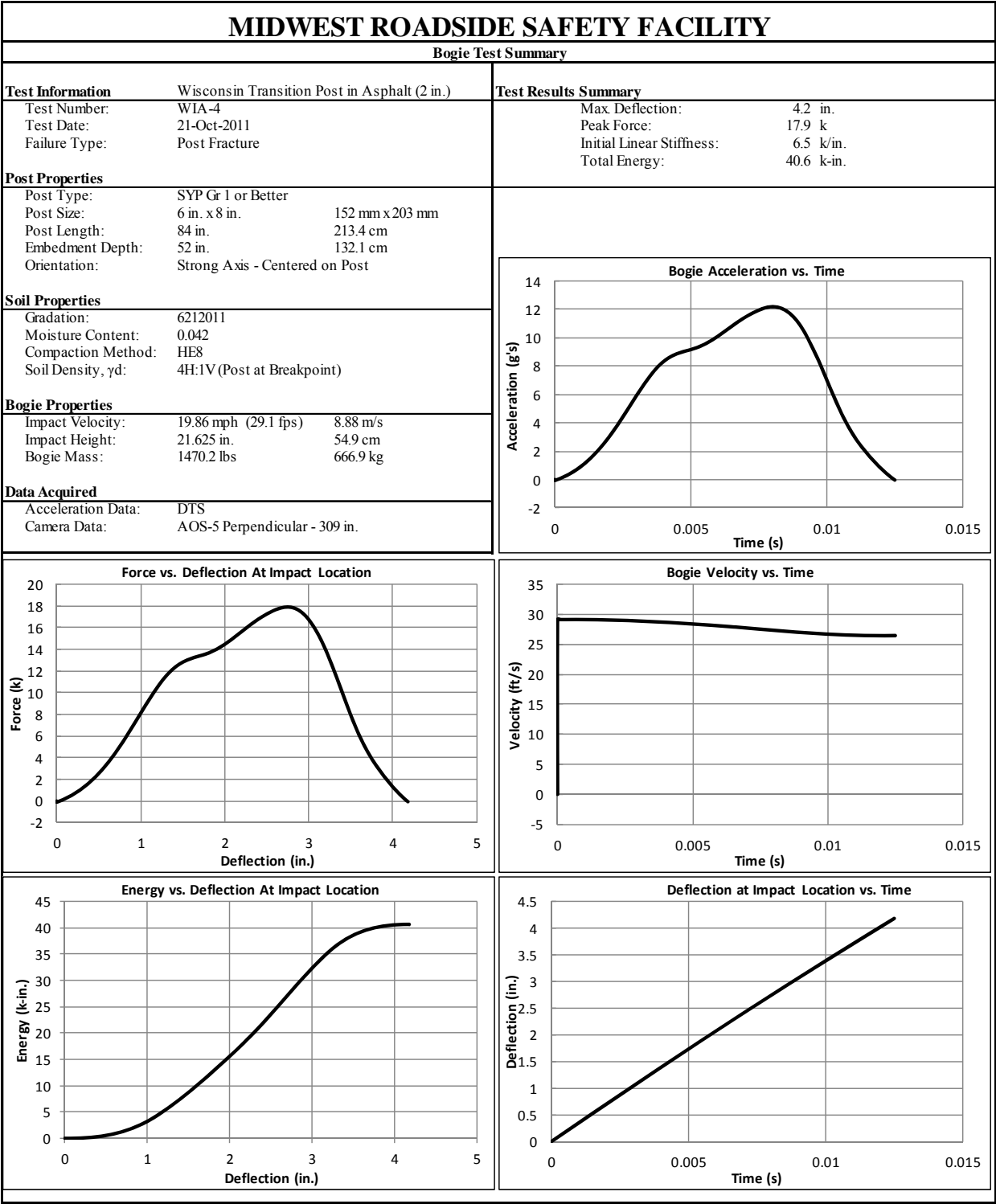


Figure E-16. Results of Test No. WIA-4 (DTS)

Appendix F. Material Specifications and Documentation

Certificates authenticating the components utilized for each dynamic bogie test are provided in this section.

Figure F-1. W6x12 Beam Material Specifications, Test No. WAGTMP-1

Figure F-2. Base Plate Material Specifications, Test No. WAGTMP-1

Figure F-3. Back-up Plate Material Specifications, Test No. WAGTMP-1

Figure F-4. W6x12 Beam Material Specifications, Test No. WAGTMP-4

Figure F-5. Base Plate Material Specifications, Test No. WAGTMP-4

Figure F-6. Back-Up Plate Material Specifications, Test No. WAGTMP-4

Figure F-7. Gusset Plate Material Specifications, Test No. WAGTMP-4

Figure F-8. 6-in. x 8-in. Wood Post Material Specifications

Figure F-9. Soil Characteristic Data, Test Nos. WITB-1 and WITB-2

Figure F-10. Soil Characteristic Data, Test Nos. WIA-1 and WIA-2

Figure F-11. Soil Characteristic Data, Test Nos. WIA-3 and WIA-4

Chemical and Physical Test Report
Made and Melted in USA

G-158850

(770)

SHIP TO SIOUX CITY FOUNDRY INC 801 DIVISION STREET 800-831-0874 SIOUX CITY, IA 51102	INVOICE TO SIOUX CITY FOUNDRY INC ACCTS PAYABLE PO BOX 3067 SIOUX CITY, IA 51102	SHIP DATE 08/19/10 CUST. ACCOUNT NO 60044062
---	---	---

PRODUCED IN: CARTERSVILLE

SHAPE + SIZE	GRADE	SPECIFICATION															SALES ORDER	CUST P.O. NUMBER										
W6 X 12#	A57250/692	ASTM A572 GR50-07, ASTM A992-06A, ASTM A709 GR50-09A															0101729-04	127527-W-04										
HEAT I.D.	C	Mn	P	S	Si	Cu	Ni	Cr	Mo	V	Nb	B	N	Sn	Al	Ti	Ca	Zn	C Eqv									
G104740	.16	.90	.015	.022	.20	.28	.09	.08	.023	.016	.001	.0002	.0091	.009	.001	.00100	.00070	.00440	.389									

Mechanical Test: Yield 55400 PSI, 381.97 MPA Tensile: 78800 PSI, 543.31 MPA %El: 21.1/8in, 21.1/200MM

Customer Requirements CASTING: STRAND CAST
Comment NO WELD REPAIRMENT PERFORMED. STEEL NOT EXPOSED TO MERCURY.

Mechanical Test: Yield 56600 PSI, 390.24 MPA Tensile: 79300 PSI, 546.75 MPA %El: 20.6/8in, 20.6/200MM

Customer Requirements CASTING: STRAND CAST
Comment NO WELD REPAIRMENT PERFORMED. STEEL NOT EXPOSED TO MERCURY.

PRODUCED IN: CARTERSVILLE

SHAPE + SIZE	GRADE	SPECIFICATION															SALES ORDER	CUST P.O. NUMBER										
F1/2 X 7	A36	ASTM A36-08, SA-36 08, ASTM A709 GR36-09A															0101729-02	127527-W-02										
HEAT I.D.	C	Mn	P	S	Si	Cu	Ni	Cr	Mo	V	Nb	B	N	Sn	Al	Ti	Ca	Zn	C Eqv									
G104895	.18	.88	.018	.012	.21	.36	.09	.07	.026	.017	.002	.0003	.0092	.012	.002	.00100	.00050	.00500	.413									

Mechanical Test: Yield 55900 PSI, 384.73 MPA Tensile: 78100 PSI, 538.48 MPA %El: 21.8/8in, 21.8/200MM

Customer Requirements CASTING: STRAND CAST
Comment NO WELD REPAIRMENT PERFORMED. STEEL NOT EXPOSED TO MERCURY.

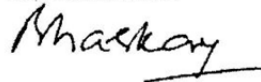
Mechanical Test: Yield 55900 PSI, 385.42 MPA Tensile: 77700 PSI, 535.72 MPA %El: 21.3/8in, 21.3/200MM

Customer Requirements CASTING: STRAND CAST
Comment NO WELD REPAIRMENT PERFORMED. STEEL NOT EXPOSED TO MERCURY.

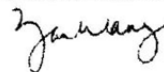
Customer Notes

NO WELD REPAIRMENT PERFORMED. STEEL NOT EXPOSED TO MERCURY.
 All manufacturing processes including melt and cast, occurred in USA. MTR
 complies with EN10204 3.1B

THE ABOVE FIGURES ARE CERTIFIED EXTRACTS FROM THE ORIGINAL CHEMICAL AND PHYSICAL TEST RECORDS
 AS CONTAINED IN THE PERMANENT RECORDS OF COMPANY.



Bhaskar Yalamanchili
 Quality Director
 Gerdau Ameristeel



Metallurgical Services Manager
 CARTERSVILLE STEEL MILL

Seller warrants that all material furnished shall comply with specifications subject to standard published manufacturing variations. NO OTHER WARRANTIES, EXPRESSED OR IMPLIED, ARE MADE BY THE SELLER, AND SPECIFICALLY EXCLUDED ARE WARRANTIES OF MERCHANTABILITY AND FITNESS FOR A PARTICULAR PURPOSE. In no event shall seller be liable for indirect, consequential or punitive damages arising out of or related to the materials furnished by seller. Any claim for damages for materials that do not conform to specifications must be made from buyer to seller immediately after delivery of same in order to allow the seller the opportunity to inspect the material in question.

287

Figure F-1. W6x12 Beam Material Specifications, Test No. WAGTMP-1

MWRSF Report No. TRP-03-266-12
 August 21, 2012



CALVERT CITY STEEL MILL
1035 SHAR-CAL ROAD
CALVERT CITY KY 42029 USA
(270) 395-3100

Chemical and Physical Test Report
MADE IN UNITED STATES

Y-057407

SHIP TO STEEL AND PIPE SUPPLY CO INC 401 NEW CENTURY PARKWAY 785-587-5185 NEW CENTURY, KS 66031	INVOICE TO STEEL AND PIPE SUPPLY CO. INC. PO BOX 1688 MANHATTAN, KS 66505-1688	SHIP DATE 01/08/10 CUST. ACCOUNT NO 40130833
--	--	---

PRODUCED IN: CALVERT CITY

SHAPE + SIZE	GRADE	SPECIFICATION														SALES ORDER	CUST P.O. NUMBER					
F38 X 8	A36	ASTM A36-08, ASTM A709 GR36														9177198-03	4500125002-03					
HEAT I.D.	C	Mn	P	S	Si	Cu	Ni	Cr	Mo	V	Nb	B	N	Sn	Ti	C Eqv						
Y013646	.15	.67	.011	.016	.25	.29	.08	.04	.022	<.008	<.008	.0002	.0093	.009	.00100	.34						

Mechanical Test: Yield 52000 PSI, 358.53 MPA Tensile: 71000 PSI, 489.53 MPA %El: 24.0/8in, 24.0/203.2mm Corrosion Index: 5.48

Customer Requirements CASTING: STRAND CAST

Comment: ASTM A36-05 & ASTM A709 GR36

Mechanical Test: Yield 51000 PSI, 351.63 MPA Tensile: 71000 PSI, 489.53 MPA %El: 24.0/8in, 24.0/203.2mm Corrosion Index: 5.48

Customer Requirements CASTING: STRAND CAST

Comment: ASTM A36-05 & ASTM A709 GR36

PRODUCED IN: CALVERT CITY

SHAPE + SIZE	GRADE	SPECIFICATION														SALES ORDER	CUST P.O. NUMBER					
F1/2 X 12	A36	ASTM A36-08, A709 GR36, ASME SA36														9177198-17	4500125002-17					
HEAT I.D.	C	Mn	P	S	Si	Cu	Ni	Cr	Mo	V	Nb	B	N	Sn	Ti	C Eqv						
Y013672	.15	.70	.010	.027	.22	.28	.08	.04	.023	.001	<.008	.0002	.0073	.010	.00100	.34						

Mechanical Test: Yield 49000 PSI, 337.84 MPA Tensile: 69000 PSI, 475.74 MPA %El: 24.0/8in, 24.0/203.2mm Corrosion Index: 5.35

Customer Requirements CASTING: STRAND CAST

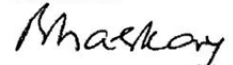
Comment: ASTM A36-05 & ASTM A709 GR36

Mechanical Test: Yield 49000 PSI, 337.84 MPA Tensile: 70000 PSI, 482.63 MPA %El: 24.0/8in, 24.0/203.2mm Corrosion Index: 5.35

Customer Requirements CASTING: STRAND CAST

Comment: ASTM A36-05 & ASTM A709 GR36

This material, including the billets, was melted and manufactured in the United States of America

 Bhaskar Yalamanchili
Quality Director
Gerdau Ameristeel

THE ABOVE FIGURES ARE CERTIFIED EXTRACTS FROM THE ORIGINAL CHEMICAL AND PHYSICAL TEST RECORDS AS CONTAINED IN THE PERMANENT RECORDS OF COMPANY.

 Alice L. Plech
Metallurgical Services Manager
CALVERT CITY STEEL MILL

Seller warrants that all material furnished shall comply with specifications subject to standard published manufacturing variations. NO OTHER WARRANTIES, EXPRESSED OR IMPLIED, ARE MADE BY THE SELLER, AND SPECIFICALLY EXCLUDED ARE WARRANTIES OF MERCHANTABILITY AND FITNESS FOR A PARTICULAR PURPOSE. In no event shall seller be liable for indirect, consequential or punitive damages arising out of or related to the materials furnished by seller. Any claim for damages for materials that do not conform to specifications must be made from buyer to seller immediately after delivery of same in order to allow the seller the opportunity to inspect the material in question.

Beam Test

288

MWR/SF Report No. TRP-03-266-12 August 21, 2012

Figure F-2. Base Plate Material Specifications, Test No. WAGTMP-1

VER. 29. 2/11 2:27PM

NO. 7396 P. 5

CERTIFICATE OF CONFORMANCE

1/20/11

Page# 1

TO:
SIOUX CITY FOUNDRY CO.
PO BOX 3067
SIOUX CITY IA 51101

SHIP TO:
SIOUX CITY FOUNDRY CO.
801 DIVISION STREET
SIOUX CITY IA 51105
712-252-4181

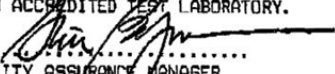
SIZE: .1250 X 6.00 X 240.00
GRADE: HOT ROLLED STRIP - CQ

Bill/Ladng# 189239 B/L Date 1/20/11 Sales Ord# 818226 05
Cust. P/O#: 131047W

Tag# P134700	01	Heat# 10323707	MasterTag# 134567	01	
C : 0.058		Mn: 0.41	P : 0.008	S : 0.004	Al: 0.044
Ti: 0.003		Co: 0.000	Mo: 0.017	Cu: 0.135	Var: 0.000
				N : 0.008	B : 0.0000
					Si: 0.018
					Cr: 0.062
					Ni: 0.046

Tag# P134860	01	Heat# 208361	MasterTag# 134803	01	
C : 0.20		Mn: 1.09	P : 0.009	S : 0.001	Al: 0.035
		Co: 0.003	Mo: 0.016	Cu: 0.093	Var: 0.002
					Si: 0.018
					Cr: 0.047
					Ni: 0.029

WE HEREBY CERTIFY THE ABOVE FIGURES ARE ACCURATELY STATED, MEET YOUR MATERIAL REQUIREMENTS AND ARE TRACEABLE IN OUR RECORDS BACK TO THE PRODUCER AND/OR AN ACCREDITED TEST LABORATORY.


.....
QUALITY ASSURANCE MANAGER
STEVE BERGMAN

))) 100% MELTED AND MANUFACTURED IN THE USA < < <

Figure F-3. Back-up Plate Material Specifications, Test No. WAGTMP-1

59732

10-JUN-2005 10:51

TXI - NITELAX 1-800-645-4155

Page 13/2:

Bill To:
STEEL AND PIPE SUPPLY
P.O. BOX 1688

Ship To: 9
STEEL AND PIPE SUPPLY
401 NEW CENTURY PARKWAY

Order Date:06/03/2005
PO No:45/59732
Mill Order No:2930688
Load No:951072
Manifest No:1674844

CHAPARRAL STEEL
CERTIFIED MATERIAL TEST REPORT
CHAPARRAL STEEL
300 Ward Rd.
Midlothian, TX
76065-9651
(972) 775-8241

MANHATTAN
66502

KS
US

GARDNER
66031

KS
US

SIZE
W 6 X 12# / W150 X 18.0

GRADE
992/572-50

LENGTH
50 FT / 15.24 M

PRODUCT
WF BEAMS

SPECIFICATION
ASTM A6-02, A992-02, A572-01

HEAT NO:22274610

CHEMICAL ANALYSIS

C	Mn	P	S	Si	Cu	Ni	Cr	Mo	Sn	V	Al	Nb	CE
.10	.90	.014	.012	.21	.37	.10	.13	.029	.009	.001	.006	.012	.31

PHYSICAL PROPERTIES

Yield Strength		Tensile Strength		Specimen Area		Elongation		Bend Test		ROA
KSI	MPa	KSI	MPa	Sq In	Sq cm	%	Gage Length	Dia.	Result	%
58.2	401.3	76.6	528.1	0.330	2.13	23.8	8In	200 mm		
57.6	397.1	75.3	519.2	0.340	2.19	24.0	8In	200 mm		

All manufacturing processes of this product, including electric arc melting and continuous casting, occurred in the U.S.A. CMTR complies with DIN EN 10204 3.1.B

"I hereby certify that the contents of this report are correct and accurate. All tests and operations performed by this material manufacturer or its sub-contractors, when applicable, are in compliance with the requirements of the material specifications and applicable purchaser designated requirements."

Signed: Tom L. Barrington Date: Jun. 10, 2005 Signed: _____ Date: _____
Tom L. Barrington: Quality Assurance Manager Notary Public (if applicable) Page: 13 of 22

376120050

290

Figure F-4. W6x12 Beam Material Specifications, Test No. WAGTMP-4



MILL TEST CERTIFICATE

1700 HOLT RD N.E.
Tuscaloosa, AL 35404-1000
800-827-8872

Load Number	Tally	Mill Order Number	P.O. Number	Part Number	Certificate Number	Date
386513	00000000410154	N-105963-007	4500156614		L325787-1	05/19/2011 08:58
Grade				Customer:		
Order Description: A572/A709, 0.5000 IN x 96.000 IN x 240.000 IN				Sold TO: STEEL & PIPE SUPPLY CO., INC. MANHATTAN KS		
Quality Plan Description: A57250/A70950: ASTM A572-07 GR 50/A709-08 GR 50				Ship TO: Kansas City Warehouse New Century KS		

Shipped Item	Heat/Slab Number	Certified By	C	Mn	P	S	Si	Cu	Ni	Cr	Mo	Cb	V	Al	Ti	N2	B	Ca	Sn	CEV
1E0881C	B1R6601-01 ***	B1R6601	0.06	1.18	0.007	0.005	0.06	0.27	0.08	0.06	0.019	0.000	0.047	0.033	0.001	0.009	0.0001	0.0029	0.009	0.31

Shipped Item	Certified By	Heat Number	Yield ksi	Tensile ksi	Y/T %	ELONGATION %		Bend OK?	Hard HB	Charpy Impacts (ft-lbf)				Shear %			Test Temp				
						2"	8"			Size mm	1	2	3	Avg	1	2		3	Avg		
1E0881C	S1E0881FTT	B1R6601 ***	54.8	68.6	79.9	38.8															
1E0881C	S1E0881MTT	B1R6601 ***	65.6	74.8	87.7	31.5															

Items: 1 PCS: 8 Weight: 26137 LBS

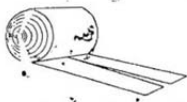
Mercury has not come in contact with this product during the manufacturing process nor has any mercury been used by the manufacturing process. Certified in accordance with EN 10204 3.1. No weld repair has been performed on this material. Manufactured to a fully killed fine grain practice. ** Produced from Coil ** ISO 9001:2008 Registered, PED Certified

**** indicates Heats melted and Manufactured in the U.S.A.

We hereby certify that the product described above passed all of the tests required by the specifications.

April Pitts
April Pitts - QA Engineer

Figure F-5. Base Plate Material Specifications, Test No. WAGTMP-4



THE STEEL WORKS, L.L.C.
P.O. BOX 366 • 1020 NIEDRINGHAUS
GRANITE CITY, ILLINOIS 62040
PHONE 618-452-2833
FAX 618-452-2904

CHEMICAL CERTIFICATION

V E N D O R	THE STEEL WORKS, L.L.C. P.O. BOX 366 1020 NIEDRINGHAUS BLDG.4 GRANITE CITY IL 62040	BILL OF LADING NO. 130323	DATE SHIPPED 08/12/10
		SHIPPER NO.	INVOICE NUMBER
		PURCHASE ORDER NO.	INVOICE DATE / /
S O L D T O	STEEL & PIPE SUPPLY CO. INC. P.O. BOX 1688 MANHATTAN, KS 66502	CUSTOMER WILL CALL	
		SALES ORD. NO. 99143550	

TSW COIL NO.	DESCRIPTION				YIELD	TENSILE	% ELONG	BEND	R.W.	OLSON		
605963	HR FB 0.1250 X	A36 6.0000	H/T # 20599201 Length: 240.0000		55800	66500	29.5					
605964	HR FB 0.1250 X	A36 6.0000	H/T # 20599201 Length: 240.0000		55800	66500	29.5					
605752	HR FL 0.1250 X	A36 4.0000	H/T # 20599201 Length: 240.0000		55800	66500	29.5					
602605	HR FL 0.1250 X	A36 4.0000	H/T # 20459201 Length: 240.0000		49300	76900	28.5					
TSW COIL NO.	C	MN	P	S	SI	AL	CB	V	CU	NI	CR	MO
605963	.060	0.670	.008	.001	.032	.030	.002	.050	.171	0.070	0.08	.023
	SN	N	B	TI								
	.009	.013	.001	.002								
TSW COIL NO.	C	MN	P	S	SI	AL	CB	V	CU	NI	CR	MO
605964	.060	0.670	.008	.001	.032	.030	.002	.050	.171	0.070	0.08	.023
	SN	N	B	TI								
	.009	.013	.001	.002								
TSW COIL NO.	C	MN	P	S	SI	AL	CB	V	CU	NI	CR	MO
605752	.060	0.670	.008	.001	.032	.030	.002	.050	.171	0.070	0.08	.023
	SN	N	B	TI								
	.009	.013	.001	.002								
TSW COIL NO.	C	MN	P	S	SI	AL	CB	V	CU	NI	CR	MO
602605	.220	1.130	.005	.002	.016	.026	.001	.001	.088	0.031	0.04	.018
	SN	N	B	TI								
	.004	.006	.001	.003								

MELTED & ROLLED IN THE U.S.A.

WE HEREBY CERTIFY THE ABOVE IS CORRECT AS CONTAINED IN THE RECORDS OF THE CORPORATION.

May Macko



Figure F-6. Back-Up Plate Material Specifications, Test No. WAGTMP-4

SPS Coil Processing Houston
1550 North Witter Rd
Pasadena, TX 77506



METALLURGICAL TEST REPORT

PAGE 1 of 2
DATE 11/16/2010
TIME 11:04:59
USER 065SHIP2

S
O
L
D
T
O

S
H
I
P
T
O

17238
Longview Warehouse
4750 West Marshall Ave
LONGVIEW TX 75604

Order	Material No.	Description	Quantity	Weight	Customer Part	Customer PO	Ship Date
40149040-0010	70872120TM	1/4 - 72 X 120 A36 TEMPERPASS STPMLPL	16	9,801.600			11/16/2010

Chemical Analysis

Heat No.	Vendor	SEVERSTAL COLUMBUS	DOMESTIC	Mill	SEVERSTAL COLUMBUS	Melted and Manufactured in the USA									
Batch	0000891836	16 EA	9,801.600 LB												
Carbon	Manganese	Phosphorus	Sulphur	Silicon	Nickel	Chromium	Molybdenum	Boron	Copper	Aluminum	Titanium	Vanadium	Columbium	Nitrogen	Tin
0.2030	0.4660	0.0080	0.0030	0.0200	0.0400	0.0500	0.0100	0.0001	0.0900	0.0280	0.0010	0.0020	0.0020	0.0068	0.0050

Mechanical/ Physical Properties

Mill Coil No.	A017368-01														
Tensile	Yield	Elong	Rckwl	Grain	Charpy	Charpy Dr	Charpy Sz	Olsen							
73800.000	53700.000	28.25	0	0.000	0	NA	0								
76200.000	55400.000	23.60	0	0.000	0	NA									
75600.000	54900.000	29.50	0	0.000	0	NA									

Chemical Analysis

Heat No.	Vendor	SEVERSTAL COLUMBUS	DOMESTIC	Mill	SEVERSTAL COLUMBUS	Melted and Manufactured in the USA									
Batch	0000891850	16 EA	9,801.600 LB												
Carbon	Manganese	Phosphorus	Sulphur	Silicon	Nickel	Chromium	Molybdenum	Boron	Copper	Aluminum	Titanium	Vanadium	Columbium	Nitrogen	Tin
0.2030	0.4660	0.0080	0.0030	0.0200	0.0400	0.0500	0.0100	0.0001	0.0900	0.0280	0.0010	0.0020	0.0020	0.0068	0.0050

Mechanical/ Physical Properties

Mill Coil No.	A017368-01														
Tensile	Yield	Elong	Rckwl	Grain	Charpy	Charpy Dr	Charpy Sz	Olsen							
73800.000	53700.000	28.25	0	0.000	0	NA	0								
76200.000	55400.000	23.60	0	0.000	0	NA									
75600.000	54900.000	29.50	0	0.000	0	NA									

THE CHEMICAL, PHYSICAL OR MECHANICAL TESTS REPORTED ABOVE ACCURATELY REFLECT INFORMATION AS CONTAINED IN THE RECORDS OF THE CORPORATION

293

Figure F-7. Gusset Plate Material Specifications, Test No. WAGTMP-4

MwRSF Report No. TRP-03-266-12 August 21, 2012

PERMA-TREAT OF ILLINOIS, INC.

1800 PERMA-TREAT DRIVE, P.O. BOX 99
 MARION, IL 62959
 PH# 800.572.7384 FAX# 618.993.8680

This is to certify that the guardrail material has been treated and inspected according to the Iowa Department of Transportation Specification requirements and IM 462.

This material has been processed from Rough Sawn #1 Southern Yellow Pine.

Company: Midwest Guardrail

Bill of Lading: 23516

Quantity	Description	Charge #	Date of Treatment	QC Name	Treatment	MC prior to treatment
288	6x8x18	4189-09	10/21/09	Martin	.60 CCA-C	20%
180	6x8x7 2 H	4202-09	10/28/09	Martin	.60 CCA-C	20%
120	6x8x7 2 H	4203-09	10/28/09	Martin	.60 CCA-C	20%
				Martin	.60 CCA-C	20%
				Martin	.60 CCA-C	20%
				Martin	.60 CCA-C	20%
				Martin	.60 CCA-C	20%
				Martin	.60 CCA-C	20%
				Martin	.60 CCA-C	20%
				Martin	.60 CCA-C	20%
				Martin	.60 CCA-C	20%
				Martin	.60 CCA-C	20%

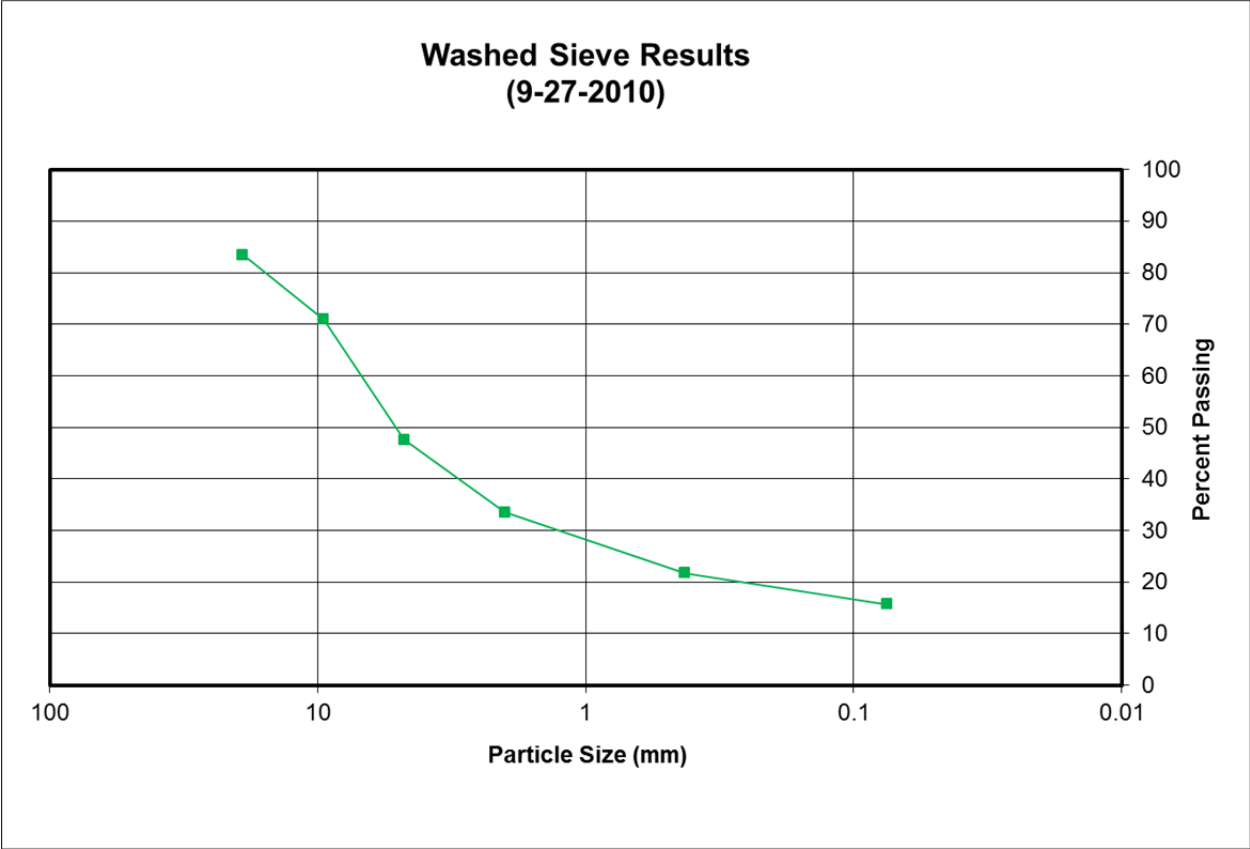
Perma-Treat of Illinois, Inc
 By: [Signature]
 Title: President
 Date: 10-2-09

NOTARIZED
 Sworn to and described
 Before me this 2 day of
October 2009.
 By: [Signature]

Official Seal



Figure F-8. 6-in. x 8-in. Wood Post Material Specifications

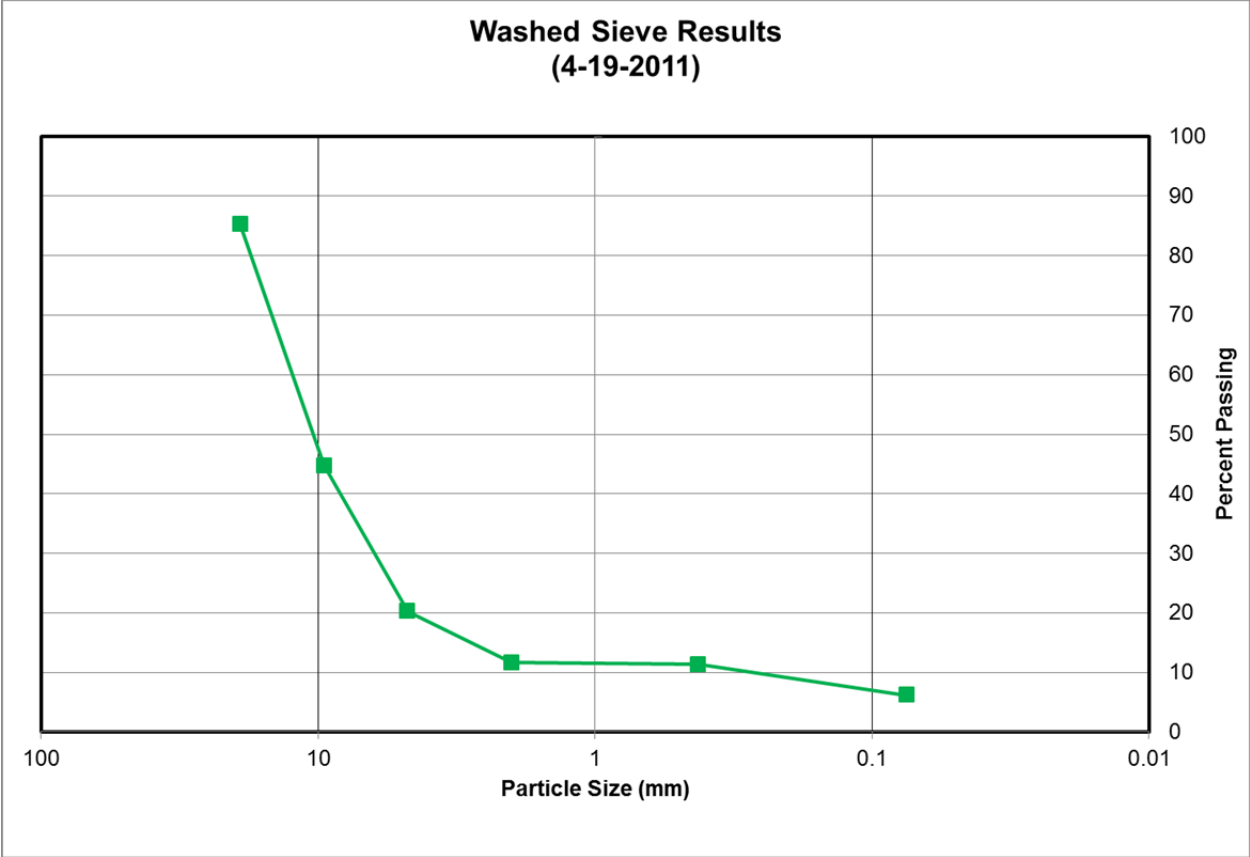


Soil Test #		9272010	Moisture Content %	#VALUE!
Wet Soil Test Weight (kg)		n/a		
Dry Soil Test Weight (kg)		1.438		
Date		9/29/2010		

Sieve Pan #	Sieve Opening (mm)	Pan Weight (kg)	% passing
3 / 4	19.05	1.212	83.032
3/8	9.5	1.194	69.680
4	4.75	1.082	44.228
10	2	1.054	27.955
40	0.425	0.824	12.239
200	0.075	0.724	3.477

Loss		0.050
------	--	-------

Figure F-9. Soil Characteristic Data, Test Nos. WITB-1 and WITB-2



Soil Test #		4192011	Moisture Content %	3.404
Wet Soil Test Weight (kg)		7.504		
Dry Soil Test Weight (kg)		7.257		
Date		4/19/2011		
Sieve Pan #	Sieve Opening (mm)	Pan Weight (kg)	% passing	
3 / 4	19.05	1.196	83.535	
3/8	9.5	1.194	44.983	
4	4.75	1.068	22.761	
10	2	1.056	11.111	
40	0.425	0.822	8.249	
200	0.075	0.716	3.670	
Loss		0.098		

Figure F-10. Soil Characteristic Data, Test Nos. WIA-1 and WIA-2



Soil Batch #		6212011	Moisture Content %	5.007
Wet Soil Test Weight (kg)		7.508		
Dry Soil Test Weight (kg)		7.15		
Date		6/24/2011		

Sieve Pan #	Sieve Opening (mm)	Pan Weight (kg)	% passing
3 / 4	19.05	1.192	87.304
3/8	9.5	1.174	69.752
4	4.75	1.07	45.543
10	2	1.042	32.447
40	0.425	0.818	24.222
200	0.075	0.712	21.933

Loss		0.658
------	--	-------

Figure F-11. Soil Characteristic Data, Test Nos. WIA-3 and WIA-4

END OF DOCUMENT